University of Dundee

University of Dundee

DOCTOR OF PHILOSOPHY

VHL inhibitors as chemical probes of the hypoxia signalling pathway

Frost, Julianty

Award date:
2018

Link to publication

General rights
Copyright and moral rights for the publications made accessible in the public portal are retained by the authors and/or other copyright owners and it is a condition of accessing publications that users recognise and abide by the legal requirements associated with these rights.

- Users may download and print one copy of any publication from the public portal for the purpose of private study or research.
- You may not further distribute the material or use it for any profit-making activity or commercial gain
- You may freely distribute the URL identifying the publication in the public portal

Take down policy
If you believe that this document breaches copyright please contact us providing details, and we will remove access to the work immediately and investigate your claim.

Download date: 04. May. 2023

VHL INHIBITORS AS CHEMICAL PROBES OF THE HYPOXIA SIGNALLING PATHWAY

Julianty Frost

Supervisors: Prof. Alessio Ciulli and Prof. Sonia Rocha

Submission for the degree of

Doctor of Philosophy

31st January 2018

Declaration

This thesis, submitted for the Doctor of Philosophy at the University of Dundee, has been performed in the laboratories of Prof. Alessio Ciulli at the Division of Biological Chemistry and Drug Discovery and Prof. Sonia Rocha at the Centre for Gene Regulation and Expression within the School of Life Sciences, Dundee. The presented work was performed under the guidance of Prof. Alessio Ciulli and Prof. Sonia Rocha, and contains no material, which has been accepted for the award of any other degree in my university.

Julianty Frost

We declare that Julianty Frost has spent the equivalent of a least nine terms in the research department of the School of Life Sciences at the University of Dundee, and that he has fulfilled the conditions of Ordinance General No. 39 of the University of Dundee and is qualified to submit the accompanying thesis in application for the degree of Doctor of Philosophy.

Prof. Alessio Ciulli

Supervisor

Prof. Sonia Rocha

Supervisor

Abstract

Von Hippel–Lindau (VHL) is the E3 ubiquitin ligase targeting hypoxia-inducible transcription factor-alpha (HIF-α) for proteasomal degradation. The crucial function of VHL in response to hypoxia and cellular oxygen sensing are well established, owing to the use of genetic tools through knockout and knockdown that inactivate VHL. However, the functional consequences of specifically interrupting the interaction between VHL and HIF-α remain to be elucidated. The development of a chemical probe that unambiguously blocks the VHL:HIF-α interaction downstream of HIF-α hydroxylation by prolyl hydroxylase domain (PHD) enzymes, would address biological questions about VHL molecular targets and functional consequences of disrupting the interaction.

Here, small molecules inhibiting the VHL:HIF-α interaction were shown for the first time to stabilise HIF-α and elicit HIF transcriptional activity in cells. The most potent VHL inhibitor identified is VH298. VH298 is potent, cell-permeable, selective, and not toxic at the concentration required for HIF-α stabilisation. Further characterisation shows that VHL inhibitor exclusively induces HIF-dependent changes in global gene and protein expression, demonstrating the specificity of the inhibitor. VHL protein level was found to increase in the presence of VHL inhibitor, which in turn promotes the degradation of HIF-α in prolonged inhibition.

The work herein characterises the VHL inhibitor as a chemical probe of the hypoxia signalling pathway with great potential to address biological questions regarding the roles and regulation of VHL. The VHL inhibitor is a unique tool due to its on-target selectivity and specificity in inducing HIF activity, without affecting HIF-independent response, and exerts its effect further downstream than PHD hydroxylation. This work provides a foundation and cellular proof-of-concept for future studies evaluating

therapeutic potential of VHL inhibitor in diseases, such as chronic anaemia, ischaemia, and inflammation-driven diseases.

Acknowledgements

First, many thanks to both my PhD supervisors, Alessio and Sonia. Thank you for accepting me as your PhD student, for your guidance, helps, supports, and encouragement throughout my PhD. You've been excellent mentors and I've learnt a lot from you. Thank you very much!

I would also like to thank every lab member in both the Ciulli and Rocha labs! You have all been very helpful, in terms of work and non-work related. Thank you for the fun and friendly environment you've created. It was great working together! I would like to thank Pedro in particular for the VHL inhibitors, and Carles who started this project! There's so many of you that I can't list. Thank you all for the fun time together.

I would like to thank everyone who has helped and advised me with experiments, everyone in BCDD and GRE division, and School of Life Sciences, lab managers, cleaning staff, Wellcome Trust store, and every staff who make my life here so much easier! Many thanks to my thesis committee Mark Field and Greg Findlay, especially for the helpful discussion and guidance.

I would also like to thank Wellcome Trust for my PhD fellowship.

Special thanks to a brother in Christ, who became my fiancé, and now a husband – Mark. Thank you for your help, encouragement, patience, love and prayer. Thank you for the company in thesis writing, it's so fun writing together and encouraging each other! Also many thanks to family in Christ for your love and prayer, and feeding me during my busy time. Thanks to my family for your love and support.

Most importantly, I would like to dedicate this thesis to the One who never leaves me nor forsakes me – heavenly Father. Thank You for Your love, Your Word, and the assurance and hope that I can have in You.

"*When you pass through the waters, I will be with you; and through the rivers, they shall not overwhelm you; when you walk through fire you shall not be burned, and the flame shall not consume you"*

Isaiah 43:2

"... even there your hand shall lead me, and your right hand shall hold me."

Psalm 139:10

His eternal power and divine nature have been clearly seen, being understood from what has been made!

Table of Contents

List of Figures

List of Tables

List of Abbreviations

2OG – 2-oxoglutarate

ABC – ATP-binding cassette

ABCA1 – ABC subfamily A member 1

ABCG1 – ABC subfamily G member 1

AhR – Aryl hydrocarbon Receptor

AK4 – Adenylate kinase 4

AMP – Adenosine 5’ monophosphate

AMPK – AMP-activated protein kinase

AMY1 – Amylase Alpha A1

ANKZ1 – Ankyrin repeat and zinc finger domain containing 1

ARNT – Aryl hydrocarbon receptor nuclear translocator

ATCC – American type culture collection

ATF6 – Activating transcription factor 6

ATP – Adenosine triphosphate

bHLH – Basic-helix-loop-helix domain

BMDAC – Bone marrow-derived angiogenic cell

BNIP3 – BCL2/adenovirus E1B 19kDa interacting protein 3

CA9 – Carbonic anhydrase 9

CAND1 – Cullin-associated NEDD8-dissociated protein 1

CBP – CREB-binding protein

ccRCC – Clear-cell renal cell carcinoma

CCT – Chperonin-containing TCP1

Cep192 – Centrosomal protein 192

CETSA – Cellular thermal shift assay

ChIP – Chromatin-immunoprecipitation

CHX - Cycloheximide

CKD – Chronic kidney disease

CMA – Chaperone-mediated autophagy

Co-IP – Co-immunoprecipitation

CO_2 – Carbon dioxide

$CoCl_2$ – Cobalt chloride

CODDD – C-terminal oxygen dependent degradation domain

CREB – cAMP response element binding protein

CRL – Cullin RING E3 ubiquitin ligase complex

CSN – COP9 signalosome

CTAD – C-terminal transactivation domain

CTL – Cytotoxic T lymphocyte

DDB1 – DNA-binding protein 1

DFX/DFO – Desferroxamine/desferrioxamine

DIA – Data independent acquisition

DMOG – Dimethyloxalylglycine

DRE – Dioxin response element

DUB – Deubiquitinase

EGFR – Epidermal growth factor receptor

EGLN – Egg-laying defective gene nine

EloB/C – Elongin B–Elongin C

EPAS-1 – Endothelial PAS domain protein 1

EPO – Erythropoietin gene

ER – Endoplasmic reticulum

FBS – Fetal bovine serum

FDR – False discovery rate

FIH – Factor inhibiting HIF

FP – Fluorescent polarisation

FT – Flow-through

G1 – Gap phase 1

G2 – Gap phase 2

GFP – Green-fluorescent protein

GLUT1 – Glucose transporter 1

GSK3β – Glycogen synthase kinase 3β

HECT – Homologous to E6AP C-terminus

HFF – Human foreskin fibroblast

HIF – Hypoxia inducible factor

HK2 – Hexokinase 2

HRE – Hypoxia response element

Hpx - Hypoxia

HSP70 – Heat shock protein 70

HSP90 – Heat shock protein 90

IBD – Inflammatory bowel disease

IgG – Immunoglobulin G

iNOS – Inducible-nitric oxide syntase

IPAS – Inhibitory PAS domain

IRE1 – Inositol-requiring enzyme 1

IKKβ – Inhibition of κB kinase β

ITC – Isothermal titration calorimetry

K_d – Dissociation constant

LZIP – Leucine zipper domain

M Phase – Mitosis

MAPK – Mitogen-activated protein kinase

MCT4 – Monocarboxylate transporter 4

MS – Mass spectrometry

mTOR – Mammalian mechanistic target of rapamycin

NAE – NEDD8-activating E1 enzyme

NHE1 – Sodium-hydrogen exchanger 1

NF-κB – Nuclear factor κ-light-chain-enhancer of activated B cells

NODDD – N-terminal oxygen dependent degradation domain

NOG – *N*-oxalylglycine

NTAD – N-terminal transactivation domain

O_2 – Molecular oxygen

ODD – Oxygen degradation domain

OTUB7B – Ovarian tumour protease DUB

PAS – Per/Arnt/Sim domain

PCC - phaeochromocytoma

PDK1 – pyruvate dehydrogenase kinase

PER2 – Period circadian clock 2

PERK – PKR-like ER kinase

PHD – Prolyl hydroxylase domain

PI3K – Phosphoinositide-3-kinase

PCK – Protein kinase C

PKR – Protein kinase R

PPI – Protein–protein interaction

PROTAC – Proteolysis targeting chimera

pO_2 – Partial pressure of oxygen

RACK1 – Receptor for activated protein kinase C

RBR – RING-in-between-RING

RCC4 – Renal cell carcinoma 4

RGC32 – Response gene to complement 32, also known as RGCC

RGCC – Regulator of cell cycle, also known as RGC32

RING – Really interesting new gene

S Phase – Synthesis phase

SGC – Structural genomics consortium

Spry2 – Sprouty

SRS – Substrate recognition subunit

STUB1 – STIP1 homology and U-box containing protein 1

TCA – Tricarboxylic cycle

TCP1 – T-complex protein 1

TMT – Tandem mass tag

TriC – TCP1 ring complex

TSC1/2 – Tuberous sclerosis protein 1 and 2

TXNIP – Thioredoxin interacting protein, also known as VDUP1

UPR – Unfolded protein response

UPS – Ubiquitin–proteasome system

VDUP1 – Vitamin D upregulated protein

VEGF – Vascular endothelial cell growth factor

VBC – VHL:Elongin B:Elongin C

VHL – von Hippel–Lindau

1. Introduction

1.1. Hypoxia

Oxygen is required for the survival of metazoan organisms. It is an essential molecule for many cellular processes, primarily the oxidative–phosphorylation system, which utilises oxygen to generate cellular adenosine triphosphate (ATP), energy for the cell, in mitochondria (1). Therefore, a tight control on oxygen homeostasis is important to maintain proper cellular functions. Importantly, the demands of oxygen level in an organism differ depending on the tissue. The normal physiological level of oxygen, termed normoxia, is therefore specific to each tissue (2). While the atmospheric oxygen concentration at sea level is 20.95% (760 mmHg), the micro-environmental oxygen level in adult human tissues varies between 7-100 mmHg (Figure 1.1). When oxygen levels drop below the physiological level in tissues, it is termed as hypoxia; whereas the opposite case makes the tissue hyperoxic.

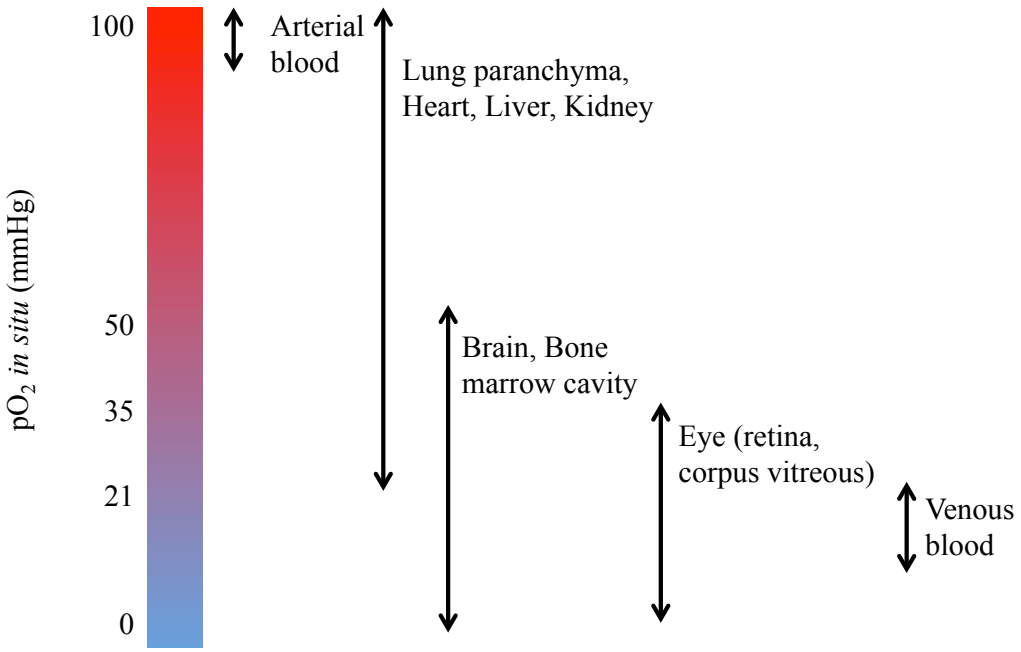

Figure 1.1 – Oxygen partial pressure (pO_2) found in various human tissues *in situ*. Figure was adapted from (2).

Hypoxia occurs when oxygen demand exceeds supply. Hypoxia has been shown to contribute to many physiological and pathological processes. Hypoxia is involved in physiological adaptation to high altitude (3,4), embryonic development (5), and angiogenesis (6,7). For instance in embryonic development, hypoxia triggers angiogenesis via vascular endothelial cell growth factor (VEGF) that is induced in hypoxia. The stimulation of angiogenesis subsequently affects the development of the labyrinth layer of placenta, vascularisation of heart and formation of bone of the embryo (5).

Hypoxia also plays a role in several pathophysiological conditions, such as cancer (8,9), anaemia (10) and ischemia including both cerebral and myocardial (11). The association of hypoxia in some of these are further discussed in section 1.2. As oxygen homeostasis is important for survival, as well as being physiologically and pathologically relevant, organisms have developed mechanisms to tightly regulate oxygen levels in cells. A major regulator of oxygen sensing and response is the family of transcription factors called hypoxia-inducible factors (HIFs). HIFs are activated in response to hypoxia to initiate a transcriptional program, and ultimately restore oxygen homeostasis and promote cell survival. This is achieved as cells switch off energy demanding processes in hypoxia such as cell proliferation, DMSO replication and translation (12-14), and trigger metabolic switch to glycosis (15). Besides HIF, there are also other hypoxia responsive transcription factors, including NF-κB, Myc, p53 and AP-1 [reviewed in (16)].

1.1.1. Hypoxia-inducible factor (HIF)

The response to hypoxia is transcriptionally regulated at the molecular level largely, but not exclusively, by HIFs. HIF was first identified in 1995, in work trying to identify the transcription regulator of the erythropoietin (EPO) gene (17). In this work, an 8-bp

DNA sequence in the enhancer of EPO gene was found to interact with HIF-1 through biochemical assays. The study led to the identification of HIF-1 and a consensus motif termed the hypoxia response element (HRE, '5 – RCGTG – 3') that interacts with HIF-1. The transcription factor was found be composed of two different subunits: an oxygen-labile α-subunit and a constitutively stable β-subunit (17,18).

1.1.1.1. HIF-α

The transcription factor HIF family has since been found to be composed of three HIF-α subunits: HIF-1α, HIF-2α (also known as endothelial PAS (Per/Arnt/Sim) domain protein-1 [EPAS-1]) (19), and HIF-3α (20); encoded by three different genes. Amongst the three-α subunits, HIF-1α is the most studied and characterised. HIF-1α is ubiquitously expressed in nearly all cell types, while HIF-2α is detected only in specific tissues, including endothelium, lung, kidney, liver, heart, and brain (21). In contrast to the restricted pattern *in vivo*, almost all transformed cell lines express HIF-2α (22). In recent years, there has been increasing interest in studying HIF-2α due to the association of elevated HIF-2α levels and poor patient survival in multiple tumours (23,24). HIF-1α and HIF-2α are the most structurally similar and contribute to the majority of HIF transcriptional responses to hypoxia. The two HIFs each transcriptionally regulate both a unique and an overlapping set of target genes. HIF-1 transcriptional activity begins early in response to hypoxia, whereas HIF-2 governs the adaptation in prolonged hypoxia (25-27). Although HIF-1 and HIF-2 are both known to attribute to poor prognosis of many cancers, only one of the HIF-α seem to be driving the progression in some tumours. For instance, HIF-2α acts as a tumour suppressor in the lung tumour, whereas HIF-1α is important for supressing tumour progression in the renal cancer [reviewed in (24)]. The opposing roles of HIF-1 and HIF-1 in cancers will be further discussed in section 1.2.1. Importantly, the two α-subunits play a role in embryonic

development as the knockout of either subunit in mice is embryonic lethal, albeit at different stages [reviewed in (28)].

HIF-3α is still very poorly understood. The protein expression of HIF-3α is restricted to a subset of tissues [reviewed in (29)]. HIF-3α was initially identified as a dominant negative regulator of HIF-1α and HIF-2α through one of its splice variant, termed as inhibitory PAS domain protein (IPAS). IPAS binds to the PAS domain of HIF-1α and HIF-2α, and prevents their dimerisation with HIF-1β, and thus the interaction with HRE of target genes. This negative regulator was later found to be the product of alternative splicing (30), and since, at least six splice variants of HIF-3α have been identified with different functions and response to hypoxia, as well as transcriptional activity [reviewed in (31,32)]. Recent studies showed that HIF-3α also functions as transcriptional activator in the zebra fish – it binds to HREs of target genes to induce their expression, indicating that HIF-3α is more than a HIF negative regulator (33). However, the association between HIF-3α expression and patient prognosis has not been established, or conclusively characterised in mammalian systems.

Structurally, HIF-α proteins are characterised by the presence of an N-terminal transactivation domain (NTAD) and an oxygen-dependent degradation domain (ODD), which contains conserved proline residues important for mediating the sensitivity of these proteins to changes in oxygen levels (Figure 1.2). Additionally, HIF-1α and HIF-2α, which share a sequence identify of 48%, also contain another domain not found in HIF-3α, the C-terminal transactivation domain (CTAD). CTAD is required for HIF transcriptional activity through the interaction with the co-activators CREB-binding protein/p300 [CBP/p300] (34).

The α- and β-subunits of HIF belong to the bHLH/PAS (basic helix–loop–helix/PAS) family of transcription factors, sharing highly similar domain regions in the N-terminus

(Figure 1.2). Each subunit is characterised by the presence of bHLH and PAS domain, required for DNA binding, and heterodimerisation between the α- and β-subunits, respectively, and several crystal structures of these domain regions of HIF-1α/HIF-1β and HIF-2α/HIF-1β heterodimers have been solved (35).

1.1.1.1. HIF-1β

HIF-1β is also known as aryl hydrocarbon receptor nuclear translocator (ARNT). Unlike the α-subunits, HIF-1β does not have an ODD domain, rendering it unaffected by changes in oxygen, such as hypoxia (Figure 1.2). In addition, its gene and protein expressions are constitutively active in normoxia (36). In hypoxia, HIF-1β can protect the hypoxia-induced HIF-1α from being degraded by the proteasome and is required for HIF transcriptional activity. Through the bHLH/PAS domains present in both proteins,

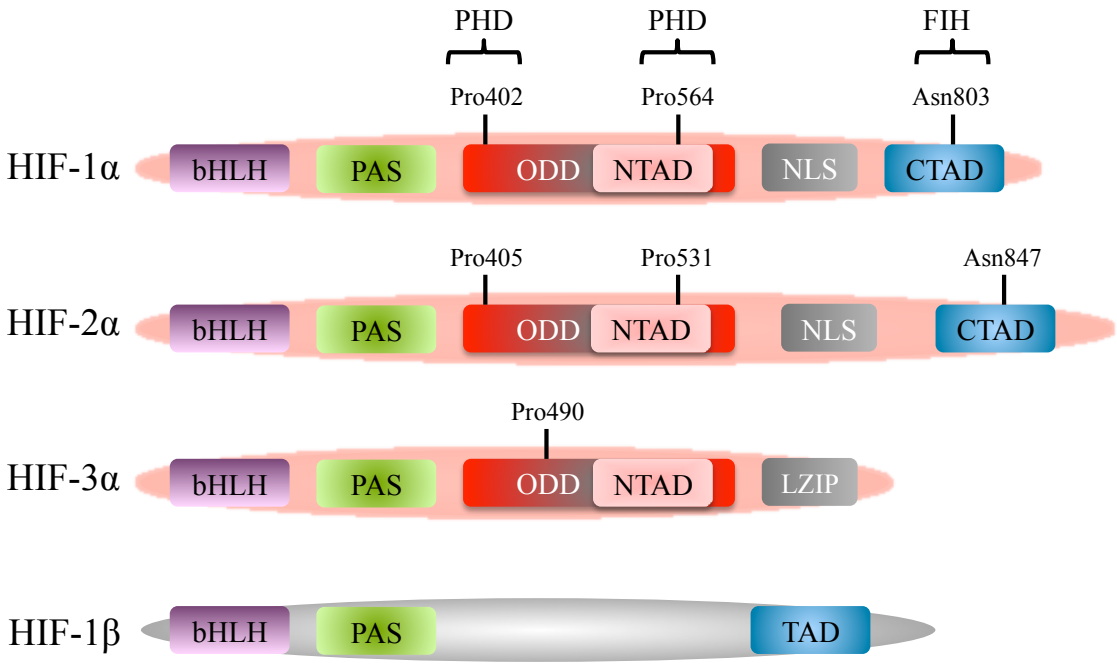

Figure 1.2 – HIF subunits domain structure: bHLH – basic helix–loop–helix domain; PAS – Per/ARNT/Sim domain; ODD – oxygen-dependent degradation domain; NTAD – N-terminal transactivation domain; CTAD – C-terminal transactivation domain; TAD – terminal transactivation domain; NLS – nuclear localisation signal; LZIP – leucine zipper domain. Hydroxylation sites by PHDs and FIH for HIF-1α and HIF-2α are noted. Adapted from (16).

HIF-1β interacts with HIF-α to form a transcriptionally active HIF dimer to regulate responses to hypoxia. HIF-1β also forms heterodimer with aryl hydrocarbon receptor (AhR) through the PAS domain of each protein (37), and binds to the dioxin response element (DRE), required for the activation of drug-metabolising enzymes (38).

Importantly, similar to the α-subunits, HIF-1β is essential for embryonic development. The knockout of HIF-1β in mice has been shown to develop abnormal vascular and is embryonically lethal [reviewed in (28)].

1.1.2. Canonical regulation of HIF in hypoxia

Unlike the constitutively expressed HIF-1β that is not affected by oxygen changes, HIF-α proteins are extremely labile. In the presence of normal oxygen level, HIF-α is rapidly degraded by the proteasome with a short half-life of 5 min (39). The ODD domain of HIF-α is subjected to hydroxylation by a family of dioxygenase enzymes called prolyl hydroxylases (PHDs). PHDs use 2-oxoglutarate (2OG), Fe^{2+}, ascorbate, and molecular oxygen as co-factors to hydroxylate two proline residues within the HIF-α ODD domains (40,41). The hydroxylated prolines create a recognition site with 1000-fold increased affinity, over the parent protein containing unmodified proline, for the E3 ubiquitin ligase, von–Hippel Lindau (VHL) tumour suppressor (42), which polyubiquitinates HIF-α, rapidly targeting it for degradation by the proteasome (Figure 1.3) (43). at the protein levels. The accumulated HIF-α dimerises with HIF-1β and binds to the consensus motif HREs of HIF-target genes in the nucleus to activate the transcription of genes in order to adapt to the hypoxic stress (Figure 1.3) (44). In hypoxia, due to the insufficient oxygen molecules, PHDs are unable to efficiently hydroxylate HIF-α. As a result, HIF-α evades degradation by the proteasome and is stabilised.

In addition to the regulation by the PHDs, another 2-oxoglutarate-dependent oxygenase, factor inhibiting HIF (FIH), is involved in regulating HIF-α (45). FIH is part of another hydroxylase family different to PHDs, the Jumonji-C family, and was the first of the family shown to have the 2OG oxygenase activity (46). In normoxia, FIH utilises Fe^{2+} to bind molecular oxygen, as well as 2OG as co-factors to hydroxylate a conserved asparagine residue (Asn803 of HIF-1α) within the CTAD, preventing the recruitment of transcriptional co-activators CBP/p300 (47). FIH is less sensitive to oxygen changes compared to PHDs; hydroxylation activity of FIH occurs in the presence of much lower oxygen levels than the required for PHDs, and becomes inactive in extreme hypoxia (48). The differential response of the two hydroxylases provides an additional HIF control in response to hypoxia.

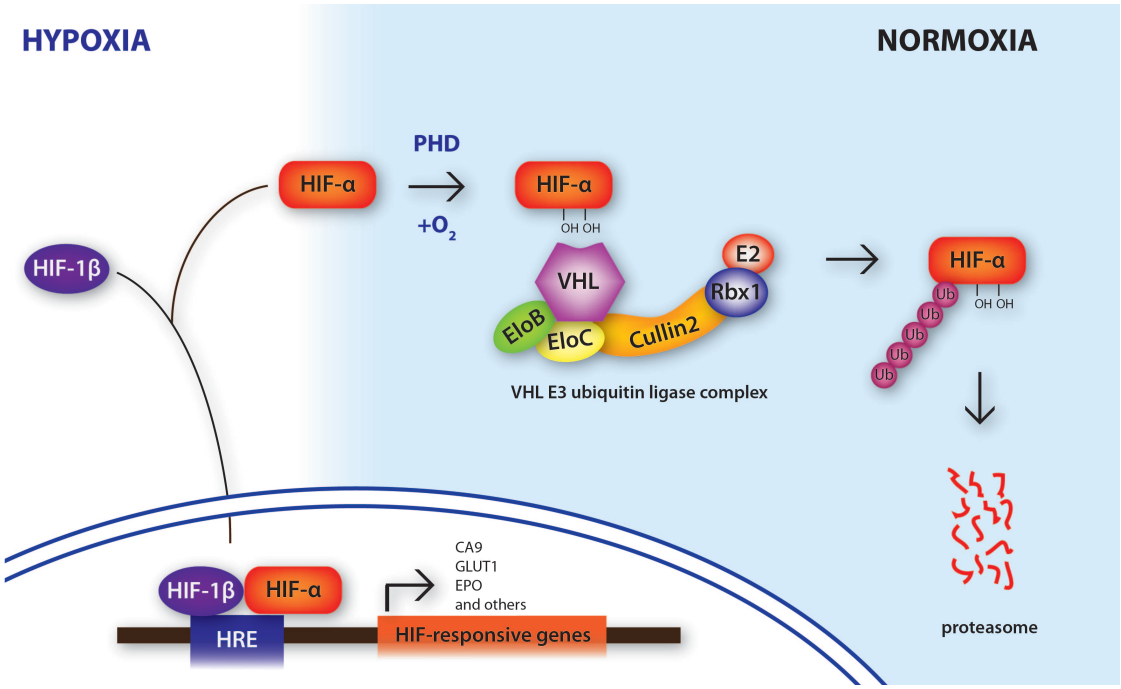

Figure 1.3 – Canonical HIF regulation pathway. In normoxia, PHDs use oxygen molecules to hydroxylate two proline residues within the HIF-1α subunit. Hydroxylated prolines allow the binding of VHL and ubiquitination by the E3 ubiquitin ligase, targeting HIF-1α/ HIF-2α for proteasomal degradation. As the oxygen level decreases to hypoxia, PHDs are gradually inhibited and this leads to the accumulation of HIF-1α, which dimerises with HIF-1β. HIF dimer interacts with endogenous HREs to drive the transcription of HIF-target genes including *CA9*, *GLUT1* and *EPO*.

1.1.3. Prolyl hydroxylase (PHD) enzymes

HIF prolyl hydroxylase (PHD) enzymes are 2OG-dependent dioxygenases that hydroxylate HIF-1α at two proline residues (Pro402 and Pro564) within the ODD domain (49,50). The two proline residues are found in consensus sequence LXXLAP, where P is the proline subjected to hydroxylation (51). While HIF-1α and HIF-2α have the LXXLAP motif, there are other PHD substrates found without this motif (discussed further in section 1.1.3.2). This suggests that substrate recognition for PHD hydroxylation is more than the consensus motif.

1.1.3.1. PHD isoforms

There are three known PHD isoforms: PHD1, PHD2, and PHD3; or EGLN 2, EGLN1, and EGLN3, respectively (51). All three isoforms display high sequence homology in the C-terminal catalytic domain, but not the N-terminus. A fourth isoform has been identified, but not well-characterised (52). Amongst the isoforms, PHD2 is the most studied and characterised, and is thought to be the most important oxygen sensor (47).

The three PHDs regulate HIF-1α and HIF-2α in a non-redundant manner (53). PHD1 shows a preference for HIF-2α over HIF-1α in normoxia, while PHD2 shows the opposite specificity; but both PHDs hydroxylate the two prolines of HIF-α. On the other hand, PHD3 hydroxylates exclusively Pro564, and acts equally on HIF-1α and HIF-2α under normoxia, but preferentially HIF-2α in hypoxia (53). In addition, the subcellular and tissue localisations for the three PHDs are different (Table 1.1). PHD2 is the most abundant of the three isoforms and expressed in all tissue types, while PHD1 and PHD3 expressions are more restricted (54,55). PHD2 and PHD3 are also induced in response to hypoxia. PHD2 is specifically induced by HIF-1α, whereas PHD3 is a target of both HIF-1α and HIF-2α (56).

Table 1.1 – PHD isoforms. Preferred target, cellular and tissue localisation, as well as phenotypes of knockout mice of PHDs are summarised.

PHD isoforms	**Preferred target in normoxia** (53)	**Subcellular localisation** (54,55)	**Tissue expression** (56)	**Phenotypes of knockout mice**
PHD1	HIF-2α over HIF-1α	Nucleus	Mainly in testes, also in heart, brain, liver and kidney	Viable offspring (57), tolerance to ischaemia, but not to exercise (58)
PHD2	HIF-1α over HIF-2α	Cytoplasm	All tissues, abundant in heart	Embryonic lethal due to cardiac and placental defects (57). Conditional knockout is viable with increased angiogenesis (59), and polycythaemia (60,61).
PHD3	HIF-1α and HIF-2α, but HIF-2α in hypoxia	Nucleus and cytoplasm	Abundant in heart	Viable (57), with reduced resting blood pressure and distinct CNS changes in innervation (57) (62)

Given the differential localisation patterns and activities towards HIF-α, the PHD isoforms may have distinct functions. Unlike HIF knockouts, PHD knockout mice are not as lethal, except for PHD2 knockout, which are embryonically lethal due to developmental defects (57). However, conditional knockout mice of PHD2 are viable, but show increase in angiogenesis (59) and are polycythaemic (60,61). Although the knockouts of PHD1 and PHD3 produce viable offspring, they display cardiovascular defects (61).

1.1.3.2. PHD-targets

Beyond HIF-1α and HIF-2α, PHDs have been shown to have other substrates, including inhibition of κB kinase β (IKKβ), Cep192, RNA polymerase II subunit Rpb1, and the β-adrenergic receptor II (63-66). These proteins also contain the motif LXXLAP recognised for proline hydroxylation and are hydroxylated by a specific PHD isoform.

The IKKβ plays a role in the activation of the nuclear factor kappa-light-chain-enhancer of activated B cells (NF-κB), a transcription factor that is constitutively active in some cancer and associated with inflammatory and innate immune responses (67). Under hypoxia, IKKβ has been shown to be inhibited by PHD1 and PHD3 (68), presumably mediated by their prolyl hydroxylase activities within the evolutionarily conserved LXXLAP motif on IKKβ, leading to reduced NF-κB activity (68,69). However, another study has found that PHD3 inactivates the phosphorylation activity of IKKβ in a hydroxylation-independent manner by preventing the interaction between IKKβ and the heat shock protein 90 (HSP90) (70). The centrosomal component Cep192, essential for cell-cycle regulation, is hydroxylated specifically by PHD1 on proline residue within the LXXLAP motif. Hydroxylation lead to Cep192 degradation as the hydroxylated protein is polyubiquitinated by Skp2 E3 ubiquitin ligase, resulting in proteasomal degradation (63). The RNA polymerase II subunit Rpb1 and the β-adrenergic receptor II also contain the same hydroxylation motif and hydroxylated by PHD1 under oxidative stress (65,71), and PHD3 (66), respectively, for degradation in a VHL- and subsequent proteasome-dependent manner (65,71).

Interestingly, PHDs have recently been found to also hydroxylate another motif that is not consensus LXXLAP, called the 'FOXO3a-like' motif. An *in vitro* hydroxylation screening assay identified FOXO3a protein as a substrate of PHD1, but FOXO3a does not have the LXXLAP consensus motif. PHD1 hydroxylates two proline residues within 'GPSS' and 'GSPT' sequences on FOXO3a, and this triggers the degradation of the protein by the proteasome (72), and may be in a manner independent of VHL (73). Another protein with similar motif to the FOXO3a prolyl hydroxylation motif is Akt, a serine/threonine kinase that promotes growth and survival of various cancers (74). Akt is frequently activated in *VHL*-defective ccRCC patients (75) and this is later on found to be due to direct regulation by VHL (74). Phosphorylated Akt is hydroylated by

PHD2 on two proline residues within ‘GSPS’ and ‘GTPE’ motifs, and subsequently recognised by VHL, which inhibits Akt activity and promotes tumorigenesis and cell survival (74).

1.1.4. Other HIF regulators

In addition to the canonical regulation of HIF through the proteasomal degradation system mediated by hydroxylation and polyubiquitination, HIF is also controlled via other mechanisms, and can be induced by other stimuli including growth factors, viral proteins, cytokines, hormones and inflammation.

Several chaperone proteins have been shown to regulate HIF-1α stability. The heat shock protein 90 (HSP90) is a molecular chaperone that binds to HIF-1α. This interaction prevents HIF-1α from misfolding and subsequent degradation as it protects HIF-1α from the receptor for activated protein kinase C (RACK1)/Elongin-C-mediated degradation (76). HSP70 also regulates HIF-1α degradation not by the proteasome, but by the lysosome via the chaperone-mediated autophagy (CMA). HSP70 interacts with the E3 ubiquitin ligase STUB1 (STIP1 homology and U-Box containing protein 1) and promotes STUB1 to catalyse K63 polyubiquitination of HIF-1α and subsequent degradation by the lysosomal machinary (77). Besides RACK1 and STUB1, other E3 ligases that regulate HIF-1α are MDM2, HAF, and TRAF6 (77). Interestingly, the deubiquitinase (DUB) enzymes that catalyse the removal of ubiquitin linkages have also been shown to regulate HIF-1α. One example is the ovarian tumour protease (OTU) DUB (OTUD7B [also known as Cezanne]) that has been shown to modulate the expression of both HIF-1α (78) and HIF-2α (79), in a proteasome-independent manner.

HIF is also regulated at the translational levels by the phosphoinositide-3-kinase/mammalian mechanistic target of rapamycin (PI3K/mTOR) and ERK mitogen-activated protein kinase (MAPK) pathways, which increase HIF-1α translation and

subsequent protein levels (80). Although HIF is the master regulator of the hypoxia signalling, other transcription factors have been shown to play a role in concert with HIF in cellular response to hypoxia. Examples are NF-κB, Myc, p53 and AP-1 [reviewed in (16)]. Furthermore, chromatin remodellers including SWI/SNF and ISWI complex also affect HIF-1α mRNA levels, as well as acting as transcriptional co-activators of in the HIF pathway (81). The multiple mechanisms and regulators highlight the importance of controlling HIF-α.

1.1.5. HIF-target genes

In response to the hypoxic stress, HIF activates a large number of genes required for many cellular processes including metabolism, angiogenesis, autophagy, apoptosis, and cell differentiation, with the ultimate aim to restore oxygen homeostasis. These pathways promote tumour growth and progression, and therefore HIFs are considered as attractive targets for therapeutic approach for cancer (73). To date, more than 100 HIF-target genes have been identified (Figure 1.4) (82), and there are estimates that HIFs could regulate up to 2% of human genes (83). These genes then mediate the response to hypoxia. The roles of some of these genes are further discussed in section 1.2.1. In addition to direct upregulation of genes by HIF, HIF can also repress gene expression indirectly through its interaction with other transcription factors, such as Myc and p53 [reviewed in (16)].

A computational study that integrates gene expression profiles from several cell lines and computational binding-site analyses identified hundreds of potential HIF-targets and interestingly, 70% of genes altered in hypoxia do not contain the canonical HRE motif (5'- [A/G]CGTG -3') in their proximal promoters, important for transcriptional activation by HIF (84). A narrower and highly reliable list of 217 genes was generated by a study that combines transcription profiling meta-analysis and chromatin-

immunoprecipitation (ChIP) analysis (85). Through this study, the authors compiled a list of 100 known and validated HIF-1 target genes (Appendix Table 9.4).

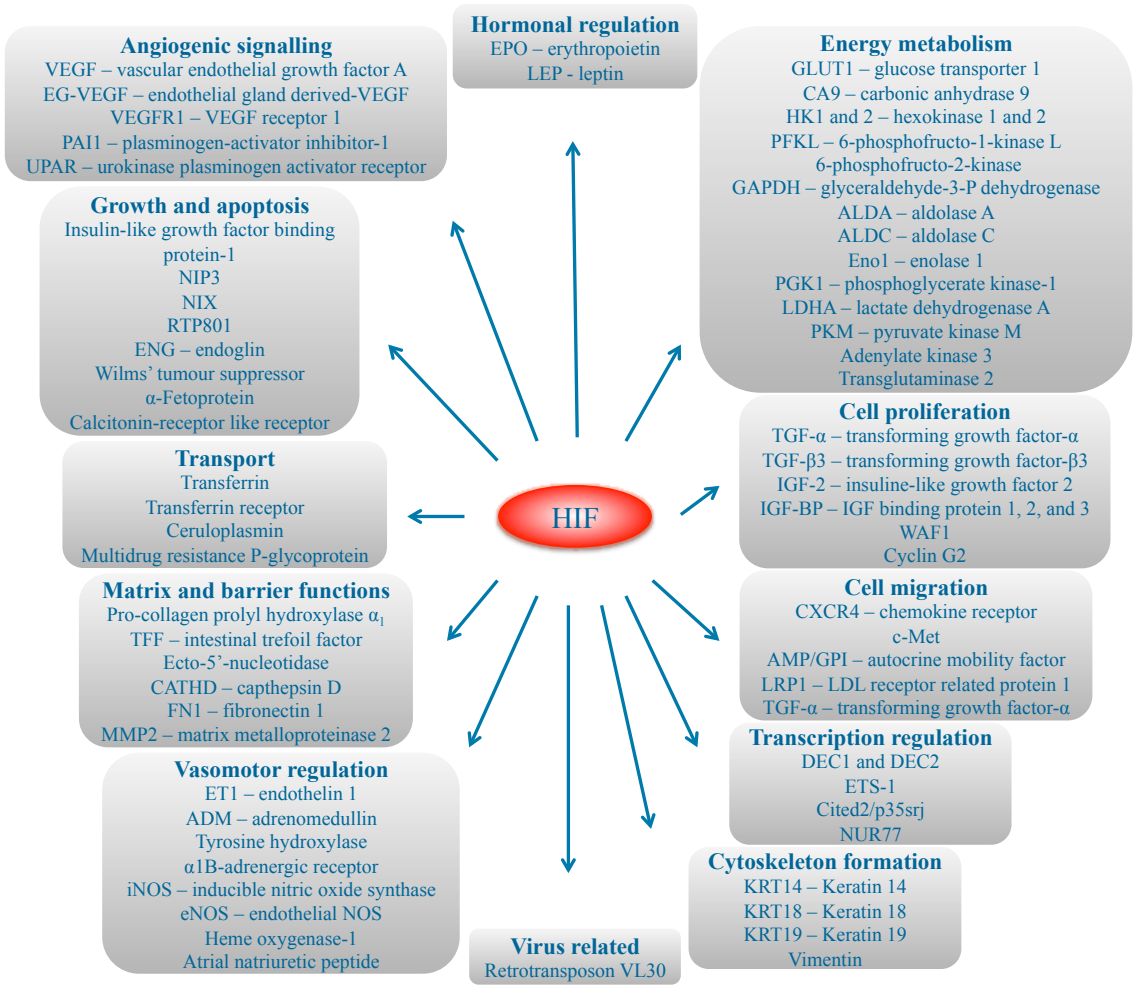

Figure 1.4 – HIF-target genes. HIF upregulates many genes involved in many biological processes. Figure is adapted from (82).

1.1.6. HIF-independent hypoxia responses

In addition to the transcriptional programme induced by HIF, cells also utilise other signalling pathways independent of HIF to mediate cellular responses to hypoxia. Examples of these HIF-independent oxygen-sensitive pathways are the mTOR and unfolded protein response (UPR).

The mTOR pathway is important for the activation of several biological processes, including metabolism, ribosomal biogenesis, mRNA translation, apoptosis and autophagy (86). Under hypoxia, particularly prolonged (chronic) hypoxia or in combination with other stresses, the mTOR signalling is inhibited in order for cell to adapt and survive the stressful condition (16). The downstream signalling of mTOR is inhibited through multiple pathways mediated by the activation of the tuberous sclerosis protein 1 and 2 (TSC1/2) complex (86). The complex can be activated via the hypoxia-inducible AMP-activated protein kinase (AMPK) or REDD1. Under hypoxia, AMPK phosphorylates the TSC1/2 complex to inhibit mTOR activity (13), whereas the induction of REDD1 releases TSC2 from a complex to allow the re-activation of TSC1/2 (87). The inhibition of mTOR activity also leads to reduced phosphorylation of S6K, S6 ribosomal protein and 4E-BP1 important for mRNA translation, inhibiting translation initiation (13).

The UPR is a pathway that activates transcriptional and translational changes in response to endoplasmic reticulum (ER) stress (86). The ER is a cellular organelle important for the maturation of membrane or secreted proteins. Under severe hypoxia, ER stress occurs, and this leads to the accumulation of unfolded or misfolded proteins, which act as sensors to rapidly activate the UPR. The activation of UPR is essential for regulating several downstream processes, including cell metabolism and cell death, protein maturation and degradation, and protein production that collectively promote hypoxia tolerance and cell survival (88). The UPR activation in hypoxia is mediated by PKR-like ER kinase (PERK) that inhibits overall mRNA translation, presumably to relieve ER function and promote overall survival (89). Besides PERK, there are two additional ER stress sensors: activating transcription factor 6 (ATF6) and inositol-requiring enzyme 1 (IRE1) that mediate the UPR; however their regulation in hypoxia is not yet well-characterised (88).

1.2. HIF and disease

The HIF transcription factor is involved in many pathological diseases including cancer, myocardial ischaemia, chronic anaemia, and gastrointestinal diseases. Although HIF activation in cancers can promote cancer progression, it is also therapeutically beneficial for the other diseases, and also aids in medical treatments including wound healing and organ transplantation.

1.2.1. Cancer

The HIF pathway regulates many biological processes including metabolism, angiogenesis and cell proliferation required for the survival of fast-proliferating tumoural cells. Therefore it is not a surprise that HIFs are induced in many tumour types (90). Owing to the rapid cell proliferation in tumour, oxygen supply is quickly exhausted from poor vascularisation, and this results in intra-tumour hypoxic regions (91). Hypoxic environment, and in turn, HIF activation, have been associated with increased metastasis and patient mortality in many human cancers. Furthermore, increased HIF-1α and/or HIF-2α levels have been observed in brain, head/neck, breast, lung, colon, gastric, kidney, pancreas, stomach, skin, endometrium, bladder, rectum, cervix, ovarian, and prostrate cancers (92).

HIF regulates processes in response to hypoxia via its target genes. For instance, HIF promotes angiogenesis, a process that renews blood vessels, required for the poorly-vascularised intra-tumour via the regulation of many pro-angiogenic genes including *vascular endothelial cell growth factor* (*VEGF*) and *inducible-nitric oxide synthase* (*iNOS*) (93). HIF also reduces oxygen demand by promoting glycolysis through upregulation of glucose uptake via glucose transporter 1 (GLUT1), increasing glycolytic enzymes such as aldolase A and phosphoglycerate kinase, and induction of pyruvate dehydrogenase kinase (PDK1) to inhibit mitochondrial respiration [reviewed in (7)].

Furthermore, HIF upregulates proteins involved in cellular pH regulation; as such the carbonic anhydrase 9 (CA9) that reversibly hydrates carbon dioxide to form bicarbonate and hydrogen ions (94); sodium-hydrogen exchanger 1 (NHE1) that pumps hydrogen ions into extracellular space (95); as well as, monocarboxylate transporter 4 (MCT4) that pumps lactate out of tumour cells (96). Collectively, these proteins promote an alkaline intracellular environment required for cell proliferation and acidic extracellular environment for invasion (90).

Hypoxic tumour activates both HIF-1α and HIF-2α, and both have been associated with poor clinical outcomes in patients with cancers. Interestingly, the functions of HIF-1α and HIF-2α can vary depending on the cancer types. In some cancers, HIF-1α promotes cancer progression, while HIF-2α acts as tumour suppressor, and the opposite is also found in other cancers. For instance, HIF-2α has been shown to contribute to disease progression and mortality in the renal clear cell carcinoma, whereas HIF-1α is suppressed due to gene deletion and the absence of HIF-1α is associated with worse patient prognosis (97,98). On the other hand, the two HIF-α act oppositely in colon cancers, where HIF-1α is overexpressed, while HIF-2α is silenced (99). The loss of HIF-2α expression was strongly correlated with advanced cancer stage, but not HIF-1α (99). Thus, the effect of HIF-α activation is dependent on the tumour type. Importantly, selective stabilisation or inhibition of either isoforms may be therapeutically beneficial for cancer treatments.

1.2.2. Anaemia-associated chronic kidney diseases

Patients with chronic kidney disease (CKD) often suffer from anaemia, a condition of red blood cell deficiency as their kidneys fail to produce adequate erythropoietin (EPO), and hepatic EPO production cannot compensate. EPO is a hormone required for the production of red blood cells in the bone marrow (100). Anaemia associated with CKD

is often linked to increased morbidity and mortality (101). Recombinant human EPO has been used to treat anaemia associated with kidney failure since 1989 (102). Since then, many other EPO analogues have been made and used for correcting anaemia. However, these treatments have shown several issues including high cost, resistance and side-effects (103), such as increased risk of cardiovascular events and blood pressure as the intermittent treatment may result in excessive EPO levels (104).

In recent years, HIF stabilisers have been explored as new strategy for treating anaemia. HIF-1α is known to transcriptionally activate *EPO* (17), thus stimulating EPO production. Examples of HIF stabilisers for this therapeutic approach are PHD inhibitors. Five PHD inhibitors are currently in clinical trials for anaemia associated with CKD, with FG-4592 (Roxadustat) as the most advanced in phase III (105); these PHD inhibitors will be discussed in 1.4.2.5.

1.2.3. Myocardial ischaemia-reperfusion injury

Myocardial ischaemia-reperfusion injury is a condition with initial restriction of blood supply to the heart muscle (myocardium), causing tissue hypoxia, followed by the restoration of blood flow (perfusion) and concomitant re-oxygenation that associate with reperfusion injury (tissue injury and profound inflammatory response) (106). Several studies have shown that ischaemic preconditioning (pre-exposure to short, non-lethal episodes of ischaemia) reduces myocardial tissue injury during subsequent ischaemia-reperfusion injury, in which HIFs play a functional role. Studies have shown that HIF-1α was stabilised in preconditioning of the myocardium in mice, and the knockdown of HIF-1α by siRNA abolished this cardioprotection effect. Similarly, cardioprotection was also achieved with HIF activator DMOG (107). In addition, the role of HIF-1α in myocardial ischaemia was found to be dependent on its interaction with the circadian rhythm protein period 2 (PER2), and this interaction promotes

anaerobic glycolysis, important for preconditioning to myocardial ischaemic tissue (108).

1.2.4. Inflammatory bowel disease

Inflamed tissues are often hypoxic owing to increased metabolism required by the inflamed resident cells and infiltrating immune cells. These processes decrease blood flow within the tissue (109). An example of inflammatory diseases associated with hypoxia is the inflammatory bowel diseases (IBDs). IBD is an inflammatory disorder due to deregulated mucosal immune system, and is divided into two types according to their distribution patterns: ulcerative colitis that is limited to the colon, and Crohn's colitis that affects any part of the gastrointestinal tract (110). The hypoxic environment and pro-inflammatory molecules enhanced in the inflamed tissues can induce HIF stabilisation (103). Activation of HIF-1α and HIF-2α has been observed in IBDs, and shown to protect against the intestinal inflammation in several ways. The stabilised HIFs can promote tissue reparation by inducing and inhibiting apoptosis in neutrophils and epithelial cells, respectively (109,110). In addition, HIF-1α also enhances the production of anti-inflammatory molecules including adenosin and netrin-1, to protect the intestinal mucosa (111).

Due to the protective role of HIF in IBD, pharmacologic activation of HIF has been an attractive therapeutic approach. Several studies have shown that HIF stabilisation induced by PHD inhibitors greatly improves intestinal inflammation in mice (112,113). The PHD inhibitor dimethyloxalylglycine (DMOG) displayed protective adaptation in an *in vivo* model of chemically induced murine colitis (112,114). Other PHD inhibitors, FG-4497 and also AKB-4924, also showed the same protective effect in murine colitis (113,115).

1.2.5. Wound healing

During wound healing, the metabolism of tissue is significantly shifted to the site of vascular damage, and tissue oxygen demand increases, resulting in hypoxia (106). HIF is stabilised during re-epithelialisation at the site of wounds and promotes mucosal barrier. HIF stimulates angiogenesis (the budding of new blood vessels from pre-existing vessels) and vasculogenesis (the *de novo* formation of blood vessels from precursor cells) required for wound healing through its targets including VEGF and iNOS (116). Furthermore, HIF also mediates the recruitment of bone marrow-derived angiogenic cells (BMDACs) to the wound. BMDACs are involved in angiogenesis or vasculogenesis, thus play an important role in wound healing (92). HIF-1 activation, by the use of PHD inhibitors has also been shown to improve impaired wound healing in diabetic mice (117-120). Therefore, therapeutic approach to stabilise HIFs would be beneficial for the treatment of conditions with defective wound healing.

1.2.6. Organ transplantation

Many solid organ transplantations display chronic rejection, resulting in graft failure and are associated with high rates of mortality and morbidity (106). Ischaemia-reperfusion injury has been shown to contribute to chronic rejection and early graft failure in liver transplantation (121), as well as the recurrence of hepatitis after transplantation in patients with the liver failure of hepatitis C (122). Owing to the role of HIF in ischemia-reperfusion injury, HIF activator may prevent early graft failure during solid organ transplantation (106). Studies have also suggested that HIF activators may be used to improve the outcomes of β-cell transplantation in diabetic patients with dysregulated β-cell function (123).

1.3. Von Hippel–Lindau (VHL)

The von Hippel–Lindau (VHL) E3 ubiquitin ligase is part of a multi-subunit Cullin RING ligase, acting as the substrate-recognition subunit of the complex. The VHL complex mediates polyubiquitination of HIF-α, important for targeting HIF-α for proteasomal degradation (43).

1.3.1. The ubiquitin–proteasome system (UPS)

The molecular machines responsible for catalysing almost all processes inside the cells including signalling, regulation, transport, movement, catalysis, membrane fusion and many more, are composed of proteins. Cellular proteins are continuously synthesised and degraded to maintain protein homeostasis (also known as proteostasis). Proteostasis is an important process, as deregulated proteins would lead to the destabilisation of entire networks and pose a danger to cells (124). For instance, many cancers occur primarily due to mutations in genes, which affect proteins and ultimately the molecular networks involved. Furthermore, as amino acids are limited recourses in the cells, and the energy required for amino acid synthesis is high, recycling them via degradation contributes to proteostasis maintenance (125).

Protein degradation in eukaryotic cells is mediated by two major protein degradation systems: the ubiquitin–proteasome system (UPS) and lysosomal proteolysis (124). While lysosomal pathway mainly degrades long-lived proteins, aggregated proteins, and cellular organelles, the UPS targets short-lived, regulated proteins, as well as abnormal, damaged or denatured proteins for degradation, degrading up to 80-90% cellular proteins (125).

The ubiquitin–proteasome system (UPS) is an essential biological pathway that regulates intracellular protein levels by polyubiquitination, and subsequent proteasomal

degradation of proteins (126). The UPS is involved in regulating many cellular processes including protein quantity control, cell cycle progression, transcription, DNA repair, apoptosis, stress response, and endocytosis (127), and therefore deregulation of the UPS is associated with many diseases (128). Proteins targeted for the UPS are tagged with a highly conserved 76-residue polypeptide, ubiquitin, an important post-translational modification that can guide a protein to the degradation machinery. This tagging process is catalysed in a stepwise mechanism primarily by three enzymes: E1 (ubiquitin-activating enzyme), E2 (ubiquitin-conjugating or carrier enzymes) and E3 (ubiquitin ligase). Briefly, E1 activates the C-terminus of ubiquitin by catalysing a thioester linkage to a Cys residue of E1 in an ATP-dependent manner. Activated ubiquitin is then transferred to a conserved active site Cys of E2 that prepares ubiquitin for conjugation. Lastly, E3 recognises a target protein substrate, and catalyse the transfer of ubiquitin from the loaded-E2 to substrate protein by forming an isopeptide bond between C-terminal of ubiquitin and a ε-amino group of a specific lysine of substrate, either directly or via an additional E3-ubiquitin thioester bond (126).

The human genome encodes two E1s, approximately 40 E2s, and more than 600 E3s ubiquitin ligases (129). As the E3 ligases confer substrate specificity to the UPS for degradation, it is not a surprise that there are so many E3s. The eukaryotic E3 ligases divided into three different types: homologous to E6AP C-terminus (HECT) E3s, really interesting new gene (RING) E3s, and RING-in-between-RING (RBR) E3s, that transfer ubiquitin to substrate via different mechanisms (130). Ubiquitin can be added on target substrates in the form of monoubiquitin/multi-monoubiquitin, and polyubiquitin chains. With seven lysine residues and the ε-amino group of ubiquitin, further ubiquitin molecules can be attached to form polyubiquitin chain that is linear, mixed or branched. The types and length of the ubiquitin chain greatly determine the biological outcome of the substrate, varying from proteasomal or lysosomal

degradation, to regulate protein function, interaction and localisation (131,132). Ubiquitination can also be reversed by a class of enzymes called deubiquitinases (DUBs), of which over 100 have been identified in the human genome .

1.3.2. Cullin RING E3 ubiquitin ligases

VHL is the substrate-recognition subunit (SRS) of a Cullin RING E3 ubiquitin ligase (CRL), a superfamily of RING E3s. CRL is the largest class of ubiquitin ligases, and is involved in regulating diverse cellular processes (133,134). Each CRL is characterised by: 1) a Cullin protein (Cullin1, 2, 3, 4a, 5 or 7), which is a scaffold protein that functions as a docking platform for assembling E3 ligase complex; 2) a small RING protein (examples are Rbx1, Roc1, and Hrt1) that recruits an ubiquitin-loaded E2 to promote the transfer of ubiquitin to substrate; 3) an adaptor protein that interchangeably binds the SRS to the Cullin complex (examples are Skp1, Elongin B:Elongin C [EloB/C] complex, damage-specific DNA-binding protein 1 [DDB1]); and finally, 4) a SRS that confers substrate specificity (133,135).

CRL is activated by a post-translational modification called neddylation, occurring on the Cullin protein. The neddylation process covalently attaches the ubiquitin-like protein NEDD8 onto a lysine residue in the Cullin C-terminus, leading to conformational changes on the Cullin and RING proteins, in order to promote ubiquitin transfer (136). Cullin can also be de-neddylated by COP9 signalosome (CSN) and de-neddylated CRL is sequestered by the interaction with Cullin-associated NEDD8-dissociated protein 1 (CAND1) that keep the CRL in an inactive state (137).

1.3.3. The VHL E3 ubiquitin ligase

1.3.3.1. The history of VHL – VHL disease

VHL is a known tumour suppressor. The gene encoding VHL was first identified in 1993, by positional cloning (138). However, long time before then, VHL has been

associated with VHL disease, an autosomal-dominant, hereditary disease caused by germline inactivating mutations in the *VHL* gene, which is associated with various types of cancers. In 1894, Treacher Collins first described familial retinal angiomatosis, now identified as a VHL-associated tumour, and in 1906, Eugen von Hippel also reported similar patients (139,140). Later in 1927, Arvid Lindau described patients with central nervous system haemangioblastomas, and recognised how it linked to the retinal angiomas reported by Collins and von Hippel. Thus, the name von Hippel–Lindau was derived and first used in 1936 (139,140).

Retinal angiomatosis and cerebellar haemangioblastomas are two of the most frequent tumours related to VHL disease, alongside with clear-cell renal cell carcinomas (ccRCCs), phaeochromocytomas (PCCs), endolymphatic sac tumours and pancreatic islet tumours. Visceral cysts in kidney, epididymis and pancreas are also common, but rarely affect the function of organ (141). Clinically, VHL disease is divided into type 1 characterised by the absence of PCCs, and type 2 with the presence of PCCs (142). Type 2 is further classified into three: type 2A (with PCCs, but not RCCs); type 2B (presence of PCCs and RCCs); and type 2C (only PCCs) (143). VHL disease and associated tumours occur in patients with biallelic inactivation of *VHL* (139). Despite being a familial disease, approximately 20% of VHL patients do not have a family history and *VHL* inactivation occurs due to *de novo* mutations (144).

1.3.3.2. The *VHL* gene and VHL isoforms

The *VHL* gene is located on chromosome 3p25 with three exons (138). *VHL* encodes two major VHL isoforms: a 213 amino acids isoform ($pVHL_{1-213}$), and a protein containing 160 amino acids ($pVHL_{54-213}$) (Table 1.2). These two isoforms are often referred as $pVHL_{19}$ and $pVHL_{30,}$ respectively, based on their apparent molecular masses upon protein electrophoresis. $pVHL_{19}$ arises from an internal translation initiation from Met54 within the open reading frame of VHL, and thereby missing the N-terminal

pentameric acidic repeat domain (145-147). $pVHL_{30}$ was first identified in 1995 and displayed tumour suppression activity, and thus was described as tumour suppressor (148). Further studies later on showed that both isoforms are functional tumour suppressors as the reintroduction of either protein suppressed tumour formation in nude mice (148). In addition, both isoform are believed to have the E3 ligase activity as they are able to bind to components of VHL E3 ubiquitin ligase (Cullin2, Elongin B and Elongin C) (145-147). *VHL* also encodes another transcript that is produced by an alternative splicing of exon 2, and found to be low in abundance (149,150) with no tumour suppression capability (149).

1.3.3.3. Expression and subcellular localisation of VHL

The VHL protein is evolutionarily conserved across species and ubiquitously expressed in embryonic and adult human tissues (150,151). Biallelic inactivation of *VHL* is embryonic lethal in mice (*VHL* –/–) owing to placental vasculogenesis deficiency, whereas heterozygous *VHL* mice (*VHL* +/–) are phenotypically normal and do not develop tumours in their short life spans (152). A conditional deletion of *VHL* in the liver of mice resulted in steatosis, formation of blood-filled vascular cavities and foci of increased vascularisation, depicting the role and importance of VHL in regulating angiogenesis (153).

$pVHL_{30}$ and $pVHL_{19}$ differ slightly in their subcellular localisation (Table 1.2). $pVHL_{30}$ is localised primarily in the cytosol, and less in the nucleus or associated with the endoplasmic reticulum (ER), whereas $pVHL_{19}$ is distributed equally in the cytosol and nucleus, but not found associated with the ER (145,154). The association with ER is thought to be related to the binding of $pVHL_{30}$ with fibronectin as both localised to the ER, and its role in assembling proper extracellular fibronectin matrix (154,155).

Table 1.2 – VHL isoforms. Protein length, apparent molecular weight, subcellular localisation, capability of tumour suppression and E3 ubiquitin ligase activity are summarised.

VHL isoforms	Protein length (amino acids)	Apparent molecular weight (kDa)	Subcellular localisation	Tumour suppression activity (145-147)	E3 ligase activity (145-147)
$pVHL_{30}$	213	30	Mainly cytosol. Little in nucleus or associated with ER (145,154)	Yes	Yes
$pVHL_{19}$	160	19	Nucleus and cytosol, but not ER (145,154)	Yes	Yes

1.3.3.1. VHL as E3 ubiquitin ligase

VHL associates with Cullin2, EloB/C, Rbx1 to form an E3 ubiquitin ligase complex (156,157), primarily known for polyubiquitinating HIF-α to form K48-linked ubiquitin chain (77), which directs HIF-α for degradation by the 26S proteasome (Figure 1.3). Cullin2 functions as a scaffold core of the complex, important for the docking of EloB/C, Rbx1 and a cognate E2 ubiquitin-conjugating enzyme (158). Rbx1 is a RING box protein containing catalytic activity of the E3 complex, and assists the recruitment of the ubiquitin-loaded E2, whereas EloB/C bridges the Cullin2 scaffold and the VHL SRS. VHL interacts with EloB/C via a conserved sequence motif in EloB/C called BC box (159). VHL is divided into two functionally distinct domains: an α domain at the C-terminus (amino acid 155-192) and a β domain at the N-terminus (amino acid 63-154 and 193-204) (Figure 1.5) (160). The α domain contains three α-helices and directly interacts with EloB/C to form the multi-protein complex with Cullin2 and Rbx1, whereas the β domain is comprised of two β-sheets arranged as a sandwich with a α-helix on top (140), importantly, contains binding pocket for target proteins, such as the HIF-α subunits.

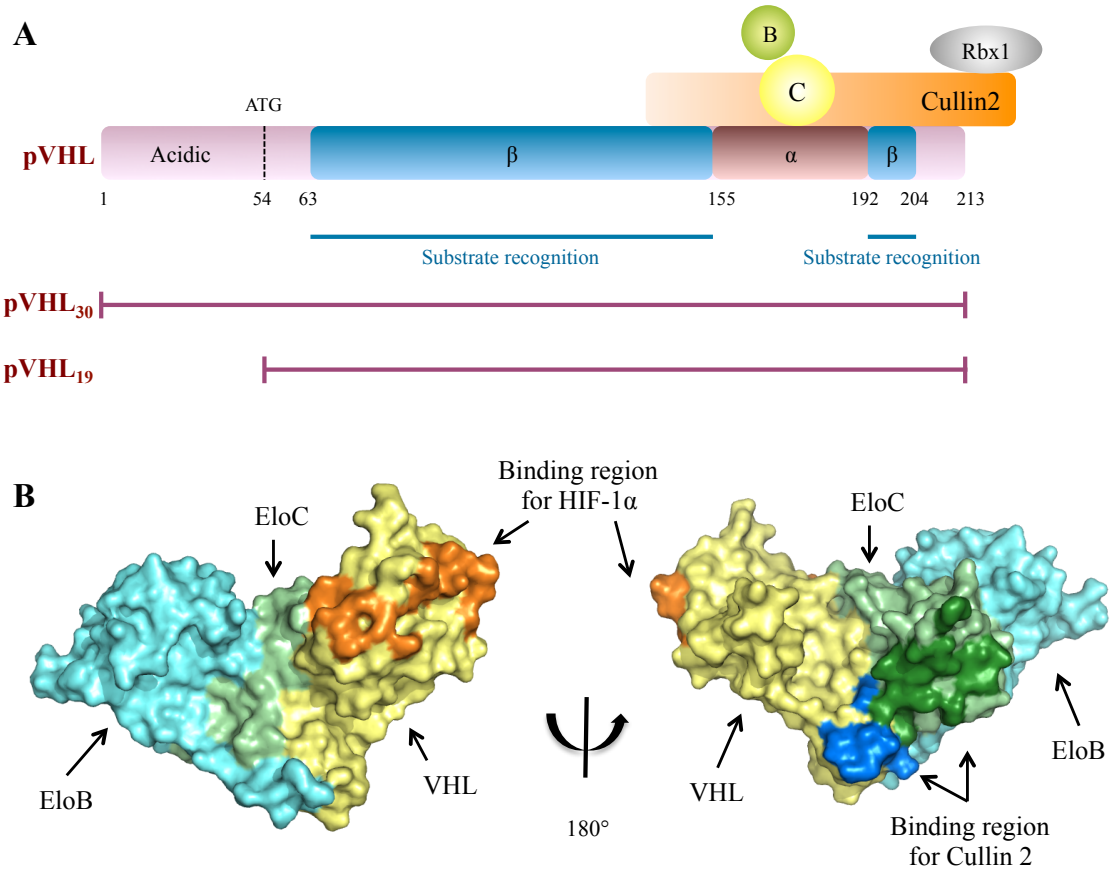

Figure 1.5 – The VHL protein. (**A**) The *VHL* gene encodes two proteins: $pVHL_{30}$ and $pVHL_{19}$. $pVHL_{19}$ is a product of alternative translation initiation sites (ATG coding for Met 54) and lacks an N-terminal acidic domain. The structure of pVHL reveals two structural subdomains: α and β. The α domain contains three α-helices and binds to EloB/C. The β domain contains a surface region that is required for binding substrates such as HIF-1α. Figure was adapted from (139). (**B**) Crystal structure of VHL_{54-213}:EloB:EloC (VBC) in two orientations. VBC is coloured according to the following: VHL is in yellow; EloC is in light green; EloB is in cyan. The surface region on VHL that is required for binding HIF-1α is highlighted in orange. The surface region on VHL that interacts with Cullin2 is highlighted in blue, whereas the surface region on EloC that interacts with Cullin2 is in dark green. Crystal structures of figure **B** is provided by Guilherme Castro.

1.3.3.2. HIF-independent VHL-targets and functions

Apart from HIF-α subunits, several other proteins have been identified as potential substrates of VHL E3 complex. Sprouty (Spry2), a protein associated with tumour growth and progression, was found to be hydroxylated on proline residues by PHDs in normoxia, and subsequently recognised by VHL for polyubiquitination and degradation (161). VHL was also shown to polyubiquitinate several atypical protein kinase C

(PKCs) involved in the tight junction structure formation and maintenance of cell polarisation (162). VHL was also found to mediate the polyubiquitination and degradation of epidermal growth factor receptor (EGFR), presumably to suppress tumour growth induced by prolonged signalling of EGFR (163). The largest subunit of RNA polymerase II, Rpb1, is also polyubiquitinated by VHL for protein degradation (71). However, in another cell context, RCC cells, Rpb1 was polyubiquitinated, but not degraded. The same study also discovered that Rpb1 possess an ODD-like domain, which contains the LXXLAP motif, and the proline residue of this motif was hydroxylated by PHD1 under oxidative stress (65).

In addition to these substrates, VHL was also found to associate directly with fibronectin to promote proper fibronectin matrix assembly, a process important for cell growth and differentiation (154). Dysregulation of the matrix formation is often associated with tumour. Interestingly, this interaction between VHL and fibronectin is impaired in VHL type 2C VHL disease, but the VHL E3 ligase activity is still functional (143). In addition, VHL has also been shown to regulate tight junctions and integrins, adherin, MMP and collagen IV important for the assembly of the extracellular matrix [reviewed in (140)].

It is also claimed that VHL appears to regulate other functions, including transcription regulation via the binding to SP1 transcription factor in a HIF-independent manner; regulation of apoptosis; cell senescence control via SWI2/SNF2 chromatin remodeller p400, independent of HIF; and cell cycle through regulation of cyclin D1 in a HIF-dependent manner [reviewed in (140,164)].

1.3.3.3. VHL regulation

The regulation of VHL protein is still not well studied and characterised. The formation of VHL-EloB/C (VBC) requires two chaperone proteins, heat shock 70 kDa protein

(HSP70) (165) and hetero-oligomeric chaperonin TCP1 ring complex (TriC; also called as chaperonin-containing TCP1 [CCT]) (165,166). The newly synthesised VHL is shuttled from the ribosomal machinery by HSP70, and the formation of VHL with EloB/C (VBC) is mediated by TriC. TriC associates with VHL to facilitate the folding of VHL, and thereby promotes the assembly of VHL into EloB/C complex (165). Failure of protein folding or formation of VBC leads to VHL degradation via the UPS, and this process requires another chaperone protein, heat shock 90 kDa protein (HSP90), which is involved in protein folding (167).

1.4. Pharmacology modulation of oxygen sensing

As HIF plays a key role in regulating many cellular processes and is implicated in diseases, it is a very attractive therapeutic target. Depending on the context and the role of HIF in the disease, activation or repression of HIF activity can be beneficial for the treatment of the disease. For instance, as HIF often promotes tumour growth, inhibition of HIF might be ideal for therapy against certain cancer types. However, as HIF-1α and HIF-2α can play opposing roles to promote tumour progression or suppression, therefore, inhibition of a specific isoform is important. On the other hand, activation of HIF would be beneficial for the treatment of chronic anaemia, ischaemia, gastrointestinal disease, and aiding wound healing process and organ transplantation. Below are examples of HIF activators and repressors, activating or repressing HIF via pharmacological modulation of protein components involved in regulating HIF activity. In addition to these, there are many small-molecules targeting different components or pathways affecting oxygen sensing that are not mentioned or discussed here.

1.4.1. HIF repressors

Pharmacological inhibition of HIF has been challenging owing to its intracellular localisation, and absence of deep and well-defined active sites, which are normally

targeted for small-molecule inhibition (168). Nonetheless, there are several HIF inhibitors available that inhibit HIF via different mechanisms; including targeting mRNA expression, protein translation, and more recently, direct small-molecule inhibition. Below are a few examples of HIF inhibitors: digoxin and acriflavine that inhibit both HIF-1α and HIF-2α, bortezomib that inhibits HIF transcriptional activity, and PT2399 that selectively inhibits HIF-2α.

1.4.1.1. Digoxin – inhibits HIF-1α and HIF-2α

A study identified digoxin and other cardiac glycosides (including proscillaridin A and ouabain) as inhibitors of HIF-1α through a high-throughput cell-based screen of drugs that are in clinical trials or approved for use (169). These drugs were shown to inhibit translation of HIF-1α and HIF-2α, as well as the induction of HIF-1α target genes in tumour cells, but their mechanisms of action remained elusive and found to be in an mTOR-independent manner (169). In addition, digoxin treatment inhibited growth of subcutaneous xenografts and established tumours in mice (169). Digoxin and the other cardiac glycosides are used in patients with congestive heart failure to inhibit the Na^+/K^+ ATPase, but the HIF-α inhibition by digoxin is not dependent on this mechanism (169). Digoxin and acriflavine (also a HIF inhibitor; 1.4.1.2) have been shown to block early step of breast cancer metastasis in mice (170). A phase II breast cancer trial begins evaluating HIF-1α level in tumour tissues of patients on daily oral digoxin for two weeks before surgery compared to no drug study (NCT01763931).

1.4.1.2. Acriflavine – inhibits HIF-1α and HIF-2α

Another HIF inhibitor, acriflavine, was also identified in a cell-based screen of drugs approved by FDA or previously in clinical use (171). Through *in vitro* pulldown assays, acriflavine was shown to bind directly to the PAS-B domains of HIF-1α and HIF-2α, preventing the dimerisation of the α-subunits to HIF-1β, thereby inhibiting HIF transcriptional activity (171). Acriflavine reduced growth of tumour in mice

xenografted with prostate cancer or hepatocellular carcinoma, and also arrested tumour growth in established prostate cancer, presumably mediated by its anti-angiogenic effects as acriflavine inhibits tumour vascularisation, expression of angiogenic cytokine and mobilisation of angiogenic cells (171). Other studies have shown that acriflavine also induces anti-cancer effects in murine breast cancer model (172) or mice with human breast cancer xenografts (170). It has also been shown that pre-treatment of acriflavine improves photodynamic therapy (a cancer therapy that induces cell death) in cultured cells (173). A very recent study shows that acriflavine reduces the maintenance of leukaemia stem cells and leukaemia development in chronic myeloid leukaemia *in vitro* and *in vivo* (174).

1.4.1.3. Proteasome inhibitor: bortezomib, carfilzomib and MG132

Bortezomib (Velcade™) is a 26S proteasome inhibitor approved by the FDA for treating multiple myeloma and mantle cell lymphoma (175). Bortezomib can induce opposite effects in cells regarding HIF regulation: bortezomib inhibits the proteasome and leads to the accumulation HIF-α and proteins degraded by the proteasome when used at sufficiently high concentrations; but it also inhibits HIF transcriptional activity by blocking the interaction between HIF-α and p300, a HIF transcriptional co-activator, when used at nanomolar concentrations (176,177). The activity and cytotoxicity of bortezomib also seems to differ depending on the cell lines tested [discussed in (176)]. Another FDA-approved proteasome inhibitor is carfilzomib (Kyprolis), also used for the treatment of multiple myeloma. Carfilzomib has been shown to be more potent than bortezomib, and able to induce responses in multiple myeloma resistant to bortezomib (178).

MG132 is another proteasome inhibitor, but has never been tested clinically due to rapid oxidation. MG132 is widely used in research and has proved to be a valuable research tool (179).

1.4.1.4. PT2399 – inhibits HIF-2α

As HIF-1α and HIF-2α are structurally similar and regarded as undruggable, there was no inhibitor that could bind to HIF-α protein directly, let alone that could selectively inhibit a particular isoform. However, early structure-guided medicinal chemistry led to the development of artificial small molecules targeting a cryptic pocket in the HIF-2α PAS domain (180). As this pocket adopts a different size in HIF-1α, it could be possible to selectively bind the small molecule to HIF-2α over HIF-1α (181). More recently, two recent studies simultaneously revealed an optimised HIF-2α-selective inhibitor – PT2399 (182,183), demonstrating that it is possible to selectively inhibit a single α-subunit. PT2399 was optimised through structure-guided design, and shown to directly inhibit HIF-2α by binding to its PAS-B domain, thereby disrupting the interaction between HIF-2α and HIF-1β and inhibiting HIF-2 transcriptional activity (183). PT2399 inhibits HIF-2 dimerisation in mice with patient-derived xenografts of *VHL*-null ccRCCs, renal carcinoma that are commonly associated with HIF-2α accumulation. Furthermore, the inhibitor suppresses tumorigenesis in 56% of these tumourgrafts, validating HIF-2α as therapeutic target in ccRCC (182). PT2399 has also been shown to minimally affect a group of 68 enzymes, receptors, and ion channels (183), thus may require further optimisation.

An additional analogue of PT2399, PT2385, which also selectively inhibits HIF-2 via the same mechanism, showed similar anti-cancer activity (184).

1.4.2. HIF activators

As discussed in 1.2. , inducing HIF activity can be therapeutically beneficial. Below are examples of HIF activators via modulating different components that are involved in HIF regulation.

1.4.2.1. 2-oxoglutarate mimics: dimethyloxalylglycine (DMOG), *N*-oxalylglycine (NOG) and *N*-oxalyl-D-phenylalanine

2-oxoglutarate (2OG) is a co-factor required by all 2OG-dependent dioxygenases including PHDs and FIH. 2OG binds to the catalytic domain that docks an essential Fe^{2+} ion, important for enzymatic activity of these dioxygenases. *N*-oxalylglycine (NOG) and dimethyloxalylglycine (DMOG, a pro-form of NOG) have been shown to inhibit both the prolyl and asparaginyl hydroxylation of PHDs and FIH, respectively (185). DMOG and NOG are structurally similar to 2OG, mimicking 2OG and binding to the active site of PHDs and FIH. NOG has been shown to also inhibit other 2OG oxygenases, and deemed unlikely to be suited for medicinal use (186). A study showed that 2OG dioxygenase inhibitors display similar transcriptional profile to hypoxia, as compared to selective PHD inhibitors (187). *N*-oxalyl-D-phenylalanine is another 2OG mimic, designed based on crystal structures of FIH–Fe^{2+}–2OG/NOG with fragments of HIF-1α CTAD, and shown to be a selective inhibitor of FIH by competing with 2OG, but it could not inhibit PHD2 at 1 mM concentration (186).

DMOG has been extensively used and reported to induce HIF activities in cells and animals. As mentioned in the previous section (1.2.), DMOG has been shown to have protective roles in many diseases, including ischaemia (heart, brain and kidney), inflammation (such as intestinal inflammation) and wound healing in diabetic mice (107,112,114,117,188).

1.4.2.2. Fe^{2+} substitutes: Co^{2+}, Ni^{2+} and Cu^{2+}

Fe^{2+} substitutes including Co^{2+}, Ni^{2+} and Cu^{2+}, replace Fe^{2+} in the active site of Fe^{2+}-containing dioxygenases including PHDs and FIH, resulting in the inhibition of their enzymatic activity and subsequent HIF stabilisation. The most commonly used substitute is $CoCl_2$. $CoCl_2$ is a water-soluble compound that was traditionally used for anaemia treatment in infants and pregnant women. $CoCl_2$ has been shown to induce EPO in cells and *in vivo*, elicits hypoxia response, and has cardioprotective effect via HIF-1α (189,190).

1.4.2.3. Fe^{2+} chelators: deferoxamine/desferrioxamine and AKB-4924

In addition to substituting Fe^{2+}, chelating Fe^{2+} also induces HIF stabilisation. There are many Fe^{2+} chelators known to stabilise HIFs, including deferoxamine/desferrioxamine (DFX/DFO), AKB-4924, $_L$-mimosine, hydralazine, FG-2229, and TM-6008 [reviewed in (106)]. Fe^{2+} is crucial for enzymatic reaction of PHDs and FIH. Therefore enzymatic activity of these enzymes would be inhibited with the sequestering of Fe^{2+}.

DFO was the first FDA-approved iron chelator, and has been systematically used to treat chronic iron overload since 1970s (191). DFO has been commonly used in stabilising HIF-1α in cells, and known to stabilise HIF-1α in almost every cell type. DFO was first shown in 1993 to induce HIF-1α by chelating iron and also activate gene expression of EPO (before the discovery of HIF as the transcription factor of EPO) (190). DFO has been shown to aid wound healing in diabetic mice (120) and possess neuroprotective effects (192,193) via its HIF stabilisation activity.

AKB-4924 (Aerpio Therapeutics) is a PHD inhibitor that predominantly targets HIF-1α and not HIF-2α (194). AKB-4924 was originally identified in a screen for antimicrobial agent against bacterial iron-dependent enzyme and it contains an α-hydroxycarbonyl

group similar to the iron-chelator L-mimosine, suggesting similar mechanism of inhibition on PHDs by chelating iron bound on the active site (194). A study shows that AKB-4924 stabilises HIF-1α to enhance host cell immunity and indirectly induces anti-microbial activity through promoting the bactericidal capacity of host cells (194). Recently, a phase I clinical trial using AKB-4924 for treating IBD has commenced (NCT02914262), since the inhibitor has been shown to regulate innate immune response and maintain epithelial barrier function in murine colitis, mediated by the stabilised HIF-1α (195).

1.4.2.4. Inhibitors of Cullin neddylation: MLN4924

MLN4924 inhibits NEDD8-activating E1 enzyme (NAE) and prevents the neddylation of Cullin1 and Cullin2 (196). MLN4924 is structurally related to adenosine 5' monophosphate (AMP), a tight binding product of NAE. In the first step of the neddylation cascade reaction, AMP binds to the nucleotide-binding site on NAE, which catalyses the formation of NEDD8 adenylate (NEDD8-AMP). The mechanism of neddylation inhibition by MLN4924 is similar – MLN4924 competes with AMP for the binding to NAE, and NAE subsequently catalyses the formation of a covalent adduct of MLN4924 with NEDD8, thereby preventing the activation and conjugation of NEDD8 to target proteins (197). The action of MLN4924 on Cullin2 results in stabilisation of HIF-α (198), and other CRL substrates (199). Many studies have shown the anti-cancer effects of MLN4924 (196-198), and the inhibitor is currently in clinical trials for patients with acute myeloid leukaemia and myelodysplastic syndromes (200). In addition, MLN4924 also decreases inflammation and disease severity in murine model of colitis (199).

1.4.2.5. PHD inhibitors

Most HIF activators mentioned above inhibit PHDs by blocking their 2OG- and Fe^{2+}-dependent catalytic activity; these HIF activators may also target other 2OG- and/or

Fe^{2+}-containing enzymes resulting in off-target effects from deregulating HIF-independent hydroxylase pathways. Below are examples of compounds that inhibit PHDs directly.

1.4.2.5.1. Roxadustat/FG-4592

Roxadustat/FG-4592 is an oral PHD inhibitor that induces erythropoiesis (red blood cell production), and regulates iron metabolism (54). FG-4592 inhibits all three PHD isoforms (201). FG-4592 is currently in phase III clinical trial for the treatment of anaemia associated with CKDs (NCT01750190) – the most advanced PHD inhibitor in clinical trial. The inhibitor could be a first-in-class treatment option – FG-4592 may be a better treatment than the purely-EPO based therapy ones as HIF stabilised in the presence of PHD inhibitor could induce cellular processes such as iron metabolism to promote erythropoiesis (202). Another potential advantage of PHD inhibition is that endogenous EPO is induced instead of administering recombinant EPO, and thereby might have reduced side effects (202). No serious drug-related side effects have been observed with in the clinical trials of FG-4592 (201).

Beside FG-4592, there are more PHD inhibitors in clinical trials: vadadustat/AKB-6548 (phase III), daprodustat/GSK1278863 (phase III), molidustat/BAY 85-3934 (phase II), JTZ-951 (phase II), and JNJ-42905343 (preclinical). A recent detailed review on these inhibitors can be found in (201).

1.4.2.5.2. IOX2

IOX2 was reported as a selective PHD inhibitor (203). Although there is no crystal structure of IOX2 itself bound to PHD2, a close analogue of IOX2 has been shown to bind to the active site of PHD2, replacing 2OG in the active site (203). This was the expected binding mode, given IOX2 was designed to mimic closely the structure of 2OG. Due to the similar catalytic domains present in all three PHD isoforms, and the

fact that they all bind 2OG similarly, it is considered likely that IOX2 also potently inhibits PHD1 and PHD3 (204). IOX2 inhibits PHD2 with IC_{50} of 22 nM in an *in vitro* binding assay (203), and is at least 431-fold more selective for PHD2 over a panel of 2OG dioxygenases (204). A more potent inhibitor than IOX2, IOX4, has also been described recently (204), but is not discussed here.

1.5. VHL inhibitors as HIF stabilisers

Chemical intervention in the ubiquitin–proteasome system (UPS) has therapeutic potential, demonstrated by the clinical success of proteasome inhibitors (128). However, this approach is not specific to a given substrate as proteasome inhibitors affect all processes that exploit the UPS for regulation. In contrast, the E3 ubiquitin ligases (>600 E3 predicted in humans) confer substrate specificity to the UPS for degradation (205), and are associated with many diseases (128), therefore E3 ubiquitin ligase would potentially provide more attractive targets and a more selective chemical intervention than the proteasome.

As mentioned previously, the tumour suppressor von Hippel–Lindau (VHL) is a biologically relevant E3 ubiquitin ligase that targets hypoxia-inducible factor-α (HIF-α) transcription factor for degradation via the UPS. Inhibition of VHL would be expected to prevent polyubiquitination and subsequent degradation of HIF-α, resulting in HIF-α stabilisation. Development of a potent inhibitor of the interaction between VHL and HIF-α would allow intervening in the HIF pathway downstream of prolyl hydroxylases and potentially in a more selective fashion. Most importantly, this would provide a tool useful for further understanding VHL.

1.5.1. Targeting protein–protein interactions

Protein–protein interactions (PPIs) are ubiquitous in nature. Owing to the diverse and crucial roles of PPIs in regulating many biology processes, the therapeutic targeting of PPIs is of great interest (179,206). However, the development of drug-like small molecule modulators that targets PPIs has proven challenging as the interacting surfaces between proteins are generally large and involve flat surface or shallow grooves, not suitable for small molecule to bind; this includes targeting the UPS (179). A variety of strategies have been employed to identify hits and leads against PPIs including: high-throughput screening of a library of compounds; fragment screening and optimisation; rational design of mimicking peptides; computational approaches to analyse 'druggability' (the likelihood of modulating a target protein by small-molecules) and predict possible small-molecule binding pockets; and lead optimisation [reviewed in (207)].

1.5.2. Chemical probes

A chemical probe is a small-molecule modulator of the function of a target protein that allows addressing mechanistic and phenotypic questions on the target protein in biochemical, cell and animal studies (208). In order to serve as a powerful tool for research, a chemical probe has to be of high-quality – potent, selective and cell-permeable. Evidence for target engagement, and an understanding of the mechanism by which the compound modulates the target should be ideally provided. The recent development of high-quality chemical probes has facilitated substantial progress in basic and translational research, and has provided a starting point for drug development (208,209).

1.5.2.1. Requirements for high-quality small molecule

A small molecule is different to chemical probe. The low molecular weight small molecule is a modulator of a target protein. However, to be approved as a chemical probe, the small molecule has to be fully assessed and meets a number of minimal requirements, or so-called "fit-for-purpose criteria". The followings are guidelines set by the Structural Genomics Consortium (SGC) (http://www.thesgc.org/chemical-probes):

- *In vitro* binding affinity towards target protein of <100 nM
- Displays >30-fold selectivity compared to other proteins of the same family
- Exhibits on-target effects in cells at 1 μM
- Screened against 'industry standard' off-targets and against large protein families relevant to drug discovery (208)
- Preferably accompanied by an inactive close analogue of the small-molecule as negative control

These are ideal criteria of a chemical probe and others have put together a more thorough review on factors to be considered in assessing the small molecules (210). It is advocated and well acknowledged that these criteria should not be rigid, and could vary depending on the specific target and pathway in question.

A chemical probe is different to a small-molecule drug in terms of their purposes and characteristics. For instance, whilst selectivity profile is very important for chemical probe, it may be less important for a drug; and indeed many drugs manifest their clinical effects through affecting multi-targets or disease pathways (208). Furthermore, a chemical probe does not need to possess optimised pharmacodynamics or oral bioavailability like a medicine, at least for use in cellular studies. Instead, a chemical

probe has to be potent, selective, and with defined on-target mechanism of action, in order to be a useful tool to address biological questions (208).

1.5.2.2. Advantages

Chemical probes have proven to be very impactful in modulating target protein due to following [reviewed in (208)]:

- Complementary to genetic tools including RNAi, and more recently, CRISPR-Cas9, specifically because a chemical probe typically inhibits a particular function of the target protein rather than removing the entire protein
- Able to inhibit a protein or a protein domain in cells or organisms rapidly and reversibly
- Can be used in any type of cell
- Uncover temporal characteristics of target inhibition
- Comparison with RNAi would help dissect between effects due to scaffolding (abolished in protein knockdown with RNAi) and inhibition of protein interaction or catalytic activity (blocked by small molecule)
- Combination with other chemical probes in synthetic lethal screens can be useful to study the link between separate pathways involved
- Crucially, the results from chemical probes can be applicable to clinical studies because chemical probes are often starting points, and provide the core scaffold to a drug, thus they likely behave similarly to small molecule drugs

1.5.2.3. Limitation

As of any approaches, chemical probe may also have off-target effects. Unbiased transcriptome and proteasome profiling may provide valuable means to analyse on- and off-target effects of a chemical probe in cells (210). In addition, a negative control, especially an inactive close analogue of the chemical probe containing ideally the same

chemical scaffold would help to distinguish between effects from on- and off-target (210).

As small molecule is not part of the endogenous system, the compound may face issues with regards to transport out of cells by efflux pumps and metabolism/stability liabilities, which could limit its applicability despite being cell-permeable. In addition, the molecule may also be toxic to cells. However, a small molecule that is deemed as chemical probe should not have these issues if well-characterised.

1.5.3. VHL inhibitors

The first series of VHL inhibitors was first described in collaborative research between the Ciulli group and scientists from Yale University (211-213). The inhibitors contain a hydroxyproline fragment, designed rationally based on the hydroxyproline residue on HIF-1α, which makes key interactions with VHL. Thus the inhibitors were expected to compete with hydroxylated HIF-1α to bind to VHL, and lead to HIF-1α stabilisation. However, these inhibitors were ineffective in inducing HIF-1α stabilisation in cells, owing to their limited potency and suboptimal physiochemical properties (211-213).

The Ciulli group later reported a series of VHL inhibitor developed by stepwise structure-guided design, with *in vitro* nanomolar binding affinities (214). The most potent inhibitor according to the *in vitro* binding affinity measured was VH032 (also called ligand 7 in the published article), however no cellular data was reported (214).

This thesis describes the characterisation of VH032 in cells and the discovery of the most potent VHL inhibitor so far, VH298, which was first disclosed by the Ciulli group in 2016 (215). In addition, a suitable negative control was also generated for each of the two inhibitors – *cis*VH032 and *cis*VH298. The two compounds maintain the chemical scaffold of respective parent binder, but do not bind to VHL because of the change in

stereochemistry at the carbon atom bearing the hydroxyl group on the hydroxyproline ring (Table 3.1 and Table 3.2).

1.5.4. The use of VHL inhibitors in proteolysis targeting chimeras (PROTACs)

Besides stabilising HIF-1α, VHL inhibitors have been used in a novel strategy that recruits a degradation system such as the VHL E3 ubiquitin ligase to degrade a specific target protein. This approach is commonly called proteolysis-targeting chimeras (PROTACs) (216). PROTAC compounds contain two recruiting ligands connected via a linker: one ligand specifically binds to a target protein that is to be degraded and the other ligand recruits an E3 ubiquitin ligase (217). PROTACs thus recruit the two targets in close proximity and promote the polyubiquitination, and subsequent proteasomal degradation of the target protein by the E3 ubiquitin ligase (217).

VHL inhibitor VH032 has been used as the VHL-recruiting moiety in several reported PROTACs. VH032 is linked to different target ligands to induce proximity-driven ubiquitination of a specific target protein by VHL and subsequent proteasomal degradation. Target proteins that have been degraded via this mechanism are: BET proteins (217,218), ERRα and RIPK2 proteins (219), and intracellular green-fluorescent protein (GFP) fused to HaloTag7 (220).

1.6. Aims and objectives

A series of small molecules that disrupts the interaction between VHL and HIF-α (VHL inhibitors) with nanomolar binding affinities have been developed and more potent VHL inhibitors were also designed by the Ciulli group, but the biological and functional activity of the VHL compounds in cells have not been elucidated.

We hypothesise that the VHL inhibitor is able to disrupt the interaction between VHL and HIF-α, leading to the stabilisation of HIF-α in cells. The binding of the small molecule on the VHL pocket for HIF-α would also indicate that the inhibitor may manipulate only the function of VHL on targeting HIF-α. The inhibitor is potentially able to also inhibit VHL rapidly and reversibly, and therefore a better tool to repress VHL function than genetic or RNAi knockdown.

To test this hypothesis, we describe the following aims:

1.6.1. To characterise VHL inhibitors as chemical probes of the hypoxia signalling pathway.

Poorly characterised chemical probe may have major off-targets, and their usage may lead to misrepresentative or incorrect conclusions (208). Therefore, it is important to characterise a small molecule for its potency, selectivity, and mode-of-action. To do so, a biased approach was initially employed to assess the ability of VHL inhibitors in stabilising and activating HIF, followed by unbiased gene and protein expression global profiling of representative inhibitors via RNA-sequencing and TMT-labelling proteomic approaches, respectively.

1.6.2. To determine the regulation of VHL using VHL inhibitors.

The VHL E3 ubiquitin ligase is not well characterised with regards to how it is regulated. Usage of a VHL inhibitor that binds specifically to the binding pocket recognised by hydroxylated HIF-α as chemical tool may shine light into the regulation and function of VHL, in the context of the blockade of this specific interaction site. In addition, there have been small molecules that bind to an E3 ligase and *de novo* "hijack" the ligase activity toward a new substrate as a new binding site is created and exposed (221). Co-IP experiment using the VHL inhibitor was performed with the goal to collect

valuable information on changes on VHL interactome in the presence and absence of the inhibitor.

2. Methods and Materials

2.1. Cell Culture

2.1.1. Cell lines and growth conditions

Human cervix carcinoma cells HeLa, human osteosarcoma cells U2OS, human embryonic kidney cells HEK293, human foreskin fibroblasts HFF, renal carcinoma cells RCC4-HA and RCC4-HA-VHL were obtained from the American Type Culture Collection (ATCC). All cells were propagated in Dulbecco's Modified Eagle Medium (Gibco) supplemented with 10% fetal bovine serum (Gibco), l-glutamine (Lonza), 100 mg ml^{-1} of penicillin/streptomycin (Lonza; DE17-602E) at 37°C and 5% CO_2. RCC4-HA and RCC4-HA-VHL were maintained in the same condition with the addition of 400 mg ml^{-1} G418 (ForMedium; G4181). Stable cell lines HeLa-HRE and U2OS-HRE luciferase cells were generated previously by others as described (222) and maintained in 0.1 mg ml^{-1} puromycin (Fisher; P8833). All cell lines were routinely tested for mycoplasma contamination using MycoAlert kit from Lonza every three months and discarded if tested positive for mycoplasma contamination.

2.2. Treatments

2.2.1. Hypoxia treatment

For hypoxia induction, cells were incubated at 1% O_2 (5% CO_2 and 94% N_2) in an InVIVO 300 hypoxia workstation (Ruskin Technologies). To prevent reoxygenation, cells were lysed for protein extract (refer to section 2.1.) or RNA extraction (refer to section 2.4.) in the hypoxia workstation. Normoxic control was included by placing cells in the 37 °C incubator chamber at 5% CO_2.

2.2.2. Compound treatments

DMSO was used as vehicle control at 1% v/v. Hypoxia mimetic agents cobalt chloride ($CoCl_2$) was obtained from Sigma (catalogue number C8661) and used at a final concentration of 100 μM for 4 h. The proteasome inhibitor MG132 was obtained from Merck (474790) and mostly used at the final concentration of 20 μM for 3 h unless indicated otherwise. PHD inhibitors IOX2 and FG-4592 were purchased from Sigma (SML0652) and Selleckchem (S1007), respectively. Drugs were added to cells at indicated concentration and for indicated length of time.

VHL inhibitors used were synthesised by Pedro Soares from Alessio Ciulli Group (Dundee) and used in a stock concentration of 25 mM.

2.3. Cell transfections

2.3.1. siRNA transfections

Small interfering RNA (siRNA) oligonucleotides were purchased from Eurofins/MWG, and used in a stock concentration of 20 μM. siRNAs were transfected using Interferin from Polyplus according to the manufacturer's instructions with some modification. Briefly, HeLa cells were seeded at 1.5×10^5 cells per well in a six-well plate one day prior to transfection. A mixture of 200 μL Opti-MEM reduced serum medium (Invitrogen; 51985-026), 3 μL INTERFERin (Polyplus; 409-50) and 3 μL of 20 μM siRNA was incubated at room temperature for 15-20 min. Meanwhile, medium was aspirated from the plate of cells and replaced with fresh pre-warmed medium. The transfection mixture was then transferred to cells in drop-by-drop. Media was changed after 24 h of transfection and transfected cells were incubated for another 24 h before lysis. The oligonucleotide sequences used for siRNA knockdown are shown in Table 2.1.

Table 2.1 – Oligonucleotide sequences used for siRNA knockdown

siRNA	Sequence (5' → 3')
Control	AAC AGU CGC GUU UGC GAC UGG
VHL	GGA GCG CAU UGC ACA UCA ACG

2.4. RNA extraction and quantitative PCR analysis

2.4.1. RNA extraction and quantification

Following treatment, medium was removed from each well or plate, and cells were washed with 1 × PBS twice. Total RNA from mammalian cells was extracted using the RNeasy Mini Kit (Qiagen; 74104/74106) according to manufacturer's protocol. Note that a total of 250 µL or 400 µL of RLT buffer (part of the RNeasy Mini Kit) supplemented with 40 mM mL^{-1} of DTT (ForMedium; DTT010) was used to lyse cells in 24-well plate or 12-well plate, respectively. RNA was quantified using NanoDrop™ 2000c spectrophotometer (Thermo Scientific), using the elution buffer (RNase-free H_2O) as blank.

2.4.2. cDNA synthesis

A total of 500 ng of RNA was reverse transcribed in a total volume of 20 µL mixture per reaction using the iScript™ cDNA Synthesis Kit (BIO RAD; 170-8891) according to the manufacturer's protocol. RNA was reverse transcribed in the Applied Biosystems 2720 thermal Cycler. Following reverse transcription, cDNA generated was diluted in RNase-free H_2O at 1:1 volume ratio.

2.4.3. Real time quantitative PCR

Real time quantitative PCR (RT qPCR) was performed in triplicates in 96-well plate using PerfeCTa SYBR Green FastMix (Quanta Biosciences; 733-1378) in C1000 Touch Thermal Cycler (Bio-Rad Laboratories). RT qPCR was performed according to manufacturer's protocol with the modification that 6 µL of the diluted cDNA was used in a total of 15 µL mixture per reaction. For all primers used in this study, an annealing temperature of 60 °C was used. mRNA levels were calculated based on averaged CT values and normalised to β-actin mRNA levels. The primers used for RT qPCR are shown in Table 2.2.

2.1. Protein lysis

2.1.1. Whole cell protein lysis

Following treatment, medium was removed from each well or plate, and cells were washed with 1 × PBS twice. Cells were harvested using whole cell protein lysis buffer (20 mM Tris pH 7.6, 150 mM NaCl, 1% Triton X100, and one protease inhibitor cocktail tablet [Roche; catalogue number 11873580001] per 10 mL of buffer). Lysis buffer containing protease inhibitor was stored in fridge (4 °C) and used for no longer than 3 months. A total of 90 µL of lysis buffer was used for a six-well plate, 200 µL for 10 cm plate, and 300 µL for 15 cm plate. Cells were collected and kept on ice for 15-30 min before centrifugation at 17,000 × *g* in the cold room (4 °C) for 10 min. The supernatant was collected and stored at –80 °C.

Table 2.2 – List of primers used for real time quantitative PCR

Gene	Sequence (Forward) 5' → 3'	Sequence (Reverse) 5' → 3'
β-actin	CTCTTCCAGCCTTCCTTCCTG	GAAGCATTTGCGGTGGACGAT
HIF-1α	GCAAGCCCTGAAAGCG	GGCTGTCCGACTTTGA
HIF-2α	GTCTCTCCACCCCATGTCTC	GGTTCTTCATCCGTTTCCAC
CA9	CGGAAGAAAACAGTGCCTATGAG	CAGGGCGGTGTAGTCAGAGA
PHD2	ACCTGATACGCCACTGTAACG	CCCGGATAACAAGCAACCAT
VEGF	TACCTCCACCATGCCAAGTG	ATGATTCTGCCCTCCTCCTTC
GLUT1	TTCACTGTCGTGTCGCTGTTT	AGCGCGATGGTCATGAGTAT
CITED2	CCTAATGGGCGAGCACATACA	GGGTGATGGTTGAAATACTGGT
PAG1	GGACAGATGCAGATCACCCT	TGAACGGCTGAACATCTCCT
EPO	GCTGAACACTGCAGCTTGAA	CAGACTTCTACGGCCTGCTG
VHL	CCTTGGCTCTTCAGAGATG	TGACGATGTCCAGTCTCCT
ABCA1	CCTGTCATCTACTGGCTCTCTA	CAGATTGGTGGAGGACACATAG
ABCG1	CTCCGCCTCATTGCCTATTT	CTCGGCCACAGTGTCTAATC
DHRS2	GCCCACGTGGTCATCAG	CCCACGTGGCACACAAT
EFR3B	CCTCATGGAGGATGCAGAAAT	ACTGAGGGTACTGATGGTAGAG
LAMC2	CCCTGGGTTGAACAGTGTATATG	CAGTCTCGCTGAATCTCTCTTG
CNN1	GTGCTACAGGGTCCAACATAG	TACCCACTTGTGAGGGAGT
MICALCL	GGAGAGCCAGAAAGATGAGAAG	CTCTGATGCGTTGTTCCTCTAA
GREM1	GCAAGCCCAAGAAATTCACTAC	TGCAACGACACTGCTTCA

DUSP2	AGTATCCCTGTGGAGGACAA	ACCCAGTCAATGAAGCCTATG
TAF9B	TCGAGCCATGCTAAGAAACC	CTGCCTTGCGATATCCAGTAA

2.1.2. SDS lysis

Cells were lysed as described in section 2.1.1, but using the SDS lysis buffer (20 mM Tris pH 7.6, 1% SDS, 5 mM NaF, 500 mM Na_3VO_4, and one protease inhibitor cocktail tablet [Roche; catalogue number 11873580001] per 10 mL of buffer). SDS lysis buffer containing protease inhibitor was stored in fridge (4 °C) and thawed at room temperature before usage. Lysis buffer was used for no longer than 3 months.

2.1.3. RIPA lysis

Cells were lysed as described in section 2.1.1, but using the RIPA lysis buffer (50 mM Tris pH 8, 150 mM NaCl, 0.1% SDS, 1% NP-40, 0.5% Sodium deoxycholate, 5 mM NaF, 500 mM Na_3VO_4, and one protease inhibitor cocktail tablet [Roche; catalogue number 11873580001] per 10 mL of buffer). Lysis buffer containing protease inhibitor was stored in fridge (4 °C) and used for no longer than 3 months.

2.1.4. MS lysis

Cells were lysed as described in 2.1.1, but using the MS lysis buffer (50 mM Tris HCl pH 8.0, 150 mM NaCl, 0.5% C7BzO (Sigma), 5 mM NaF, 500 mM Na_3VO_4, and one protease inhibitor cocktail tablet [Roche; catalogue number 11873580001] per 10 mL of buffer). Tris HCl, NaCl, NaF and Na_3VO_4 had been sterile-filtered prior to preparing the MS lysis buffer. The 0.5% C7BzO was prepared fresh in sterile-filtered MilliQ water. The lysis buffer was prepared and used fresh on the day of cell lysis.

2.2. Protein quantification

2.2.1. Bradford assay

Protein concentrations of cells lysed in the whole cell protein lysis buffer or RIPA buffer were determined using Bradford (BioRad), following manufacturer's instructions. Briefly, 2 µL of protein lysates was pipetted into a cuvette containing 798 µL of MilliQ water, followed by the addition of 200 µL Bradford reagent. 2 µL of MilliQ water was used as blank. The mixture was mixed by brief vortexing and absorbance value was measured at 595 nM. Protein concentration was determined using the absorbance value against a previously generated BSA standard curve.

2.2.2. BCA protein assay

Protein concentration of cells lysed in SDS lysis buffer were quantified using Pierce™ BCA Protein Assay Kit (Thermo Scientific), following manufacturer's instructions. Briefly, 2 µL of protein lysates was added into a microcentrifuge tube containing 1 mL of BCA reagent mixture. The mixture was incubated in a water bath at 37 °C for 30 min, followed by cooling at room temperature for 10 min. The mixture was transferred into a cuvette and absorbance value was obtained using a NanoDrop™ 2000c spectrophotometer (Thermo Scientific) at 562 nm. Protein concentration was calculated using the absorbance value against a BSA standard curve.

2.3. Western blot

2.3.1. Western blotting – semi-dry transfer

Following protein quantification in the previous section, a total of 20 to 30 µg of proteins were prepared in 2 × loading buffer (100 mM Tris HCl pH 6.8, 20% (v/v) glycerol, 4% (w/v) SDS, 200 mM DTT and bromophenol Blue), and incubated for 5 min at 95 °C. Samples were loaded into a SDS-page gel (Tris-HCl poly-acrylamide

gel) previously prepared (5% stacking and 10% resolving for all proteins, except for VHL protein that requires 12% resolving gel), and run at 80-120 volts in running buffer (25 mM Tris, 0.195 M glycine, and 0.1% SDS). A total of 3 µL of SeeBlue® Plus2 Pre-Stained Standard (Thermo Scientific; LC5925) was loaded as protein ladder. The gel was then transferred in a semi-dry transfer system (BioRad) into a PVDF membrane (Merck/Millipore; 10344661) for 2 h at 15 volts/0.80 mA in transfer buffer (50 mM Tris, 40 mM glycine, 0.001% SDS and 10% methanol). The membrane was then blocked with 10% milk in TBS-tween buffer (20 mM Tris pH 7.6, 150 mM NaCl, 0.1% Tween) for 10 min. After 3 × 5 min washes with TBS-tween buffer, the membranes were incubated with primary antibody for 1 h at room temperature or overnight at 4 °C. Antibodies manufacturers and dilutions are shown in Table 2.3. The membranes were then washed with TBS-tween (3 × 5 min) and incubated with the appropriate secondary HRP antibody (anti-mouse from Cell Signalling [7076S] at 1:2000 dilution, anti-rabbit from Cell Signalling [7074S] at 1:2000 dilution, or anti-goat from Thermo Fisher [A-11020] at 1:10000 dilution). After washes, membranes were developed using ECL solution (Pierce). β-actin was used as loading control.

2.3.1. LI-COR system

VHL inhibitor was screened for its ability to stabilise HIF-1α and hydroxylated HIF-1α using the LI-COR system to detect and quantify protein level. A total of 20 to 30 µg of proteins were prepared in 4 × NUPAGE LDS sample buffer (Thermo Fisher; NP0007) supplemented with DTT (ForMedium; DTT010, and incubated for 5 min at 95 °C. Samples were loaded into a NUPAGE 4-12% Bis-Tris protein gel (Life Technologies; NP0323BOX), and run at 200 volts for 50 min (or until the blue front line reached the bottom of the gel) in 1 × MOPS SDS running buffer (Thermo Scientific; NP0001). A total of 3 µL of PageRuler Plus Prestained protein ladder (Thermo Scientific; 26619)

was loaded as protein ladder. Samples from co-immunoprecipitation experiments (2.5.1) were also resolved via the LI-COR system.

Table 2.3 – List of antibodies along with species, manufactures and dilutions used. M – mouse; R – rabbit; G – goat; S - sheep

Antibody	Manufacture	Species	Dilution
β-actin	Cell Signalling, #3700s	M	1:5000
HIF-1α	BD Biosciences, 610958	M	1:1000
HIF-1α-OH (Hyp564)	Cell Signalling, #3434	R	1:1000
HIF-2α	R&D, AF2886	G	1:1000
VHL	Cell Signalling, #2738	R	1:1000
VHL	Cell Signalling, #68547	R	1:1000
CA9	Novus Biologicals, NB100-417	R	1:1000
PHD2	Bethyl Laboratories, A300-322A	R	1:1000
PHD3	Bethyl Laboratories, A300-327A	R	1:1000
GLUT1	Cell Signalling, #12939	R	1:1000
BNIP3	Abcam, ab10433	M	1:10000
HK2	Cell Signalling, #2867S	R	1:2000

2.4. Luciferase assay

HeLa and U2OS cells stably expressing a luciferase reporter gene (HRE luciferase reporter) as described in (222) were used to examine HIF transcriptional activity. HeLa-HRE and U2OS-HRE cells were seeded in 12-well plate at 2.5×10^5 and

2.0×10^5 cells per well, respectively, one day prior to treatment with compounds. Medium was replaced with fresh pre-warmed medium, followed by treatment of cells with indicated compounds for optimised treatment time of 24 h (HeLa) or 32 h (U2OS). Following compound treatment, medium was removed, and cells were washed gently with 1 × PBS twice. After removing the final wash, cells were lysed in 200 µL of 1 × passive lysis buffer (Promega). The 12-well plate containing lysed cells was stored in freezer at −20 °C to be frozen (at least 1 h) and thawed at room temperature on a shaking platform to enhance cell lysis. From here onwards, cell lysates were handled at room temperature and stored in −80 °C freezer. Cells were scraped off the well and lysates from each well were transferred to a microcentrifuge tube. Cell debris was pelleted by centrifugation at 13,200 rpm, and supernatant was transferred to a new microcentrifuge tube. Luciferase assays were performed according to the manufacturer's instructions (Promega). Briefly, 5 µL of the supernatant was pipetted into a Sarstedt round-bottom polystyrene tube (Thermo Scientific; 50-809-212) that is compatible with Berthold Lumat LB 9507 Luminometer. The tube containing supernatant was placed in the Luminometer that had been set to add 50 µL of luciferase assay reagent (Promega) into the tube. Luciferase activity was measured 10 sec after the addition of reagent by the Luminometer. Results were normalised for protein concentration (quantified using Bradford assay [Biorad]), with all experiments being performed a minimum of three times before calculating means and standard deviations.

2.5. Co-immunoprecipitation

2.5.1. Co-immunoprecipitation for hydroxylated HIF-1α using sepharose beads

HeLa cells were seeded onto 15 cm plate one day prior to treatment with compounds. Compounds were added to cells in fresh media and left for two hours in the 37 °C

incubator. After treatment, cells were washed with 1 × PBS twice and lysed in 350 µL of whole cell lysis buffer as described in section 2.1.1. Protein was quantified using Bradford assay as described in 2.2.1. A total of 300 µg of cell lysates were used per immunoprecipitation condition. Protein lysates were incubated with 1 µg of HIF-1α-OH antibody (Hydroxy-HIF-1α [Pro564], Cell Signalling, rabbit, #3434) or 1 µg of rabbit IgG antibody in a rotating platform at 4 °C overnight. Packed protein-G-sepharose beads (20 µl, Generon; PC-G5) were used to recover the immuno-complexes, by incubation in a rotating platform for 1.5 h at 4 °C. Lysates were collected as flow-through (FT) prior to 5 washes with 0.1% Tween-20 in 1 × PBS buffer. The complexes were eluted from beads with 20 µL of 2 × SDS-loading buffer (0.1 M Tris-HCL pH 6.8, 20% glycerol, 4% SDS, 0.2 M DTT, and a touch of bromophenol blue) and resolved as described above by immunoblotting (2.3.1).

2.6. Cellular Thermal Shift Assay

Cellular thermal shift assay (CETSA) was adapted from the supplementary of (223). HeLa cells were seeded on two 15 cm plates and left to incubate for one to two days until the cells grew to 85-90% confluent. Media was removed and cells were washed once with 1 × PBS. Cells were harvested with trypsin/EDTA and resuspended in 0.8 mL of 1 × PBS containing one protease inhibitor cocktail tablet [Roche] per 10 mL of buffer. Cells were lysed by four freeze-thaw cycles using liquid nitrogen (thawing at room temperature). The soluble fraction (lysate) was separated from the cell debris by centrifugation at 13,200 rpm for 20 min at 4 °C. The lysate was divided into two aliquots, with one aliquot being treated with 100 µM of VH298, and the other aliquot with vehicle (1% DMSO). After 10-30 min incubation at room temperature, the two fractions were divided into smaller aliquots (50 µL), and heated individually at different temperatures (40.4, 42.4, 44.6, 48.1, 49.9, 53.3, and 55.4 °C) in a PCR machine for

3 min followed by cooling for 3 min at room temperature. Note that these temperatures can be adjusted according to the PCR machine used. The heated lysates were centrifuged at 13,200 rpm for 20 min at 4 °C, pellets were removed and the soluble fractions were analysed by SDS-PAGE (refers to 2.3.1), and immunoblotted for VHL (Cell Signalling), stripped (0.25 M glycine pH 2, 1% SDS), and washed before being immunoblotted for PHD2 (Bethyl Laboratories). Raw images were processed using ImageJ. Non-heated cell lysates were established as 100% intensity for each condition, and data quantified relative to that condition and plotted with Graphpad.

2.7. Flow cytometry analysis of cell cycle profile

HeLa or U2OS cells were seeded one day prior at the dentisity 2×10^5 to compound treatment on 6-well plate. Cells were treated with indicated compounds for 24 h and harvested by trypsin/EDTA. Cells were pelleted and washed once in 1 × PBS before fixing in 1 mL ice cold 70% ethanol. Fixed cell suspensions can be stored in the freezer (-20 °C) until ready for cell cycle profiling. A total of 400 µL fixed HeLa cells or 1 mL of fixed U2OS cells were centrifuged at 450 × g for five min to pellet cells. Ethanol was removed and cell pellet was washed in 500 µL of 1 × PBS. Following another centrifugation at 450 × g for five min, 200 µL of pre-warmed Guava Cell Cycle reagent (Millipore) was added to the pelleted cells and mixed gently by pipetting. After incubation at room temperature for 30 min in the dark, cells were analysed for their cell cycle profile with Guava easyCyte HT software. Red fluorescence was evaluated on a linear scale and pulse width analyses were used to determine cell doublets and cellular aggregation. Cells with DNA content between 2N and 4N were designated as being in G1, S or G2/M phase of the cell cycle. The number of cells in each phase was expressed as a percentage of the total number of cells counted.

2.8. Cell viability assay

2.8.1. CellTiter-Glo luminescent cell viability assay

Cell viability was analysed using CellTiter-Glo luminescent cell viability assay (Promega) according to manufacturer's instruction. Briefly, the number of cells seeded onto the 384-well plate was optimised for each cell line. Note that cells were plated with the Matrix WellMate liquid dispenser to ensure uniform plating. Cells were plated in 384-well plates (1000 RCC4 cells per well and 1500 HFF, HeLa or U2OS cells per well) in a total volume of 25 µL media one day prior to treatment with VHL inhibitors and respective non-binding *cis*-analogues. Following 24 h treatment with the compounds, cells and CellTiter-Glo reagent were equilibrated at room temperature for 30 min. Cells were then incubated with 25 µL CellTiter-Glo reagent in the dark on an orbital shaker to induce cell lysis, followed by 10 min incubation at room temperature in the dark to stabilise luminescent signal. Luminescence was measured using a PHERASTAR plate reader (BMG LabTech).

2.8.2. Proliferation assay

A total of 1.5×10^5 cells were seeded in six-well plates one day prior to treatments with VHL compounds. At treatment times of 0, 24, 48, and 72 h, cells were detached using 400 µL of trypsin, followed by the addition of 600 µL of media to stop the trypsinisation reaction. Cells were then counted using haemocytometer.

2.8.3. Colony formation assay

A total of 500-2000 cells were seeded in a six-well plate one day prior to treatments with VHL compounds. After 24 h of treatment, media was changed and cells were further incubated for one week. Cells were washed with 1 × PBS twice and stained with 2 mL 0.005% (w/v) crystal violet in 25% (v/v) methanol for 10 min at room

temperature. The staining was washed off with water and plates were left to dry overnight. Numbers of colonies formed were counted with the M-tools suite from OMERO on the scanned plates.

2.9. RNA Sequencing

2.9.1. Sample Preparation

HeLa cells were seeded in 35 mm dishes at 2×10^5 one day prior to treatments with 1% DMSO, hypoxia (1% O_2), 250 µM IOX2, or 250 µM VH032 for 16 h. RNA was extracted as described in section 2.4. , and DNAse treatment (RNase free DNase from Qiagen; 79254) was included according to manufacturer's instruction. Experiments were performed in six replicates. RNA samples were handed to Andrew Cassidy from the Genetic Core Services Unit in Dundee, who performed the quality control test, library preparation and running of the samples on the NextSeq 500 platform. RNA ERCC ExFold RNA Spike-In Mix (Mix1 and Mix2) was distributed throughout the RNA-Seq experiment.

2.9.2. Data Analysis

FastQ files containing reads were quality-controlled with *fast*QC (http://www.bioinformatics.bbsrc.ac.uk/projects/fastqc). The raw sequence reads from each replicate were aligned to the Ensembl human genome GRCh37 and ERCC sequence with STAR. The aligned reads were combined and number of read for each gene was counted with subread-featureCounts pipeline (224). The files were found to contain ribosomal DNA (rDNA) contaminations, majority of which were the following two mitochondrial DNA: ENSG00000211459 and ENSG00000210082 – which were removed manually. Differential gene expression analysis was then performed by the R--package *edgeR* according to its user guide (225).

2.10. Tandem mass tag labelling mass spectrometry

2.10.1. Sample preparation

A total of 1×10^6 HeLa cells were seeded on four 6 cm plate one day prior to cell treatment. Cells were treated with 0.05% DMSO, hypoxia, 250 μM IOX2 and 250 μM VH032 for 24 h. Cells were lysed as described in section 2.1.1, but in 4% SDS in 100 mM Tris-HCl, pH 8.5 and one protease inhibitor cocktail tablet [Roche] per 10 mL of buffer. Lysates were sonicated for 6 cycles of 30 sec on low power setting with Bioruptor™ Twin (Diagenode). Wenzhang Chen from the FingerPrints Proteomic group, Dundee, performed protein digestion, TMT-labelling (TMT 10 plex™ Isobaric label reagent set from Thermo Scientific; 90110), fractionation of peptides and database search against human protein sequences (Sprot) using the Mascot search engine (Matrix Science, Version 2.2) through proteome discovery software (version 1.4).

2.11. Co-immunoprecipitation mass spectrometry

2.11.1. Sample preparation

HeLa cells were seeded on five 15 cm plates one day prior to treatment with 1% DMSO (two plates, one for IgG control), 20 μM MG132, 100 μM VH298, or a mix of 20 μM MG132 and 100 μM VH298. After 3 h compound treatment, cells were lysed in the 250 μL of MS lysis buffer as described in section 2.1.4. Protein was quantified by Bradford assay as described in section 2.2.1. A total of 750 μg of protein lysate were used per immunoprecipitation condition. Prior to immunoprecipitation, 50 μg of Dynabeads® Protein G (Thermo Scientific, 10003D) were incubated with 6 μg of VHL antibody (BD Biosciences, mouse, 556347) or negative control mouse IgG in a rotating platform at 4°C for 10 min. The antibodies-coated beads were then incubated with 750 μg of cell lysates in a rotating platform at 4°C overnight. Following

immunoprecipitation, the beads were washed with 300 µL of ice-cold 50 mM ammonium bicarbonate thrice. Before removing the last wash, one-third of the total complexes (100 µL) was transferred to a fresh Eppendorf tube, supernatant was removed and the co-IP complex was eluted from beads with 20 µL SDS-loading buffer for immunoblotting.

The following protocol was mainly carried out by Kelly Hodge from GRE proteomic support group, Dundee. The remaining beads (two-third of the total complexes) were resuspended in 50 µL of 50 mM ammonium bicarbonate supplemented with 10 mM DTT, and incubated at ambient temperature for 1 h on a shaking platform. 20 mM iodoacetamide was added to the mixture and incubated on a shaking platform in the dark for 15 min at ambient temperature. Immuno-bound proteins were digested on the beads with 1 µg trypsin (Roche) at 37°C for 1 h. The supernatant was removed and the remaining beads were resuspended in 40 µL of 50 mM ammonium bicarbonate for subsequent re-trypinisation (1 µg, 37°C, overnight). All supernatants were pooled. The acquired peptide mixture was cleaned using a C18 resin matrix and eluted with 25% acetonitrile prior to drying. Resuspended peptides were analysed by on-line nanoLC-MS/MS using a LTQ OrbiTrap Velos Pro (Thermo Scientific) coupled to the Ultimate 3000 RSLCnano system (Thermo Scientific). Peptides were loaded on a PepMap 100 C18 column (100 µM x 2 cm, Dionex) in 0.1% formic acid, and subsequently separated on an Easy-Spray PepMap RSLC C18 column (75 µM x 50 cm, Dionex), using 80% acetonitrile in 0.08% formic acid buffer. Separation was performed with a 2-40% gradient and a 0.3 µL/min flow rate for 156 m. The OrbiTrap Velos Pro was operated in data dependent acquisition mode. MS spectra were acquired in the mass range of 335-1800 m/z at a resolution of 60,000 full width at half maximum (FWHM). The 15 most abundant ions were analysed by Ion Trap MS/MS.

3. Characterisation of VHL inhibitors

3.1. Introduction

Hypoxia, which occurs when oxygen demand exceeds supply, is an important physiological and pathological stimulus (11). Furthermore, components of the hypoxia response pathway are evolutionary conserved in multicellular organisms (226). The cellular response to hypoxia is mediated by the action of the Hypoxia-Inducible Factors (HIFs), a family of transcription factors activated in hypoxia.

The hypoxia pathway represents a compelling therapeutic target, given that it plays a major role in a wide range of diseases. The pathway has been historically targeted to enhance or inhibit the stabilisation of HIFs through the knockdown/knockout of the HIFs or PHDs and more recently through pharmacological approaches. HIF stabilisers described in 1.4. have been widely used as in biochemical and biomedical research, however they affect multiple pathways and have poor target selectivity, which limit their scope as chemical tools for understanding the hypoxia signalling.

Alternative to the abovementioned targets for activating HIFs, the VHL E3 ubiquitin ligase, which is the master regulator of HIFs also represents an attractive target for the stabilisation HIFs. Development of a potent inhibitor of the VHL:HIF-α protein–protein interaction would allow intervening in the HIF pathway downstream of PHD enzymes and potentially in a more selective fashion; this may avoid the HIF-independent off-target effects observed with PHD inhibitors (211).

Small molecules disruptors of the VHL:HIF-α interaction had been previously developed, but were ineffective in the induction of HIFs in cells because of their limited potency (211-213). In order to achieve compound-induced HIF-α activity and a pseudo-hypoxic response, inhibitors would have to bind VHL as strongly as possible to be able

to compete with its high affinity for the endogenous hydroxylated HIF-α substrates inside cells (215).

At the beginning of my PhD project, the Ciulli group had just reported a VHL inhibitor series with *in vitro* nanomolar binding affinities, which included VH032 (also called ligand 7 in the published data) (214). VH032 was the most potent VHL inhibitor reported in this study, with a dissociation constant (K_d) of 150±30 nM as assessed in competitive fluorescence polarisation (FP) assay and 185±6 nM as determined by isothermal titration calorimetry (ITC) (Table 3.1). Based on the X-ray crystal structure of VH032 bound to VHL:ElonginB:ElonginC (VBC) complex, the Ciulli group designed and synthesised a new series of VHL inhibitors. Carles Galdeano and Pedro Soares of the Ciulli group performed FP and ITC to measure the binding of these VHL inhibitors and identified VH101 to be the first double-digit nanomolar affinity binder to VBC, with a measured Kd of 90±10 nM by FP and 44±9 nM by ITC Table 3.1.

The Ciulli group also generated suitable negative control compounds that do not bind to VHL, but maintain as closely as possible the physiochemical properties of the parent binder. For VH032 and VH101, the respective inactive epimers are the *cis*-hydroxyproline analogues *cis*VH032 and *cis*VH101, respectively. This change in stereochemistry at the carbon atom bearing the hydroxyl group of the hydroxyproline ring results in the loss of binding for VBC as shown by ITC by Pedro Soares (Table 3.1). This result confirmed that the stereospecific effect that had previously been observed in the context of the HIF peptide (227) is retained in the context of VHL inhibitors. These inhibitors, however, had not been investigated with regards to their effectiveness at stabilising HIF-α in cells.

Therefore, the aim of the work presented in this chapter was to determine whether VHL inhibitors are able to activate HIFs and presented suitable alternative chemical tools for

studying the hypoxia signalling pathway in cells. Here, VHL inhibitors VH032 and VH101 were shown to stabilise transcriptionally active HIF-α, but VH101 was discovered to be cytotoxic at the concentration used. A new series of VHL inhibitors were then screened for their ability to accumulate HIF-α, and VH298 was found to be the best and not toxic at the maximum concentration used (250 μM).

Table 3.1 – Chemical structures, and dissociation constants measured by FP and ITC of VH032 and VH101 by Carles Galdeano and Pedro Soares. Figures of chemical structures were provided by Pedro Soares

Inhibitor	Chemical Structure	Kd FP (nM)	Kd ITC (nM)
VH032	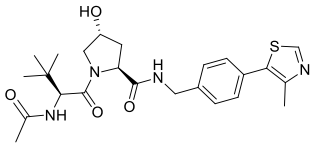	150 ± 30	185 ± 6
VH101	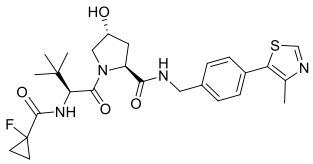	90 ± 10	44 ± 9
*cis*VH032	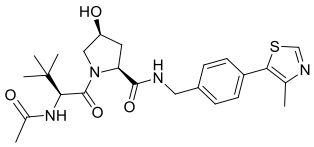	Not tested	No binding
*cis*VH101	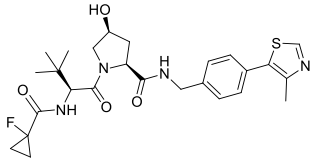	Not tested	No binding

3.2. VHL inhibitors VH032 and VH101 stabilise hydroxylated HIF-1α

To determine the ability of VHL inhibitors VH032 and VH101 to stabile HIF-1α protein in cells, HeLa cells were treated with VH032 or VH101 at different concentrations for 2 h; time course experiments showed that the level of accumulated HIF-1α was the highest at 2 h (not shown). In the presence of VH032 (Figure 3.1**A)** or VH101 (Figure 3.1**B**), HIF-1α protein levels increased in HeLa cells in a dose-dependent manner, but not when the inactive epimers *cis*VH032 and *cis*VH101 were used (Figure 3.1**A** and **B**). The maximum HIF-1α protein level was achieved with 250 μM VH032 inhibitor (Figure 3.1**A**) and 150 μM VH101 (Figure 3.1**B**). Immunoblots with antibodies specific for HIF-1α hydroxylated at Pro564 (HIF-1α-OH) showed increased levels of this HIF-1α form only after treatment with the VHL inhibitors VH032 and VH101, and proteasome inhibitor MG132, but not with $CoCl_2$ and IOX2 (PHD inhibitors). This observation is consistent with notion that disruption of the VHL:HIF-α interaction by VHL inhibitors occurs downstream of HIF-α hydroxylation by PHDs.

Serum proteins may bind to small molecule drug-like compounds and subsequently decrease the concentration of free active drugs that can penetrate into cells. In cell treatment experiments, 10% fetal bovine serum (FBS) is used in the growth medium. To investigate if the presence of serum affects the activity of VHL inhibitors, HeLa cells were treated with VH032 and VH101 in the presence of growth medium containing 0-10% of FBS (Figure 3.1**C** and **D**). The presence of FBS did not alter the stabilisation profiles of HIF-1α and hydroxylated HIF-1α induced by VH032 (Figure 3.1**C**) or VH101 (Figure 3.1**D**), indicating that VH032 and VH101 activity is not significantly altered by the presence of serum in the growth medium.

Here, VH032 and VH101 were shown to be the first VHL inhibitors that stabilise HIF-1α in mammalian cells, demonstrating the ability of these inhibitors to enter the cells, and leading specifically to the accumulation of hydroxylated HIF-1α. This indicates that the mode of action of the VHL inhibitors is downstream of hydroxylation by PHD enzymes. Moreover, the activity of these small molecules was not affected by the presence of serum in the growth medium.

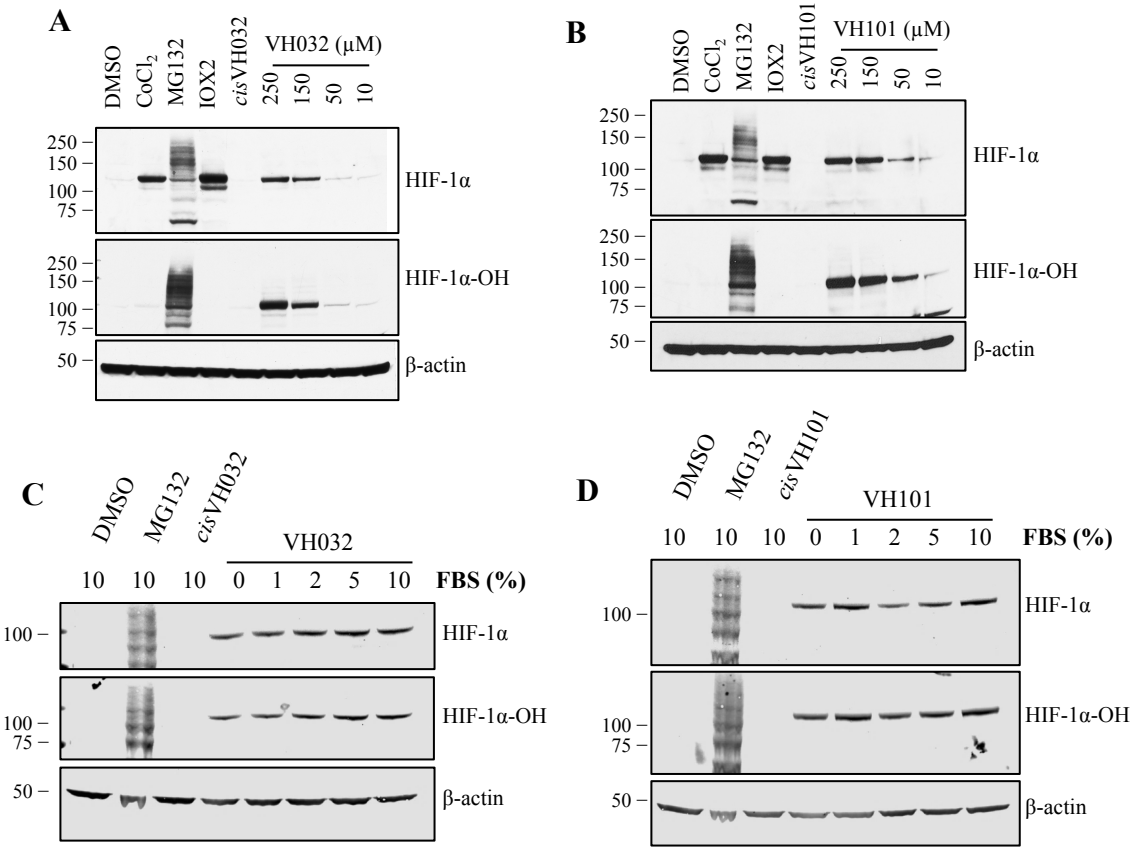

Figure 3.1 – VHL inhibitors VH032 and VH101 increase HIF-1α and hydroxylated HIF-1α levels independent of the presence of serum in the growth medium. HeLa cells were seeded on 6-well plates and treated for 4 h with 1% DMSO only (vehicle control), 4 h of 100 μM CoCl2 (hypoxia-mimetic condition), 4 h of 20 μM proteasome inhibitor MG132, 6 h of 250 μM PHD inhibitor IOX2, 2 h of 250 μM negative control of VHL inhibitor *cis*VH032 (**A**) or *cis*VH101 (**B**), and VHL inhibitor VH032 (**A**) or VH101 (**B**) at the concentration indicated. 150 μM VH032 (C) or VH101 (**D**) was used to treat HeLa cells in 6-well plates in the presence of 0, 1, 2, 5, and 10% FBS in fresh growth medium for 2 h. HeLa cells were also treated with 20 μM MG132 for 3 h and 150 μM *cis*VH032 (**C**) or *cis*VH101 (**D**) for 2 h in the presence of 10% FBS in fresh growth medium as positive and negative control, respectively. Protein levels were analysed by immunoblotting using antibodies against HIF-1α, HIF1α-OH (Hyp564), and β-actin, which acted as a loading control. Precision Plus protein standards (Bio-Rad) were used, ladder size in kDa.

3.3. VHL inhibitors VH032 and VH101 induce transcriptionally active HIF-α

To investigate the ability of VHL inhibitors to promote HIF activity, a luciferase reporter assay was performed. In HRE-luciferase reporter cells, HeLa-HRE and U2OS-HRE, treatments with VHL inhibitors VH032 and VH101 exhibited marked concentration-dependent increase of HIF-dependent luciferase activity, consistent with hypoxia and IOX2 treatments, while no activity was observed with high concentration of non-binding epimers *cis*VH032 and *cis*VH101 (Figure 3.2**A** and **B**). Since VH101 is more potent than VH032 (Table 3.1), VH101 required a lower concentration (50 μM) than VH032 (150 μM) to reach the same level (threefold increase relative to control) of HIF activity in U2OS-HRE cells (Figure 3.2**A**). Consistently, at the concentration of 150 μM, VH101 induced a higher HIF activity (fourfold increase relative to control) than VH032 (threefold increase relative to control) in HeLa-HRE cells (Figure 3.2**B**). HIF activity of VH101 at 150 μM was comparable to hypoxia exposure and inhibition of PHDs by IOX2 at the same concentration, while VH032 required a higher dose (250 μM) in U2OS-HRE cells (Figure 3.2**A**). Peculiarly, VH101-induced HIF activity profile diminished in HeLa-HRE cells at high dosage of 250 μM (Figure 3.2**B**). Nonetheless, this analysis revealed that VHL inhibitors-induced HIFs are able to bind to HRE motifs and be transcriptionally active.

Increase of HRE-luciferase activity in the presence of VHL inhibitors would suggest that HIF-α stabilised by VHL inhibitors forms HIF dimer and binds to the HRE motifs of its target genes to drive the transcription process. To further assess HIF transcriptional activity induced by VHL inhibitor, mRNA levels of known HIF-target genes including *VEGF*, *GLUT1*, *CA9*, and *PHD2* were monitored in HeLa cells by

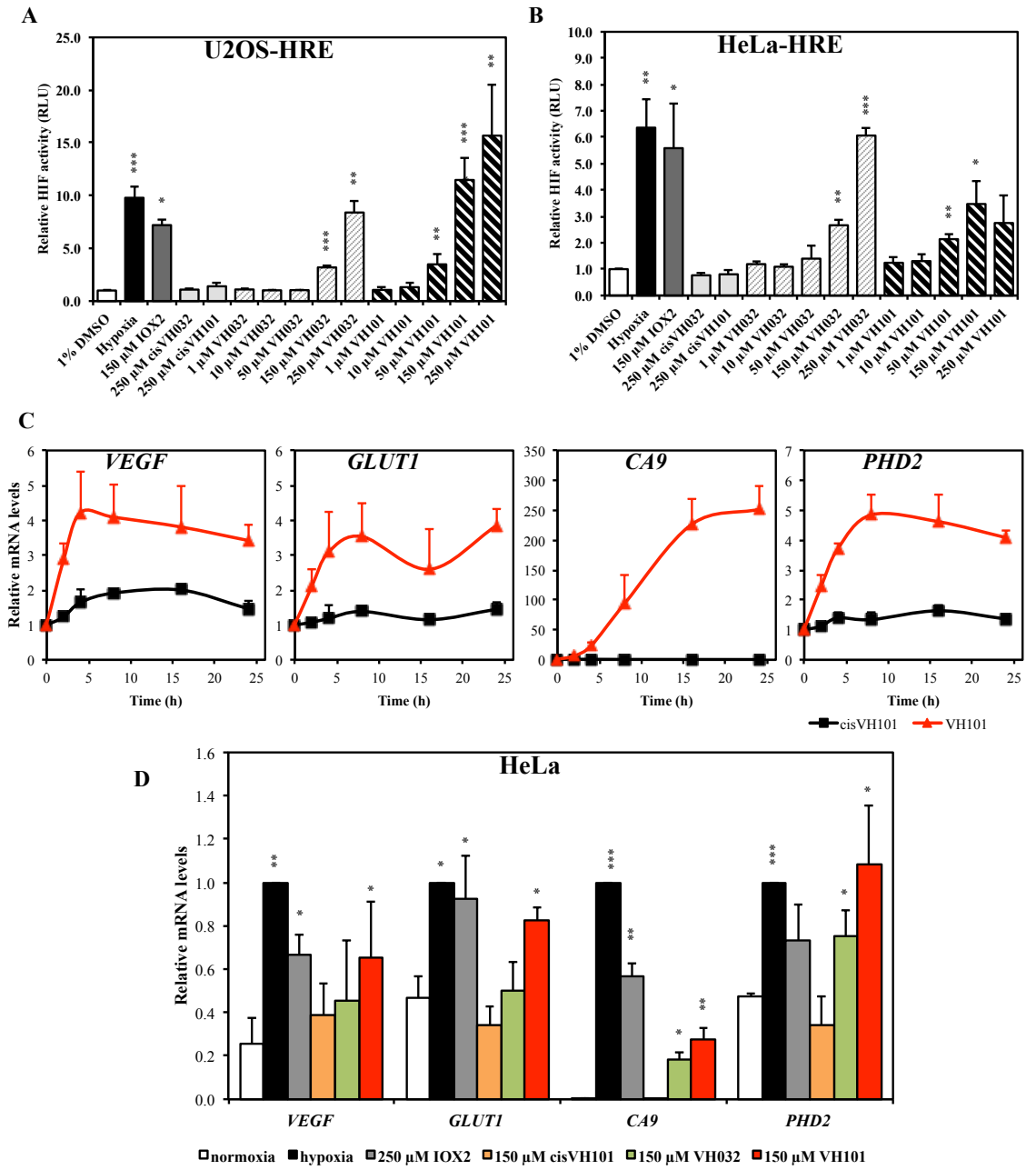

Figure 3.2– VHL inhibitors VH032 and VH101 induce HIF-α transcriptional activity. U2OS (**A**) and HeLa (**B**) cells stably expressing an HRE-luciferase reporter plasmid were treated with indicated conditions for 32 h and 24 h, respectively. (**C**) Time-dependent curves of HIF targets (*VEGF*, *GLUT1*, *CA9* and *PHD2*) mRNA expression in HeLa cells treated with 150 µM *cis*VH101 or VH101. (**D**) mRNA expression of HIF targets (*VEGF*, *GLUT1*, *CA9* and *PHD2*) in HeLa cells treated with 1% DMSO (normoxia control), 1% O_2 (hypoxia), IOX2, *cis*VH101, VH032 and VH101 for 16 h. mRNA was collected, reverse transcribed and analysed by qRT-PCR. The levels of the indicated mRNAs were normalised to those of β-actin. Graphs depict the mean + SD of three independent biological replicates. Two-tailed student's t-test was performed to calculate p values, and levels of significance are denoted as follows: *P<0.05, **P<0.01, and ***P<0.001.

quantitative real-time PCR (qRT-PCR). Time-course treatment with VH101 resulted in marked upregulation of HIF-target genes, but not with inactive epimer *cis*VH101 (Figure 3.2**C**). mRNA of *VEGF* reached the maximum levels with the shortest treatment time (4 h) amongst the HIF-target genes examined, whereas *CA9* required the longest presence of VH101 (16 h) (Figure 3.2**C**). Since 16 h treatment with VH101 induced significant increase in mRNA levels of the four genes tested, 16 h treatment time was used in the coming experiments assessing mRNA levels of HIF-target genes. VH032 and VH101 resulted in significant increase in the mRNA levels of the genes monitored, but this was not observed when the negative control *cis*VH101 was added to HeLa cells (Figure 3.2**D**). The more potent cellular activity of VH101, when compared with VH032, was further confirmed as VH101 treatment induced higher increase in mRNA levels of all the genes analysed than treatment with VH032 at equimolar concentration and identical treatment time (Figure 3.2**D**). Together, the results obtained demonstrate that pharmacological inhibition of VHL by small molecules stabilises transcriptionally active HIFs and that VH101 is a more potent VHL inhibitor than VH032.

3.4. VHL inhibitors VH032 and VH101 do not alter cell cycle

In addition to its role in oxygen sensing, VHL has been associated with other biological processes (140), and one of such is mitosis (228-230). VHL suppresses spindle misorientation by protecting microtubules from depolymerisation and thereby stabilising the microtubules (228). In addition, VHL plays a role in maintaining normal mitotic checkpoint control and resultant chromosomal stability as the inactivation of VHL causes reduced level of Mad2 that controls the spindle checkpoint function (229). To determine whether the inhibition of VHL at the interface where HIF-α binds might affect VHL function on mitosis, cells treated with VHL inhibitors were analysed by flow cytometry for their cell cycle profiles. Whereas inhibition of PHD2 by IOX2 and VHL by VH032 caused little or no significant alteration of the cell cycle profile in

U2OS cells (Figure 3.3**B**), both increase the G1 population of HeLa cells (Figure 3.3**A**). Apart from altering the cell cycle profile of cells, VH101 and its non-binding inactive analogue *cis*VH101 also resulted in an increase of cell death (Figure 3.3**A** and **B**), thus rendering their effect on cell cycle unreliable. Nonetheless, the increase in G1 population exhibited in IOX2- and VH032-treated cells may be the effect of the stabilised HIF-1α, which has been shown to result in G1 cell cycle arrest due to the HIF-1α-dependent upregulation of CDK inhibitors p27 and p21 (231).

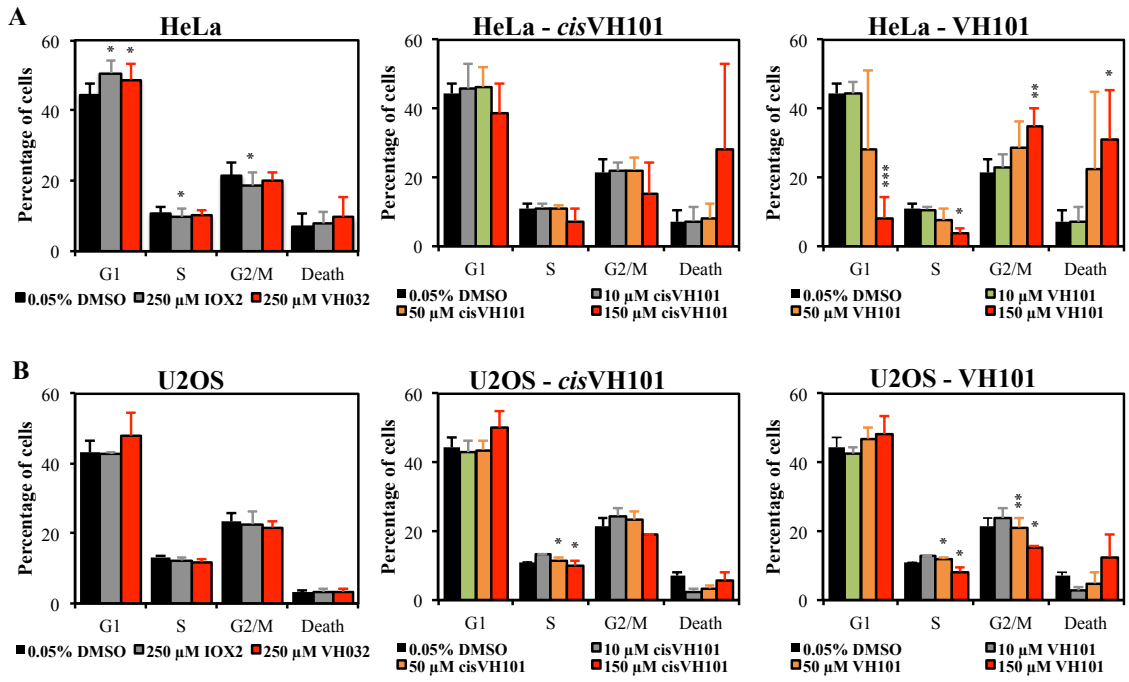

Figure 3.3 – VHL inhibitors VH032 and VH101 do not significantly alter cell cycle. Cell cycle profile graphs of HeLa (**A**) and U2OS (**B**) cells were treated with indicated conditions for 24 h. Graphs depict the mean + SD of three independent biological replicates. Two-tailed student's t-test was performed to calculate p values, and levels of significance are denoted as follows: *P<0.05 and **P<0.01.

3.5. VH101 is cytotoxic, but not VH032

VHL inhibitors could serve as a useful tool for the study of the biological functions of VHL and may have the potential to be an alternative therapeutic target in the hypoxia pathway. Therefore, it is important that VHL inhibitors are not toxic and act selectively on-target inside cells. However, analysis of the cell cycle profile of cells (Figure 3.3) showed that treatment with VH101 and its non-binding epimer *cis*VH101 resulted in cell death. To further investigate if VHL inhibitors are cytotoxic, several experiments assessing cellular viability were performed.

3.5.1. Cell proliferation and viability assay by trypan blue exclusion

First, cell proliferation in the presence of VHL inhibitors VH032 and VH101, and their respective negative control compounds (*cis*VH032 and *cis*VH101) were assessed. The number of HeLa and U2OS cells were counted from starting time point of 0 h (cells were seeded one day prior) to 72 h in the presence of compounds for every 24 h using trypan blue exclusion assay (Figure 3.4). VH032 and PHD inhibitor IOX2 treatments resulted in reduced proliferation (Figure 3.4**A**), which could be due to the abovementioned G1 cell cycle arrest observed in the analysis (Figure 3.3). VH101 and *cis*VH101 also resulted in a significant reduction in proliferation, particularly at higher concentrations: 50 μM for VH101 in both HeLa and U2OS cells, but 50 μM *cis*VH101 in U2OS and 150 μM *cis*VH101 in HeLa cells (Figure 3.4**B**). At 50 μM, VH101 reduced cell proliferation more efficiently than its non-binding analogue in both cell lines (Figure 3.4**B**), suggesting the inhibition of VHL could lead to reduced proliferation. Nevertheless, the reduced proliferation in the presence of *cis*VH101 indicates that the chemical composition of VH101 may be causing cytotoxicity.

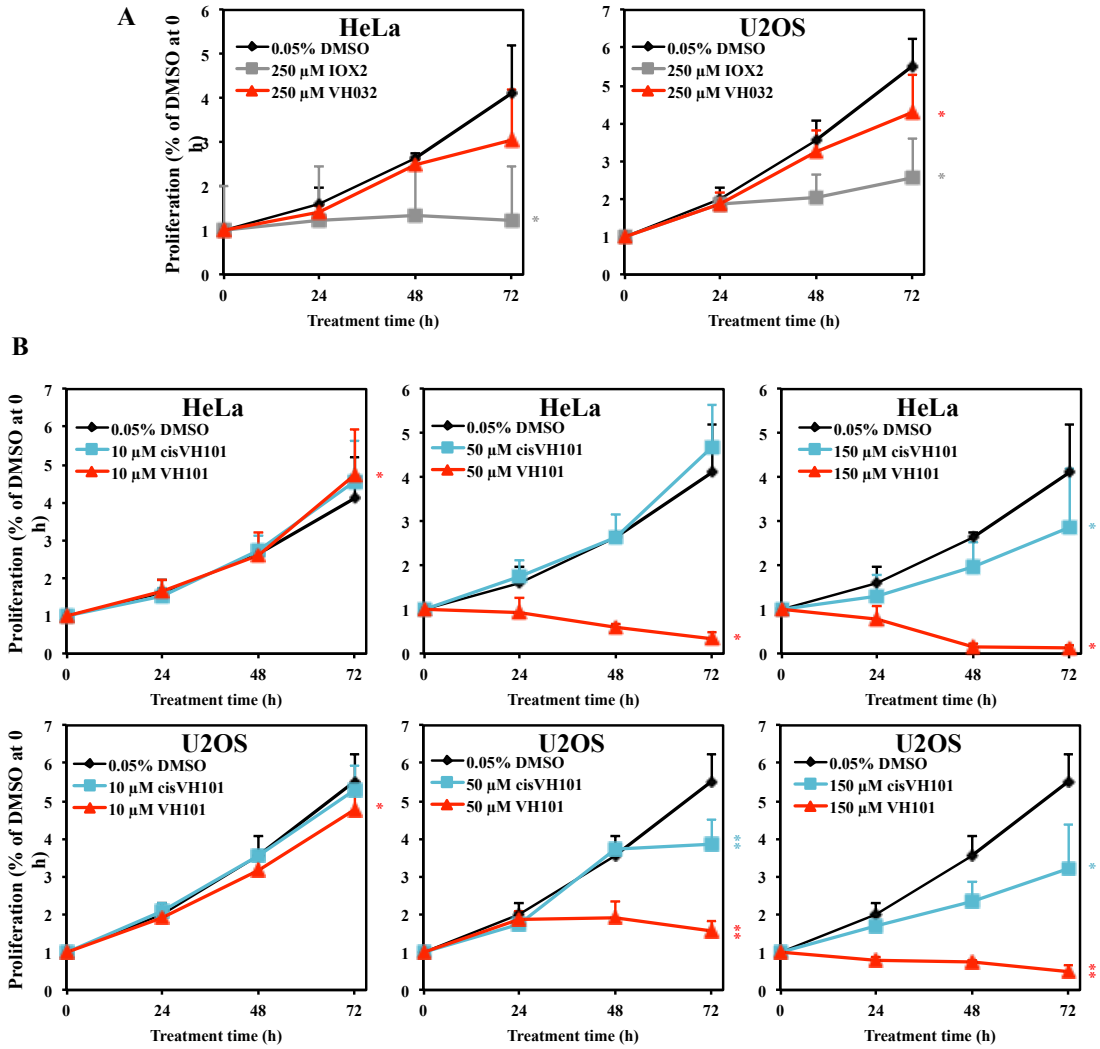

Figure 3.4 – VH101 impairs cell proliferation and viability, but not VH032. (**A** and **B**) Time-dependent proliferation curves of HeLa and U2OS cells treated with indicated compounds for 0, 24, 48, and 72 h. At the end of each treatment, cells were trypsinised and stained with trypan blue for counting. The levels of significant changes at 72 h treatments were determined. Graphs depict the mean + SEM of three independent biological replicates. Two-tailed student's t-test was performed to calculate p values, and levels of significance are denoted as follows: *P<0.05 and **P<0.01.

3.5.2. Clonogenic assay

To further substantiate the proliferation results, colony formation assay was performed. Low density of cells were treated for 16 h with compounds and allowed to grow for 1-2 weeks. Cells were stained with crystal violet to observe the ability of cells to form colonies. After the treatment with IOX2 and VH032, HeLa and U2OS cells were able to form colonies (Figure 3.5**A**) and quantification showed that there were no significant decreases in the colony numbers, with the exception of VH032 resulting in a slight drop of colony numbers in U2OS cells (Figure 3.5**B**). In contrast, cells treated with VH101 exhibited significant decrease of colonies formed and its inactive epimer *cis*VH101 also decreased the number of colonies, particularly in U2OS cells (Figure 3.5**A** and **B**).

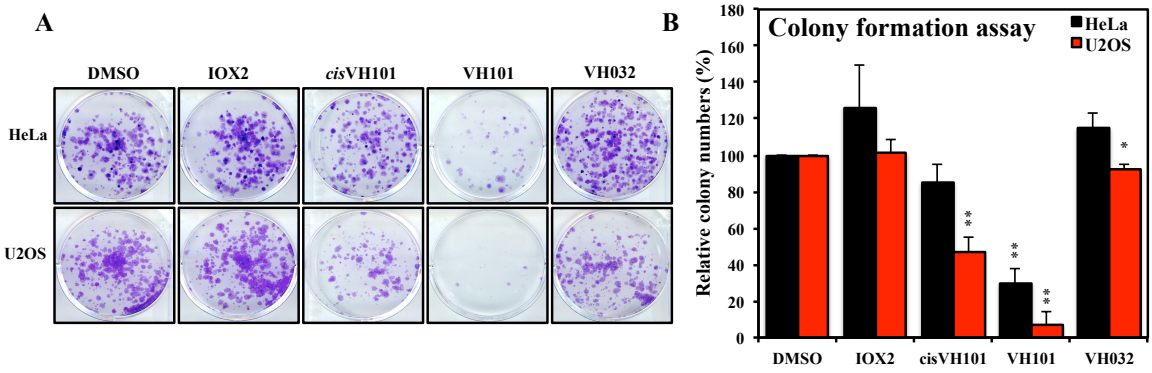

Figure 3.5 – VH101 impairs colony formation ability of cells, but not VH032. (**A** and **B**) HeLa and U2OS cells were seeded in 6-well plates at 1000-2000 cells per well and treated with 0.05% DMSO, 250 µM IOX2, 150 µM *cis*VH101, 150 µM VH101 and 250 µM VH032 for 16 h. After treatment, media were changed and incubated for 1-2 weeks. Cells were stained with crystal violet (**A**) and colonies formed were counted (**B**). Graphs depict the mean + SEM of three independent biological replicates. Two-tailed student's t-test was performed to calculate p values, and levels of significance are denoted as follows: *P<0.05 and **P<0.01.

3.5.3. CellTiter-Glo luminescent cell viability assay

To further confirm whether the decreased proliferation and colony formation are due to the inhibition of VHL by the inhibitors or the nature of the chemical composition of the VHL inhibitors, a high-throughput cytotoxicity assay (CellTiter-Glo luminescent cell viability assay) was performed for VH032 and VH101, as well as their respective inactive analogues (*cis*VH032 and *cis*VH101) in six cell lines: HeLa, U2OS, HFF, HEK293, and VHL-null RCC4 cells constituted with HA-tag (RCC4-HA) or HA-tagged VHL (RCC4-HA-VHL). The use of the two RCC4 cell lines would be ideal for differentiating cytotoxicity effect of the inhibitors from reduced cell proliferation due to VHL inhibition.

The viability of cells treated with VH032 or *cis*VH032 did not seem to be affected in the cell lines tested, up to the dosage of 250 μM and even a twofold increase to 500 μM (Figure 3.6**A**). However, in the presence of VH101 as well as *cis*VH101, cell viability notably decreased in all cell lines (Figure 3.6**B**), and crucially in a similar fashion for RCC4-HA compared to RCC4-HA-VHL, suggesting that the cytotoxicity of VH101 is due to its chemical properties and not the effect of VHL inhibition by VH101.

Collectively, cell proliferation, colony formation and CellTiter-Glo assay indicate that VH101 is cytotoxic, presumably via a mechanism other than due to on-target binding, and this is not case with VH032.

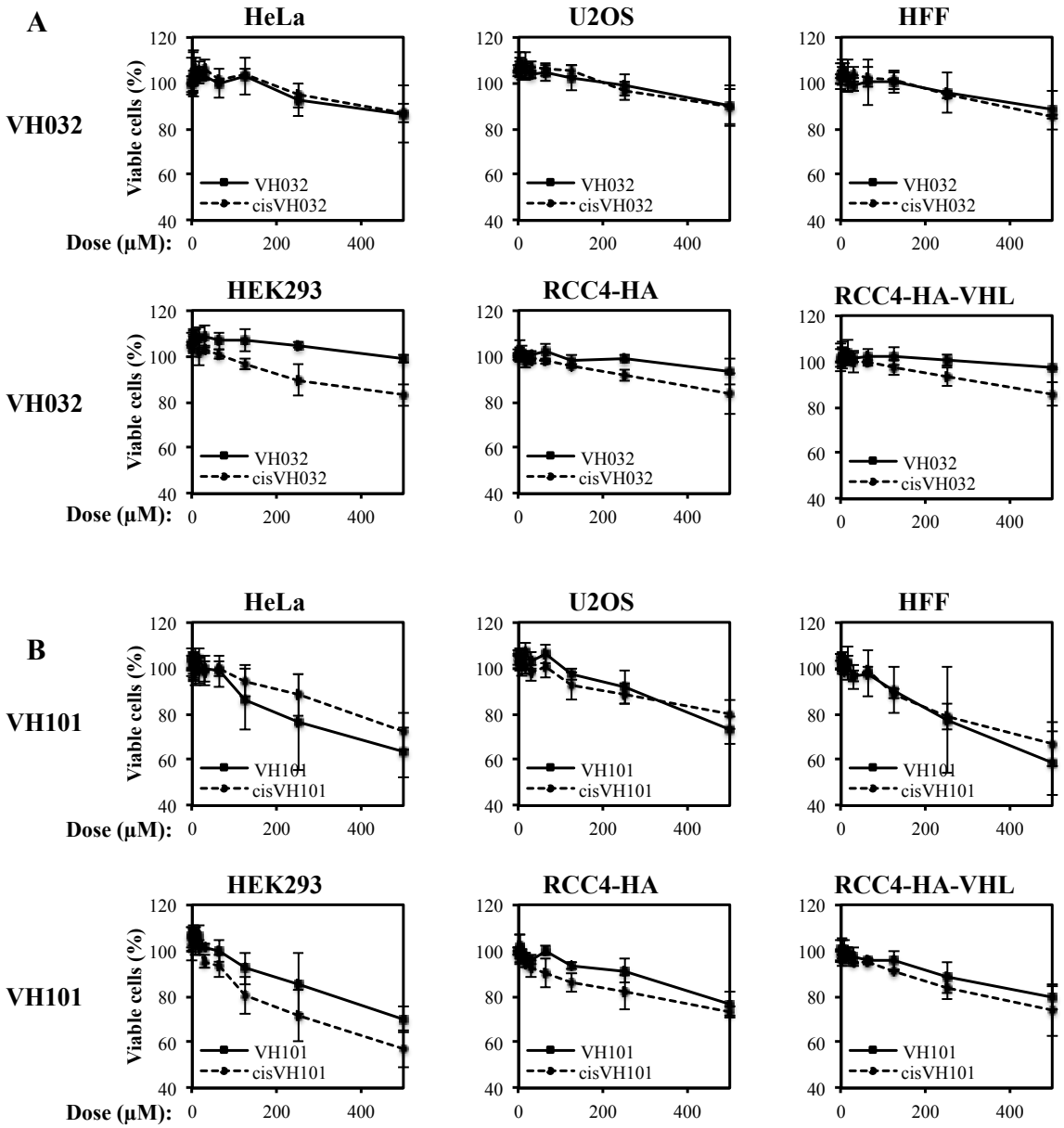

Figure 3.6 – VH101 induces cytotoxicity in cells, but not VH032. The viability of HFF, HeLa, U2OS, RCC4-HA and RCC4-HA-VHL cells treated with *cis*VH032, *cis*VH101, VH032 and VH101 for 24 h was determined using the CellTiter-Glo Luminescent Cell Viability Assay kit. Graphs depict the mean + SEM of three independent biological replicates.

3.6. VHL inhibitor screen

At this point, the discovery that the most potent VHL inhibitor VH101 is cytotoxic prompted the dropping of this compound from further biological studies. While the less potent inhibitor VH032 was not cytotoxic and able to upregulate transcriptionally active HIF-1α, it required to be used at relatively high dose to elicit HIF stabilisation in cells

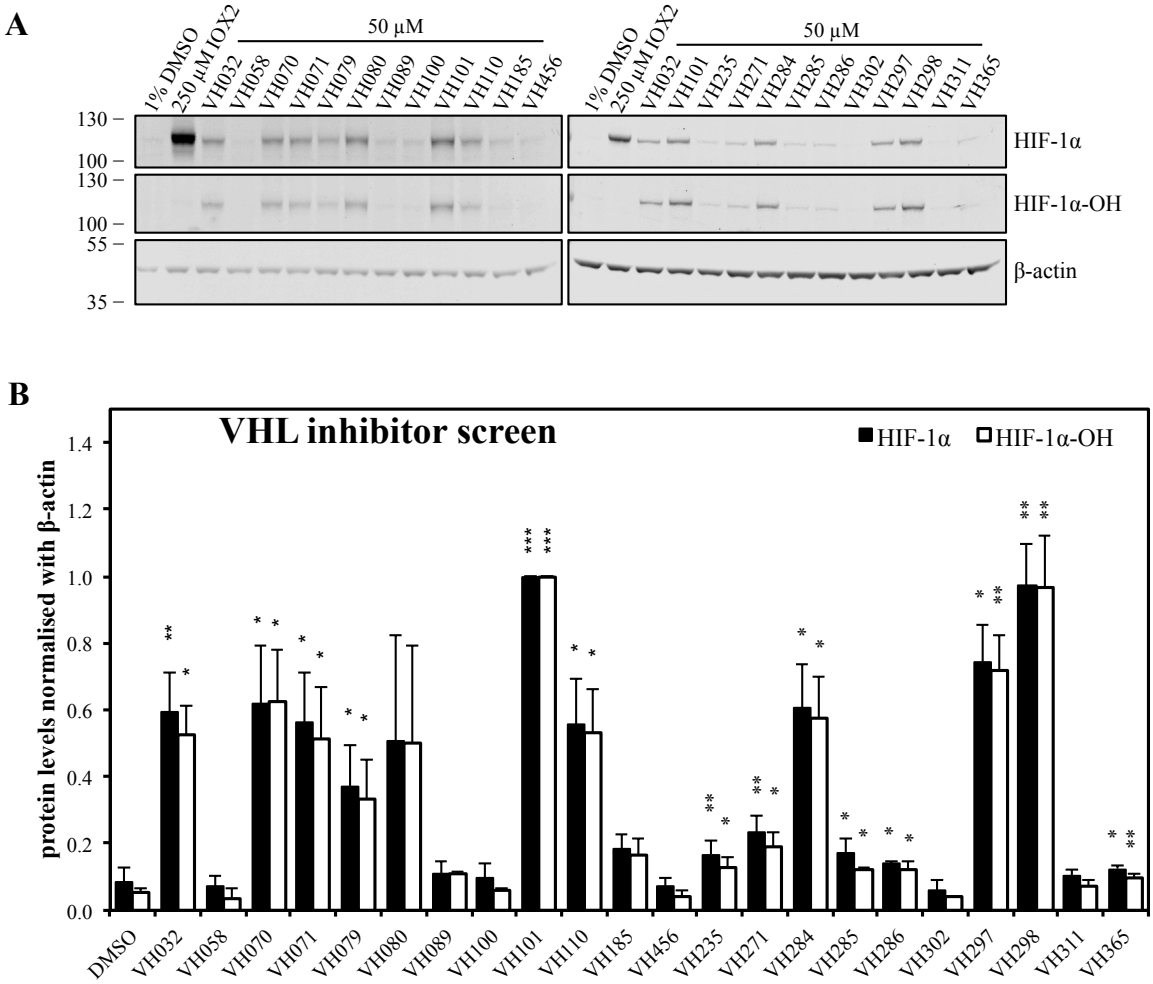

Figure 3.7 – VHL inhibitor screen. HeLa cells were treated with 50 μM VHL inhibitors for 2 h. DMSO (2 h) was used as vehicle control and PHD inhibitor IOX2 (2 h) as positive control for HIF-1α and negative control for HIF-1α-OH. (**A**) Protein levels were analysed by immunoblotting using antibodies against HIF-1α, HIF1α-OH (Hyp564), and β-actin, which acted as a loading control. PageRuler Plus Prestained protein ladder (Thermo Fisher) was used, ladder size in kb. (**B**) HIF-1α and HIF1α-OH (Hyp564) protein levels were quantified with LI-COR system. Graphs depict the mean + SD of three independent biological replicates. Two-tailed student's t-test was performed to calculate p values, and levels of significance are denoted as follows: *P<0.05, **P<0.01, and ***P<0.001.

Table 3.2 – Chemical structures, and dissociation constants measured by FP and ITC of VH284, VH297, VH298 and *cis*VH298 by Pedro Soares. Figures of chemical structures were provided by Pedro Soares.

Inhibitor	Chemical Structure	Kd FP (nM)	Kd ITC (nM)
VH284	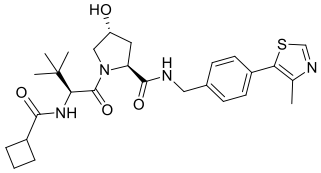	245 ± 50	210 ± 12
VH297	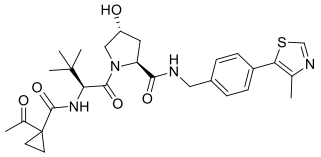	167 ± 30	106 ± 14
VH298	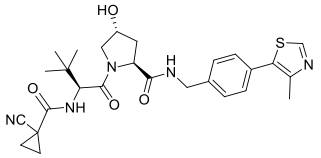	79 ± 30	90 ± 5
*cis*VH298	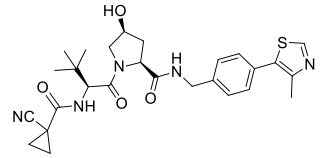	No binding	No binding

(Figure 3.1 and Figure 3.2). This inspired the Ciulli group to design a new series of VHL inhibitors by changing the left-hand side of VH032 and VH101 to structure that fits better to the VHL pocket with improved chemical property (key compounds tested further are listed in Table 3.2 and the rest are in Appendix Table 9.1), with the goal to identify a new inhibitor that would be more potent in cells than VH032, and not cytotoxic. FP, SAR and ITC were performed by Pedro Soares of the Ciulli group on these compounds, and based on the measured binding affinity of the inhibitors to VBC, number of them were selected to be screened by Western blotting for their ability to accumulate HIF-1α in cells (Figure 3.7). Western blots of lysates from HeLa cells treated with 2 h of VHL inhibitors were generated and HIF-1α and its hydroxylated form on Pro564 (HIF-1α-OH) were quantified using the LI-COR system. Consistent with its ability to induce a higher HIF transcriptional activity (Figure 3.2**A** and **C**),

VH101 stabilised a higher level of HIF-1α than VH032 (Figure 3.7). VH298 was the most potent of the novel compounds tested and stabilised HIF-1α and HIF-1α-OH, to a level similar to that observed using VH101. This was closely followed by VH297 (Figure 3.7**B**). The most active compounds VH298 and VH297, as well as VH284 that induced similar HIF-1α levels as VH032, were selected to be examined for their cytotoxicity effects.

3.7. Cytotoxicity screen for VH284, VH297 and VH298

To select non-toxic VHL inhibitor, the high-throughput screen CellTiter-Glo luminescent assay, for the assessment of cell viability was performed using VH284, VH297 and VH298 VHL inhibitors (Figure 3.8). The overall cell viability profiles of the three VHL inhibitors showed a higher decrease in cell viability at high concentrations of 500 μM (Figure 3.8), compared to that of VH032 (Figure 3.6). However, their respective inactive epimers (*cis*VH284, *cis*VH297 and *cis*VH298) demonstrated different cell viability profiles. In all the cell lines tested, *cis*VH284 cell viability curves were similar to that of VH284, except in HEK293, in which the inactive negative control *cis*VH284 induces a higher decrease in cell viability than its parent binder (Figure 3.8**A**). Treatment with inactive epimers, *cis*VH297 (Figure 3.8**B**) and *cis*VH98 (Figure 3.8**C**), resulted in smaller decreases in cell viability compared to their respective parent binders, VH297 and VH298, respectively, indicating the reduced cell viability of VH297 and VH298 could be due to the effect of VHL inhibition and not the cytotoxic effect of the compound composition. In addition, among the three negative control compounds, only *cis*VH284 exhibited cytotoxicity, suggesting that chemical properties of VH284 may be cytotoxic.

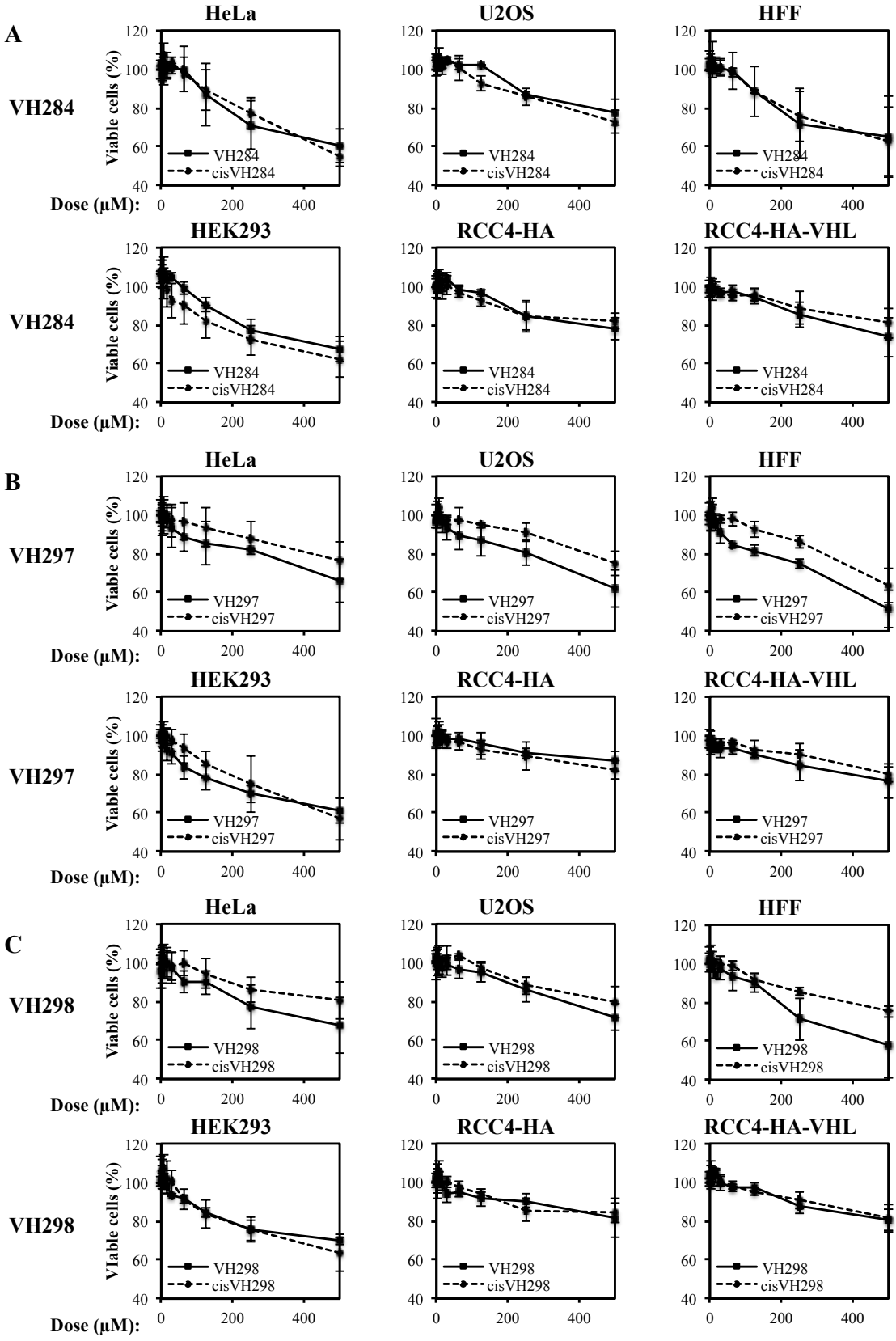

Figure 3.8 –VH298 and VH297 are not cytotoxic, but VH284 is. The viability of HFF, HeLa, U2OS, RCC4-HA and RCC4-HA-VHL cells treated with *cis*VH284, *cis*VH297, *cis*VH298, VH284, VH297 and VH298 for 24 h was determined using the CellTiter-Glo Luminescent Cell Viability Assay kit. Graphs depict the mean + SEM of three independent biological replicates.

3.8. VH298 is not cytotoxic

VH298 is the most potent VHL inhibitor screened (Figure 3.7) and its *cis*-hydroxyproline analogue shows no apparent cytotoxicity effect (Figure 3.8). However, to further confirm that levels of VH298 cytotoxicity were limited and tolerable, cell proliferation and colony formation assays were carried out in HeLa cells. VH298 and its inactive negative control *cis*VH298 did not alter cell proliferation rate (Figure 3.9**A**) and the ability of HeLa cells to form colonies (Figure 3.9**B** and **C**). Altogether, these data suggested that VH298 is not cytotoxic at the high micromolar concentrations required to be used in cells.

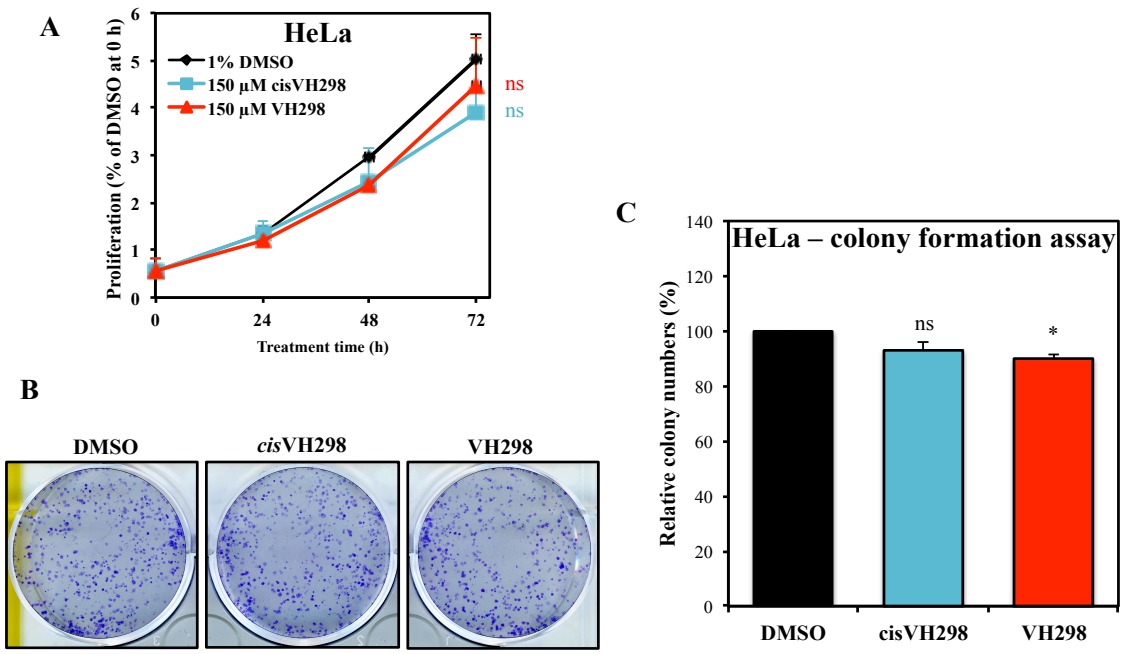

Figure 3.9 – VH298 is not cytotoxic in HeLa cells. (**A**) Time-dependent proliferation curve of HeLa cells treated with indicated compounds for 0, 24, 48, and 72 h. At the end of each treatment, cells were trypsinised and stained with trypan blue for counting. The levels of significant changes at 72 h treatments were determined. (**B**) HeLa cells were seeded in 6-well plates at 1000-2000 cells per well and treated with 0.05% DMSO, 150 µM *cis*VH298 and 150 µM VH298 for 24 h. After treatment, media were changed and incubated for 1-2 weeks. Cells were stained with crystal violet (**B**) and colonies formed were counted (**C**). Graphs depict the mean + SD of three independent biological replicates. Two-tailed student's t-test was performed to calculate p values, and levels of significance are denoted as follows: *P<0.05 and ns: P>0.05.

3.9. Discussion

Chemical probes that target different components of the hypoxia signalling to activate HIFs are useful tools for the study of this signalling pathway. One of the targets is the VHL E3 ubiquitin ligase. Previous studies have reported small molecules that bind the VHL protein at the interface where hydroxylated HIF-1α would normally bind, disrupting the interaction between VHL and HIF-1α (211-214). However, these VHL inhibitors were proven to be inactive in cells or had yet to be investigated for their activity in cells. The Ciulli group optimised the best inhibitor VH032 [ligand 7 from ref. (214)] at the time to improve binding affinities of VHL inhibitors, leading to the discovery of a more potent compound, VH101, possessing double-digit nanomolar binding affinity.

Herein, VH032 and VH101 were shown for the first time to stabilise hydroxylated HIF-1α that is transcriptionally active in cells. Consistently, the more potent binder VH101 induced a higher transcriptional activity than VH032 in HRE-reporter cell lines. Moreover, mRNA levels of HIF-target genes were higher in VH101-treated cells than following VH032 treatment. Altogether revealing that VH101 is more potent than VH032 in cells.

Unfortunately, VH101 and its non-binding analogue *cis*VH101 were found to be severely cytotoxic at the concentrations needed to be used in cells. Following cell cycle analysis, both compounds were found to result in cell death. VH101 and *cis*VH101 also greatly reduced cell proliferation and viability, and prevented HeLa and U2OS cells from forming colonies, suggesting that these compounds caused these cells to die. Although VH032 was active and non-toxic at concentration required in cells, a relatively high dose of up to 250 μM inhibitor was required to induce HIF activity to levels comparable to a hypoxic response.

To overcome these problems, the Ciulli lab designed another series of VHL inhibitors by optimising the left-hand side of VH032 and VH101, in order to improve the permeability of the inhibitor as well as alter the inhibitor to fit better to the VHL pocket; the latter was possible by assessing the crystal structure of VHL with the inhibitor. To identify the best compound, these compounds were initially screened by western blotting for HIF-1α protein levels. VH298 was found to be the best in stabilising HIF-1α protein levels, followed by VH297 and VH284. The three compounds were screened for cytotoxicity effects, which demonstrated that only VH284 was cytotoxic. VH298 was selected for further studies as the most potent VHL inhibitor, and at the same time was not cytotoxic at micromolar concentrations required to be used for biological studies in cells.

Potential contribution for the observed mismatch between the micromolar concentrations of the inhibitors required to stabilise HIF-1α in cells despite the nanomolar-binding affinities were also investigated. Amongst one possible reason considered was the presence of serum protein in the growth medium, which could affect the activity of VHL inhibitors in case of high serum protein binding. However, this was found not to be the case for the inhibitors tested (VH032 and VH101). With the discovery of VH298, the goal to improve the inhibitor activity in cells and reduce the dose required was ultimately achieved.

In summary, small molecule disruptors of VHL:HIF-α interaction were shown for the first time to stabilise hydroxylated HIF-1α that is transcriptionally active in cells.

4. Characterisation of VH298: a potent and selective VHL inhibitor

4.1. Introduction

Small molecules that bind, potently and selectively, to their protein target inside the cell can be useful chemical tools to study and perturb the molecular target in biological systems. These small molecule modulators are also known as chemical probes. In recent years, development of high-quality chemical probes (potent, with known target selectivity and proven mechanism of action) has enabled significant progress in both basic and translational research, and provided a starting point for the development of drugs (208,209). This is achieved through their unique advantages of being complementary to genetic approaches such as CRISPR and RNAi, as well as the probes' ability of rapidly and reversibly inhibit a target in any cell types or animals. Small molecule disruptors of VHL:HIF-α interaction could therefore serve as useful chemical probes to study the biology of the hypoxia signalling pathway.

In the previous chapter, VH298 was identified to be the best VHL inhibitor in accumulating hydroxylated HIF-1α and its cytotoxicity was tolerable in cells. In order for VH298 to meet the criteria for use as a potential chemical probe to address biology (i.e. potency, selectivity, on-target effect, lack of toxicity, amongst others), it is essential to fully characterise its cellular activity.

Here, the aim of the work presented was to characterise VH298 as chemical probe and elucidate further its potency, target engagement and mode of action in disrupting VHL:HIF-α interaction inside cells. The ability of VH298 to stabilise transcriptionally active hydroxylated HIF-α and consequently HIF-targets were also explored. One HIF-target gene increased was EPO that is required for the treatment of anaemic patient,

demonstrating possible therapeutic potential of VHL inhibitor. Overall, the results validated VH298 as the most potent VHL inhibitor thus far and a high-quality chemical probe.

4.2. Biophysical and structural characterisation of VH298

As VH298 was the best compound assessed in the cellular activity assay (Figure 3.7) amongst the VHL inhibitor screened, VH298 and its inactive *cis*-hydroxyproline analogue *cis*VH298 were first characterised for their binding affinity to recombinant VHL protein by other members of the Ciulli Lab. VH298 and *cis*VH298 (Figure 4.1**A**) (compounds synthesised by Pedro Soares) both bear a cyanocyclopropyl group in place of the terminal methyl group of VH032 (Table 3.1). Pedro Soares assessed the binding affinity of VH298 for the VHL:ElonginB:ElonginC (VBC) complex, using isothermal titration calorimetry (ITC) and fluorescence polarisation (FP) assays. VH298 showed a dissociation constant (K_d) of 90 nM as determined by ITC, while no binding could be detected for *cis*VH298 (Figure 4.1**C**), confirming that *cis*VH298 is inactive. In a competitive FP assay, VH298 confirmed a higher binding affinity (80 nM) than VH032 (150 nM) (Figure 4.1**D**).

Crystal structure of VH298-bound VBC solved by Dr. Morgan Gadd showed that VH298 maintains the same overall binding mode as VH032 (214), binding to the pocket on VHL where hydroxylated HIF-1α would normally bind (Figure 4.1**B**), thus confirming that VH298 is anticipated to compete with HIF-1α for the binding on VHL.

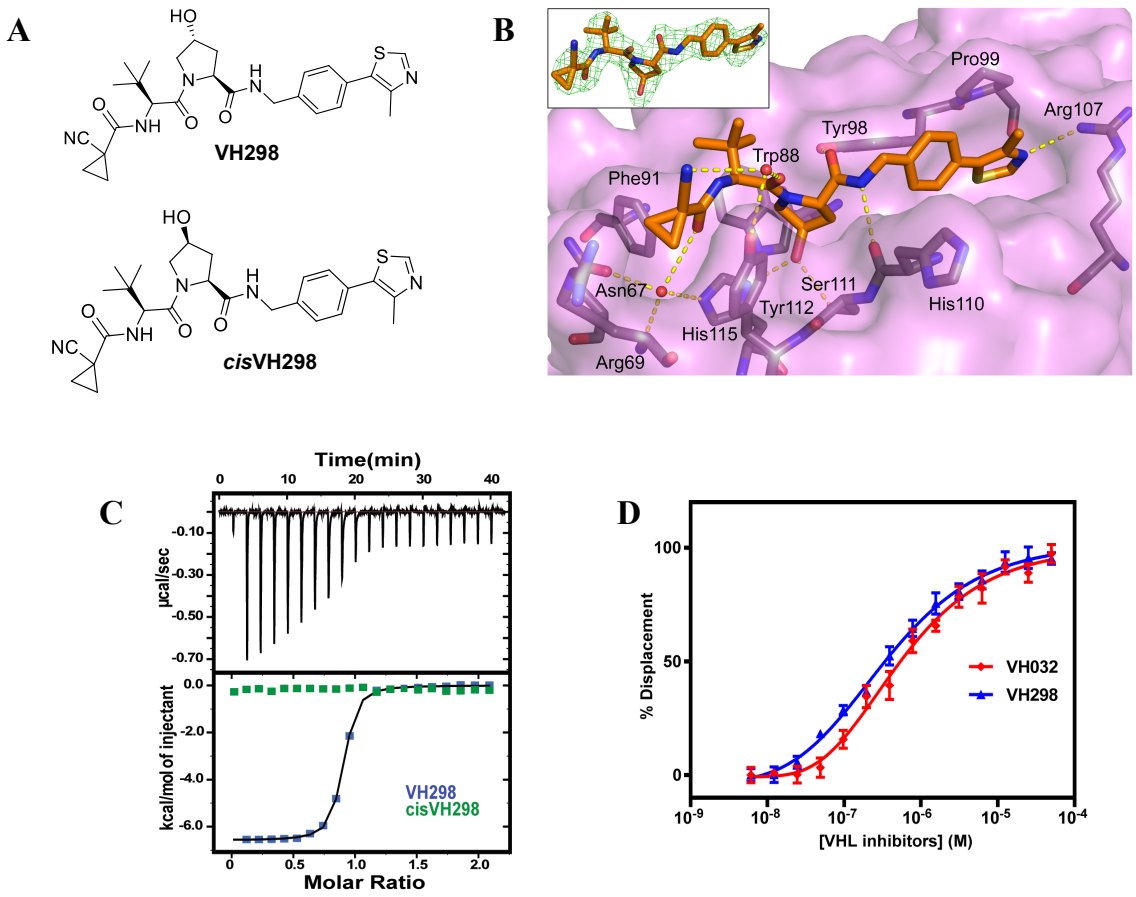

Figure 4.1 – Biophysical and structural characterisation of VH298, a new potent VHL inhibitor. (**A**) Chemical structure of VH298 VHL inhibitor and its non-binding derivative *cis*VH298. Figures were from Pedro Soares. (**B**) Crystal structure of VBC in complex with VH298 (orange carbons, PDB code 5LLI) solved by Dr. Morgan Gadd (who also provided the figure). VHL is shown as a purple surface and the VHL residues forming the binding pocket as grey stick representations. The bound ligand is shown as sticks representation with orange carbons, nitrogen atoms in blue, oxygen in red and sulfur in dark yellow. The inset panel shows the Fo-Fc omit map contoured at 3 σ around the ligand. (**C**) ITC titrations of 300 µM VH298 (blue) and 300 µM *cis*VH298 (green) into 30 µM VBC protein were performed by Pedro Soares. (**D**) Competitive fluorescence polarisation binding assays of VH298 and VH032 displacing a 20-mer FAM-labelled HIF-1α peptide binding to VBC (K_d = 3 nM), confirming the relative potency observed by ITC. (**C** and **D**) Figures were made by Pedro Soares who performed the assays.

4.3. VH298 selectively engages VHL

To investigate whether VH298 could interact with cellular VHL protein, a cellular thermal shift assay (CETSA) (223) was performed. CETSA utilises the thermal denaturation temperature of a protein from cell lysates. The binding of a ligand to target protein can increase the thermal denaturation temperature of a protein, and thus if VH298 binds to VHL protein, melting curve of VHL will shift.

Protein levels of both the on-target VHL and the primary potential off-target PHD2 were monitored at different temperatures of incubation in HeLa cell lysates treated with VH298 using western blotting. PHD2 enzyme could be an off-target for at least two reasons. Firstly, at the biological level, it is essential to ensure that HIF-dependent hypoxic response is not due to the inhibition of PHD enzymes. Secondly, at the molecular level, products of enzymatic reaction are known to be able to bind to their enzyme, resulting in a feedback inhibition. Therefore, it is important to ensure that the small molecule VHL inhibitor, which contains hydroxyproline residue found also in hydroxylated-HIF-α (the primary product of PHDs), does not bind to PHD enzymes.

PHD inhibitor FG-4592 was used as a control in the assay for PHD2 stabilisation. In the presence of VH298, a significant shift in the VHL melting curve was observed, demonstrating compound-induced target stabilisation inside cells (Figure 4.2**A**). In contrast, no thermal stabilisation was observed for PHD2 upon VH298 treatment (Figure 4.2**B**). A shift in the melting curve of PHD2, but not VHL, was observed in the presence of FG-4592 (Figure 4.2**A** and **B**) confirmed the validity of the assay.

The initial VHL antibody used for western blotting was purchased from Cell Signalling (#2738). This antibody was discontinued and replaced with a latest one (#68547), which detects multiple VHL bands (Figure 4.2**C**). The multiple bands were proven to be VHL bands as shown by the VHL knockdown via siRNA approach in HeLa cells and the

absence of all VHL bands in VHL-null renal cells 786-O and RCC4-HA (Figure 4.2**C**). The CETSA experiment with VH298 treatment (Figure 4.2**A**) was repeated and blotted with the new VHL antibody (Figure 4.2**D**). In the presence of VH298, all the VHL bands detected were stabilised, suggesting that VH298 binds to all the multiple forms of VHL (Figure 4.2**D**).

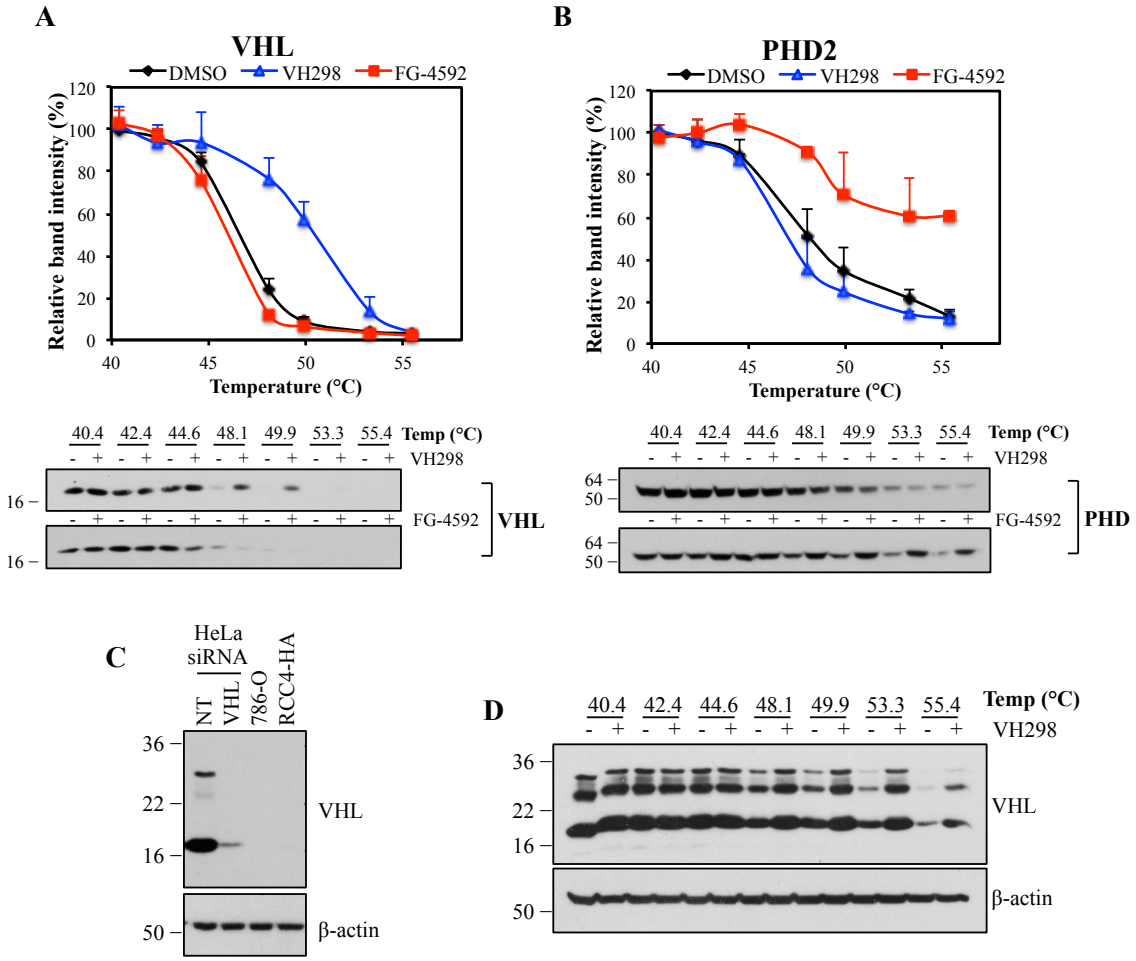

Figure 4.2 – VH298 selectively engages VHL. Cellular thermal shift assay (CETSA) to monitor cellular target engagement of (**A**) VHL and (**B**) PHD2. VH298 and FG-4592 (100 µM) were incubated in HeLa cell lysates for 15-30 min. Representative western blots and quantifications are shown. Data are presented as means ± SEM from three independent experiments. (**C**) HeLa cells were transfected with siRNA non-targeting (NT) control and VHL. Represented western blot includes cell lysates from renal cells 786-O and RCC4-HA that lack VHL. (**D**) CETSA of (**A**) was repeated with a newer VHL antibody (Cell Signalling; #68547) that detects multiple bands of VHL.

4.4. VH298 leads to HIF-α accumulation inside cells

VH298 had been shown to stabilise hydroxylated HIF-1α in cells at a concentration of 50 μM in the VHL inhibitor screen assay (Figure 3.7). To determine the concentration of VH298 required to induce the stabilisation of HIF-1α, HeLa cells were treated with VH298 in a dose-dependent manner for 2 h (Figure 4.3**A**). VH298 induced concentration-dependent accumulation of HIF-1α levels, with detectable HIF-1α bands visible as low as 10 μM and the strongest HIF-1α accumulation at 150 μM (Figure 4.3**A**). *cis*VH298 was inactive even at high concentration (250 μM), demonstrating that the inhibitor's activity is strictly dependent on the binding to VHL. The accumulation of HIF-1α was also observed in non-tumoural cell lines, including human foreskin fibroblast (HFF) cells (Figure 4.3**B**) and mouse cytotoxic T lymphocyte (CTL) cells (215), demonstrating that the cellular activity of VH298 is not limited to immortalised cancer cells, but also active in other mammalian cell types.

Beside HIF-1α, HIF-2α was also stabilised in the presence of VH298 (Figure 4.3**B**). The extent of VH298-induced HIF-α subunit accumulation after 2 h was comparable to that observed on treating cells over the same time with 1% O_2 (hypoxia) for 2 h or PHD2 inhibitors (IOX2 or FG-4592) at identical concentrations (100 μM) for 2 h in all cell lines tested (Figure 4.3**A** and **B**). Immunoblots with an antibody specific for HIF-1α hydroxylated at Pro564 (HIF-1α-OH) showed increased levels of this species only upon treatment with VH298 (Figure 4.3**A** and **B**) and proteasome inhibitor MG132 (Figure 4.3**A**), but not with IOX2 and FG-4592 (Figure 4.3**A** and **B**), consistent with disruption of the VHL:HIF-α interaction by VH298 downstream of HIF-α hydroxylation.

To further evaluate the activity of VH298, time-course experiments in HeLa cells following treatment with VH298 and hypoxia (1% O_2) were performed and levels of HIF-1α and HIF-2α were independently monitored by immunoblots (Figure 4.3**C** and

D). VH298 induced a more rapid and pronounced accumulation of HIF-1α and HIF-2α compared to hypoxia (Figure 4.3**C**), and both HIF-1α and HIF-2α (Figure 4.3**D**) remained accumulated over the treatment time, with protein levels detectable already after 5 min and persisting beyond 24 h after treatment.

To confirm that the increase of HIF-α was indeed due to the inhibition of VHL activity, clear cell renal cell carcinoma *VHL*$^{-/-}$ renal cell carcinoma 4 (RCC4) cells were treated with VH298. In the complete absence of functional VHL proteins in RCC4 cells expressing only the haemagglutinin (HA) tag, the levels of HIF-α subunits did not increase further upon VH298 treatment (Figure 4.3**B**). In contrast, RCC4 cells expressing HA-tagged VHL showed accumulation of HIF-α subunits in the presence of VH298 (Figure 4.3**B**), demonstrating the on-target specificity of VH298.

Taken together, these data show that VH298 is able to induce the stabilisation of HIF-α subunits in tumoural and non-tumoural cell lines, resulting from effective and specific blockade of the VHL: HIF-α interaction.

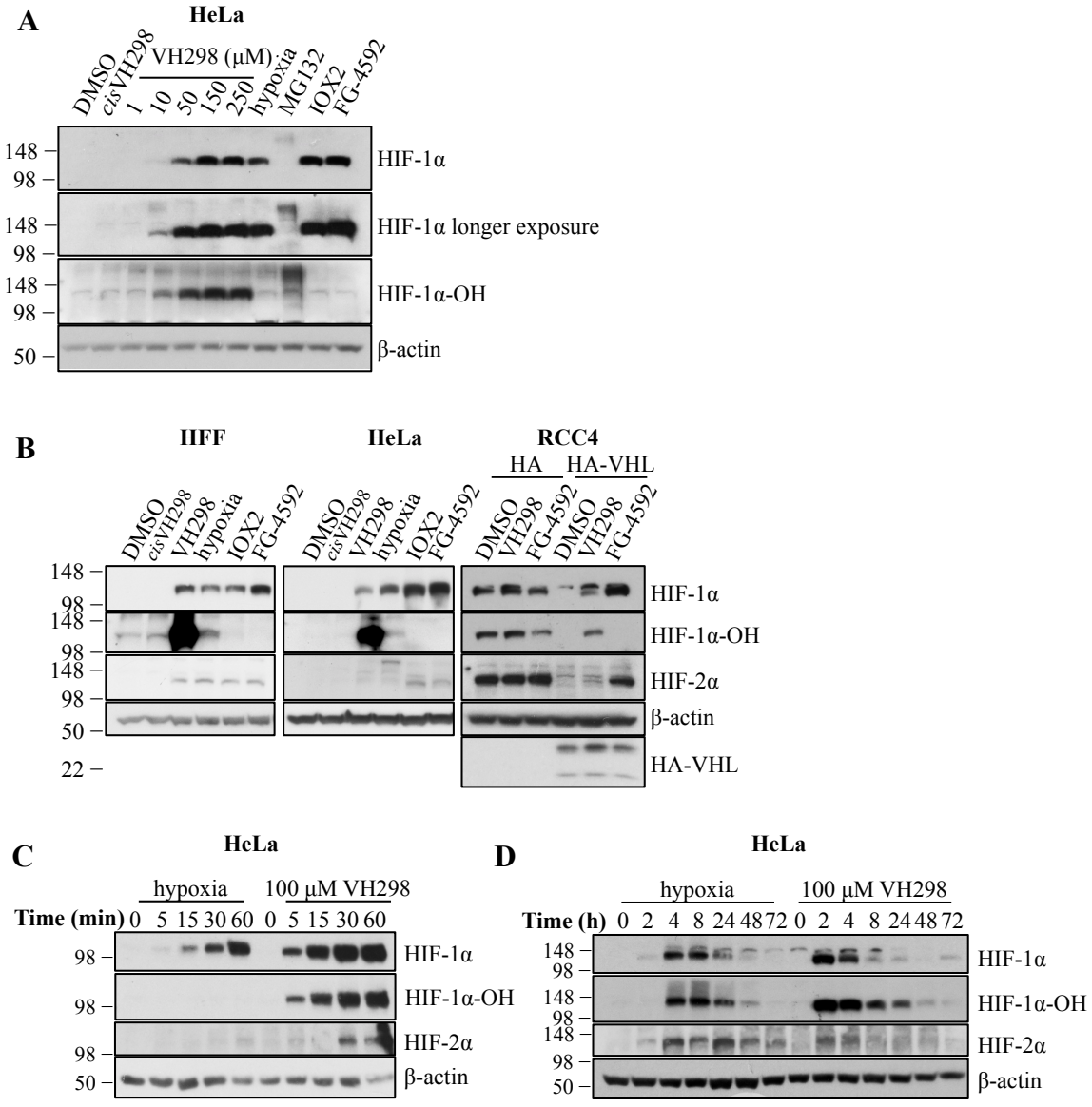

Figure 4.3 – VH298 induces concentration- and time-dependent on-target specific accumulation of hydroxylated HIF-α in human cell lines. (**A**) Immunoblots of HIF-α subunits in HeLa cells treated with increasing concentrations of VH298, 1% DMSO, hypoxia, 250 μM *cis*VH298, 100 μM IOX2, 100 μM FG-4592 for 2 h, and 20 μM MG132 for 3 h. (**B**) Treatment of 1% DMSO, hypoxia (1% O_2), and 100 μM of indicated compounds in HFF, HeLa, RCC4-HA and RCC4-HA-VHL cells for 2 h. (**C** and **D**) Time-course immunoblots of lysates from HeLa cells subjected to hypoxia (1% O_2) or 100 μM VH298. The blots shown are representative of three independent experiments.

4.5. VH298 selectively stabilises hydroxylated HIF-1α

To further interrogate the specificity of the compound's mode of action, the stabilised HIF-1α induced by VH298 was examined for the levels of its hydroxylated form. Since the HIF-1α antibody recognises both hydroxylated and non-hydroxylated HIF-1α species, while the HIF-1α-OH antibody is specific for the hydroxylated species on Pro564, co-immunoprecipitation (co-IP) experiments with the HIF-1α-OH antibody were performed. In the presence of VH298, the accumulated HIF-1α was found mainly in the IP fraction, and not in the flow-through (FT) (Figure 4.4**C**), indicating that majority of the HIF-1α species stabilised by VH298 were hydroxylated. A similar result was observed with the proteasome inhibitor MG132, which blocks the pathway downstream of HIF hydroxylation. In contrast, when cells were treated with the PHD inhibitor IOX2, that inhibit HIF hydroxylation, HIF-1α was found in the FT and not in the IP fractions, demonstrating that the HIF-1α-OH antibody pulled down only the hydroxylated HIF-1α (Figure 4.4**C**).

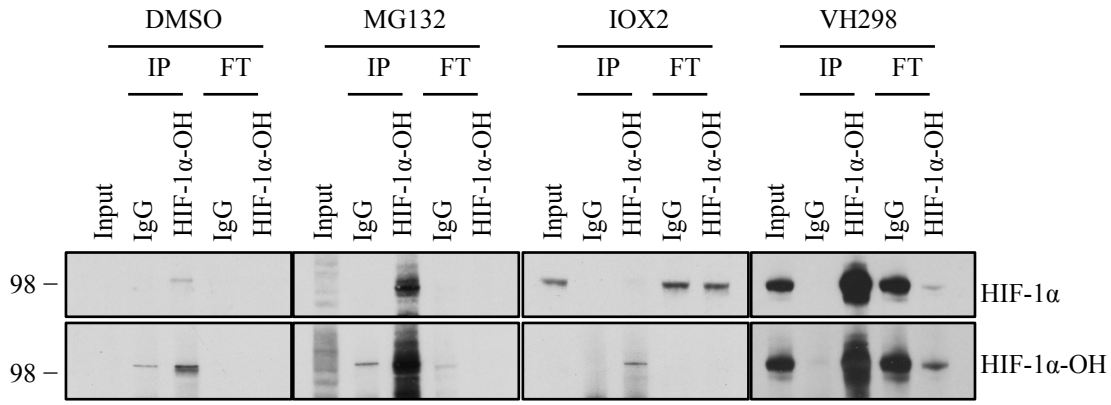

Figure 4.4 – The majority of the VH298-induced HIF-1α is hydroxylated. Co-immunoprecipitation experiments on lysates from HeLa cells treated with vehicle DMSO (1% for 2 h), MG132 (20 μM for 3 h), IOX2 (250 μM for 6 h), or VH298 (100 μM for 2 h) prior to lysis. 300 μg of protein were used to immunoprecipitate with the HIF-1α-OH (Pro564) antibody. Rabbit immunoglobulin G (IgG) was used as a control. Inputs represent 10% of the starting material used per immunoprecipitation (IP) and flow-through (FT) represents 20% of the flow-through collected after IP. The blots shown are representative of three independent experiments.

Taken together, these results are consistent with the VHL inhibitor VH298 engaging potently and selectively the VHL E3 ubiquitin ligase (Figure 4.2**A**-**B** and **D**) as its cellular target downstream of HIF hydroxylation, leading to specific intracellular accumulation of the hydroxylated HIF-α form.

4.6. VH298 induces HIF transcriptional activity

To assess the ability of VH298 to promote HIF activity, a luciferase reporter assay was initially performed. In addition, quantitative real-time PCR (qRT-PCR) analysis for endogenous HIF-dependent targets was also conducted to confirm the ability of VH298 to stabilise transcriptionally active HIF. To further ensure that VH298 is indeed the best VHL inhibitor, VH032 and VH297 were included in the qRT-PCR assay. Cytotoxicity effects of VH032 and VH297 were previously shown to be limited (Figure 3.8). In addition, VH297 was found to be the second best VHL inhibitor in its ability to stabilise HIF-1α in the VHL inhibitor screen, followed by VH032 (Figure 3.7).

4.6.1. Luciferase assay

In HRE-luciferase reporter cells, U2OS-HRE, treatments with VH298 exhibited marked concentration-dependent increase of HIF-dependent luciferase activity, consistent with hypoxia and IOX2 treatments, while no activity was observed with high concentration of non-binding epimer *cis*VH298 (Figure 4.5**A**).

4.6.1. Quantitative real-time PCR

The ability of VH298 to induce transcriptionally active HIF was further confirmed in qRT-PCR assays monitoring mRNA levels of known HIF-target genes including *CA9* and *GLUT1* in different cellular backgrounds. Optimum treatment time with VH298 was determined to be 24 h in HFF cells as observed in a qRT-PCR assay that monitored

expression of *GLUT1* mRNA levels of six known HIF-target genes including *CA9*, *GLUT1*, *GLUT3*, *BNIP3*, *PHD2* and *VEGF* (Figure 4.6**A**).

Treatments with VH032, VH297 and VH298 showed marked increase of HIF-target genes, but not with inactive epimers *cis*VH032, *cis*VH297 and *cis*VH298 (Figure 4.6**B**). Different responses to VHL inhibitor treatment were observed in different cell lines. For instance, HFF was the most sensitive to VHL inhibitors among the cell lines used; maximum mRNA levels of *CA9* and *GLUT1* were reached with 100 and 25 µM of VH298, respectively, in HFF cells. VH297 showed the weakest induction profiles of *CA9* and *GLUT1* mRNA amongst the three VHL inhibitors (Figure 4.6**B**). Consistently in all cell lines, even when used at 250 µM concentration, VH297 could not achieve the maximum increase of *CA9* and *GLUT1* mRNA levels as seen with VH298, with the

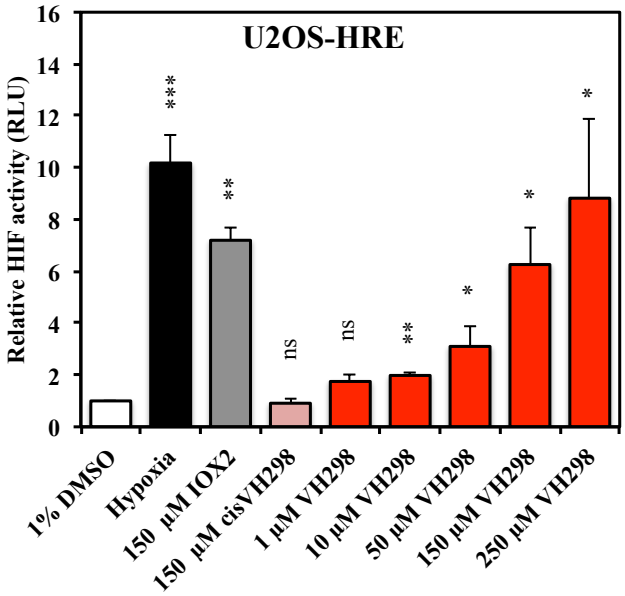

Figure 4.5 – VH298 induces HIF-α transcriptional activity in U2OS-HRE. (**A**) U2OS cells stably expressing an HRE-luciferase reporter plasmid were treated with indicated conditions for 32 h. Graphs depict the mean + SD of three independent biological replicates. Two-tailed student's t-test was performed to calculate p values, and levels of significance are denoted as follows: *P<0.05, **P<0.01, ***P<0.001, and ns: P>0.05.

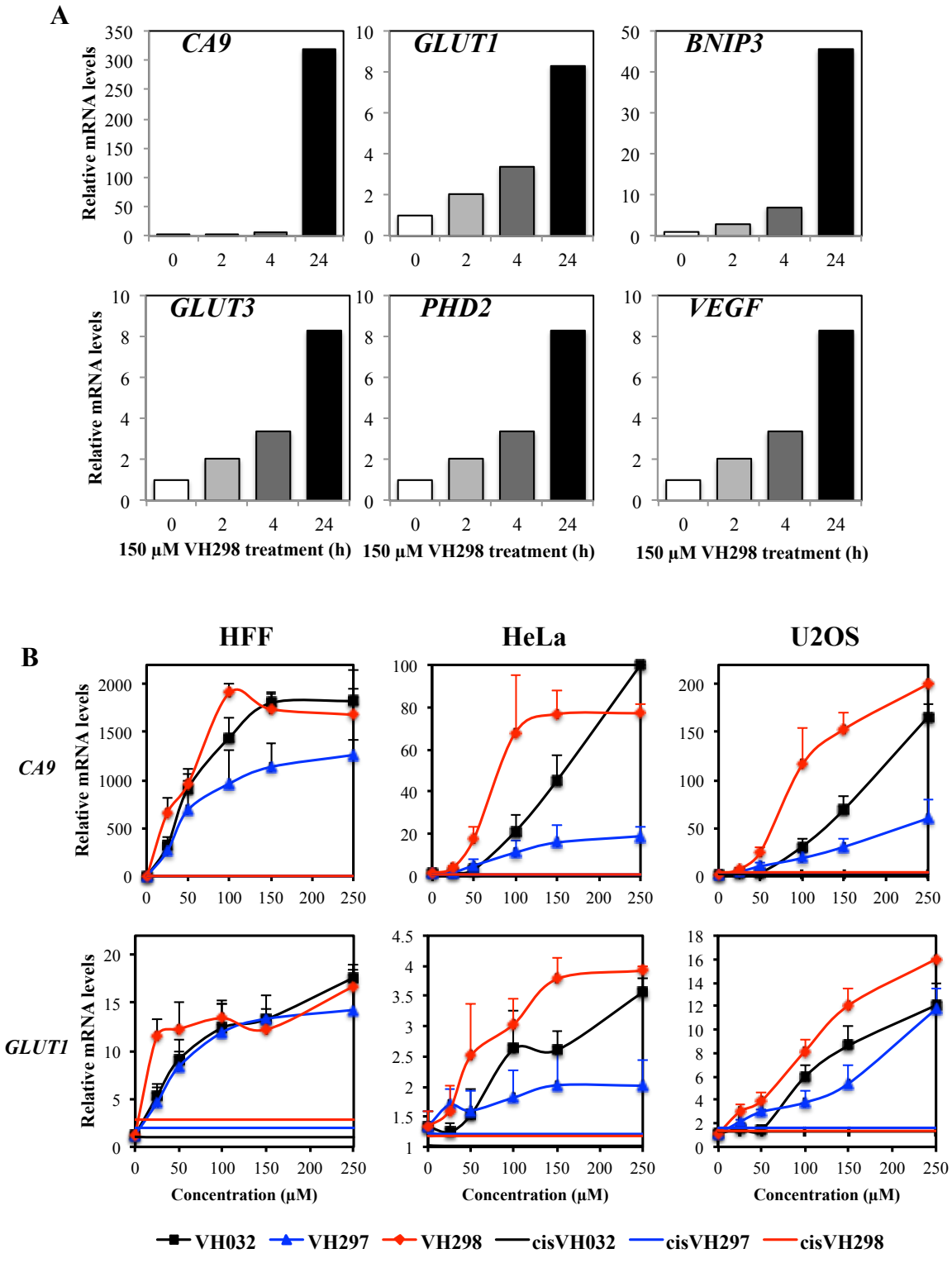

Figure 4.6 – VHL inhibitors induce HIF-α transcriptional activity in various cell lines. (**A**) HFF cells were treated with 150 µM of VH298 for 0, 2, 4, and 24 h. Experiment was performed once. (**B**) Dose-response curves of *CA9* and *GLUT1* mRNA expressions in HFF (24 h), HeLa (16 h) and U2OS (16 h) cells in the presence of *cis*VH032, *cis*VH297, *cis*VH298, VH032, VH297 and VH298. Graphs depict the mean + SD of three independent biological replicates. (**A** and **B**) mRNA was collected, reverse transcribed and analysed by qRT-PCR. The shown levels of the indicated mRNAs were normalised to those of β-actin.

exception of *GLUT1* in HFF cells (achieved with 100 μM of VH297). Comparing the remaining two VHL inhibitors, VH298 required a lower concentration than VH032 to increase mRNA levels of target genes analysed.

Altogether, these results indicate that VHL inhibitor-induced hydroxylated HIF proteins are transcriptionally active and confirm the superiority of VH298 over VH032 and VH297 with regards to its cellular potency.

4.7. VH298 upregulates HIF-dependent gene products

To examine whether the observed VH298-dependent increases of HIF target mRNAs would be translated into proteins, protein levels of known HIF target gene products (CA9, GLUT1, PHD2, PHD3, BNIP3, and HK2) were monitored in mammalian cells treated for 24 h with VH298 or PHD inhibitors IOX2 and FG-4592 (each at concentration of 100 μM), or hypoxia (1% O_2). Accumulation of all the HIF targets analysed was detected following prolonged treatment of VH298 in cells, to levels consistent to those observed with hypoxia or PHD inhibition treatments (Figure 4.7**A-B**). In all cell lines tested, hypoxia induced the highest levels of protein expression for the majority of HIF targets screened, with GLUT1 and CA9 being the most prominent (Figure 4.7**A-C**). PHD3 levels were also the highest under hypoxia in most cell lines, but not in RCC4-HA-VHL (Figure 4.7**B**), in which PHD3 levels were not affected by any treatments. VH298 proved as effective as hypoxia in increasing PHD2 and HK2 protein levels (Figure 4.7**A-B**), however in HFF cells, BNIP3 protein level increased more with VH298 treatment than hypoxia treatment. By contrast, VH298 treatment resulted in similar levels of induction of the protein analysed when compared with PHD inhibition in all cell lines tested. The exception was RCC4-HA-VHL cells, in which IOX2 and FG-4592 treatments were the most effective conditions, as observed by higher levels of target proteins, including CA9, PHD2, BNIP3 and HK2 (Figure 4.7**B**).

Of note, a higher concentration (150 μM) of VH298 was required in RCC4-HA-VHL cells to detect a good response to VHL inhibition, which was likely due to the high level of HA-tagged VHL expressed in these cells, as compared to the VHL level in HFF, HeLa or U2OS (Figure 4.7**D**).

Time course treatments with 1% O_2 (hypoxia) and VH298 in HeLa cells showed that most HIF-target genes examined were stabilised at similar time points in both

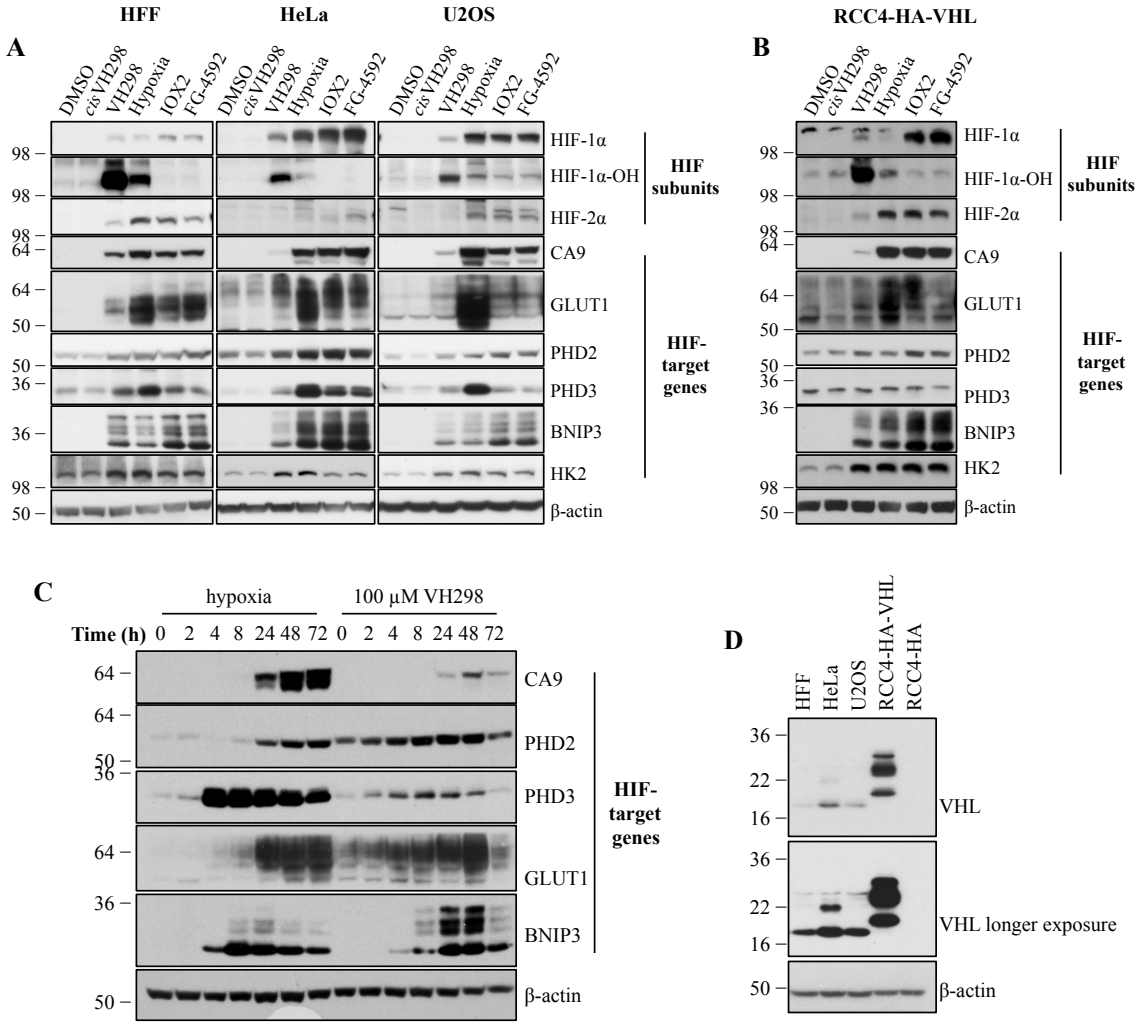

Figure 4.7 – VH298 elicits a HIF-dependent hypoxic response in various cell lines. 1% DMSO, hypoxia (1% O_2) and indicated compounds at 100 μM were introduced to (**A**) HFF, HeLa, U2OS and (**B**) RCC4 cells expressing HA-tagged VHL (with the exception of *cis*VH298 and VH298 used at 150 μM) for 24 h. (**C**) Time-course immunoblots of HIF targets from HeLa cells subjected to hypoxia (1% O_2) or 100 μM VH298. (**D**) VHL protein levels were analysed by western blotting in HFF, HeLa, U2OS, RCC4 expressing HA tag or HA-tagged VHL. Protein levels were analysed by immunoblotting using antibodies against the indicated proteins, with β-actin as the loading control. The blots shown are representative of three independent experiments.

conditions, but reaching the maximum levels at different times (Figure 4.7**C**). PHD3 was the first to reach the maximum level in hypoxia treatment at 4 h, but not increased much in VH298 treatment, while CA9 was the last to be upregulated and reached maximum level at 48-72 h of hypoxia or 48 h of VH298 treatment (Figure 4.7**C**).

In prolonged treatment of 72 h, all target genes tested had started to decrease in protein levels when treated with VH298, but not so much with hypoxia treatment (Figure 4.7**C**). Altogether, the results suggested that all HIF-target genes were upregulated in response to HIF stabilisation by the different stimuli used, albeit at different rate. Overall, the data presented here supports the application of VH298 as chemical probe to elicit effective HIF-dependent hypoxic response inside cells.

4.8. VH298 stimulates EPO production in VHL-dependent manner

HIF transcriptional activities are known to stimulate the production of the hormone erythropoietin (EPO), which is primarily expressed in the kidney and liver. To investigate whether VH298-induced HIF activity is able to stimulate EPO production, mRNA levels of *EPO* in RCC4 cells reconstituted with HA-tag or HA-VHL were analysed by qRT-PCR. While VH298 had no effect on the mRNA level of *EPO* in RCC4-HA cells that lack VHL, the VHL inhibitor increased mRNA levels of *EPO* in RCC4-HA-VHL, restoring to a similar level compared to the VHL-null RCC4-HA cells (Figure 4.8**A**). This indicates that pharmacological inhibition of VHL is able to stimulate endogenous EPO synthesis.

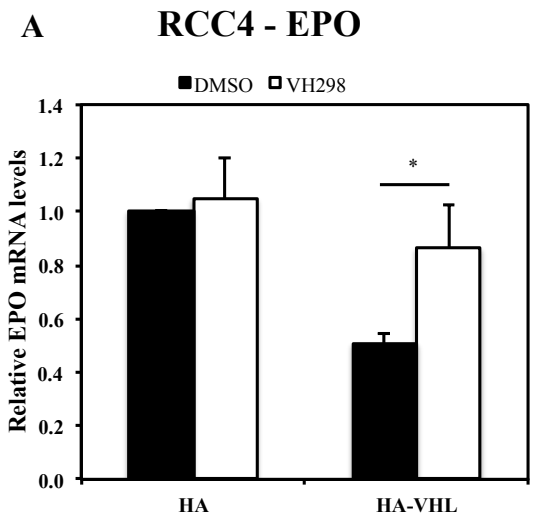

Figure 4.8 – VH298 stimulates EPO production in VHL-dependent manner. (**A**) EPO production in RCC4-HA and RCC4-HA-VHL cells subjected to 100 μM VH298. Graphs depict the mean + SD of three independent biological replicates. Two-tailed student's t-test was performed to calculate p values, and level of significance is denoted as follows: *0.01<P<0.05.

4.9. Discussion

Small molecule that selectively binds to VHL on the interface where HIF-α normally binds would compete with HIF-α. If the VHL inhibitor binds with sufficient potency relative to the natural substrate, it could fully occupy the target-binding site, leading to the stabilisation of HIF-α subunits and subsequently induce HIF transcriptional activity. Work from the Ciulli lab showed that the best VHL inhibitor in stabilising HIF-1α, VH298, was able to compete with 20-mer HIF-1α peptide in the FP assay and bind to VBC complex with high potency on the VHL pocket where hydroxylated HIF-1α would normally bind. Importantly, the *cis*-hydroxyproline analogue *cis*VH298 does not show any detectable binding to VHL, and is thus inactive in cells (Figure 4.1) (215). Because *cis*VH298 has a very similar structure to VH298, and consequently similar physiochemical properties, it provides ideal negative control.

To provide a useful chemical tool to study the biology of VHL and HIF, it was important to fully characterise VH298 for its ability to stabilise HIF subunits and activate HIF transcriptional activity in cells. Here, VH298 was shown to stabilise both HIF-α subunits: HIF-1α and HIF-2α in various mammalian cell lines. Importantly, in the absence of *VHL* in renal cell carcinoma cell line RCC4 that stably expresses HA tag, VH298 could not stabilise HIF-α subunits. However, when RCC4 cells express HA-tagged VHL, VH298 induced HIF-α accumulation (Figure 4.3**B**). This mode of inhibition by binding to VHL was further confirmed by the stabilisation of HIF-1α that was in its majority hydroxylated, proving that VH298 acts downstream of HIF-α hydroxylation. Furthermore, CETSA analysis that showed that VH298 specifically engaged VHL as its target but not PHD2 (Figure 4.2).

The stabilisation of HIF-α subunits when cells were treated with VH298 led to the upregulation of HIF activity, as displayed by the luciferase assay and qRT-PCR assay

that monitored two known HIF-target genes (*CA9* and *GLUT1*). Previously published VHL inhibitor, VH032 (214), and the second best VHL inhibitor screened by western blotting for HIF-1α protein levels, VH297, also upregulated *CA9* and *GLUT1* mRNA, but to lower levels when compared to VH298 (Figure 4.5**B**), making VH298 the most potent VHL inhibitor tested. Gratifyingly, mRNA of these two HIF-target genes, as well as others (*PHD2*, *PHD3*, *BNIP3* and *HK2*) was translated into protein products in multiple mammalian cells (HeLa, U2OS, HFF, and RCC4-HA-VHL) treated with VH298, confirming the ability of VH298 to elicit effective HIF-dependent hypoxic response inside cells.

An important observation to consider was the dose of VH298 required in cells. Although being more potent and more permeable (215) than VH032, a high concentration of up to 100 μM VH298 was still required to stabilise HIF-1α. One reason for this could be the amount of VHL present in cells (Figure 4.7**D)**. Cells with more VHL such as RCC4-HA-VHL (Figure 4.7**D)** required a higher dose of 150 μM to stabilise detectable HIF-α (Figure 4.7**B**), while in cells with less VHL such as HFF (Figure 4.7**D)**, increased HIF-target mRNAs at lower concentration than HeLa and U2OS (Figure 4.6**B**). These results provide additional evidence for the on-target activity of the VHL inhibitors, and suggest that target abundance affects the dose of VH298 required. Another reason could conceivably be the requirement of the compound to occupy fully the VHL binding site, e.g. to 99.9%, in order to effectively block its activity – consistent with even a small percentage of unbound VHL being sufficient to effectively catalyse HIF polyubiquitination and subsequent degradation. Such a high-bar to target engagement for effective inhibition means that at least 100-fold higher concentration relative to K_d is required for cellular activity (i.e. 10 μM concentration in spite of a K_d of ~ 100 nM). This feature, combined with potential limitations to cell permeability, give rise to an apparent large difference between cellular activity and the

binding affinities measured. These features are common to many chemical probes used for biochemical and biomedical research, which also show huge differences between binding affinity measured *in vitro* to concentration required for cell treatment. One of such example is the PHD inhibitor used here, IOX2, which possesses IC_{50} of 22 nM, but is used at micromolar range (203). Nonetheless, despite requiring micromolar range for cell treatment, the dose administered to achieve required HIF-α stabilisation and transcriptional activity is tolerable for the period of experimentation. Therefore, VH298 is suitable for use as chemical probe and is now available through the newly established Chemical Probes Portal (http:www.chemicalprobes.org/vh298).

Besides being a potential chemical probe of the hypoxic signalling pathway, VH298 may have therapeutic potential as a HIF stabiliser. Over the years, a number of strategies have been developed to stabilise HIF-α through escaping or blocking its degradation by the proteasome, with the most promising being the inhibition of HIF-α hydroxylation catalysed by PHDs (232). A number of PHD inhibitors are currently in clinical trials for the treatment of anaemia in patients with chronic kidney disease, and this is because the transcriptional HIF activity is able to stimulate the production of EPO that benefits anaemic patients lacking sufficient EPO synthesis (105). Here, VH298 was shown for the first time to have the ability to stimulate the production of endogenous EPO (Figure 4.8), indicating that it may have therapeutic potential for the anaemic patients. In addition to EPO production, the stabilisation of HIF is known to stimulate angiogenesis via HIF-mediated *VEGF* expression (233). The increase of *VEGF* mRNA expressions in HFF fibroblasts in the presence of VH298 (Figure 4.6**A**) suggests that VH298 may also have the potential in stimulating angiogenesis.

Although not shown here, we have screened VH298 against > 100 tested cellular kinases, ion channels, and GPCRs *in vitro* at the concentration of 50 μM, and found VH298 to exhibit negligible off-target effects (215).

Taken together, the data presented in this chapter identified VH298 as the most potent VHL inhibitor tested and a high-quality chemical probe with potential for the study of HIF-dependent responses, as it is potent, has known selectivity and a proven mechanism of action. The data further provides evidence for the potential of VH298 as therapeutic lead for conditions requiring EPO or VEGF induction.

5. Transcriptome and proteome changes induced by VHL inhibitors

5.1. Introduction

The HIF transcription factor is known to regulate many genes by binding directly to the HRE motif on the promoter of HIF-target genes, resulting in the increase of mRNA levels of these genes, and subsequently protein levels. In previous chapters, the inhibition of VHL using small molecule that binds to the pocket of hydroxylated HIF-1α binding site on VHL, were shown to lead to the stabilisation of transcriptionally active hydroxylated HIF-1α. However, the investigation of the VHL inhibitor so far was focused on monitoring HIF-α levels and the effects on a selected panel of few HIF-target genes.

As a chemical probe to study the biology of VHL, it is important to fully evaluate the effects of the inhibition of VHL by the small molecule in an unbiased manner. Here, the aim of the work presented in this chapter is to gain a more complete understanding of the effect of VHL inhibitor in cells at a global level. To achieve this, global transcriptome and proteome analyses were performed.

5.1.1. Transcriptomic analysis by RNA-sequencing

Transcriptome analysis would provide an understanding of the global changes of transcripts in the cells in the presence of the VHL inhibitor. Such an analysis would allow validating the anticipated effects on the HIF pathway, as well as identifying potential new pathways involved and novel regulatory units activated by the inhibition of VHL. To analyse the transcriptome, the deep-sequencing approach, RNA-sequencing (234), was employed. Briefly, RNA is converted to cDNA fragments, which are then flanked by specific short sequences known as adaptors to serve as tags for sequencing.

Each cDNA fragment is sequenced in a high-throughput fashion to obtain short sequences of 30-400 bp, which are called ‘reads’. The resulting reads are aligned to a reference genome. This produces a transcriptome profile containing the number of aligned reads for each gene, which is used as input for differential expression analysis. RNA-sequencing has been shown to be highly sensitive, reproducible, and reliable technique to accurately measure transcriptome changes in the cell (234).

With the use of RNA-sequencing, analysis comparing several conditions is possible. In addition to the analysis of changes in gene expression following treatment with the VHL inhibitor (in this case, VH032 was used, because VH298 has not yet been designed) comparing to vehicle control DMSO; the conditions of hypoxia and PHD inhibitor (IOX2) were also included. These additional treatments represent standard methods in the field of stabilisation of HIF-α, but each also affects different and additional pathways in the cell.

5.1.2. Proteomic analysis by TMT labelling

Proteomic analysis was conducted using the 10-plex tandem mass tags (TMTs)-labelling method. 10-plex TMT labelling approach enables simultaneous identification and quantification of protein levels from up to 10 different samples. Each sample is labelled separately with one of the TMT isobaric reagents, after which all samples are pooled together. Although the mass difference between these reporters is extremely small, they can be resolved with the current generation of mass analysers (235,236). Like the RNA-sequencing analysis, proteomic analysis of VH032, hypoxia, IOX2 and DMSO treatments were performed.

Overall, through the RNA-sequencing approach, it was found that the VHL inhibitor VH032 induced mostly gene expression changes dependent on HIF stabilisation.

Interestingly, the proteomic approach identified that besides HIF-1α and HIF-target genes, VH032 treatment increased VHL protein levels.

5.2. RNA-sequencing – quality control of samples

To determine the global transcriptome changes induced by the small molecule-inhibition of VHL, an unbiased RNA-sequencing approach was used. HeLa cell line was selected for this study as most of the characterisation of VHL inhibitor had been carried out in this cell line. Importantly, there are transcriptomic data of hypoxia and HIF study in HeLa.

RNA-sequencing experiments and analysis were performed in HeLa cells following treatment of 1% DMSO (vehicle/negative control), 1% O_2 (hypoxia), PHD inhibitor IOX2 or VHL inhibitor VH032 (Figure 5.1). IOX2 and VH032 were used at the concentration of 250 µM, which showed good induction of HIF activity. VH032 was

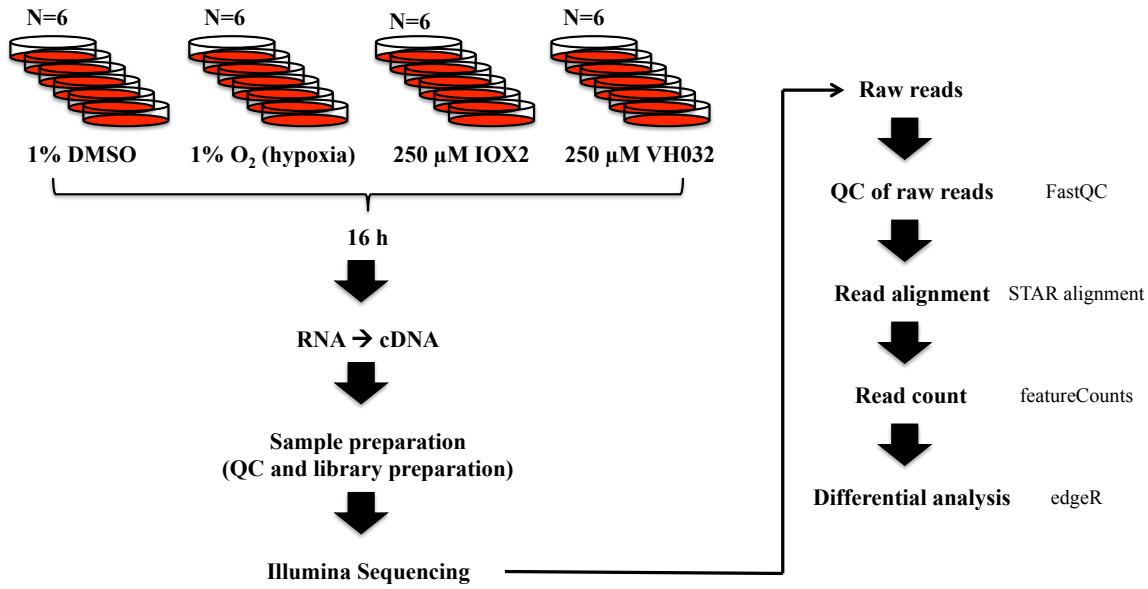

Figure 5.1 – RNA-sequencing workflow. HeLa cells were treated with 1% DMSO, 1% O_2 (hypoxia), 250 µM of IOX2 or VH032 for 16 h prior to harvesting. RNA was extracted and converted to cDNA. Library preparation and quality control (QC) were performed by Andrew Cassidy from the Genetic Core Services Unit in Dundee. RNA samples were submitted for Illumina sequencing. The following data analysis was performed with guidance from Christian Cole from the Data Analysis Group in Dundee. Raw reads obtained from sequencing was quality-controlled using FastQC software. Raw sequence reads were aligned to Ensembl human genome GRCh37 with STAR and counts for the reads aligned to each gene were obtained with subread-featureCounts pipeline. Differential gene expression analysis was performed using the R package edgeR according to edgeR user guide.

used in this experiment instead of VH298 because VH298 had yet to be designed and synthesised at the time these experiments were performed. Treatment time of 16 h was used to ensure that the treatment was long enough to induce optimum transcriptome changes, and in hope that it was insufficient to observe secondary transcriptome changes stimulated by the initial transcription products.

For this experiment, six biological replicates for each condition were carried out, as it had been shown that six replicates provide sufficient statistical mean to strengthen robustness of the result (237). Before submitting samples for sequencing, a portion of RNA extracted from each sample was used for qRT-PCR to monitor mRNA levels of HIF-target genes since the treatment of hypoxia, IOX2 or VH032 led to the transcription of HIF-target genes including *VEGF*, *GLUT1*, *CA9*, and *PHD2* (Figure 3.2**D**). The three conditions in all six replicates successfully upregulated mRNA of the HIF-target genes tested significantly (Figure 5.2**A**). Samples of these six replicates were prepared, quality-controlled, and sequenced in an Illumina sequencer by Andrew Cassidy from the Genetic Core Services Unit in Dundee (Figure 5.1).

The data obtained from the sequencing unit was analysed with the help of Christian Cole from the Data Analysis Group of the Centre for Gene and Regulation & Expression at the University of Dundee (Figure 5.1). The quality of the six replicates for each condition was determined by statistical analysis of the correlation between replicates, and the relationship between variance and mean (Figure 5.2**B** and **C** and Figure 5.3).

The correlation between replicates measures the similarity between expression values for transcripts between the samples. In this case, DMSO samples clustered together and showed weak correlation to the other conditions (Figure 5.2**B**). Replicates of hypoxia, IOX2 and VH032 conditions did not cluster within their respective condition in the

heat-map (Figure 5.2**B**), suggesting that the three conditions may result in similar transcriptome changes.

Nevertheless, replicates of each condition clustered together in the multidimensional scaling plot generated according to the 2000 largest leading logFC for genes between samples (Figure 5.2**C**) and heat-maps for each condition showed a strong correlation between 0.92 and 1 across replicate of the same condition (Figure 5.3), suggesting that replicates of the same condition were similar and statistically close to each other.

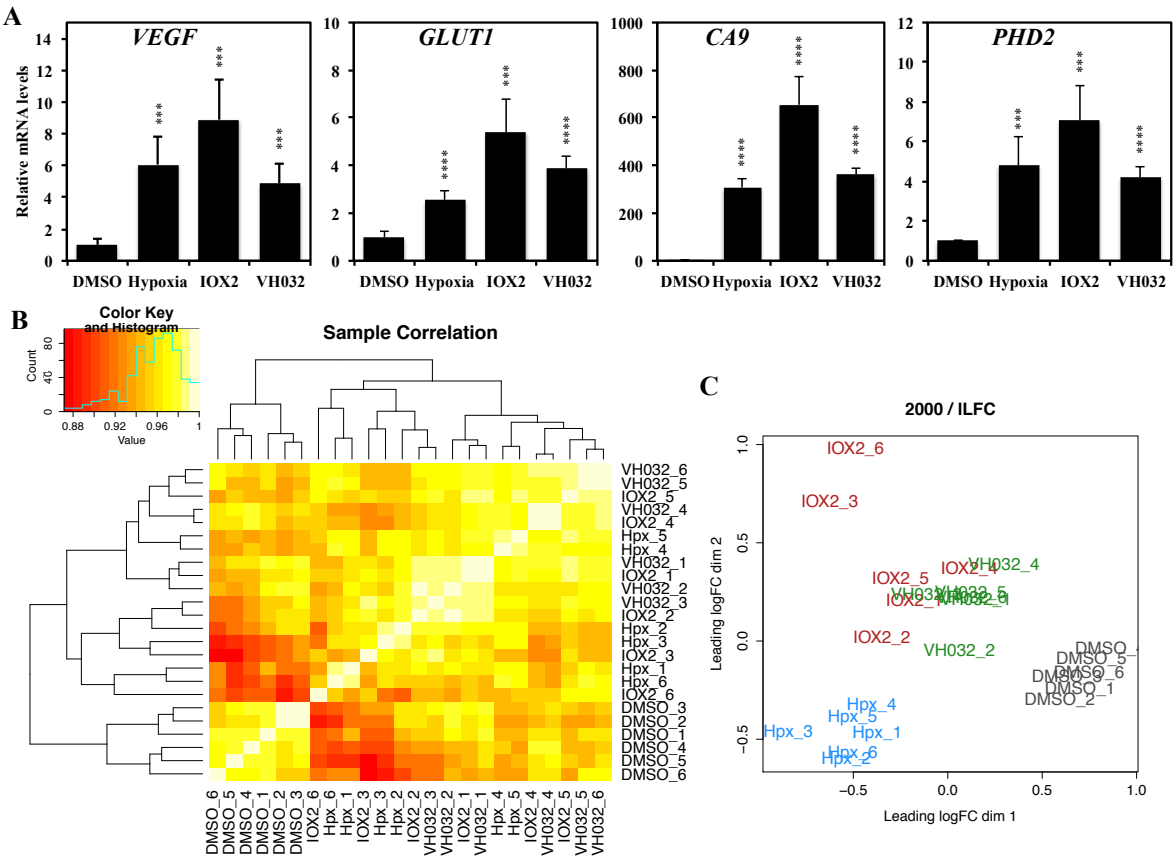

Figure 5.2 – RNA-sequencing – quality control of samples. (**A**) HeLa cells were treated with 1% DMSO, 1% O_2 (hypoxia), 250 µM of IOX2 or VH032 for 16 h prior to harvesting. mRNA was extracted and qRT-PCR was performed for HIF-target genes (*VEGF*, *GLUT1*, *CA9* and *PHD2*) to confirm the expected effect on those genes. (**B**) Heat-map of Pearson correlations among RNA-sequencing samples that had been normalised to their total counts. (**C**) Multidimensional scaling plot of RNA-sequencing data generated by edgeR's plotMDS. The distance between two samples reflects the leading logFC of the corresponding RNA samples. The leading logFC is the average (root mean square) of the 2000 largest absolute logFCs for genes between those two samples.

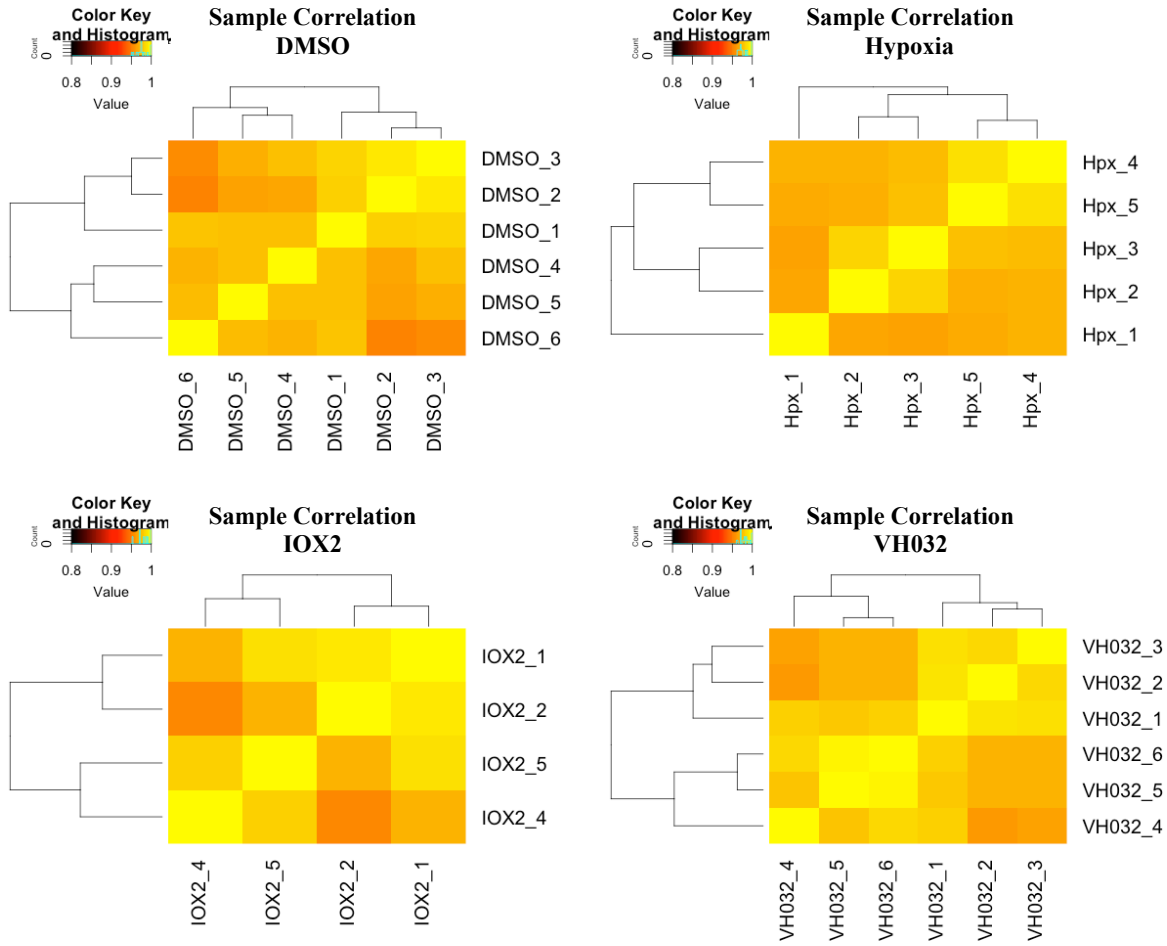

Figure 5.3 – RNA-sequencing – quality control of replicates. Heat-map of Pearson correlations between replicates for DMSO, hypoxia, IOX2 or VH032 treatment. Each data had been normalised to their total counts.

5.1. RNA-sequencing – differential expression

To investigate the differences in gene expression between treatments, volcano plots were generated to show the gene expression changes between pairs of conditions (Figure 5.4**A**). In addition, to observe the overall changes of transcriptome induced by the treatment of hypoxia, IOX2 or VH032 comparing to DMSO control, Venn diagrams were generated (Figure 5.4**B** and **C**). Differentially expressed genes were selected with the criteria of a false discovery rate (FDR) under 0.05 (5% of the results was expected to be false positive), and logarithm base 2 of the fold change between conditions ($\log_2$FC) > 1 for upregulated genes and $\log_2$FC < –1 for downregulated genes.

Overall, when compared to DMSO control, hypoxia induced the broadest transcriptional changes, followed by IOX2 and VH032 (Figure 5.4**A**). Hypoxia treatment resulted in the largest transcriptome changes: 734 mRNAs upregulated and 508 mRNAs downregulated (Figure 5.4**B** and **C**). In contrast, IOX2 and VH032 led to changes in a smaller set of genes, mainly resulting in increased gene expression (714 increased and 45 decreased in IOX2; 274 increased and 21 decreased in VH032). In the volcano plot comparing VH032 to IOX2 treatment, little difference in differential gene expression was observed, with only slightly more genes upregulated in IOX2 than VH032 (Figure 5.4**A**). However, when VH032 or IOX2 treatments were individually compared to DMSO treatment, more genes were increased in expression in the presence of IOX2 (714 genes) than VH032 (274 genes) (Figure 5.4**B**), suggesting that small molecule inhibiting PHD2 (IOX2) induced a broader transcriptome change than the small molecule inhibiting VHL (VH032).

Majority of genes upregulated in the presence of VH032 overlapped with hypoxia and IOX2 treatments – 232 genes (Figure 5.4**B** and Appendix Table 9.3). Since the three conditions activated HIF transcription activity of the hypoxia signalling pathway, most

of the 232 genes were presumed to be HIF-targets. To confirm this, the subset of genes shared by the three conditions was compared to a number of publicly available datasets (Table 5.1).

A total of 83 genes out of the 232 genes upregulated in hypoxia, IOX2 and VH032 were found in at least one of these lists (Figure 5.5) and noted in Appendix Table 9.3, suggesting that these overlapped genes consisted of HIF-targets and confirming the validity of the experiment and analysis.

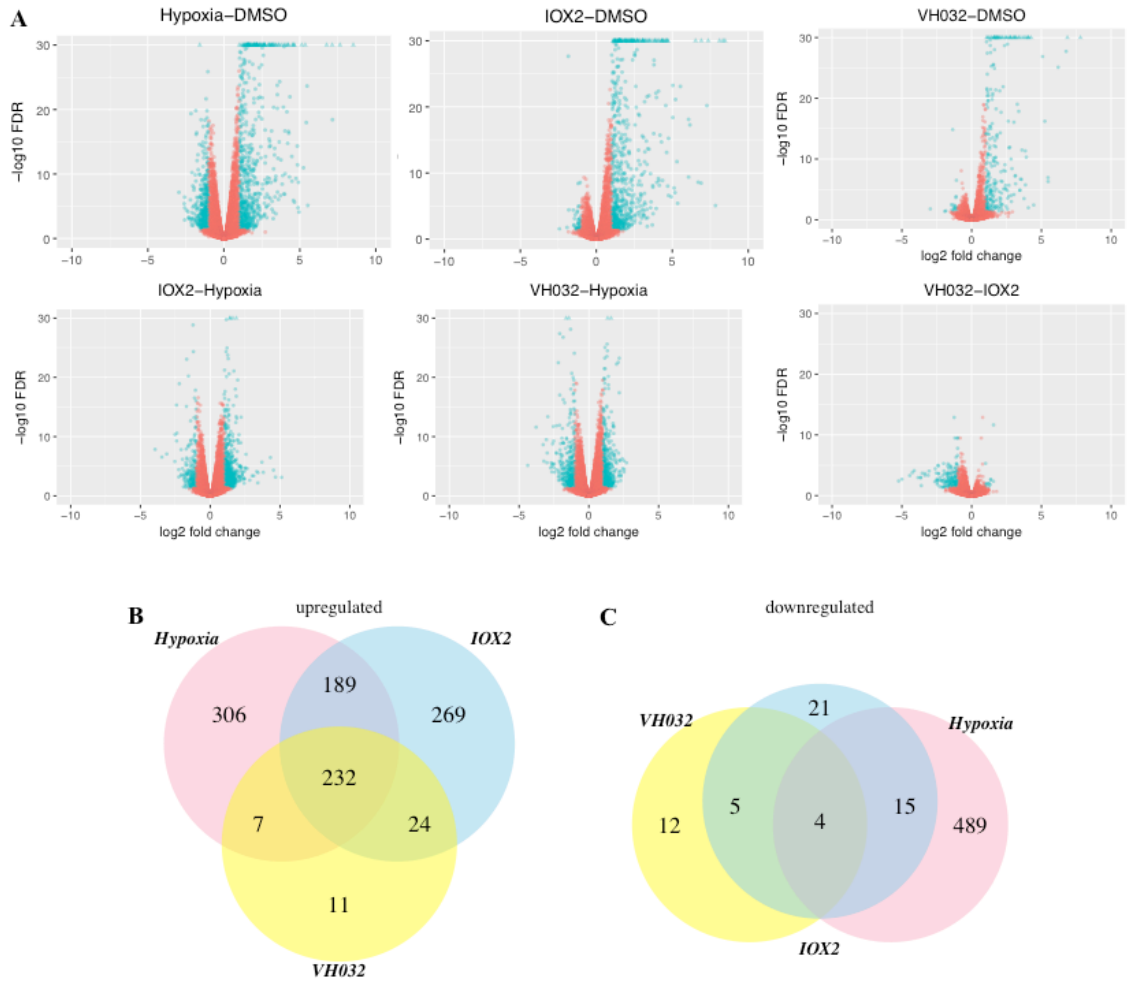

Figure 5.4 – RNA-sequencing – volcano plots and Venn diagrams of differential gene expression analysis. (**A**) Each dot represents a differentially expressed gene comparing the two conditions stated in the heading legend; comparing the condition on the left to the right, i.e., hypoxia to DMSO on the top left figure. Blue dots represent genes with increased expression (logFC > 1; to the right) or decreased expression (logFC < –1; to the left) at FDR<0.05. Blue triangles (present at –log10 FDR of 30) represent genes with logFC > 1 or < –1 and –log10 FDR > 30. (**B** and **C**) Venn diagrams showing the number of genes (**B**) upregulated (logFC > 1) or (**C**) downregulated (logFC < –1) with FDR < 0.05 in hypoxia, IOX2 and VH032 treated cells compared to DMSO control.

Table 5.1 – Publicly available datasets on validated and known HIF-targets, hypoxia-inducible genes, and genes containing HIF-1 or HIF-2 binding sites.

Reference	Description	Number of genes
(84)	Validated known HIF-targets adapted from the reference manuscript and listed in Appendix Table 9.4	100
(85)	Genes induced in hypoxia across 16 cell lines. Data was provided by Prof. Luis del Peso Ovalle, Madrid, Spain. Authors performed meta analysis of hypoxia-treated gene profiling datasets across 19 experiments and 16 cell lines and listed in Appendix Table 9.5	259
(238)	Genes upregulated in hypoxia in HeLa cells. Data was provided by Prof. Luis de Peso Ovalle, Madrid, Spain, after re-analysis of reference paper and listed in Appendix Table 9.6	1141
(239)	Genes upregulated in hypoxia in MCF7 cells	356
(240)	Genes containing HIF-1 binding sites identified by ChIP-sequencing	301
(240)	Genes containing HIF-2 binding sites identified by ChIP-sequencing	246

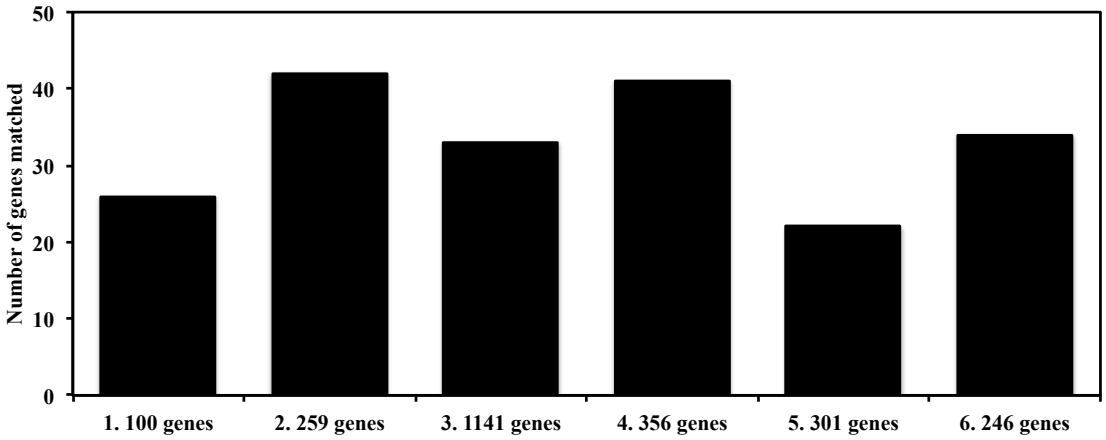

Figure 5.5 – RNA-sequencing – comparison of genes upregulated in hypoxia, IOX2 and VH032 treatments to publicly available datasets. 232 genes upregulated in hypoxia, IOX2 and VH032 was compared to publicly available datasets including (1) a list of 100 known and validated HIF targets, (2) a list of 259 upregulated genes conserved across 16 cell lines, (3) a list of 1141 genes upregulated in hypoxia in HeLa cells, (4) a list of HIF-1 (356 genes) or (5) HIF-2 (301 genes) targets identified by ChIP-sequencing, and (6) a list of 246 genes upregulated in MCF7 cells in hypoxia condition.

5.2. RNA-sequencing – validation

From the data analysis, a list of 232 upregulated genes (Appendix Table 9.3), as well as, a list of 4 downregulated genes (Appendix Table 9.2), were found overlapped in hypoxia, IOX2 and VH032 treatments comparing to DMSO negative control. Five genes (*CA9*, *PHD2* (also known as *EGLN1*), *NDRG1*, *GLUT1* (also known as *SLC2A1*), and *BNIP3*) from the upregulated list and two genes (*DUSP2* and *TAF9B*) from the downregulated list were selected for validation to confirm that the mRNA of these genes were increased or decreased, respectively.

To validate these genes shared by the three conditions, mRNA levels were measured by qRT-PCR (Figure 5.6). All the genes chosen for validation with a $\log_2FC > 1$ (upregulated genes) or $\log_2FC < -1$ (downregulated genes) presented a significant increase or decrease, respectively, in the presence of hypoxia, IOX2, VH032, when compared with DMSO control. In addition, the most potent VHL inhibitor VH298 also resulted in significant increases for the upregulated genes and decrease for the downregulated genes at 100 μM or 250 μM concentration used (with the exception that the increase of DUSP2 gene in the presence of 100 μM VH298 was not significant) (Figure 5.6). Taken together, the validation for these genes affected by hypoxia, IOX2 and VH032 was considered as successful.

A list of 11 genes (Table 5.2) and a list of 12 genes (Table 5.3) were found in the category of upregulated genes and downregulated genes, respectively, for VH032 treatment only, but not hypoxia or IOX2, when compared to DMSO control (Figure 5.4B). These genes could be potential indirect target of inhibiting VHL, independent of HIFs, PHDs or the requirement of oxygen. Four genes (*ABCA1*, *ABCG1*, *DHRS2*, and *EFR3B*) from the upregulated list (described in Table 5.2) and four genes (*LAMC2*, *CNN1*, *MICALCL*, and *GREM1*) from the downregulated list (described in Table 5.3)

were selected for validation by qRT-PCR to confirm whether the mRNA of these genes were increased or decreased, respectively, as observed in RNA-sequencing. These genes were selected as they showed increased or decreased expression from DMSO control, in

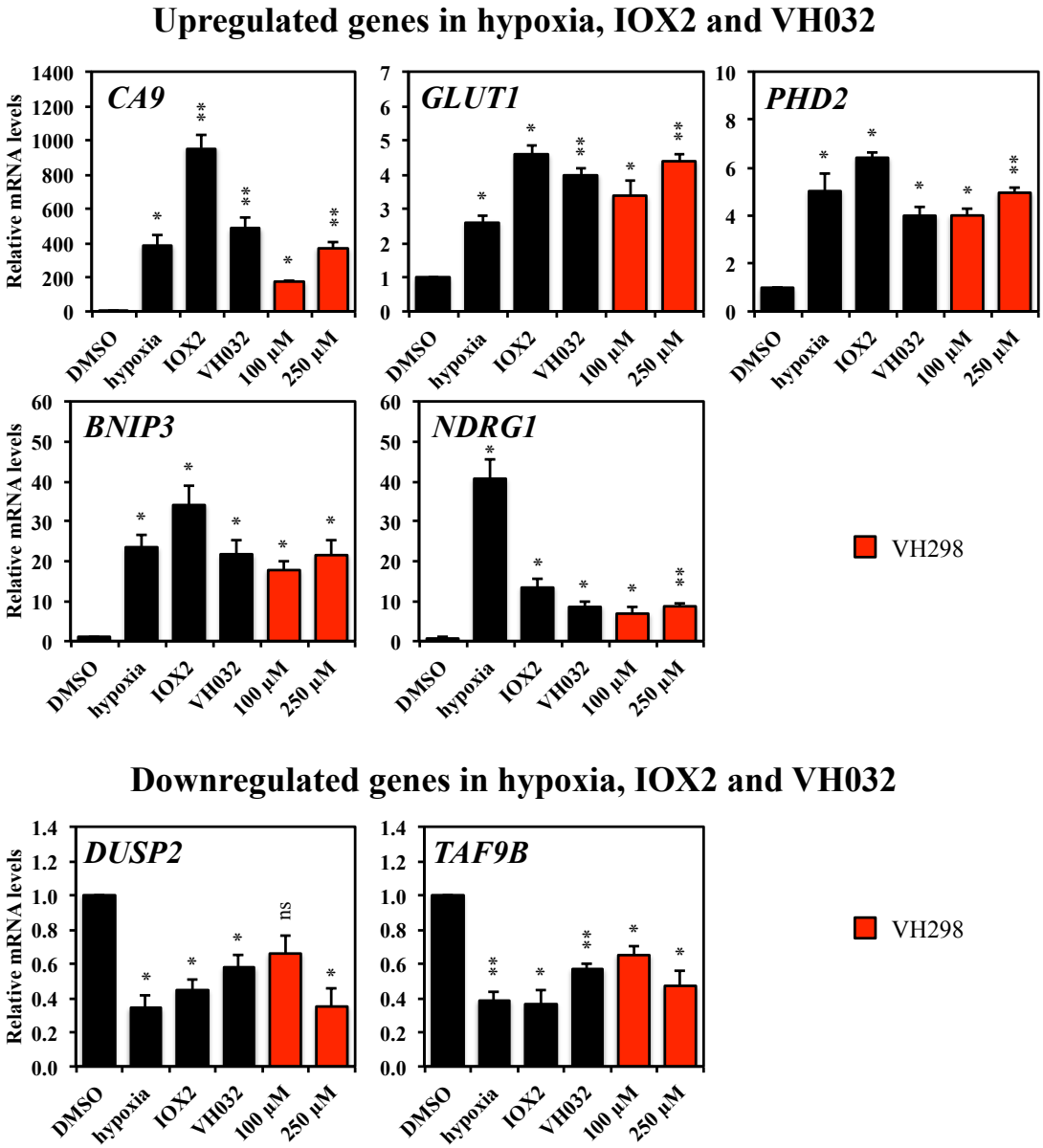

Figure 5.6 – RNA-sequencing – validation on genes upregulated or downregulated in hypoxia, IOX2 and VH032. HeLa cells were treated with 1% DMSO control, 1% O_2 (hypoxia), 250 µM IOX2 or 250 µM VH032 for 16 h prior to mRNA extraction. The graphs show relative mRNA transcripts normalised to actin mRNA levels. Black bars represent conditions as those used in RNA-sequencing experiment. Red bars represent VH298 VHL inhibitor treatments at 100 or 250 µM concentration (16 h). The mean + SEM were determined from three independent experiments. Two-tailed student t-test analysis was performed * $P \leq 0.05$, ** $P \leq 0.01$, *** $P \leq 0.001$ and ns: $P>0.05$.

particular *ABCA1* and *ABCG1*, which showed the largest log_2FC of 1.60 and 1.44, respectively, in the treatment with VH032. In addition, these selected genes are involved in important biological processes (as described in Table 5.2 and Table 5.3) and interestingly; *ABCA1* and *ABCG1* belong to the same family, the ATP-binding cassette (ABC) transporters superfamily, that function to transport cholesterol and phospholipids, suggesting that VH032 may activate the lipid transport pathway.

Table 5.2 – List of 11 genes upregulated in the presence of VH032 only, but not hypoxia or IOX2, when compared to DMSO control. Genes were selected at FDR < 0.05 and log_2FC > 1. In red: selected for validation by qRT-PCR and description for these genes were included.

Ensembl gene ID	Gene name	Description
ENSG00000076641	PAG1	
ENSG00000081665	ZNF506	
ENSG00000084710	EFR3B	Part of a complex that localise PI4K to the plasma membrane, may act as the membrane-anchoring component.
ENSG00000100867	DHRS2	Attenuates MDM2-mediated p53/TP53 degradation, leading to p53/TP53 stabilisation and increased transcription activity, resulting in the accumulation of MDM2 and CDKN1A/p21
ENSG00000140986	RPL3L	
ENSG00000149260	CAPN5	
ENSG00000149564	ESAM	
ENSG00000160179	ABCG1	ATP-binding cassette (ABC) transporters superfamily member. Involved in macrophage cholesterol and phospholipids transport and may regulate cellular lipid homeostasis in other cell types
ENSG00000165029	ABCA1	ATP-binding cassette (ABC) transporters superfamily member. Function as a cholesterol efflux pump with cholesterol as its substrate, in the cellular lipid removal pathway
ENSG00000212916	MAP10	
ENSG00000267342	RP11-552F3.10	

Table 5.3 – List of 11 genes downregulated in the presence of VH032 only, but not hypoxia or IOX2, when compared to DMSO control. Genes were selected at FDR < 0.05 and $\log_2$FC < –1. In red: selected for validation by qRT-PCR and description for these genes were included.

Ensembl gene ID	Gene name	Description
ENSG00000058085	LAMC2	Laminin is a family member of extracellular matrix glycoproteins and involved in biological processes such as cell adhesion, differentiation, migration, signalling, neurite outgrowth and metastasis
ENSG00000122367	LDB3	
ENSG00000130176	CNN1	Calponin 1 is implicated in the regulation and modulation of smooth muscle contraction.
ENSG00000133808	MICALCL	May cooperate with MAPK1/ERK2 via an intracellular signal transduction pathway in the morphogenetic development of round spermatids to spermatozoa.
ENSG00000166923	GREM1	May play a role in regulating organogenesis, body patterning and tissue differentiation. May play a role during carcinogenesis and metanephric kidney organogenesis.
ENSG00000167994	RAB3IL1	
ENSG00000236947	RP11-98G7.1	
ENSG00000242951	RP11-507E23.1	
ENSG00000254101	RP11-30J20.1	
ENSG00000257588	RP11-469H8.6	
ENSG00000260401	RP11-800A3.4	
ENSG00000261788	RP11-480G7.1	

Previously, a small portion of RNA samples was used to synthesise cDNA prior to submitting for RNA-sequencing. These cDNA samples were used for validation by qRT-PCR (Figure 5.7; black bars). All the genes chosen for validation with a $\log_2$FC > 1 (upregulated genes) presented an increase in the presence of VH032, when compared with DMSO control, particularly, a significant increase for *ABCA1* and *EFR3B*.

On the other hand, out of the four genes selected for validation with a $\log_2$FC < –1 (downregulated genes), only *CNN1* presented a significant decrease in mRNA levels (Figure 5.7; black bars). However, IOX2 treatment also resulted in a significant decrease for *CNN1*, suggesting that *CNN1* may not specifically be downregulated in the

presence of only VH032. While *LAMC2* mRNA level was not downregulated in the presence of VH032, mRNA levels of *MICALCL* and *GREM1* decreased, but not significantly.

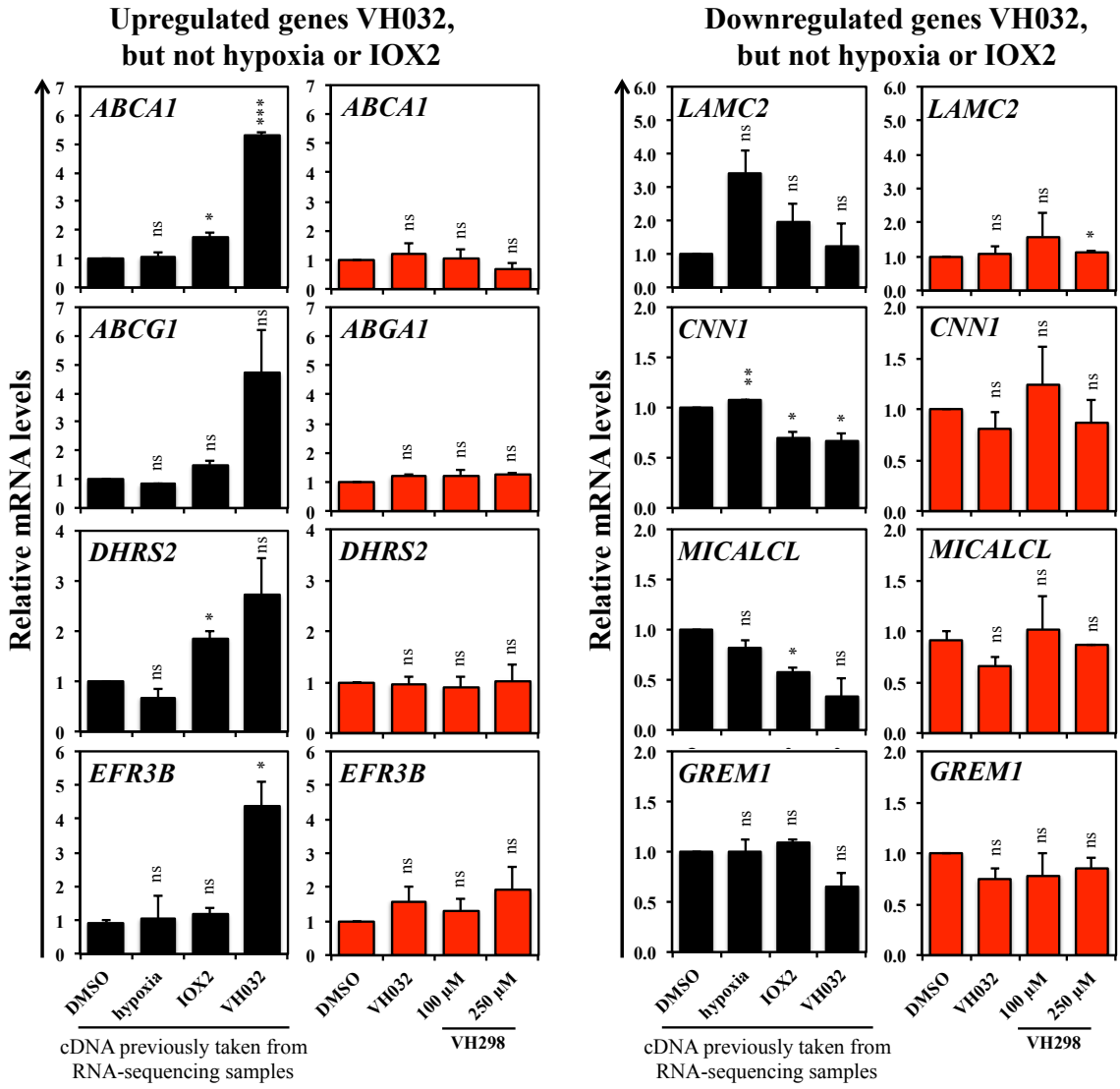

Figure 5.7 – RNA-sequencing – validation on genes upregulated or downregulated in VH032 only, but not in hypoxia, and IOX2. HeLa cells were treated with 1% DMSO control, 1% O_2 (hypoxia), 250 µM IOX2 or 250 µM VH032 for 16 h prior to mRNA extraction. The graphs show relative mRNA transcripts normalised to actin mRNA levels. Black bars: cDNA used was taken from RNA samples prior to submission for RNA-sequencing. Red bars: RNA samples were not submitted for RNA-sequencing. The mean + SEM were determined from three independent experiments. Two-tailed student t-test analysis was performed * $P \leq 0.05$, ** $P \leq 0.01$, *** $P \leq 0.001$ and ns: $P>0.05$.

To further validate these genes altered by the presence of VH032 only, qRT-PCR experiment was repeated with the same concentration of VH032 (250 μM) and VH298 (100 and 250 μM) VHL inhibitors. The two VHL inhibitors did not significantly decrease mRNA levels of any of the four downregulated genes (Figure 5.7; red bars). Strikingly, the four genes that were found upregulated in the presence of VH032 did not present significant increase in mRNA levels in the presence of VH032 or VH298. *ABCA1*, *ABCG1* an d *EFR3B* that had approximately 5-fold increase (Figure 5.7; black bars) when compared to DMSO control no longer increased when a new batch of compound was used (Figure 5.7; red bars).

Taken together these results, the validation for VH032-specific genes showed that VHL inhibitors did not affect these genes, highlighting the need for validation following RNA-sequencing experiments.

5.3. TMT-labelling – experimental setup

To gain a more complete understanding of the effects of VHL inhibitor in cells, a proteomic study was performed (Figure 5.8).

HeLa cells were treated with 250 µM VH032 (VH298 had yet to be designed), comparing with vehicle control (1% DMSO). Hypoxia (1% O_2) and PHD inhibitor IOX2 (250 µM) were included in the proteomic analysis controls. A total of four conditions were carried out with the treatment time of 24 h to observe the global proteome changes. Enabled by the 10-plex tandem mass tags (TMTs)-labelling strategy, experiment was performed in duplicate and peptides from each sample were labelled according to Figure 5.8 by Wenzhang Chen from the FingerPrints Proteomic group, Dundee. By use of the mass spectrometry-based method, more than 8,043 proteins were identified with FDR < 0.01 and quantified.

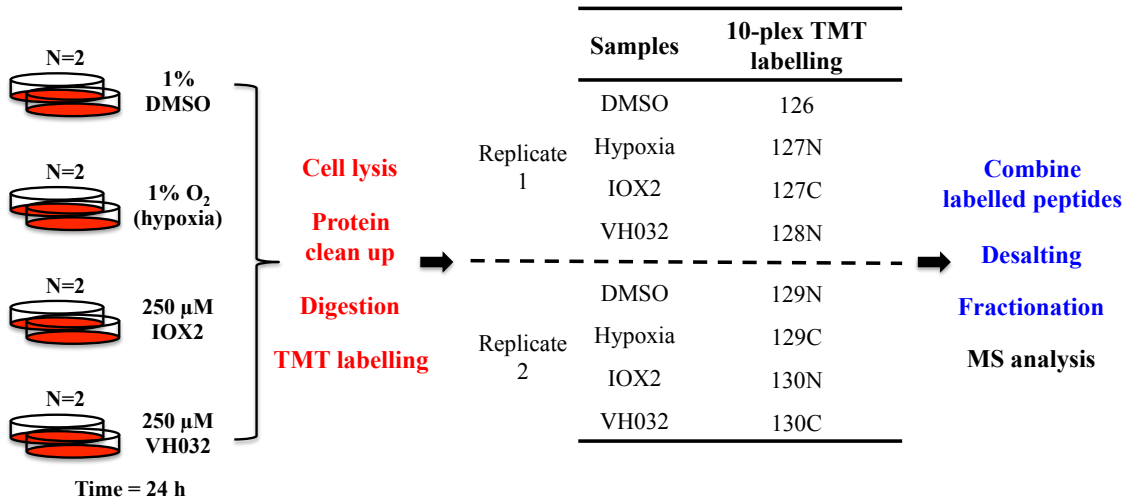

Figure 5.8 – Tandem mass tag (TMT)-labelling – workflow. HeLa cells were treated with 1% DMSO, 1% O_2 (hypoxia), 250 µM IOX2, 250 µM VH032 for 24 h – in biological duplicate. Proteins were obtained by cell lysis, cleaned up, digested by trypsinisation, and labelled with 10-plex TMT labelling reagent according to the table shown (carried out with the help of Wenzhang Chen from the FingerPrints Proteomic group, Dundee, apart from the cell lysis). Labelled peptides were combined, desalted, fractionated and analysed by mass spectrometry (MS). Red text indicates steps carried out at the protein level, and blue are performed on peptides.

To determine the reproducibility between the two replicates, the relative abundance for each protein between replicates to each respective DMSO control replicate was plotted (Figure 5.9**A**). Hypoxia treatment showed high reproducibility in protein quantification (Pearson correlation: 0.81). Instead, IOX2 and VH032 treatments were not as reproducible (Pearson correlation: 0.43, 0.30, respectively). Nonetheless, the data was used to detect possible proteome changes induced by these treatments and validation by western blotting would be performed to confirm any changes on target of interest.

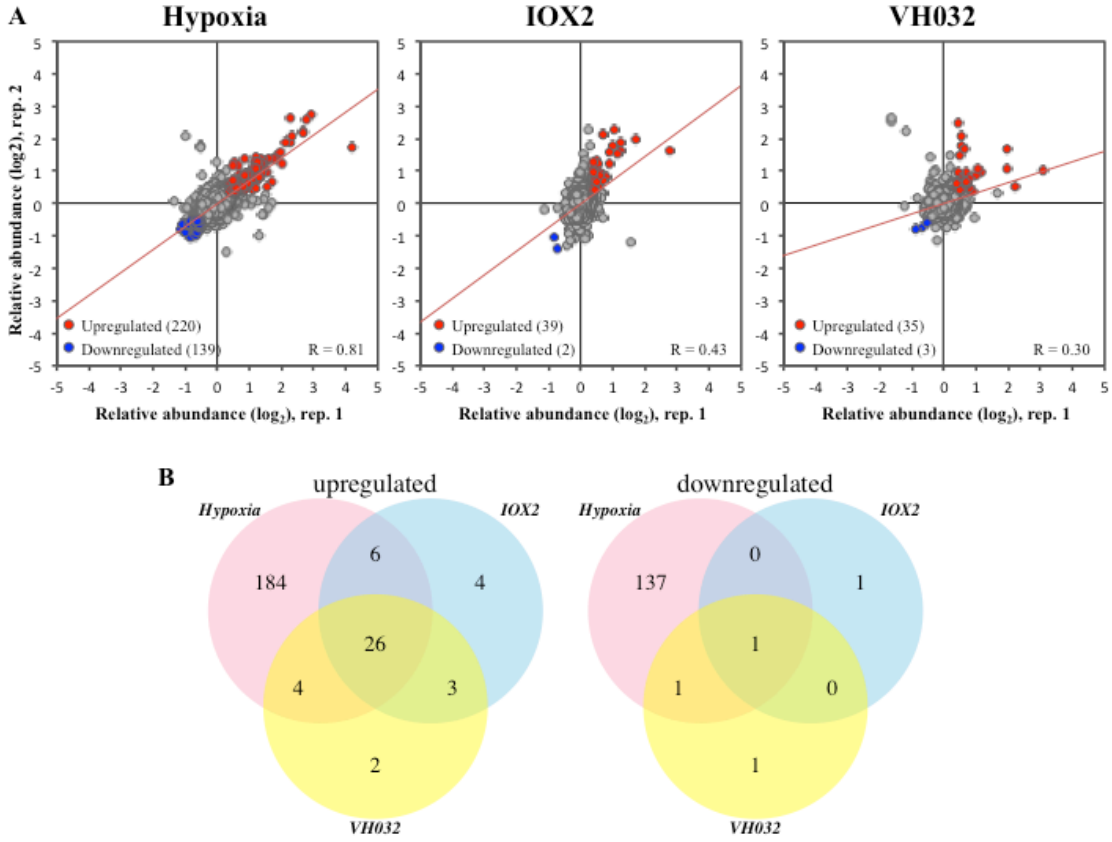

Figure 5.9 – TMT-labelling – Impact of hypoxia, IOX2 and VH032 on the cellular proteome in HeLa cells. (**A**) Scatter plot representation of relative protein abundances obtained for different treatment conditions compared to respective replicate of vehicle (DMSO)-treated cells, for a total of 8,043 proteins quantified. The two axes are relative abundance (log_2FC) from two different replicates in this experiment. Red dots represent upregulated proteins in both replicates (absolute fold change difference to DMSO > 1.3) and blue dots represent downregulated proteins in both replicates (absolute fold change difference to DMSO < 0.7). Red line is the linear fit to the data. (**B**) Venn diagrams depicting the number of upregulated proteins and downregulated proteins in the two replicates comparing the presence of hypoxia, IOX2 or VH032 to DMSO control.

5.4. TMT-labelling – differentially regulated proteins

To identify changes in protein expression, a cut-off filter of absolute fold change difference > 1.3 (a 30% increase for upregulated genes) and < 0.7 (a 30% decrease for downregulated genes) to DMSO control (FDR < 0.01) was selected. Comparing to vehicle control DMSO, treatments of hypoxia, IOX2 and VH032 altered protein expression in cells (Figure 5.9). Among the three treatments, hypoxia induced the highest number of protein expression changes; 220 proteins increased in level in hypoxia, while 139 proteins decreased. On the other hand, the majority of differentially regulated proteins were increased in the presence of IOX2 (39 versus 2 decreased) or VH032 (35 versus 3 decreased).

To investigate overall proteome changes comparing hypoxia, IOX2 and VH032 treatments, Venn diagrams for increased and decreased protein levels were plotted (Figure 5.9B). The majority of proteome changes in the presence of IOX2 and VH032 were overlapped with hypoxia (Figure 5.9B), sharing 26 upregulated targets (Table 5.4) and only one downregulated target (Table 5.5)

5.4.1. Differentially regulated proteins shared by hypoxia, IOX2 and VH032

HIF-1α was found in the list of 26 upregulated proteins in common between hypoxia, IOX2 and VH032 treatments (Table 5.4), suggesting that the cell treatments had successfully stabilised HIF-1α. Among the 26 shared upregulated proteins (Table 5.4), 22 proteins (highlighted in blue) were found in at least one of the publicly available dataset listed in Table 5.1, which contained hypoxia-inducible genes. In addition, transcripts of these 22 genes encoding these proteins (highlighted in blue) and two additional genes (*PP13G* and *KAD4*, highlighted in green) were found increased in hypoxia, IOX2 and VH032 by RNA-sequencing (Appendix Table 9.3), suggesting that

these proteins were regulated at transcriptional level. Although *KAD4* (also known as *AK4*, adenylate kinase 4) was not found in the lists in Table 5.1, it had been confirmed to be HIF-target genes (241). On the other hand, *PP13G* (also known as *PPP1R3G*) was found to be a hypoxia-inducible gene in the osteoclast microarray, but not known to be regulated by HIF (242).

Table 5.4 – List of 26 upregulated proteins shared between hypoxia, IOX2 and VH032 treatment. Proteins were selected at FDR < 0.01 and relative abundance to DMSO control > 1.3 for each replicate. Uniprot ID and gene name are listed with relative abundance to DMSO control for hypoxia (Hpx-1 and Hpx-2), IOX2 (IOX2-1 and IOX2-2), and VH032 (VH032-1 and VH032-2) in duplicate. In red: known primary target (HIF-1α). In blue: transcripts for the respective genes were found to be upregulated in hypoxia, IOX2 and VH032 by RNA-sequencing (**Appendix Table 9.3**) and found in at least one of the publicly available dataset (**Table 5.1**). In green: transcripts were found to be upregulated in hypoxia, IOX2 and VH032 by RNA-sequencing (**Appendix Table 9.3**).

Uniprot ID	Gene name	Hpx-1	Hpx-2	IOX2-1	IOX2-2	VH032-1	VH032-2
Q12983	BNIP3	18.11	3.33	11.59	2.60	8.33	2.03
P35318	ADML	6.47	4.73	2.05	4.81	1.47	3.44
O76061	STC2	3.24	1.59	1.58	4.36	1.84	1.31
P11169	GTR3	7.52	6.58	1.39	2.51	1.63	1.95
Q16790	CAH9	6.76	6.04	3.31	3.93	3.94	3.26
P06307	CCKN	1.43	2.46	1.71	1.80	1.35	1.98
Q16665	HIF1A	4.00	2.31	2.37	3.68	2.19	1.98
Q15413	RYR3	2.32	1.87	2.20	2.86	1.45	4.30
P98155	VLDLR	3.51	2.60	2.01	3.45	1.97	1.85
P05412	JUN	2.89	1.94	1.34	2.03	1.32	1.37
Q16877	F264	6.29	4.48	1.85	2.97	2.10	2.09
P11166	GTR1	3.59	2.79	1.35	1.72	1.47	1.42
Q9Y4K0	LOXL2	3.89	2.96	1.30	2.11	1.46	1.44
Q9BXL7	CAR11	2.13	1.72	1.85	2.33	1.56	3.23
Q9NX57	RAB20	2.50	1.93	1.44	2.34	1.58	1.49
P28300	LYOX	4.81	3.63	1.59	4.38	1.44	1.72
Q92597	NDRG1	5.06	4.25	1.36	1.58	1.62	1.41
B7ZBB8	PP13G	4.37	3.65	1.57	1.84	1.73	1.37
P13674	P4HA1	2.45	2.31	1.48	1.53	1.50	1.58
Q15118	PDK1	2.07	1.84	1.62	1.63	1.61	1.54
P09104	ENOG	3.03	2.62	1.39	2.23	1.70	1.74
Q9Y4C1	KDM3A	2.53	2.23	1.46	1.47	1.56	1.44
P27144	KAD4	1.42	1.38	1.31	1.38	1.33	1.37
O00469	PLOD2	2.76	2.53	1.41	1.50	1.55	1.58
Q9GZT9	EGLN1	1.87	1.61	1.37	1.44	1.39	1.34
Q9Y5U4	INSI2	2.19	2.18	1.31	2.39	1.32	1.54

Table 5.5 – A downregulated gene shared by hypoxia, IOX2 and VH032 treatments. Gene was selected at FDR < 0.01 and relative abundance to DMSO control < 0.7. Uniprot ID and gene name are listed with relative abundance to DMSO control for hypoxia (Hpx-1 and Hpx-2), IOX2 (IOX2-1 and IOX2-2), and VH032 (VH032-1 and VH032-2) in duplicate.

Uniprot ID	Gene name	Hpx-1	Hpx-2	IOX2-1	IOX2-2	VH032-1	VH032-2
Q9BRL6	SRSF8	0.60	0.58	0.56	0.49	0.62	0.60

The remaining three genes (*CCKN*, *RYR3*, and *CAR11*) (Figure 5.4) were not known to be HIF-target genes or hypoxia-inducible genes. In addition, gene expressions of *CCKN* and *RYR3* were not detected in the RNA-sequencing analysis, while *CAR11* gene expression was not significantly increased in the presence of hypoxia (log_2FC of 0.2115), IOX2 (log_2FC of -0.2106), or VH032 (log_2FC of -0.2688) with FDR < 0.01, suggesting that CAR11 could be a direct substrate of VHL or indirectly regulated in a post-translational manner by VHL target. On the other hand, CCKN and RYR3 could potentially be HIF-targets, or similar to CAR11, VHL substrates or regulated by VHL target.

Overall, the exposure to hypoxia or the treatment of PHD inhibitor IOX2 or VHL inhibitor VH032 successfully stabilised HIF-1α and known HIF-target proteins, validating the pharmacological intervention in an unbiased –omic level.

5.4.2. Differentially regulated proteins in VH032 only, and not in hypoxia or IOX2

Proteins upregulated upon VH032-mediated VHL inhibition, but not in hypoxia or PHD inhibition by IOX2 could be potential VHL targets that bind to the same pocket as HIF-α, but independent of PHD hydroxylation. In the proteomic analysis, two proteins were identified to be upregulated in VH032, but not hypoxia or IOX2: VHL and AMY1 (Table 5.6). Relative to DMSO control, protein abundance of *VHL* did not alter in IOX2

(1.02 for replicate 1 and 0.94 for replicate 2) and decreased slightly in hypoxia (0.87 for replicate 1 and 0.89 for replicate 2, thus not meeting the criteria of < 0.7). Interestingly, *VHL* protein abundance increased in VH032 (1.59 for replicate 1 and 1.53 for replicate 2) relative to DMSO control. This suggests that *VHL* protein may be altered by the small molecule-mediated inhibition of VHL. VH032 treatment also increased *AMY1* protein abundance (4.64 for replicate 1 and 1.42 for replicate 2), but not hypoxia or IOX2 (although replicate 1 of hypoxia showed a ratio of 1.25 to DMSO control). *AMY1* encodes for the salivary alpha-amylase, which is involved in catalysing the initial digestion of dietary starch and glycogen. This could potentially be a direct VHL target, but further validation would be required.

On the other hand, only one protein significantly decreased in level in the presence of VH032, but not in hypoxia or IOX2 (Table 5.7): RGCC. However, protein expression of *RGCC* also decreased in one replicate of hypoxia (0.71 in Hpx-1) and both replicates of IOX2 (0.79 in IOX2-1 and 0.45 in IOX2-2). *RGCC* fell under this category due to the selection criteria, which required the relative fold change to be < 0.7 in both replicates. RGCC (regulator of cell cycle), also known as RGC32 (response gene to complement 32), is induced by p53 in response to DNA damage and modulates the kinase activity of cell cycle. RGCC has been reported to be a hypoxia-inducible gene (243) and involved in high-altitude physiology (244). Yet, here RGCC decreased in protein levels in all three conditions. Validation would be required to further confirm the results.

Among the three genes, protein expression of *VHL* was consistent between the two replicates and significantly distinct from hypoxia or PHD inhibition treatments, and was therefore chosen for validation in subsequent work, which will be described in the next chapter.

Table 5.6 – List of two proteins with increased levels in the presence of VH032, but not hypoxia or IOX2. Genes were selected at FDR < 0.01 and relative abundance to DMSO control > 1.3. Uniprot ID and gene name are listed with relative abundance to DMSO control for hypoxia (Hpx-1 and Hpx-2), IOX2 (IOX2-1 and IOX2-2), and VH032 (VH032-1 and VH032-2) in duplicate. In red: selected for validation.

Uniprot ID	Gene name	Hpx-1	Hpx-2	IOX2-1	IOX2-2	VH032-1	VH032-2
P40337	VHL	0.87	0.89	1.02	0.94	1.59	1.53
P04745	AMY1	1.25	0.86	1.01	0.90	4.64	1.42

Table 5.7 – List of one protein with increased level in the presence of VH032, but not hypoxia or IOX2. Genes were selected at FDR < 0.01 and relative abundance to DMSO control < 0.7. Uniprot ID and gene name are listed with relative abundance to DMSO control for hypoxia (Hpx-1 and Hpx-2), IOX2 (IOX2-1 and IOX2-2), and VH032 (VH032-1 and VH032-2) in duplicate.

Uniprot ID	Gene name	Hpx-1	Hpx-2	IOX2-1	IOX2-2	VH032-1	VH032-2
Q9H4X1	RGCC	0.71	0.97	0.79	0.45	0.54	0.58

5.4.3. Differentially regulated proteins in other categories

Four proteins were found to significantly change in abundance in IOX2 treatment only and not overlapped with hypoxia or VH032 (Table 5.8). These four proteins could be target of PHD enzymes, but not recognised by VHL and independent of oxygen level. However, the fold changes in protein abundance for all four genes were > 1.3 in hypoxia replicate 1 only, and two genes (KCT2 [keratinocyte-associated transmembrane protein 2] and H2A1B [histone H2A, core component of nucleosome]) were > 1.3 in VH032 replicate 1 (Table 5.8), suggesting that they could be induced in hypoxia or upon VH032 treatment, respectively. Similar observation were seen in category of proteins shared by two of the three treatments (Table 5.9, Table 5.10, Table 5.11), where these proteins could potentially be induced in all three conditions and validation would be required to confirm these results. The followings are other examples:

- *ANKZ1* protein falls into the category of proteins induced in hypoxia and IOX2, but not VH032 (Table 5.9). However, *ANKZ1* (ankyrin repeat and zinc finger domain containing 1; involved in endoplasmic reticulum-associated degradation pathway) is one of the gene containing HIF-1 binding site identified by ChIP-sequencing (240) and RNA-sequencing analysis identified *ANKZ1* (*ANKZF1* in the RNA-sequencing list) to be common target of hypoxia, IOX2 and VH032 (Appendix Table 9.3).
- *HXK2* (hexokinase 2, also known as *HK2*) from Table 5.10 was increased in gene expression in hypoxia and VH032, but not IOX2 as analysed by RNA-sequencing (Appendix Table 9.3). However, *HK2* is a known HIF-target gene and was shown in the previous chapter to be upregulated in all three conditions by western-blotting (Figure 4.7**A**-**B**).
- TXNIP was found in the category induced by IOX2 and VH032, but not upregulated by hypoxia (Table 5.11) was identified in hypoxia treatment in MCF7 cells (239). TXNIP (thioredoxin interacting protein, also termed VDUP1 for vitamin D upregulated protein) is a major regulator of cellular redox homeostasis. Interestingly, *TXNIP* mRNA was reported to increase in hypoxic perinecrotic areas of conventional renal cell carcinoma and glioblastoma (245). However, *TXNIP* was also reported to decrease in mRNA and protein levels in hypoxia in a HIF-independent manner, but in different cell culture backgrounds (HeLa and HEK293), and decrease in mRNA in the VHL-null 786-O cells (246). Furthermore, TXNIP was found to enhance VHL:HIF-1α interaction to promote nuclear export of the complex and subsequently HIF-1α degradation (247). Unfortunately, its gene expression was not detected in the RNA-sequencing analysis presented in this chapter. Nevertheless, these published

data suggest that TXNIP plays a role in the hypoxia signalling, and it would therefore be very interesting to validate TXNIP.

Altogether, results suggest that proteins found to increase or decrease in abundance may not all be exactly correct and validation would need to be performed to confirm all these changes. In addition, there were more proteins not mentioned above that would be interesting for further pursuing, such as K1C16 and ALPK3 that seemed to increased in both hypoxia and IOX2, but not VH032, and P2RX2 and CJ011 that were increased in hypoxia and IOX2, but not VH032.

Table 5.8 – List of four proteins with increased abundance in the presence of IOX2, but not hypoxia or VH032. Genes were selected at FDR < 0.01 and relative abundance to DMSO control > 1.3. Uniprot ID and gene name are listed with relative abundance to DMSO control for hypoxia (Hpx-1 and Hpx-2), IOX2 (IOX2-1 and IOX2-2), and VH032 (VH032-1 and VH032-2) in duplicate.

Uniprot ID	Gene name	Hpx-1	Hpx-2	IOX2-1	IOX2-2	VH032-1	VH032-2
P08779	K1C16	2.80	1.21	1.34	1.49	0.98	1.11
Q8NC54	KCT2	1.44	1.05	1.34	1.35	1.44	1.12
P04908	H2A1B	1.72	1.16	1.39	1.58	1.74	1.07
Q96L96	ALPK3	2.62	0.80	1.35	1.63	1.18	0.96

Table 5.9 – List of six proteins with increased abundance that are shared by hypoxia and IOX2, but not VH032. Genes were selected at FDR < 0.01 and relative abundance to DMSO control > 1.3. Uniprot ID and gene name are listed with relative abundance to DMSO control for hypoxia (Hpx-1 and Hpx-2), IOX2 (IOX2-1 and IOX2-2), and VH032 (VH032-1 and VH032-2) in duplicate. In green: upregulated in hypoxia, IOX2, and VH032 in the RNA-sequencing analysis.

Uniprot ID	Gene name	Hpx-1	Hpx-2	IOX2-1	IOX2-2	VH032-1	VH032-2
Q86SJ2	AMGO2	2.06	1.63	1.61	1.81	1.48	1.27
Q9H7J1	PPR3E	4.73	6.23	2.33	3.06	3.20	1.25
Q9UBL9	P2RX2	2.97	1.45	1.41	1.50	1.30	1.09
Q9H8Y5	ANKZ1	1.82	1.52	1.43	1.43	1.40	1.26
O14556	G3PT	2.12	1.75	1.51	1.99	1.55	1.27
Q9H2I8	CJ011	1.78	1.86	1.30	1.32	1.13	0.90

Table 5.10 – List of four proteins with increased abundance that are shared by hypoxia and VH032, but not IOX2. Genes were selected at FDR < 0.01 and relative abundance to DMSO control > 1.3. Uniprot ID and gene name are listed with relative abundance to DMSO control for hypoxia (Hpx-1 and Hpx-2), IOX2 (IOX2-1 and IOX2-2), and VH032 (VH032-1 and VH032-2) in duplicate. In blue: HIF-target.

Uniprot ID	Gene name	Hpx-1	Hpx-2	IOX2-1	IOX2-2	VH032-1	VH032-2
Q58FG1	HS904	1.78	1.46	1.22	1.74	1.35	5.63
P52789	HXK2	1.55	1.42	1.26	1.24	1.35	1.38
P07205	PGK2	2.06	1.96	1.26	1.40	1.33	1.51
Q6ZMT1	STAC2	1.37	1.46	1.45	1.07	1.43	1.34

Table 5.11 – List of three proteins with increased abundance that are shared by IOX2 and VH032, but not hypoxia. Genes were selected at FDR < 0.01 and relative abundance to DMSO control > 1.3. Uniprot ID and gene name are listed with relative abundance to DMSO control for hypoxia (Hpx-1 and Hpx-2), IOX2 (IOX2-1 and IOX2-2), and VH032 (VH032-1 and VH032-2) in duplicate. In blue: upregulated in hypoxia in MCF7 cells (239).

Uniprot ID	Gene name	Hpx-1	Hpx-2	IOX2-1	IOX2-2	VH032-1	VH032-2
Q6ZMR3	LDH6A	2.42	0.50	6.90	3.14	3.89	2.14
Q9H6K1	CF106	1.62	1.20	1.48	1.86	1.40	2.78
Q9H3M7	TXNIP	1.22	1.16	1.30	1.97	1.64	1.57

5.5. Discussion

A chemical probe is a small molecule modulator useful for addressing questions about its target in biochemical, cell-based and animal studies. In previous chapters, VHL inhibitors were characterised as potential chemical probes for the study of hypoxia signalling. VHL inhibitors can rapidly and selectively inhibit their target protein VHL, leading to the stabilisation and subsequently transcriptional activity of HIF-α subunits.

Here, it was decided to extensively characterise the cellular effects induced by VHL inhibitor in an unbiased manner by assessing its global effect on transcriptome and proteome, using the HeLa cell-based system, which has been broadly used to assess the hypoxic response. In addition, hypoxia and the PHD inhibitor IOX2 were included in the studies. These three conditions trigger a hypoxic response – leading to the stabilisation of HIF-1α – but each affects different components involved in the hypoxia signalling pathway. The inclusion of hypoxia and PHD inhibitor treatments was postulated to allow distinguishing HIF-dependent target genes to HIF-independent target genes mediated by VHL. In addition, the proteomic analysis would also allow distinguishing HIF-target proteins from potential VHL targets independent of PHD hydroxylation.

Briefly, below are the key findings of the work presented here.

1. RNA-sequencing analysis. Hypoxia induced the largest transcriptome changes amongst the three conditions that inhibited different components of the hypoxia signalling pathway. Comparing the two inhibitors, VHL inhibitor VH032 was found to induce a less broad transcriptome alteration compared to the PHD inhibitor IOX2. Known HIF-target genes including *CA9*, *GLUT1*, *PHD2*, *NDRG1* and *BNIP3* were validated and shown to increase in all three treatments,

activating the HIF transcription activity. On the other hand, several genes was identified to specifically be altered by VH032 only and not hypoxia or IOX2 (*ABCA1*, *ABCG1*, *DHRS2*, and *EFR3B* that increased in gene expression and *LAMC1*, *CNN1*, *MICALCL*, and *GREM1* that decreased in gene expression); however the analysis of mRNA levels using a fresh batch of VH032 or in the more potent inhibitor VH298 mostly showed no significant changes, inconsistent with the RNA-sequencing results.

2. TMT-labelling analysis. Similar to the transcriptome changes, hypoxia condition resulted in the highest number of increased and decreased protein expression, while IOX2 and VH032 treatments led to mainly increased expression with similar number of proteins (39 and 35, respectively). Most interesting finding was the increase of VHL in the present of the VHL inhibitor VH032, which was not observed in hypoxia or IOX2 treatment.

Oxygen is key for survival and the deprivation of oxygen, or hypoxia, causes significant stress in living cells. To adapt to hypoxic stress, cells activate a number of cellular pathways including mTOR signalling, the unfolded protein response (UPR), and gene regulation by HIFs (44). In a HIF-dependent manner, expression of hundreds of genes is induced in hypoxia (239). Comparison of hypoxia and the two small molecule HIF stabilisers (IOX2 and VH032) showed an overlapped group of genes (Appendix Table 9.3) and proteins (Table 5.4) in the transcriptomic and proteomic data, respectively. Majority of these were HIF-target genes/proteins, which is as expected because the three conditions induce HIF activity. On the other hand, some of these hits could be novel HIF-targets, and therefore would be worth validating.

Hypoxia was also found to alter gene and protein expressions of many genes not found in IOX2 or VH032 – likely regulated in a HIF-independent manner. Many other transcription factors are known to be induced in hypoxia, including NF-κB

(68,248,249), PGC-1α (250), ATF-4, Egr-1 (249), dERR in *Drosophila melanogaster* (251) and BLMP in *Caenorhabditis elegans (252)*, could play a role in regulating HIF-independent genes, which are subsequently translated into proteins. In addition, hypoxia adaptations through mTOR signalling and the UPR are known to influence mRNA translation and consequently gene expression (44,86). Altogether, these factors could be responsible for the IOX2- or VH032-independent changes in transcriptome and proteome.

PHDs are known to have other substrates beyond HIF, including IKKβ, Cep198, the β-adrenergic receptor, and RNA polymerase (63,64). In addition, the inhibition of PHDs via genetic or pharmacologic approaches has been shown to induce mTORC1 and autophagy activation in response to amino acids, independent of HIFs (253). These signify that PHDs could potentially mediate HIF-independent responses to hypoxia and oxygen-independent responses to other stimuli such as amino acids. This may explain the induction of large number of genes in the presence of the PHD inhibitor IOX2 – 189 genes upregulated shared by IOX2 and hypoxia but not VH032 and 269 genes upregulated in IOX2 only and not hypoxia/VH032. Interestingly, these 189 genes may represent genes transcriptionally regulated by target proteins of PHD hydroxylation, independent of VHL recognition, at least by the pocket that binds to hydroxylated HIF-1α. Potential transcription binding sites present in these 189 genes were computed through the Gene Set Enrichment Analysis (GSEA) website at FDR < 0.05 (top 10 gene sets in Appendix Table 9.7, list of overlapped genes in Appendix Table 9.8). These data may be useful in identifying potential novel transcription factor induced by PHD hydroxylation, independent of VHL. In addition, the transcriptomic data combined with the proteomic data would allow the revelation of possible novel PHD-targets. On the other hand, proteins shared between IOX2 and VH032 (not in hypoxia) might be potential novel PHD targets recognised by VHL.

One flaw of the proteome analysis was the reproducibility of the replicates and detection of proteins. Only two biological replicates were performed and the reproducibility between the replicates for IOX2 and VH032 was poor. Data obtained would not be completely reliable and validation would be required to confirm any hits of interest. Furthermore, mass spectrometry detection of peptides is known to be "hit and miss" and detection of peptides from the same protein is not always consistent between replicates. Therefore, increasing the number of replicates would greatly strengthen the reliability of data obtained. The amount of protein lysates used for co-IP should be increased to ensure the pullldown of sufficient VHL protein. In addition, repeat with VH298, the most potent VHL inhibitor identified so far, would be ideal as VH298 is now available for purchase via commercial suppliers (https://www.tocris.com/products/vh-298_6156), and extensive study with VH298 would be useful for the community in hypoxia field.

Nonetheless, the analysis was sufficient as an initial screen for identifying potential targets of interest, as demonstrated by the presence of HIF-1α and HIF-targets in hypoxia, IOX2 and VH032. The proteomic analysis would be useful for distinguishing HIF-target proteins to potential VHL targets independent of PHD hydroxylation. Interestingly, *VHL* was identified to increase in protein expression in the present of VH032, but not hypoxia or IOX2, and this result led to the decision to validate and further investigate this observation, which will be discussed in the next chapter.

Although not pursued in this thesis due to time constraints, in future, it would also be interesting to further validate and investigate hits of RNA-sequencing and proteomic mentioned, and especially discussed in this chapter that may be potential novel HIF-targets, PHD-targets independent of VHL or PHD-targets recognised by VHL. Initial validation such as qRT-PCR to monitor mRNA levels of RNA-sequencing hits,

and western-blotting to confirm the changes in protein levels would be warranted, especially if good antibodies are available for the identified hits.

Most important to highlight was the overall effect of VHL inhibitor on the global transcriptome and proteome. Data showed that the VHL inhibitor was very specific – majority of gene and protein expression changes are common with hypoxia and IOX2, indicating that the VHL inhibitor may be specifically influencing primarily HIF activation. As the small molecule inhibitor was designed to possess a hydroxyproline residue, thus mimicking the hydroxylated proline residue of HIF-1α in order to compete with and stabilise hydroxylated HIF-1α, it is an important and reassuring discovery of the work presented in this chapter that the VHL inhibitor was not found to affect putative HIF-independent VHL functions. It is rare for chemical probes to be characterised so extensively at the transcriptome and proteome level. The thorough study of VHL inhibitors presented herein would therefore be useful for scientists using this compound as chemical probe. For instance, if there were a specific gene of interest that may be regulated by VHL, glimpse at transcriptomic and proteomic levels would be available.

In summary, analyses of VHL inhibitor VH032 at the transcriptome and proteome level in an unbiased fashion revealed for the first time that the VHL inhibitor was very selective and on-target – affecting primarily, if not, exclusively the canonical VHL:HIF interaction. Furthermore, the inclusion of IOX2 and hypoxia conditions in these analyses have uncovered potential novel hits, such as HIF-targets and HIF-independent PHD-targets, which provide a direction for further exploration on the functions of PHDs and VHL. These datasets would be useful for scientists using the chemical probe and would be made publicly available.

6. VHL inhibitors increase VHL protein levels

6.1. Introduction

In hypoxia, HIF-α proteins are known to be readily upregulated, but this is not sustained in prolonged hypoxia as HIF-α proteins are eventually degraded by mainly the proteasome (Figure 4.3**C** and **D**). This feedback effect is known to be due to the increase of HIF-targets, PHD enzymes, PHD2 and PHD3 (Figure 4.7**C**) (254). The downregulation of the stabilised HIF-α was also observed in cells treated with VHL inhibitor for prolonged periods (Figure 4.3**D**); however, unlike following hypoxia treatment, PHD3 was not greatly upregulated under VHL inhibition (Figure 4.7**C**). In addition, proteomic analysis (shown in the previous chapter) in the presence of VHL inhibitor VH032 revealed an increase in VHL protein levels. Interestingly, this increase was not observed when cells were treated with the PHD inhibitor IOX2 or hypoxia (1% O_2).

The aim of the work presented in this chapter was to investigate the significance of the increase of VHL proteins in the presence of VHL inhibitor.

Here, in agreement with the proteomic data, VH032 treatment led to increased VHL protein levels in HeLa cells and also in HFF cells. In addition, the most potent VHL inhibitor, VH298, also induced this upregulation. Treatment with VHL inhibitors did not result in changes in VHL at the transcriptional level. Importantly, increased levels of VHL protein, observed in the presence of VHL inhibitor, were responsible for the downregulation of HIF-1α occurring following prolonged treatment. Furthermore, this occurred primarily via the proteasomal degradation. Using a variety of approaches, results revealed that the upregulation of VHL levels was mediated by an increase in VHL half-life in the presence of VH298. Co-immunoprecipitation of VHL coupled with mass spectrometry was performed to identify potential regulators of VHL.

6.2. VHL inhibitors increase VHL protein levels in cells

TMT-labelling proteomic analysis indicated that VHL was increased at the protein level following a 24 h of treatment with the VHL inhibitor VH032, but not following treatment with hypoxia (1% O_2) or PHD inhibitor IOX2 (Table 5.6 and Figure 6.1). To validate this observation, VHL protein levels in HeLa cells treated with VH032 were monitored by western blot. VHL protein levels did not increase after a short treatment of 2 h, but showed marked upregulation in response to the longer treatment of 24 h with

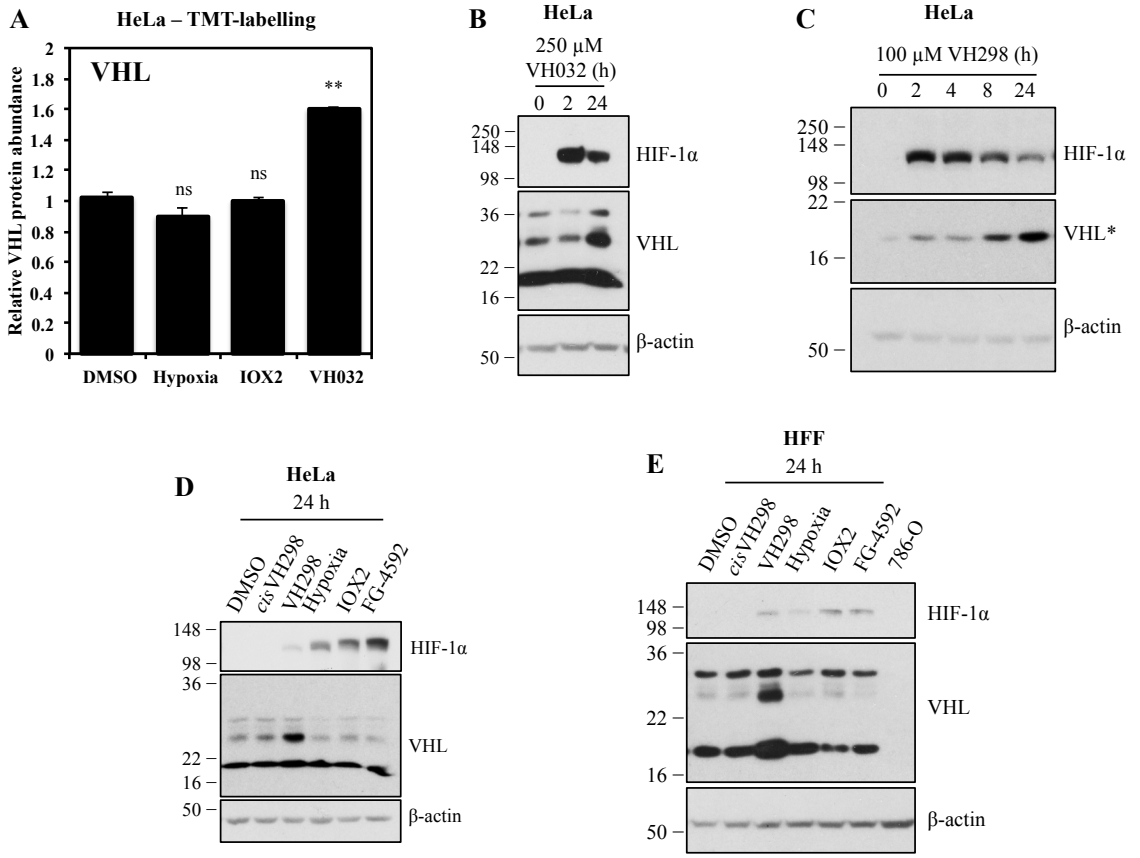

Figure 6.1 – VHL protein levels increase in the presence of VHL inhibitors. (**A**) Graph depicting relative VHL protein abundance to DMSO control for hypoxia, IOX2 and VH032 treatments after 24 h. Data are presented as means + SD from proteomic analysis (TMT-labelling) of two independent biological experiments. Two-tailed student's t-test was performed to calculate p values, and levels of significance are denoted as follows: ***0.001<P<*0.01 and, ns: *P>0.05*. HeLa cells were treated with (**A**) 250 μM VH032 or (**C**) 100 μM VH298 for indicated time. (**D**) HeLa or (**E**) HFF cells were treated with 1% DMSO, hypoxia (1% O2), and 100 μM of indicated compounds for 24 h. 786-O cell lysate was loaded in (**E**) as negative control for VHL bands. Protein levels were analysed by immunoblotting using antibodies against HIF-1α, VHL, VHL* (older VHL antibody #2738; Cell Signalling), and β-actin which acted as a loading control. The blots shown are representative of three independent experiments.

VH032 (Figure 6.1**B**). The increase in VHL protein levels was also observed with the more potent VHL inhibitor, VH298 (Figure 6.1**C**-**E**), also in a time-dependent manner (Figure 6.1**C**), confirming that this increase is due to the inhibition of VHL by the small molecules. Additionally, the increase in VHL protein levels was not observed with the non-binding epimer *cis*VH298 (Figure 6.1**D**-**E**), further demonstrating that the inhibition of VHL by small molecules results in the accumulation of VHL.

In HeLa and HFF cells, the treatment of hypoxia or PHD inhibitor IOX2 did not increase VHL protein levels (Figure 6.1**D**-**E**), in agreement with the TMT-proteomic results (Figure 6.1**A**). In addition, treatment with FG-4592, which is also a PHD inhibitor, showed similar results to those obtained with IOX2 – no alteration in VHL protein levels.

Altogether, VHL protein was confirmed to be upregulated by the small molecule VHL inhibitors, not only in HeLa cells, in which the proteomic analysis was performed, but also in HFF fibroblasts, and this increase was not observed following hypoxia or in the presence of PHD inhibitors.

6.3. Ligand-bound VHL increased protein stability

To examine whether the increase in VHL protein levels in the presence of VHL inhibitor was due to an increase in mRNA levels, qRT-PCR assays monitoring mRNA levels of *VHL* were performed. mRNA levels of *VHL* were not altered in the presence of VH032 or VH298 in HeLa (Figure 6.2**A**) or VH298 in HFF cells (Figure 6.2**B**). Similar to the unaltered VHL protein levels, hypoxia and IOX2 did not induce changes in VHL mRNA levels (Figure 6.2**A**).

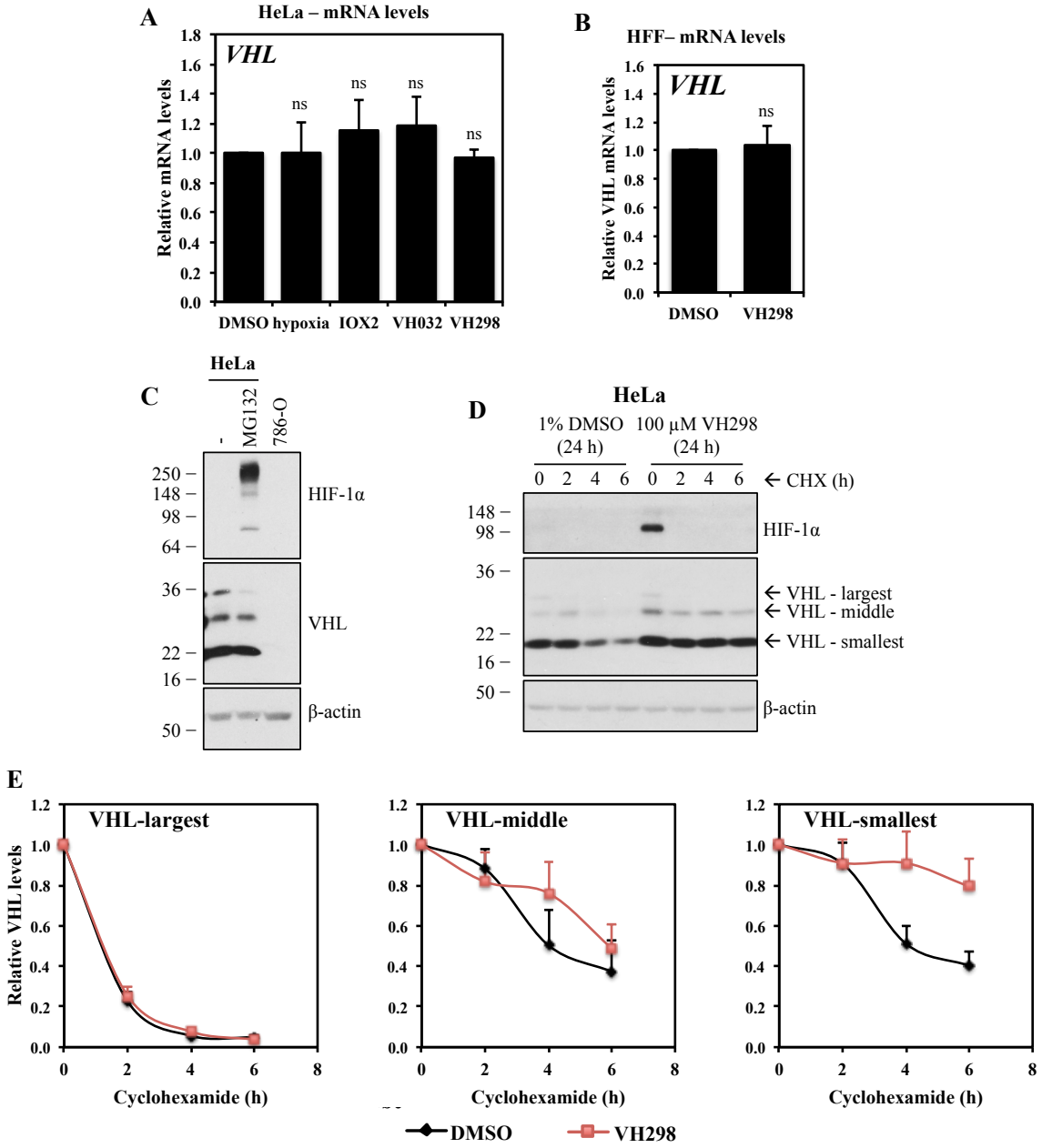

Figure 6.2 – VHL inhibitor stabilises VHL proteins. VHL mRNA expressions in (**A**) HeLa cells treated with 1% DMSO, hypoxia (1% O2), and 250 µM IOX2, 250 µM VH032 or 100 µM VH298 for 16 h or in (**B**) HFF cells treated with 1% DMSO or 100 µM VH298 for 24 h. mRNA was collected, reverse transcribed and analysed by qRT-PCR. The shown levels of the indicated mRNAs were normalised to those of β-actin. Graphs depict the mean + SEM of three independent biological replicates. Two-tailed student's t-test was performed to calculate p values, and levels of significance are denoted as follows: ns is *P>0.05*. (**C**) HeLa cells treated with 20 µM MG132 for 3 h. 786-O cell lysate was loaded as negative control for VHL and HIF-1α. (**D**) Half-life of VHL proteins of HeLa cells treated with DMSO negative control or VH298 VHL inhibitor was measured by treating cells with cycloheximide (CHX) for indicated times. (**E**) VHL protein levels (divided into largest, middle and smallest bands) were quantified from multiple blots of different exposure time by ImageJ and plotted. Protein levels were analysed by immunoblotting using antibodies against HIF-1α, VHL, and β-actin, which acted as a loading control. The blots shown are representative of three independent experiments.

Another possible cause of the increase of VHL proteins in the presence of VHL inhibitor was thought to be that VHL might be auto-regulating itself to be degraded by the proteasome, similar to how VHL regulates the proteasomal degradation of HIF-1α. To investigate whether VHL targets itself for proteasomal degradation, HeLa cells were treated with the proteasome inhibitor MG132 (Figure 6.2**C**). This analysis showed that VHL proteins were not uregulated in the presence of MG132. In fact, the largest band of VHL detected (just below 36 kDa) showed a decrease in protein level following treatment with the proteasome inhibitor.

Another possibility of the increased VHL proteins is that the ligand-bound VHL may be more stable than the unbound form. To determine if the half-life of VHL increases in the presence of VHL inhibitor, a cycloheximide chase experiment, which inhibits *de novo* protein synthesis, was performed on the endogenous VHL in cells. Multiple bands of VHL were present and divided into three categories according to their observed sizes: VHL-largest, VHL-middle and VHL-smallest. Analysis revealed a shorter half-life of around 1.5 h for the largest VHL protein and similar half-life of 4 h for VHL-middle and VHL-smallest (Figure 6.2**D**-**E**). VHL inhibitor VH298 did not alter protein stability of VHL-largest, but increased the half-life of the middle and smallest VHL proteins. Half-life of VHL-middle increased from 4 h to 6 h in the presence of VH298, while the half-life of VH298-bound VHL-smallest was beyond the 6 h cycloheximide treatment. This result correlates to the increased protein levels for VHL-middle and VHL-smallest seen in the presence of VHL inhibitors (Figure 6.1**B**-**E**).

Taken together this data indicates that the binding of VHL inhibitor leads to increased VHL protein levels, as a result of protein stabilisation.

6.4. HIF-1α protein levels decreased in prolonged VH298 treatment

In hypoxia, HIF-α proteins are known to be readily upregulated, but this is not sustained in prolonged hypoxia as HIF-α proteins are eventually degraded by the proteasome, due to the increase of HIF-targets, PHD2 and PHD3 (254). The downregulation of HIF-1α was also observed when cells were treated with VHL inhibitor (Figure 6.3**A**). Although PHD2 levels increased significantly under VHL inhibitor, PHD3 was not upregulated to the same extent as under hypoxia (Figure 4.3**D)**.

One possible cause for the decrease in HIF-1α in prolonged VH298 treatment is that VHL inhibitor was exhausted after long treatment, and therefore was not enough to inhibit VHL. To investigate this hypothesis, cells were first treated with 100 μM VH298 for 24 h, where HIF-1α levels decreased, followed by additional treatment with VH298 for 2 h at optimum concentration (concentration at which maximum HIF-1α level is induced). At 2 h treatment, the optimum doses of VH298 required to treat HeLa and HFF cells were 400 μM and 100 μM, respectively (Figure 6.3**B**). Using the optimum concentration of VH298 determined, after the initial 24 h treatment with 100 μM VH298, 400 μM and 100 μM VH298 was added to HeLa and HFF cells, respectively. The addition of more VH298 increased HIF-1α slightly, but did not rescue the degraded HIF-1α to the same level as the initially stabilised HIF-1α at 2 h in both HeLa and HFF (Figure 6.3**C**).

Results indicate that the decrease of HIF-1α levels in prolonged VH298 treatment was not due to insufficient VH298 to inhibit VHL. However, it is possible that the extra-added inhibitor may still be insufficient to fully saturate the target, given the significantly increased VHL levels under those conditions.

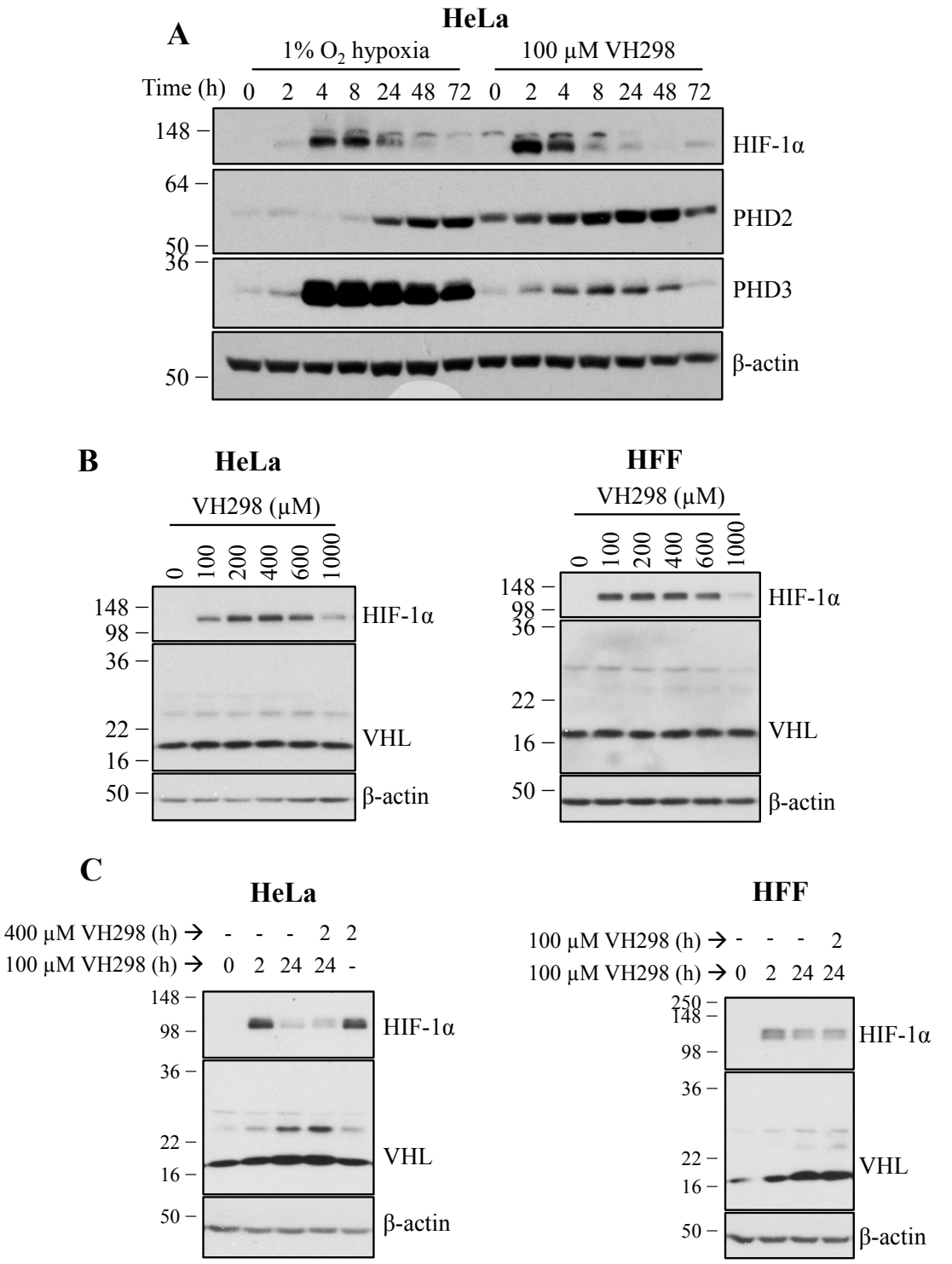

Figure 6.3 – HIF-1α protein levels decreased in prolonged VH298 treatment and could not be rescued with the re-addition of VH298. (**A**) Time-course immunoblots of HIF-1α and its targets (PHD2 and PHD3) in hypoxia (1% O_2) or 100 μM VH298. (**B**) Dose-dependent immunoblots of HIF-1α in HeLa (**left panel**) and HFF (**right panel**) cells treated with VH298 for 2 h. (**C**) HeLa and HFF cells were treated with 100 μM VH298 for 2 and 24 h. After 24 h treatment of 100 μM VH298, 400 μM VH298 was introduced to HeLa cells for 2 h and 100 μM VH298 to HFF cells for 2 h. A 2 h treatment with 400 μM VH298 was also included in HeLa cells. Protein levels were analysed by immunoblotting using antibodies against indicated proteins, and β-actin, which acted as a loading control. The blots shown are representative of three independent experiments.

6.5. The decrease in HIF-1α levels in prolonged VHL inhibitor treatment was due to increased VHL protein levels

HIF-1α is known to be degraded via the proteasomal (255) as well as lysosomal (256) pathways. To investigate if the VHL inhibitor-induced HIF-1α was degraded in prolonged treatment by either of the pathways, cells were first treated with VH298 for 24 h, followed by proteasome inhibitor (MG132) or lysosome inhibitors (chloroquine or bafilomycin A1) for the last 3 h. As expected, all three inhibitors stabilised HIF-1α, where MG132 accumulate post-translational modified HIF-1α (present as a smear) and, both chloroquine and bafilomycin A1 treatments resulted in a single band of HIF-1α (Figure 6.4**A**).

After 24 h VH298 treatment, MG132 rescued the degraded HIF-1α to similar protein levels as 3 h treatment of VH298 (Figure 6.4**A**). On the other hand, lysosomal inhibitors were not as efficient; both chloroquine and bafilomycin A1 increased HIF-1α to a much lower extent. These data indicate that the accumulated HIF-1α proteins in the presence of VHL inhibitor VH298 were degraded, in the long-term VH298 treatment, via mainly the proteasomal pathway. The lysosomal pathway also contributes to HIF-1α degradation in the presence of the VHL inhibitor, but to a lower extent.

Similar to the previous data (Figure 6.2**C**), the middle and smallest VHL proteins remained unaltered in the presence of MG132, while the largest VHL band seen was depleted (Figure 6.4**A**). The combination of VH298 and MG132 treatment resulted in the same observed depletion of VHL-largest in MG132, as well as increases in VHL-middle and VHL-smallest protein levels. Instead, the treatment of chloroquine or bafilomycin A1 alone did not seem to alter VHL protein levels, and the addition of either of the lysosome inhibitor to cells that had been treated with VH298 for 24 h also did not further change the accumulated VHL.

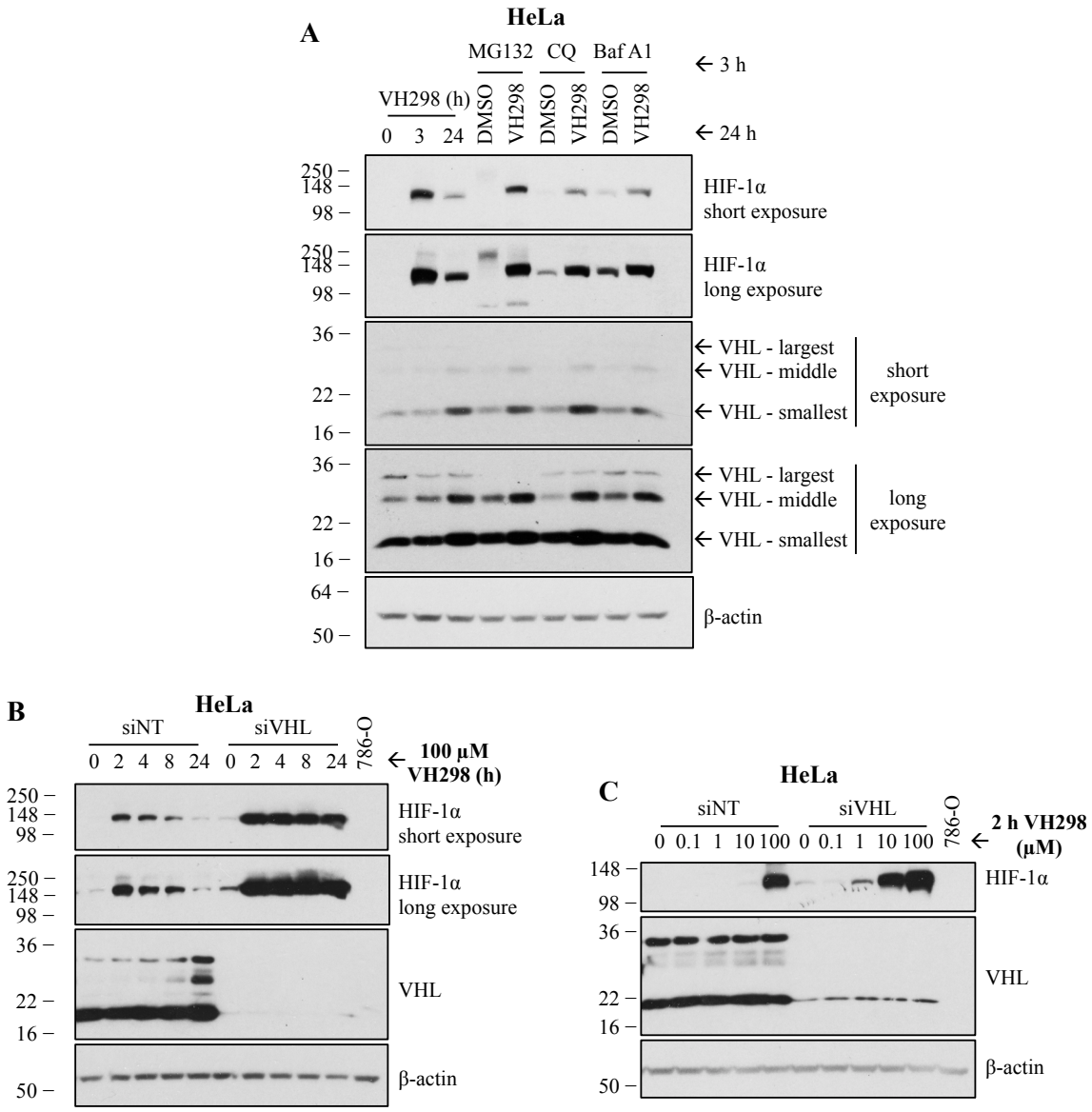

Figure 6.4 – The decrease of HIF-1α protein levels in prolonged VH298 treatment is mediated by proteasomal degradation in a VHL-dependent manner. (**A**) HeLa cells were treated with 3 and 24 h of 100 µM VH298. After 24 h treatments of 1% DMSO or 100 µM VH298, cells were treated with proteasome inhibitor MG132 (20 µM), autophagy inhibitors chloroquine (CQ; 50 µM) or bafilomycin A1 (Baf A1; 50 nM) for 3 h. (**B** and **C**) HeLa cells were transfected with non-targeting siRNA control (siNT) or VHL siRNA (siVHL). (**B**) After 24 h, media was changed and transfected cells were treated with 100 µM VH298 for indicated times. (**C**) After 46 h, media was changed and transfected cells were treated with indicated concentrations of VH298 for 2 h. Cell lysate of 786-O was included as negative control for VHL. Protein levels were analysed by immunoblotting using antibodies against HIF-1α, VHL, and β-actin, which acted as a loading control. The blots shown are representative of three independent experiments.

The results so far show that in the long treatment of VH298, the initially induced HIF-1α levels decreased and VHL increased. To investigate whether the VH298-induced HIF-1α is degraded in VHL-dependent manner, siRNA-mediated knockdown of VHL was performed in HeLa cells. In control siRNA-treated cells, VH298 treatment over time resulted in HIF-1α degradation, whereas under VHL knockdown by siRNA, HIF-1α remained stabilised over the entire course of the 24 h compound treatment (Figure 6.4**B**). This result suggests that the degradation of VH298-induced HIF-1α was mediated by VHL.

Interestingly, the knockdown of VHL only led to slight stabilisation of HIF-1α. siRNA approach might not be able to completely remove all endogenous VHL, and even very low amount of the remaining VHL appears to be enough to efficiently polyubiquitinate HIF-1α for proteasomal degradation. The high activity and catalytic efficiency of VHL might explain the requirement of relatively high concentration of VHL inhibitor in order to observe detectable levels of HIF-1α. To examine this hypothesis, a dose-dependent VH298 treatment was performed with and without siRNA-mediated VHL knockdown. In the knockdown of VHL, HIF-1α levels could be detected already at 1 μM concentration of VH298, and 10 μM inhibitor treatment under VHL knockdown could achieve similar HIF-1α stabilisation as 100 μM VH298 in the negative control siRNA background. The combination of VH298 and the knockdown of VHL clearly showed additive effect on accumulating HIF-1α.

Together, these results indicate that following treatment with VHL inhibitor VH298, HIF-1α that is initially stabilised, is eventually degraded via the proteasome pathway, still in a VHL-dependent manner, and driven likely by the prominent increase in VHL levels.

6.6. Analysis of VHL interactome in the presence of VH298

The results above demonstrate that VHL is upregulated in the present of VHL inhibitors. In an attempt to dissect the mechanism behind VHL upregulation in the present of VHL inhibitor, a proteomic analysis of VHL interactome was performed through co-immunoprecipitation (co-IP) coupled with mass spectrometry (MS) analysis. For this study, VHL antibody was used to isolate endogenous VHL in order to observe native interactors. Co-IP using VHL antibody was optimised as described below.

First, a VHL antibody obtained from BD Biosciences was confirmed to be able to immunoprecipitate VHL from HeLa cell lysates treated with MG132 (Figure 6.5). Furthermore, as MG132 blocks the proteasome, it was possible to demonstrate that, under these conditions, HIF-1α was in complex with VHL. Although sepharose protein G beads immunoprecipitated more VHL than the magnetic dynabeads protein G, sepharose beads were incubated with lysates:antibodies complex longer (overnight), compared to 1 h incubation with of lysates with antibody-coated dynabeads (Figure 6.5**A**). As both beads seemed to work equally well, it was decided to use dynabeads to minimise loss of sample through the use of magnetic separation rather than the centrifugation approach of using sepharose beads.

Next, since 10 min incubation of antibodies with dynabeads immunoprecipated comparable amount of VHL to overnight incubation, using 10 min incubation time, lysates were incubated with the antibodies-coated dynabeads for 1 h or overnight (Figure 6.5**B**). The antibodies:beads complex formed overnight immunoprecipitated much more VHL than the 1 h incubation. Therefore for this interactome study, 6 µg of antibody was first coated on the magnetic beads for 10 min, followed by overnight incubation with 750 µg of cell lysates.

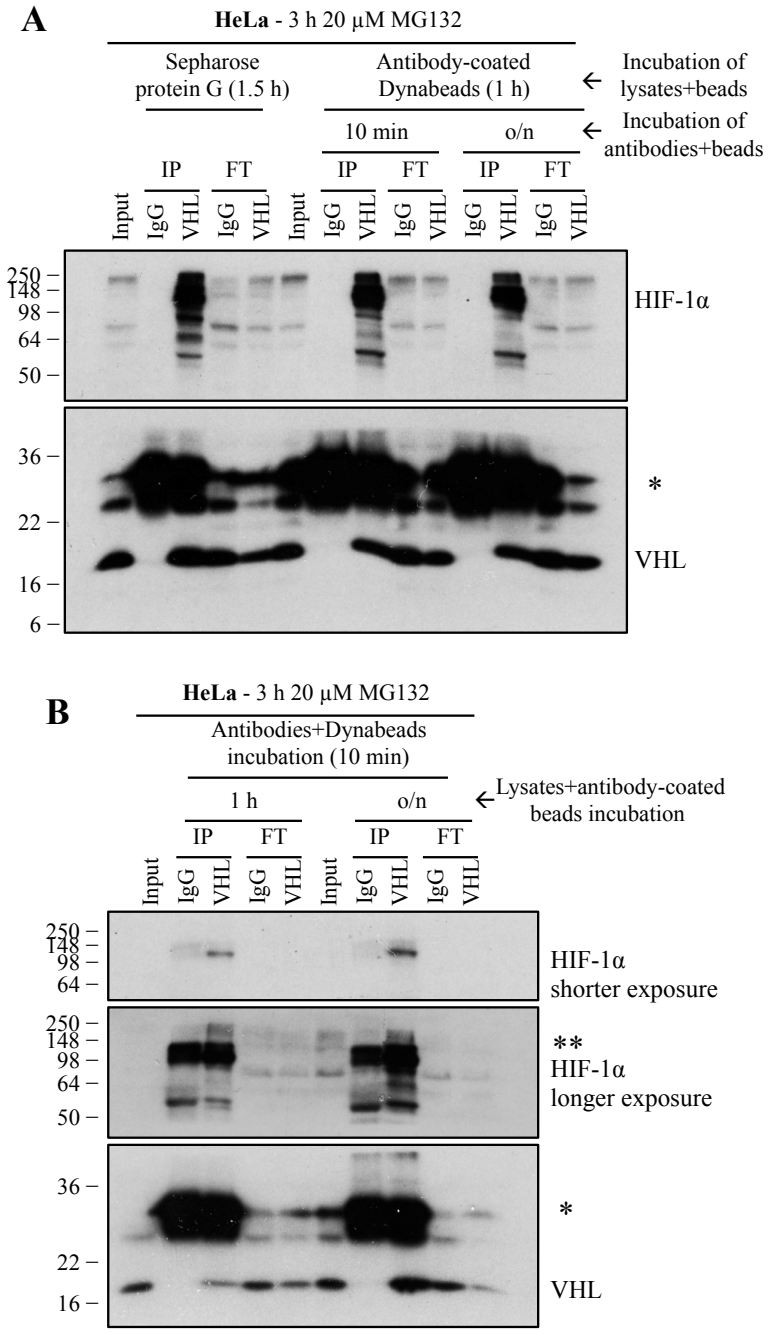

Figure 6.5 – Optimisation for co-immunoprecipitation of VHL. HeLa cells treated with MG132 (20 μM for 3 h) prior to cell lysis. 500 μg of protein lysates were used to immunoprecipitate VHL with the 4 μg VHL antibody (BD Biosciences). 4 μg Rabbit immunoglobulin G (IgG) was used as a control. Inputs represent 10% of the starting material used per immunoprecipitation (IP) and flow-through (FT) represents 10% of the flow-through collected after IP. (**A**) co-IP using sepharose beads was compared to dynabeads. Protein lysates were incubated with VHL antibodies at 4°C for overnight, followed by incubation with sepharose protein G beads for 1.5 h at 4°C on a rotating platform. On the other hand, dynabeads were first coated with antibodies for 10 min incubation at room temperature or overnight at 4°C, followed by incubation with protein lysates for 1 h at 4°C. (**B**) Dynabeads were first coated with antibodies for 10 min incubation at room temperature, followed by incubation with protein lysates for 1 or overnight at 4°C. * denotes IgG light chain at approximately 30 kDa and ** denotes non-specific band.

Co-IP experiments were performed on lysates of HeLa cells exposed to 3 h of DMSO (negative control), MG132, VH298, and a mix of MG132 with VH298 to block both the proteasome and the VHL:HIF-1α interaction (Figure 6.6). The rationale for combining MG132 and VH298 was because as VH298 binds to the VHL pocket, a new surface could be formed and may lead to interaction with new binder. Thus, blocking the proteasome may stabilise VHL:VH298:newbinder interaction, if the new binder were to be degraded via the proteasome system. While, the treatment of only MG132 was used to exclude protein complexes formed in the presence of the proteasome inhibitor, such as HIF-1α and proteins involved in HIF-1α degradation. Analysis was performed in four replicates.

Protein response to treatment was estimated by label-free quantification. Although the same amount of VHL antibodies and beads used, peptide intensity for VHL may differ between samples in the same replicate due to technical issues such as pipetting and

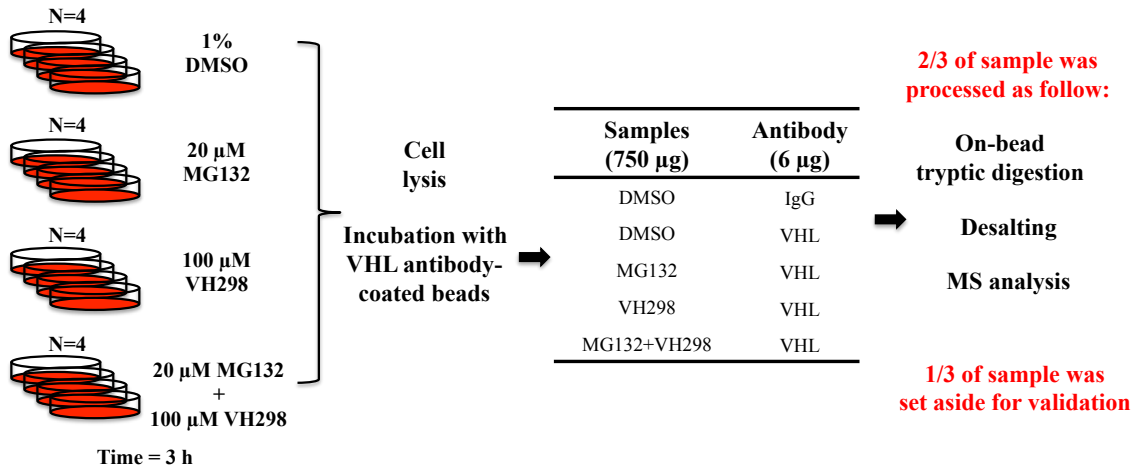

Figure 6.6 – Co-immunoprecipitation coupled mass spectrometry workflow. HeLa cells were treated with 1% DMSO, 20 µM MG132, 100 µM VH298, or a mix of 20 µM MG132 and 100 µM VH298 for 3 h prior to harvesting. 6 µg VHL antibody (BD Biosciences) was coated on 50 µL dynabeads protein G by shaking at room temperature of 24°C for 1 h. 6 µg Mouse immunoglobulin G (IgG) was used as a control. 750 µg cell lysates were then incubated with VHL-antibody-coated dynabeads protein G on a rotating platform at 4°C overnight. Two-third of samples were used for mass spectrometry (MS) analysis and the remaining was kept for validation. For MS analysis, proteins were digested by trypsinisation on beads, followed by desalting to clean up peptides, and analysed by MS.

washing of beads.

Therefore, within the same replicate, peptide intensities were normalised to the VHL intensity of DMSO control in order to set an equal intensity of VHL. Unfortunately, protein intensity for VHL was not present in two out of the four replicates (replicate 2 and replicate 3) for most conditions, as it was not detected in the MS analysis. Therefore the normalisation was only performed in replicate 1 and replicate 4. To ensure that co-IP experiments were successful, co-IP samples that were set aside previously were analysed by western-blotting for VHL protein and gratifyingly, VHL was present in all the co-immunoprecipitates of VHL (Figure 6.7**A**).

By analysing the protein abundance ratios between immunoprecipitate of treatments and immunoprecipitate of IgG control, specific interactors and contaminants can be distinguished. With the selection criterion that across all replicates, the peptide intensity of each protein in at least one condition has to be more than the intensity in IgG for the same protein, 231 out of 1,641 proteins fell under this selection and were analysed further. In order for the protein to fall into the "enriched" category, protein intensity has to be > 1.5 log two-fold change (log_2FC) in the treated samples compared to the DMSO control. In addition, these proteins have to be enriched in at least two of the four replicates.

Unfortunately, Cullin2, a component of the VHL ubiquitin ligase complex, did not pass the selection criteria, because its intensity in the IgG control in one of the replicates was larger than that in any of the treated samples. Gratifyingly, the other components including Elongin B and Elongin C were co-immunoprecipitated with VHL. Furthermore, HIF 1 α was detected in the MG132 treatment of all four replicates (Table 6.2), but not in VH298 or MG132:VH298 treatments, demonstrating that VH298

disrupted VHL:HIF-1α interaction. Amongst proteins that were enriched in any conditions, HIF-1α was the only protein that consistently enriched in all four replicates.

To distinguish proteins of interest affected by each treatment, Venn diagrams for enriched and depleted proteins were plotted (Figure 6.7**B**). Enrichment criteria was set at $log_2FC > 1.5$ compared to DMSO and depletion at $log_2FC < –1.5$ to DMSO. The combination of VH298 and MG132 co-immunoprecipitated the most number of

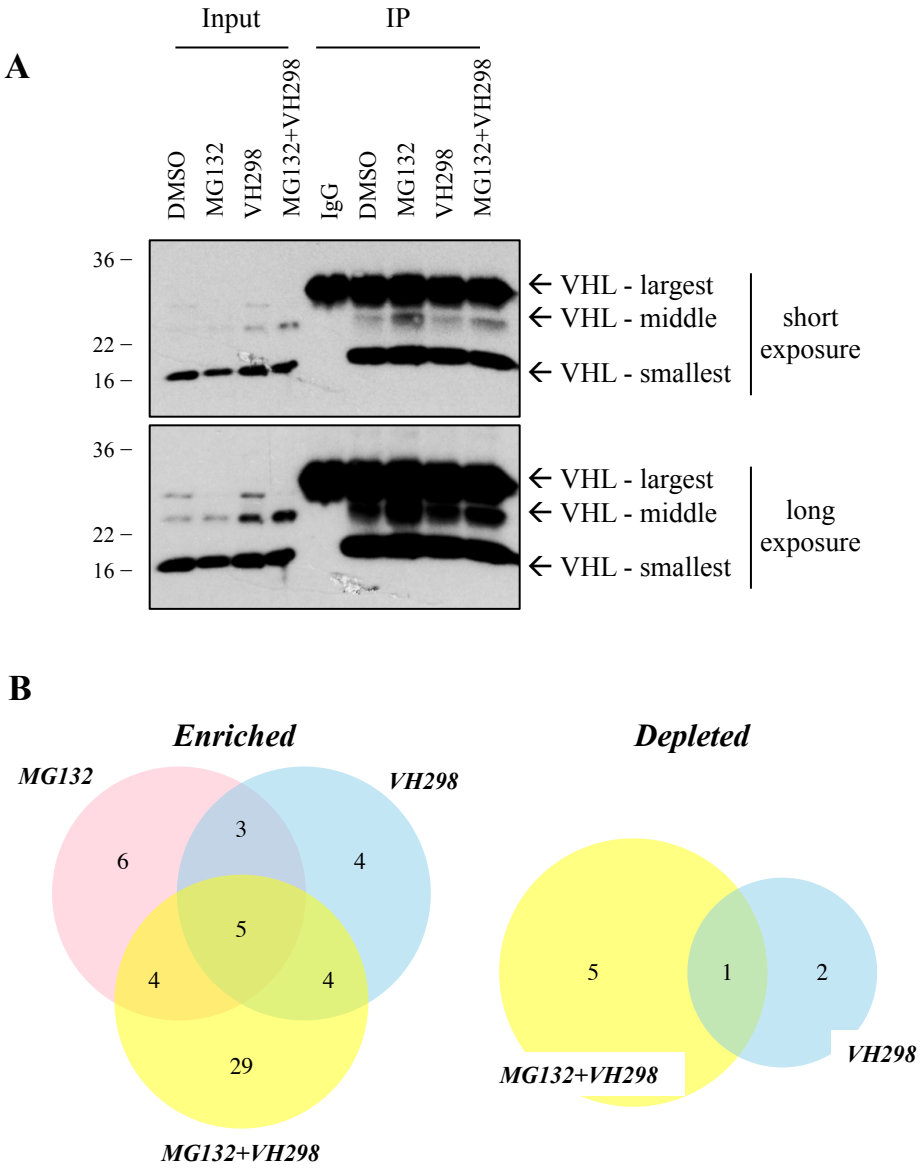

Figure 6.7 – Comparison amongst treatments. (**A**) HeLa cells treated with 1% DMSO, 20 µM MG132, 100 µM VH298 or a mix of 20 µM MG132 and 100 µM VH298 for 3 h prior to cell lysis. One-third of co-IP samples for MS analysis (described in **Figure 6.6**) were used here for western-blotting. Inputs represent 10% of the starting material used per IP (25 µg). (**B**) Venn diagrams depicting the number of enriched proteins ($log_2FC > 1.5$) and depleted proteins ($log_2FC < –1.5$) comparing the presence of MG132, VH298 or MG132 and VH298 to negative control DMSO.

proteins (42) and enriched 29 proteins not found in individual treatment of VH298 or MG132 (Table 6.7), which might be potential interactors of VH298-bound VHL, and stabilised by the blocking of proteasome. Indeed, six out of the 29 proteins are known interacting proteins of VHL (highlighted in blue), while the rest of the proteins seemed to be known ubiquitous contaminants, including keratins, cytoskeletal proteins such as actin and tubulins, and high abundance proteins including histones and translation elongation factors (257). These contaminants were also found throughout in other treatments.

Interestingly, TCEB1 (Elongin C) was depleted in VH298 and MG132+VH298 treatments (Table 6.8), and TCEB2 (Elongin B) was depleted in MG132+VH298 treatment (Table 6.10). The inhibition of VHL by VH298 seemed to induce the depletion the two components of VHL E3 ubiquitin complex. One possibility could be that as VHL levels increase in response to VH298 treatment, there is a greater relative population of VHL that is not bound to Elongin proteins, as those proteins stoichiometrically cannot cope with the increase in VHL level – leading to an apparent "depletion" of EloB/C from VHL. Another explanation may be that VH298 may interfere with the formation of the complex, or that bound HIF-1α promotes the formation of the E3 ubiquitin complex, and this effect becomes less pronounced when HIF α binding is competed by VH298.

As mentioned, the aim of this analysis was to dissect the mechanism of VHL regulation in the presence of VHL inhibitor. Therefore, the most interesting genes would be those enriched or depleted in the presence of VH298 alone (Table 6.6 and Table 6.9), as well as MG132+VH298 only (Table 6.7 and Table 6.10) as MG132 stabilised the complex formed. However, most of the proteins identified were contaminants, and only one that might be a regulatory protein: HERC6, which was depleted in cells treated with both VH298 and MG132 (Table 6.10). HERC6 belongs to the HERC family of E3 ubiquitin

ligase that contains a C-terminal HECT domain (258). The HECT domain is predicted to form a thioester with ubiquitin before transferring it to a substrate, but this ability has not been demonstrated for HERC6. If an E3 ligase were enriched in the treatment of both VH298 and MG132, it might be involved in regulating the VH298-bound VHL. However, from the results, HERC6 was depleted. The depletion of HERC6 could indicate that HERC6 might play a role in regulating VHL. The binding of a ligand, in this case VH298, might prevent HERC6 from polyubiquitinating VHL and targeting it for degradation. Nonetheless, the proteomic analysis is not sufficient to identify confident VHL regulator. Validation on HERC6 would be interesting for future investigation.

Overall, results indicate that co-IP for all four replicates had worked as HIF-1α was enriched in all replicates. However, data obtained was not enough to uncover novel regulator or interactor of VHL.

Table 6.1 – List of five proteins enriched in MG132, VH298 and MG132+VH298 treatments. Proteins were selected with $\log_2$FC > 1.5 compared to DMSO control. Ensembl ID, uniprot ID, gene name and protein name are listed.

Ensembl ID	Uniprot ID	Gene name	Protein name
ENSG00000106636	O15498	YKT6	Synaptobrevin homolog YKT6
ENSG00000119689	P36957	DLST	Dihydrolipoyllysine-residue succinyltransferase component of 2-oxoglutarate dehydrogenase complex, mitochondrial
ENSG00000159352	P55036	PSMD4	26S proteasome non-ATPase regulatory subunit 4
ENSG00000181019	P15559	NQO1	NAD(P)H dehydrogenase [quinone] 1
ENSG00000188219	Q6S8J3	POTEE	POTE ankyrin domain family member E;POTE ankyrin domain family member I;Putative beta-actin-like protein 3;Putative beta-actin-like protein 3, N-terminally processed;POTE ankyrin domain family member J

Table 6.2 – List of six proteins enriched in MG132 only, but not VH298 or MG132+VH298 treatments. Proteins were selected with $log_2FC > 1.5$ compared to DMSO control. Ensembl ID, uniprot ID, gene name and protein name are listed. In blue: proteins found to be interacting proteins of VHL when searched in the 'GeneCards' human gene database website (http://www.genecards.org/).

Ensembl ID	Uniprot ID	Gene name	Protein name
ENSG00000100644	Q16665	HIF1A	Hypoxia-inducible factor 1-alpha
ENSG00000089597	Q14697	GANAB	Neutral alpha-glucosidase AB
ENSG00000101150	O43399	TPD52L2	Tumor protein D54
ENSG00000114573	P38606	ATP6V1A	V-type proton ATPase catalytic subunit A
ENSG00000126067	P49721	PSMB2	Proteasome subunit beta type-2;Proteasome subunit beta type
ENSG00000169710	P49327	FASN	Fatty acid synthase;[Acyl-carrier-protein] S-acetyltransferase;[Acyl-carrier-protein] S-malonyltransferase;3-oxoacyl-[acyl-carrier-protein] synthase;3-oxoacyl-[acyl-carrier-protein] reductase;3-hydroxyacyl-[acyl-carrier-protein]

Table 6.3 – List of three proteins enriched in MG132 and VH298, but not the combination of MG132+VH298 treatment. Proteins were selected with $log_2FC > 1.5$ compared to DMSO control. Ensembl ID, uniprot ID, gene name and protein name are listed. In blue: proteins found to be interacting proteins of VHL when searched in the 'GeneCards' human gene database website (http://www.genecards.org/).

Ensembl ID	Uniprot ID	Gene name	Protein name
ENSG00000102144	P00558	PGK1	Phosphoglycerate kinase;Phosphoglycerate kinase 1
ENSG00000106263	P55884	EIF3B	Eukaryotic translation initiation factor 3 subunit B
ENSG00000137073	Q5T6F2	UBAP2	Ubiquitin-associated protein 2

Table 6.4 – List of four proteins enriched in MG132 and MG132+VH298, but not VH298 treatment. Proteins were selected with $log_2FC > 1.5$ compared to DMSO control. Ensembl ID, uniprot ID, gene name and protein name are listed. In blue: proteins found to be interacting proteins of VHL when searched in the 'GeneCards' human gene database website (http://www.genecards.org/).

Ensembl ID	Uniprot ID	Gene name	Protein name
ENSG00000100764	P62191	PSMC1	26S protease regulatory subunit 4
ENSG00000143870	Q15084	PDIA6	Protein disulfide-isomerase A6
ENSG00000143947	P62979	RPS27A	Ubiquitin-40S ribosomal protein S27a;Ubiquitin;40S ribosomal protein S27a;Ubiquitin-60S ribosomal protein L40;Ubiquitin;60S ribosomal protein L40;Polyubiquitin-B;Ubiquitin;Polyubiquitin-C;Ubiquitin
ENSG00000173267	O76070	SNCG	Gamma-synuclein

Table 6.5 – List of four proteins enriched in VH298 and MG132+VH298, but not MG132 treatment. Proteins were selected with $log_2FC > 1.5$ compared to DMSO control. Ensembl ID, uniprot ID, gene name and protein name are listed.

Ensembl ID	Uniprot ID	Gene name	Protein name
ENSG00000105323	Q9BUJ2	HNRNPUL1	Heterogeneous nuclear ribonucleoprotein U-like protein 1
ENSG00000124207	P55060	CSE1L	Exportin-2
ENSG00000177425	Q96IZ0	PAWR	PRKC apoptosis WT1 regulator protein
ENSG00000197956	P06703	S100A6	Protein S100-A6;Protein S100

Table 6.6 – List of four proteins enriched in VH298, but not MG132 or MG132+VH298. Proteins were selected with $log_2FC > 1.5$ compared to DMSO control. Ensembl ID, uniprot ID, gene name and protein name are listed.

Ensembl ID	Uniprot ID	Gene name	Protein name
ENSG00000105974	Q03135	CAV1	Caveolin;Caveolin-1
ENSG00000129116	Q8WX93	PALLD	Palladin
ENSG00000167767	Q6KB66	KRT80	Keratin, type II cytoskeletal 80
ENSG00000178209	Q15149	PLEC	Plectin

Table 6.7 – List of 29 proteins enriched in MG132+VH298 treatment only, but not MG132 or VH298. Proteins were selected with $log_2FC > 1.5$ compared to DMSO control. Ensembl ID, uniprot ID, gene name and protein name are listed. In blue: proteins found to be interacting proteins of VHL when searched in the 'GeneCards' human gene database website (http://www.genecards.org/).

Ensembl ID	Uniprot ID	Gene name	Protein name
ENSG00000039560	Q9P0K7	RAI14	Ankycorbin
ENSG00000077549	P47756	CAPZB	F-actin-capping protein subunit beta
ENSG00000085733	Q14247	CTTN	Src substrate cortactin
ENSG00000087365	Q13435	SF3B2	Splicing factor 3B subunit 2
ENSG00000099901	P43487	RANBP1	Ran-specific GTPase-activating protein
ENSG00000101608	P19105	MYL12A	Myosin regulatory light chain 12A;Myosin
ENSG00000118680	O14950	MYL12B	regulatory light chain 12B
ENSG00000108298	P84098	RPL19	Ribosomal protein L19;60S ribosomal protein L19
ENSG00000115091	P61158	ACTR3	Actin-related protein 3
ENSG00000128595	O43852	CALU	Calumenin
ENSG00000132341	P62826	RAN	GTP-binding nuclear protein Ran
ENSG00000133030	Q6WCQ1	MPRIP	Myosin phosphatase Rho-interacting protein;Tyrosine-protein kinase receptor
ENSG00000136810	P10599	TXN	Thioredoxin
ENSG00000140416	P09493	TPM1	Tropomyosin alpha-1 chain
ENSG00000140740	P22695	UQCRC2	Cytochrome b-c1 complex subunit 2, mitochondrial
ENSG00000143549	P06753	TPM3	Tropomyosin alpha-3 chain
ENSG00000148396	O15027	SEC16A	Protein transport protein Sec16A
ENSG00000151914	Q03001	DST	Dystonin
ENSG00000162614	Q0ZGT2	NEXN	Nexilin
ENSG00000167986	Q16531	DDB1	DNA damage-binding protein 1

ENSG00000169813	P52597	HNRNPF	Heterogeneous nuclear ribonucleoprotein F;Heterogeneous nuclear ribonucleoprotein F, N-terminally processed
ENSG00000172867	P35908	KRT2	Keratin, type II cytoskeletal 2 epidermal
ENSG00000180879	P51571	SSR4	Translocon-associated protein subunit delta
ENSG00000182944	Q01844	EWSR1	RNA-binding protein EWS
ENSG00000184009	P63261	ACTG1	Actin, cytoplasmic 2;Actin, cytoplasmic 2, N-terminally processed
ENSG00000186395	P13645	KRT10	Keratin, type I cytoskeletal 10
ENSG00000197321	O95425	SVIL	Supervillin
ENSG00000197728	P62854	RPS26	40S ribosomal protein S26;Putative 40S ribosomal protein S26-like 1
ENSG00000254772	P26641	EEF1G	Elongation factor 1-gamma

Table 6.8 – List of a protein depleted in VH298 and MG132+VH298 treatments, but not MG132. Proteins were selected with $\log_2$FC < −1.5 compared to DMSO control. Ensembl ID, uniprot ID, gene name and protein name are listed. In blue: proteins found to be interacting proteins of VHL when searched in the 'GeneCards' human gene database website (http://www.genecards.org/).

Ensembl ID	Uniprot ID	Gene name	Protein name
ENSG00000154582	Q15369	TCEB1	Transcription elongation factor B polypeptide 1

Table 6.9 – List of two proteins depleted in VH298, but not MG132 or MG132+VH298. Proteins were selected with $\log_2$FC < −1.5 compared to DMSO control. Ensembl ID, uniprot ID, gene name and protein name are listed.

Ensembl ID	Uniprot ID	Gene name	Protein name
ENSG00000138594	Q9NYL9	TMOD3	Tropomodulin-3
ENSG00000198467	P07951	HEL-S-273	Tropomyosin beta chain

Table 6.10 – List of five proteins depleted in MG132+VH298, but not MG132 or VH298. Proteins were selected with $\log_2$FC < −1.5 compared to DMSO control. Ensembl ID, uniprot ID, gene name and protein name are listed. In blue: proteins found to be interacting proteins of VHL when searched in the 'GeneCards' human gene database website (http://www.genecards.org/).

Ensembl ID	Uniprot ID	Gene name	Protein name
ENSG00000277443	P29966	MARCKS	Myristoylated alanine-rich C-kinase substrate
ENSG00000103363	Q15370	TCEB2	Transcription elongation factor B polypeptide 2
ENSG00000138642	Q8IVU3	HERC6	Probable E3 ubiquitin-protein ligase HERC6
ENSG00000136824	O95347	SMC2	Structural maintenance of chromosomes protein;Structural maintenance of chromosomes protein 2
ENSG00000107223	O60869	EDF1	Endothelial differentiation-related factor 1

6.7. Discussion

In the previous chapter, proteomic analysis of VHL inhibitor-treated HeLa cells identified VHL to be upregulated. Validation by Western-blotting confirmed that VHL protein levels indeed increased in the presence of VHL inhibitor VH032. In addition, this effect was also observed following treatment with the more potent VHL inhibitor, VH298. Furthermore, the non-binding *cis*-hydroxyproline analogue of VH298, *cis*-VH298, could not upregulate VHL. This demonstrated that the upregulation of VHL was not an off-target effect of the inhibitors and it required the binding of the VHL inhibitor. This upregulation was not only observed in HeLa cells, but also in fibroblast cells, HFF. Importantly, this effect is not dependent on oxygen availability or PHD enzymes as the treatment of hypoxia or PHD inhibitors (IOX2 and FG-4592) did not lead to an increase in VHL levels.

The increase of VHL protein levels in the presence of its inhibitor could be due to several reasons: VHL inhibitor could induce the transcription or translation of VHL; VHL could be autoregulating itself for degradation, an activity which would be blocked by the compound; or the ligand-bound VHL might be stabilised and less degradable inside the cell. Results showed that VHL inhibitor did not alter mRNA level of VHL and VHL does not autoregulate itself for the degradation by the proteasome. In contrast, the inhibitor-bound VHL showed a longer half-life, demonstrating that in the ligand-bound form, VHL might be less degradable. The antibody used for Western-blotting detected three bands of VHL, which are designated as VHL-smallest, VHL-middle and VHL-largest in this study. *VHL* encodes for two isoforms from the same transcripts: a 24-kDa longest isoform of 213-amino acid, and a 19-kDa isoform of 160-amino acid. The shorter isoform is initiated from an internal alternative start codon in frame that is 159 bp downstream the first start codon (145-147). The three bands detected by the antibody have not been characterised for which isoform each band is, although there is

sufficient evidence from the literature to suggest that the band designated as ”VHL-smallest” (which runs as an approximate ~19 kDa protein) corresponds to the short isoform [also named $pVHL_{19}$] (145-147). All three bands could potentially be from the short isoform that is post-translationally modified; alternatively the VHL-middle and VHL-largest bands could be detecting different forms of the long isoform of VHL ($pVHL_{30}$).

Nonetheless, this increase in VHL levels in the presence of VHL inhibitor was found to be responsible for the downregulation of HIF-1α that was rapidly accumulated due to the treatment. Interestingly, the siRNA-mediated knockdown of VHL in normoxia accumulated very little HIF-1α compared to VHL inhibitor. As mentioned previously, VHL inhibitor VH298 has a binding affinity in the nanomolar range as measured by ITC, but was used at micromolar range in cells. Considering that even the knockdown of VHL mediated by siRNA approach could not stabilise much HIF-1α, it is likely that all cellular VHL has to be completely engaged with the compound and inhibited to prevent the interaction between VHL and HIF-1α, which would lead to the stabilisation of HIF-1α. This was further demonstrated by the combination of siRNA-mediated knockdown of VHL and VH298 treatment – VH298 stabilised comparable amounts of HIF-1α at a 10-fold lower dose when combined with VHL knockdown.

VHL inhibitors are being widely used as part of the proteolysis targeting chimeric molecules (PROTACs) to induce degradation of a specific target-protein by recruiting the target-protein to the VHL E3 ubiquitin ligase complex for ubiquitination. Optimum degradation of protein-of-interest is typically achieved at sub-μM concentrations of PROTACs, and at these low doses, such compounds have been shown not to induce HIF-1α stabilisation in cells (217,220). This could explain the observation mentioned above. At low dose of PROTACs usage, low but sufficient VHL E3 ubiquitin ligase complexes are hijacked to polyubiquitinate, and subsequently to degrade protein of

interest. Likewise, only low amount of VHL is required to polyubiquitinate hydroxylated HIF-1α for proteasomal degradation.

To understand the mechanism of VHL regulation in the presence of VHL inhibitor, co-immunoprecipitation (co-IP) coupled mass spectrometry (MS) analysis was performed. In the VHL inhibitor-bound form, a new surface is formed on VHL, which was hypothesised might lead to the interaction with proteins that are not VHL-binding proteins as *neo*-substrates. This hypothesis is based on the knowledge that other ligands for Cullin RING ligase, such as auxin (259) and immunomodulatory drug (260) compounds, induce such mechanism of action. If these proteins are regulated by the proteosomal degradation pathway, MG132 treatment would be expected to stabilise them in a bound complex with VHL. Co-IP was performed using antibody against VHL. By isolating endogenous VHL, *VHL* expression would be controlled by the endogenous promoter and its function would not be altered by addition of a tag. Analysis showed that HIF-1α was found in the VHL co-immunoprecipitate of MG132 treatment in all four replicates performed, demonstrating that the co-IP was successful. However, there were a few caveats with this approach.

First, MS detection is rather random and not all resulting peptides can be confidently detected across replicates. Indeed, peptides (hence proteins) detected from this analysis were inconsistent across replicates. For instance, VHL was not detected in the second and third replicates of the analysis, but western blotting of the samples set aside before processing for MS showed successful isolation of VHL. Next, the current MS approaches are able to detect a large number of proteins, including non-specific interactors (contaminants). This poses a challenge for discriminating between contaminants and relevant interactors. Here, despite the inclusion of IgG negative control, it was not sufficient to filter out contaminants. As a result, these contaminants were identified as being enriched in the treatments. Furthermore, the MS analysis could

not confidently identify potential VHL regulators. All proteins listed as enriched or depleted were not consistent in all four replicates, with the exception of only HIF-1α. It would be ideal to carefully re-evaluate data obtained in the future. In addition, a change of approach to confidently identify possible VHL interactors may be worthwhile. Using data independent acquisition (DIA) analysis (261) would solve this problem and potentially identify low abundance interactors responsible for the increase in VHL protein levels following treatment with VH298.

Nonetheless, the analysis identified HERC6, a probable E3 ubiquitin ligase, as being depleted in cells treated with both VH298 and MG132. This suggests that HERC6 might play a role in regulating VHL. The adaptors of VHL E3 ubiquitin ligase complex, EloB and EloC (TCEB2 and TCEB1, respectively), were also depleted in MG132+VH298 treatment (Elongin B) and MG132+VH298 as well as VH298 alone (EloC), respectively. This suggesting that there might be insufficient EloB/C due to the increase of VHL level, or VH298 may disrupt the formation of the E3 complex, or that HIF-1α is required for the formation of the E3 ubiquitin complex. It would be interesting to validate these hits, first by repeating the co-IP experiment for immunoblotting and detecting changes in protein levels using antibodies. Size-exclusion chromatography on lysates of cells treated with DMSO vehicle control or VHL inhibitor may also reveal whether HERC6 and Elongin B/C are in complex with VHL and if they dissociate from VHL in the presence of inhibitor. As HERC6 may play a role in regulating VHL, knockdown of HERC6 using approach such as siRNA, may uncover if VHL protein level changes in response to HERC6 depletion. Ultimate proof of the role of HERC6 as an E3 ubiquitin ligase would be to perform *in vitro* ubiquitination assay.

Overall, the data presented in this Chapter together showed that VHL levels increased in the presence of VHL inhibitor, which in turn induced the degradation of the hydroxylated HIF-1α that was initially accumulated by the inhibitor. The increase of

VHL levels was due to the increase in its half-life when bound by the VHL inhibitor, presumably as a result of mere ligand-bound stabilisation. However, the mechanism that regulates the inhibitor-bound VHL remains to be fully understood. Results also indicate that VHL may be a very active E3 ubiquitin ligase and only little VHL is required to polyubiquitinate hydroxylated HIF-1α for proteasomal degradation – thus explaining the requirement of micromolar doses of VHL inhibitor to stabilise HIF-1α.

7. Discussion and conclusion remarks

VHL is the E3 ubiquitin ligase regulating HIF-1α for proteasomal degradation; its crucial function in response to hypoxia and cellular oxygen sensing are well established owing to the use of genetic tools. Genetic knockout and knockdown to inactivate VHL have been widely used in biochemical studies. Although mice with homozygous *VHL* −/− are embryonically lethal (152), heterozygous and conditional tissue-specific knockouts of *VHL* (262), as well as the use of siRNA targeting *VHL* (263), have proved to be useful tools providing important insights into the biological consequences of VHL inactivation and its critical role in HIF regulation. However, the functional consequences of specifically disrupting the interaction between VHL and HIF-α remain to be elucidated. The development of a chemical probe that unambiguously blocks the VHL:HIF-α interaction would allow addressing biological questions about VHL molecular target, and functional consequences of disrupting the interaction in a manner complementary and potentially synergistic with genetic tools.

In 2012, a collaboration work between the Ciulli group and a group at Yale University produced the first series of small molecule inhibitors of VHL E3 ubiquitin ligase (211,213), achieving what was previously thought unfeasible, as the development of E3 ligase inhibitors had been unprecedented and unsuccessful via previous approaches. The inhibitors were designed rationally to contain a hydroxyproline group as a starting point, since hydroxyproline of HIF-1α is key for interaction with VHL. The first generation of VHL inhibitors was able to bind to VHL:ElonginB:Elongin C (VBC) *in vitro* with single-digit micromolar potency, but inactive in cells. The Ciulli group further optimised the inhibitors and generated more potent VHL inhibitors with nanomolar binding affinities in 2014 (214). However, these small molecules were yet to be investigated for their cellular activities. In addition, these small molecules were only

mere inhibitors of the VHL:HIF-α interaction *in vitro* using recombinant proteins, but not characterised and qualified as chemical probes.

Therefore, this project began with the aim of characterising VHL inhibitors in cells. Here, VHL inhibitors were shown for the first time to be active in cells – able to stabilise hydroxylated HIF-α and activate HIF transcriptional activity. However, challenges were faced when some of the VHL inhibitors induced cytotoxicity at the concentration used, independent of its mode-of-action. As it is important for a compound to not cause cytotoxicity aside from its inhibition effect, the Ciulli group continued to optimise the inhibitors to increase their potency and improve their physicochemical properties, with the aim of finding inhibitors, which are not just potent, but also highly selective, and not cytotoxic. Through cellular activity and cytotoxicity screens, the most potent VHL inhibitor, VH298, was identified. This work has characterised VH298 as a VHL inhibitor that is: potent with double-digit nanomolar *in vitro* binding affinity, cell-permeable, active in cells, selectively inhibits VHL, and importantly, does not induce toxicity at the concentration required for HIF-α stabilisation (215). With the cellular studies, the initial aim of characterising VHL inhibitors in cells was achieved. In addition, the work validates VHL inhibitors as chemical probes with potential to investigate specific roles of VHL, which could help to distinguish between HIF-dependent and independent VHL functions.

Once VHL inhibitors were characterised as chemical probes, it was decided to take the validation of VHL inhibitors a step further by investigating global transcriptome and proteome changes induced by the inhibitor. Through the use of RNA-sequencing and TMT-labelling, VHL inhibitor was revealed to induce primarily HIF-dependent changes in global gene and protein expression. This was reassuring and provided confidence that the mechanism of action was by on-target effect, as the small molecule inhibits VHL on

its binding pocket for hydroxylated HIF-α, and thus should not affect HIF-independent VHL functions.

Interestingly, VHL was found upregulated in the proteomic analysis in the presence of VHL inhibitor. This was unexpected at the time, however in hindsight, it is known that it is not uncommon for inhibitors to induce an increase in protein level of their targets inside cells [for examples in the case of inhibitors of the BET proteins (264)]. Indeed, it can be envisaged that ligand-bound protein could be more stable, or evade degradation as interaction with negative regulators of the target may be disrupted. Cellular work validated that the inhibition of VHL by the small molecule indeed increases protein levels of VHL, which in turn promotes HIF-α degradation in prolonged treatment. As VHL inhibitor was found to increase the half-life of VHL in cells, the binding of inhibitor may result in increased VHL stability, thus protecting VHL from cellular degradation. To this end, VHL is a tumour suppressor protein living "on the edge" of thermal stability. The melting temperature of VHL recombinant protein bound to EloB/C is just above 37°C (212), and many mutations are known to inactivate VHL by significantly destabilising the protein (58). However, the exact mechanism underlying the upregulation of VHL in the presence of its inhibitor remains elusive. Inhibitor-bound VHL may interrupt its native binding with interactors that mediate the VHL stability. Therefore, another aim arose, to dissect the interactome of VHL in the absence and presence VHL inhibitor, with the goal to identify the mechanism behind VHL upregulation and if possible, to find novel regulators of VHL. Co-IP of VHL coupled with mass spectrometry was performed, but data from analysis was insufficient to make any conclusive remark and more work is required to validate hits identified.

Overall, the main objective of this project was achieved through characterisation of VHL inhibitors and this enables the introduction of potent VHL inhibitor as chemical probe to the scientific community (http://www.chemicalprobes.org/vh298). A tangible

impact outcome of this work is that the compound is now available to any researcher to purchase via the commercial vendor Tocris (https://www.tocris.com/products/vh-298_6156). This chemical probe would be useful to address biological questions that were previously not possible due to the lack of a tool blocking VHL:HIF-α interaction. In addition, this work also demonstrates that it is possible to inhibit an E3 ubiquitin ligase, which has been deemed challenging, and also possible to interrupt protein–protein interaction using small molecules to trigger downstream cellular signalling.

The characterisation of VHL inhibitors demonstrates the suitability of utilising VHL inhibitor as part of PROTAC compounds to recruit the VHL E3 complex as degradation machinery for a specific target protein. It is important for these PROTACs to not induce HIF-dependent response, which would be an undesired effect and may interfere with the degradation of the target protein. Indeed, this study shows that at the optimum concentration for PROTACs using VHL inhibitor (217,220), the inhibitor is unable to stabilise HIF in cells, thereby making VHL ligands suitable as part of PROTAC. An exploitable concentration window between the activities of PROTAC and VHL inhibitor was also revealed and would be useful information for researchers working on PROTACs. In addition, the work in this thesis and PROTAC data demonstrate the strong catalytic efficiency of VHL – low amount VHL is sufficient to mediate the ubiquitination and subsequent degradation of its target protein. This raises the question of why the cellular level of VHL is much higher than the amount required for adequate degradation of its target. However, considering the roles of HIF and the importance of regulating it, the presence of ubiquitous VHL would ensure tight regulation of HIF-α level. VHL appears to be additionally required for HIF-independent roles and regulation of other VHL targets.

Although the crucial role of VHL in the regulation of HIF is well established, many non-canonical HIF-independent roles of VHL remain elusive. As the VHL inhibitor is

mechanistically different from *VHL* genetic knockout or knockdown, combination and comparison of the inhibitor and *VHL* knockdown would be able to distinguish effects of HIF-dependent functions from scaffolding of VHL complex, and in this way, may uncover novel HIF-independent roles of VHL. In addition to VHL inhibition/knockout/knockdown, comparison with PHD inhibitor that targets upstream of VHL:HIF-α may reveal temporal features of target inhibition. It would also be interesting to examine whether other known VHL targets (discussed in 1.3.3.2), aside from HIF-α, are affected by VHL inhibitor, and in this way, could further validate the specificity of VHL inhibitor.

Recent studies have identified protective role of *VHL* knockout during mitochondrial dysfunction (265). However, there was no cell-penetrant VHL inhibitor available at that time. Instead, PHD inhibitor FG-4592 was used as a replacement to mimic *VHL* knockout to trigger hypoxia response, and shown to display the same protective effect (265). With the availability of a cell-penetrant and well-characterised VHL inhibitor, that is VH298, the direct rescue mechanism of VHL during mitochondrial dysfunction can now be investigated. In addition, comparison of VHL inhibition with *VHL* knockdown may determine whether the protective effect is dependent on HIF or due to a hypoxic response. Likewise, the use of VHL inhibitor may also be applicable to diseases that benefit from increased HIF response.

PHD inhibitors display protective roles in many diseases, primarily mediated by their HIF stabilisation responses. It would be interesting to investigate whether VHL inhibitor could achieve the same protective effects, and if pharmacological intervention at the VHL:HIF-α interaction might provide an alternative, complementary, and potentially more specific approach to PHD inhibition. For instance, PHD inhibitors have been shown to greatly improve inflammation-driven diseases, such as inflammatory bowel disease (112-115). VHL inhibitor could be used to determine if this

protective effect is exclusively dependent on HIF, since VHL inhibitor modulates only HIF-dependent responses. Moreover, VHL inhibitor is also able to induce EPO production required for anaemia treatment. Therefore, VHL:HIF-α inhibition should be considered and validated as a potential therapeutic target in diseases that benefit from HIF response, including chronic anaemia, inflammation-driven diseases, ischaemia, and, conditions such as wound healing and organ transplantation.

One fact to consider at the beginning of validating the therapeutic potential of VHL:HIF-α inhibition, and likely of potential concern to researchers interesting in developing such drug leads, is that the small molecule is inhibiting VHL, a tumour suppressor. Inactivation of *VHL* has been implicated with *VHL* disease-associated hemangioblastomas and clear cell renal carcinomas, in which HIF is constitutively active (139). However, it is also known that not all tissues are susceptible to tumour formation after *VHL* loss (139), and that *VHL* loss is required but not sufficient to cause tumour growth, i.e. mutations or loss of other genes are required beside that of *VHL* (266,267). Furthermore, HIF-1α and HIF-2α play opposing roles in renal cancer progression (97), whereas VHL inhibitor stabilises both isoforms. Besides, the inhibition by small molecule is acute and reversible, and very different from complete removal of the entire protein, and therefore should not contribute to the long-term progression of cancer. Nonetheless, it would be important and interesting to examine the phenotype outcomes of the inhibitor in a cell-based and animal models. Not only would this validate the potential of using VHL inhibitor in animal-based research, but it would also provide greater insights into the functional roles of VHL:HIF-α interaction.

Overall, this project characterises VHL inhibitor as a chemical probe of the VHL:HIF pathway with great potential to address biological questions regarding the roles and regulation of VHL. VHL inhibitor is a unique tool due to its on-target selectivity and specificity in inducing HIF activity without affecting HIF-independent response, as in

the case of knockout/knockdown, and exerts its effect further downstream than PHD hydroxylation.

8. References

1. Sena, L. A., and Chandel, N. S. (2012) Physiological roles of mitochondrial reactive oxygen species. *Mol Cell* **48**, 158-167
2. Stamati, K., Mudera, V., and Cheema, U. (2011) Evolution of oxygen utilization in multicellular organisms and implications for cell signalling in tissue engineering. *J Tissue Eng* **2**, 2041731411432365
3. Frisancho, A. R. (1975) Functional adaptation to high altitude hypoxia. *Science* **187**, 313-319
4. Beall, C. M. (2007) Two routes to functional adaptation: Tibetan and Andean high-altitude natives. *Proc Natl Acad Sci U S A* **104 Suppl 1**, 8655-8660
5. Simon, M. C., and Keith, B. (2008) The role of oxygen availability in embryonic development and stem cell function. *Nat Rev Mol Cell Biol* **9**, 285-296
6. Liao, D., and Johnson, R. S. (2007) Hypoxia: a key regulator of angiogenesis in cancer. *Cancer Metastasis Rev* **26**, 281-290
7. Krock, B. L., Skuli, N., and Simon, M. C. (2011) Hypoxia-induced angiogenesis: good and evil. *Genes Cancer* **2**, 1117-1133
8. Wilson, W. R., and Hay, M. P. (2011) Targeting hypoxia in cancer therapy. *Nat Rev Cancer* **11**, 393-410
9. Vaupel, P., and Mayer, A. (2007) Hypoxia in cancer: significance and impact on clinical outcome. *Cancer Metastasis Rev* **26**, 225-239
10. Kapitsinou, P. P., Liu, Q., Unger, T. L., Rha, J., Davidoff, O., Keith, B., Epstein, J. A., Moores, S. L., Erickson-Miller, C. L., and Haase, V. H. (2010) Hepatic HIF-2 regulates erythropoietic responses to hypoxia in renal anemia. *Blood* **116**, 3039-3048
11. Michiels, C. (2004) Physiological and pathological responses to hypoxia. *Am J Pathol* **164**, 1875-1882
12. Bi, M., Naczki, C., Koritzinsky, M., Fels, D., Blais, J., Hu, N., Harding, H., Novoa, I., Varia, M., Raleigh, J., Scheuner, D., Kaufman, R. J., Bell, J., Ron, D., Wouters, B. G., and Koumenis, C. (2005) ER stress-regulated translation increases tolerance to extreme hypoxia and promotes tumor growth. *EMBO J* **24**, 3470-3481
13. Liu, L., Cash, T. P., Jones, R. G., Keith, B., Thompson, C. B., and Simon, M. C. (2006) Hypoxia-induced energy stress regulates mRNA translation and cell growth. *Mol Cell* **21**, 521-531
14. Hammond, E. M., Denko, N. C., Dorie, M. J., Abraham, R. T., and Giaccia, A. J. (2002) Hypoxia links ATR and p53 through replication arrest. *Mol Cell Biol* **22**, 1834-1843
15. Semenza, G. L. (2011) Regulation of metabolism by hypoxia-inducible factor 1. *Cold Spring Harb Symp Quant Biol* **76**, 347-353
16. Kenneth, N. S., and Rocha, S. (2008) Regulation of gene expression by hypoxia. *Biochem J* **414**, 19-29
17. Wang, G. L., and Semenza, G. L. (1995) Purification and characterization of hypoxia-inducible factor 1. *J Biol Chem* **270**, 1230-1237
18. Wang, G. L., Jiang, B. H., Rue, E. A., and Semenza, G. L. (1995) Hypoxia-inducible factor 1 is a basic-helix-loop-helix-PAS heterodimer regulated by cellular O2 tension. *Proc Natl Acad Sci U S A* **92**, 5510-5514
19. Tian, H., McKnight, S. L., and Russell, D. W. (1997) Endothelial PAS domain protein 1 (EPAS1), a transcription factor selectively expressed in endothelial cells. *Genes Dev* **11**, 72-82

20. Gu, Y. Z., Moran, S. M., Hogenesch, J. B., Wartman, L., and Bradfield, C. A. (1998) Molecular characterization and chromosomal localization of a third alpha-class hypoxia inducible factor subunit, HIF3alpha. *Gene Expr* **7**, 205-213
21. Wiesener, M. S., Jurgensen, J. S., Rosenberger, C., Scholze, C. K., Horstrup, J. H., Warnecke, C., Mandriota, S., Bechmann, I., Frei, U. A., Pugh, C. W., Ratcliffe, P. J., Bachmann, S., Maxwell, P. H., and Eckardt, K. U. (2003) Widespread hypoxia-inducible expression of HIF-2alpha in distinct cell populations of different organs. *FASEB J* **17**, 271-273
22. Talks, K. L., Turley, H., Gatter, K. C., Maxwell, P. H., Pugh, C. W., Ratcliffe, P. J., and Harris, A. L. (2000) The expression and distribution of the hypoxia-inducible factors HIF-1alpha and HIF-2alpha in normal human tissues, cancers, and tumor-associated macrophages. *Am J Pathol* **157**, 411-421
23. Franovic, A., Holterman, C. E., Payette, J., and Lee, S. (2009) Human cancers converge at the HIF-2alpha oncogenic axis. *Proc Natl Acad Sci U S A* **106**, 21306-21311
24. Keith, B., Johnson, R. S., and Simon, M. C. (2011) HIF1alpha and HIF2alpha: sibling rivalry in hypoxic tumour growth and progression. *Nat Rev Cancer* **12**, 9-22
25. Koh, M. Y., and Powis, G. (2012) Passing the baton: the HIF switch. *Trends Biochem Sci* **37**, 364-372
26. Bartoszewska, S., Kochan, K., Piotrowski, A., Kamysz, W., Ochocka, R. J., Collawn, J. F., and Bartoszewski, R. (2015) The hypoxia-inducible miR-429 regulates hypoxia-inducible factor-1alpha expression in human endothelial cells through a negative feedback loop. *FASEB J* **29**, 1467-1479
27. Uchida, T., Rossignol, F., Matthay, M. A., Mounier, R., Couette, S., Clottes, E., and Clerici, C. (2004) Prolonged hypoxia differentially regulates hypoxia-inducible factor (HIF)-1alpha and HIF-2alpha expression in lung epithelial cells: implication of natural antisense HIF-1alpha. *J Biol Chem* **279**, 14871-14878
28. Ke, Q., and Costa, M. (2006) Hypoxia-inducible factor-1 (HIF-1). *Mol Pharmacol* **70**, 1469-1480
29. Bertout, J. A., Patel, S. A., and Simon, M. C. (2008) The impact of O2 availability on human cancer. *Nat Rev Cancer* **8**, 967-975
30. Makino, Y., Kanopka, A., Wilson, W. J., Tanaka, H., and Poellinger, L. (2002) Inhibitory PAS domain protein (IPAS) is a hypoxia-inducible splicing variant of the hypoxia-inducible factor-3alpha locus. *J Biol Chem* **277**, 32405-32408
31. Dengler, V. L., Galbraith, M., and Espinosa, J. M. (2014) Transcriptional regulation by hypoxia inducible factors. *Crit Rev Biochem Mol Biol* **49**, 1-15
32. Bardos, J. I., and Ashcroft, M. (2005) Negative and positive regulation of HIF-1: a complex network. *Biochim Biophys Acta* **1755**, 107-120
33. Zhang, P., Yao, Q., Lu, L., Li, Y., Chen, P. J., and Duan, C. (2014) Hypoxia-inducible factor 3 is an oxygen-dependent transcription activator and regulates a distinct transcriptional response to hypoxia. *Cell Rep* **6**, 1110-1121
34. Lando, D., Peet, D. J., Whelan, D. A., Gorman, J. J., and Whitelaw, M. L. (2002) Asparagine hydroxylation of the HIF transactivation domain a hypoxic switch. *Science* **295**, 858-861
35. Wu, D., Potluri, N., Lu, J., Kim, Y., and Rastinejad, F. (2015) Structural integration in hypoxia-inducible factors. *Nature* **524**, 303-308
36. Kallio, P. J., Pongratz, I., Gradin, K., McGuire, J., and Poellinger, L. (1997) Activation of hypoxia-inducible factor 1alpha: posttranscriptional regulation and conformational change by recruitment of the Arnt transcription factor. *Proc Natl Acad Sci U S A* **94**, 5667-5672

37. Wu, D., Potluri, N., Kim, Y., and Rastinejad, F. (2013) Structure and dimerization properties of the aryl hydrocarbon receptor PAS-A domain. *Mol Cell Biol* **33**, 4346-4356
38. Sekine, H., Mimura, J., Yamamoto, M., and Fujii-Kuriyama, Y. (2006) Unique and overlapping transcriptional roles of arylhydrocarbon receptor nuclear translocator (Arnt) and Arnt2 in xenobiotic and hypoxic responses. *J Biol Chem* **281**, 37507-37516
39. Huang, L. E., Arany, Z., Livingston, D. M., and Bunn, H. F. (1996) Activation of hypoxia-inducible transcription factor depends primarily upon redox-sensitive stabilization of its alpha subunit. *J Biol Chem* **271**, 32253-32259
40. Schofield, C. J., and Zhang, Z. (1999) Structural and mechanistic studies on 2-oxoglutarate-dependent oxygenases and related enzymes. *Curr Opin Struct Biol* **9**, 722-731
41. Ploumakis, A., and Coleman, M. L. (2015) OH, the Places You'll Go! Hydroxylation, Gene Expression, and Cancer. *Mol Cell* **58**, 729-741
42. Hon, W. C., Wilson, M. I., Harlos, K., Claridge, T. D., Schofield, C. J., Pugh, C. W., Maxwell, P. H., Ratcliffe, P. J., Stuart, D. I., and Jones, E. Y. (2002) Structural basis for the recognition of hydroxyproline in HIF-1 alpha by pVHL. *Nature* **417**, 975-978
43. Jaakkola, P., Mole, D. R., Tian, Y. M., Wilson, M. I., Gielbert, J., Gaskell, S. J., von Kriegsheim, A., Hebestreit, H. F., Mukherji, M., Schofield, C. J., Maxwell, P. H., Pugh, C. W., and Ratcliffe, P. J. (2001) Targeting of HIF-alpha to the von Hippel-Lindau ubiquitylation complex by O2-regulated prolyl hydroxylation. *Science* **292**, 468-472
44. Majmundar, A. J., Wong, W. J., and Simon, M. C. (2010) Hypoxia-inducible factors and the response to hypoxic stress. *Mol Cell* **40**, 294-309
45. Lando, D., Peet, D. J., Gorman, J. J., Whelan, D. A., Whitelaw, M. L., and Bruick, R. K. (2002) FIH-1 is an asparaginyl hydroxylase enzyme that regulates the transcriptional activity of hypoxia-inducible factor. *Genes Dev* **16**, 1466-1471
46. Hewitson, K. S., McNeill, L. A., Riordan, M. V., Tian, Y. M., Bullock, A. N., Welford, R. W., Elkins, J. M., Oldham, N. J., Bhattacharya, S., Gleadle, J. M., Ratcliffe, P. J., Pugh, C. W., and Schofield, C. J. (2002) Hypoxia-inducible factor (HIF) asparagine hydroxylase is identical to factor inhibiting HIF (FIH) and is related to the cupin structural family. *J Biol Chem* **277**, 26351-26355
47. Schofield, C. J., and Ratcliffe, P. J. (2004) Oxygen sensing by HIF hydroxylases. *Nat Rev Mol Cell Biol* **5**, 343-354
48. Masson, N., Singleton, R. S., Sekirnik, R., Trudgian, D. C., Ambrose, L. J., Miranda, M. X., Tian, Y. M., Kessler, B. M., Schofield, C. J., and Ratcliffe, P. J. (2012) The FIH hydroxylase is a cellular peroxide sensor that modulates HIF transcriptional activity. *EMBO Rep* **13**, 251-257
49. Masson, N., Willam, C., Maxwell, P. H., Pugh, C. W., and Ratcliffe, P. J. (2001) Independent function of two destruction domains in hypoxia-inducible factor-alpha chains activated by prolyl hydroxylation. *EMBO J* **20**, 5197-5206
50. Ivan, M., Kondo, K., Yang, H., Kim, W., Valiando, J., Ohh, M., Salic, A., Asara, J. M., Lane, W. S., and Kaelin, W. G., Jr. (2001) HIFalpha targeted for VHL-mediated destruction by proline hydroxylation: implications for O2 sensing. *Science* **292**, 464-468
51. Epstein, A. C., Gleadle, J. M., McNeill, L. A., Hewitson, K. S., O'Rourke, J., Mole, D. R., Mukherji, M., Metzen, E., Wilson, M. I., Dhanda, A., Tian, Y. M., Masson, N., Hamilton, D. L., Jaakkola, P., Barstead, R., Hodgkin, J., Maxwell, P. H., Pugh, C. W., Schofield, C. J., and Ratcliffe, P. J. (2001) C. elegans EGL-9

and mammalian homologs define a family of dioxygenases that regulate HIF by prolyl hydroxylation. *Cell* **107**, 43-54

52. Oehme, F., Ellinghaus, P., Kolkhof, P., Smith, T. J., Ramakrishnan, S., Hutter, J., Schramm, M., and Flamme, I. (2002) Overexpression of PH-4, a novel putative proline 4-hydroxylase, modulates activity of hypoxia-inducible transcription factors. *Biochem Biophys Res Commun* **296**, 343-349
53. Appelhoff, R. J., Tian, Y. M., Raval, R. R., Turley, H., Harris, A. L., Pugh, C. W., Ratcliffe, P. J., and Gleadle, J. M. (2004) Differential function of the prolyl hydroxylases PHD1, PHD2, and PHD3 in the regulation of hypoxia-inducible factor. *J Biol Chem* **279**, 38458-38465
54. Rabinowitz, M. H. (2013) Inhibition of hypoxia-inducible factor prolyl hydroxylase domain oxygen sensors: tricking the body into mounting orchestrated survival and repair responses. *J Med Chem* **56**, 9369-9402
55. Katschinski, D. M. (2009) In vivo functions of the prolyl-4-hydroxylase domain oxygen sensors: direct route to the treatment of anaemia and the protection of ischaemic tissues. *Acta Physiol (Oxf)* **195**, 407-414
56. Aprelikova, O., Chandramouli, G. V., Wood, M., Vasselli, J. R., Riss, J., Maranchie, J. K., Linehan, W. M., and Barrett, J. C. (2004) Regulation of HIF prolyl hydroxylases by hypoxia-inducible factors. *J Cell Biochem* **92**, 491-501
57. Takeda, K., Ho, V. C., Takeda, H., Duan, L. J., Nagy, A., and Fong, G. H. (2006) Placental but not heart defects are associated with elevated hypoxia-inducible factor alpha levels in mice lacking prolyl hydroxylase domain protein 2. *Mol Cell Biol* **26**, 8336-8346
58. Rechsteiner, M. P., von Teichman, A., Nowicka, A., Sulser, T., Schraml, P., and Moch, H. (2011) VHL gene mutations and their effects on hypoxia inducible factor HIFalpha: identification of potential driver and passenger mutations. *Cancer Res* **71**, 5500-5511
59. Takeda, K., Cowan, A., and Fong, G. H. (2007) Essential role for prolyl hydroxylase domain protein 2 in oxygen homeostasis of the adult vascular system. *Circulation* **116**, 774-781
60. Minamishima, Y. A., Moslehi, J., Bardeesy, N., Cullen, D., Bronson, R. T., and Kaelin, W. G., Jr. (2008) Somatic inactivation of the PHD2 prolyl hydroxylase causes polycythemia and congestive heart failure. *Blood* **111**, 3236-3244
61. Takeda, K., Aguila, H. L., Parikh, N. S., Li, X., Lamothe, K., Duan, L. J., Takeda, H., Lee, F. S., and Fong, G. H. (2008) Regulation of adult erythropoiesis by prolyl hydroxylase domain proteins. *Blood* **111**, 3229-3235
62. Bishop, T., Gallagher, D., Pascual, A., Lygate, C. A., de Bono, J. P., Nicholls, L. G., Ortega-Saenz, P., Oster, H., Wijeyekoon, B., Sutherland, A. I., Grosfeld, A., Aragones, J., Schneider, M., van Geyte, K., Teixeira, D., Diez-Juan, A., Lopez-Barneo, J., Channon, K. M., Maxwell, P. H., Pugh, C. W., Davies, A. M., Carmeliet, P., and Ratcliffe, P. J. (2008) Abnormal sympathoadrenal development and systemic hypotension in PHD3-/- mice. *Mol Cell Biol* **28**, 3386-3400
63. Ortmann, B., Druker, J., and Rocha, S. (2014) Cell cycle progression in response to oxygen levels. *Cell Mol Life Sci* **71**, 3569-3582
64. Karuppagounder, S. S., and Ratan, R. R. (2012) Hypoxia-inducible factor prolyl hydroxylase inhibition: robust new target or another big bust for stroke therapeutics? *J Cereb Blood Flow Metab* **32**, 1347-1361
65. Mikhaylova, O., Ignacak, M. L., Barankiewicz, T. J., Harbaugh, S. V., Yi, Y., Maxwell, P. H., Schneider, M., Van Geyte, K., Carmeliet, P., Revelo, M. P., Wyder, M., Greis, K. D., Meller, J., and Czyzyk-Krzeska, M. F. (2008) The von Hippel-Lindau tumor suppressor protein and Egl-9-Type proline hydroxylases

regulate the large subunit of RNA polymerase II in response to oxidative stress. *Mol Cell Biol* **28**, 2701-2717

66. Xie, L., Xiao, K., Whalen, E. J., Forrester, M. T., Freeman, R. S., Fong, G., Gygi, S. P., Lefkowitz, R. J., and Stamler, J. S. (2009) Oxygen-regulated beta(2)-adrenergic receptor hydroxylation by EGLN3 and ubiquitylation by pVHL. *Sci Signal* **2**, ra33
67. Dolcet, X., Llobet, D., Pallares, J., and Matias-Guiu, X. (2005) NF-kB in development and progression of human cancer. *Virchows Arch* **446**, 475-482
68. Cummins, E. P., Berra, E., Comerford, K. M., Ginouves, A., Fitzgerald, K. T., Seeballuck, F., Godson, C., Nielsen, J. E., Moynagh, P., Pouyssegur, J., and Taylor, C. T. (2006) Prolyl hydroxylase-1 negatively regulates IkappaB kinase-beta, giving insight into hypoxia-induced NFkappaB activity. *Proc Natl Acad Sci U S A* **103**, 18154-18159
69. Fu, J., and Taubman, M. B. (2010) Prolyl hydroxylase EGLN3 regulates skeletal myoblast differentiation through an NF-kappaB-dependent pathway. *J Biol Chem* **285**, 8927-8935
70. Xue, J., Li, X., Jiao, S., Wei, Y., Wu, G., and Fang, J. (2010) Prolyl hydroxylase-3 is down-regulated in colorectal cancer cells and inhibits IKKbeta independent of hydroxylase activity. *Gastroenterology* **138**, 606-615
71. Kuznetsova, A. V., Meller, J., Schnell, P. O., Nash, J. A., Ignacak, M. L., Sanchez, Y., Conaway, J. W., Conaway, R. C., and Czyzyk-Krzeska, M. F. (2003) von Hippel-Lindau protein binds hyperphosphorylated large subunit of RNA polymerase II through a proline hydroxylation motif and targets it for ubiquitination. *Proc Natl Acad Sci U S A* **100**, 2706-2711
72. Zheng, X., Zhai, B., Koivunen, P., Shin, S. J., Lu, G., Liu, J., Geisen, C., Chakraborty, A. A., Moslehi, J. J., Smalley, D. M., Wei, X., Chen, X., Chen, Z., Beres, J. M., Zhang, J., Tsao, J. L., Brenner, M. C., Zhang, Y., Fan, C., DePinho, R. A., Paik, J., Gygi, S. P., Kaelin, W. G., Jr., and Zhang, Q. (2014) Prolyl hydroxylation by EglN2 destabilizes FOXO3a by blocking its interaction with the USP9x deubiquitinase. *Genes Dev* **28**, 1429-1444
73. Zurlo, G., Guo, J., Takada, M., Wei, W., and Zhang, Q. (2016) New Insights into Protein Hydroxylation and Its Important Role in Human Diseases. *Biochim Biophys Acta* **1866**, 208-220
74. Guo, J., Chakraborty, A. A., Liu, P., Gan, W., Zheng, X., Inuzuka, H., Wang, B., Zhang, J., Zhang, L., Yuan, M., Novak, J., Cheng, J. Q., Toker, A., Signoretti, S., Zhang, Q., Asara, J. M., Kaelin, W. G., Jr., and Wei, W. (2016) pVHL suppresses kinase activity of Akt in a proline-hydroxylation-dependent manner. *Science* **353**, 929-932
75. Hager, M., Haufe, H., Kemmerling, R., Hitzl, W., Mikuz, G., Moser, P. L., and Kolbitsch, C. (2009) Increased activated Akt expression in renal cell carcinomas and prognosis. *J Cell Mol Med* **13**, 2181-2188
76. Liu, Y. V., Baek, J. H., Zhang, H., Diez, R., Cole, R. N., and Semenza, G. L. (2007) RACK1 competes with HSP90 for binding to HIF-1alpha and is required for O(2)-independent and HSP90 inhibitor-induced degradation of HIF-1alpha. *Mol Cell* **25**, 207-217
77. Ferreira, J. V., Soares, A. R., Ramalho, J. S., Pereira, P., and Girao, H. (2015) K63 linked ubiquitin chain formation is a signal for HIF1A degradation by Chaperone-Mediated Autophagy. *Sci Rep* **5**, 10210
78. Bremm, A., Moniz, S., Mader, J., Rocha, S., and Komander, D. (2014) Cezanne (OTUD7B) regulates HIF-1alpha homeostasis in a proteasome-independent manner. *EMBO Rep* **15**, 1268-1277

79. Moniz, S., Bandarra, D., Biddlestone, J., Campbell, K. J., Komander, D., Bremm, A., and Rocha, S. (2015) Cezanne regulates E2F1-dependent HIF2alpha expression. *J Cell Sci* **128**, 3082-3093
80. Semenza, G. L. (2003) Targeting HIF-1 for cancer therapy. *Nat Rev Cancer* **3**, 721-732
81. Kenneth, N. S., Mudie, S., van Uden, P., and Rocha, S. (2009) SWI/SNF regulates the cellular response to hypoxia. *J Biol Chem* **284**, 4123-4131
82. Chowdhury, R., Hardy, A., and Schofield, C. J. (2008) The human oxygen sensing machinery and its manipulation. *Chem Soc Rev* **37**, 1308-1319
83. Semenza, G. L. (2007) Life with oxygen. *Science* **318**, 62-64
84. Benita, Y., Kikuchi, H., Smith, A. D., Zhang, M. Q., Chung, D. C., and Xavier, R. J. (2009) An integrative genomics approach identifies Hypoxia Inducible Factor-1 (HIF-1)-target genes that form the core response to hypoxia. *Nucleic Acids Res* **37**, 4587-4602
85. Ortiz-Barahona, A., Villar, D., Pescador, N., Amigo, J., and del Peso, L. (2010) Genome-wide identification of hypoxia-inducible factor binding sites and target genes by a probabilistic model integrating transcription-profiling data and in silico binding site prediction. *Nucleic Acids Res* **38**, 2332-2345
86. Wouters, B. G., and Koritzinsky, M. (2008) Hypoxia signalling through mTOR and the unfolded protein response in cancer. *Nat Rev Cancer* **8**, 851-864
87. DeYoung, M. P., Horak, P., Sofer, A., Sgroi, D., and Ellisen, L. W. (2008) Hypoxia regulates TSC1/2-mTOR signaling and tumor suppression through REDD1-mediated 14-3-3 shuttling. *Genes Dev* **22**, 239-251
88. Ron, D., and Walter, P. (2007) Signal integration in the endoplasmic reticulum unfolded protein response. *Nat Rev Mol Cell Biol* **8**, 519-529
89. Koumenis, C., Naczki, C., Koritzinsky, M., Rastani, S., Diehl, A., Sonenberg, N., Koromilas, A., and Wouters, B. G. (2002) Regulation of protein synthesis by hypoxia via activation of the endoplasmic reticulum kinase PERK and phosphorylation of the translation initiation factor eIF2alpha. *Mol Cell Biol* **22**, 7405-7416
90. Semenza, G. L. (2013) HIF-1 mediates metabolic responses to intratumoral hypoxia and oncogenic mutations. *J Clin Invest* **123**, 3664-3671
91. Balamurugan, K. (2016) HIF-1 at the crossroads of hypoxia, inflammation, and cancer. *Int J Cancer* **138**, 1058-1066
92. Semenza, G. L. (2012) Hypoxia-inducible factors in physiology and medicine. *Cell* **148**, 399-408
93. Semenza, G. L. (2001) Regulation of hypoxia-induced angiogenesis: a chaperone escorts VEGF to the dance. *J Clin Invest* **108**, 39-40
94. Swietach, P., Wigfield, S., Cobden, P., Supuran, C. T., Harris, A. L., and Vaughan-Jones, R. D. (2008) Tumor-associated carbonic anhydrase 9 spatially coordinates intracellular pH in three-dimensional multicellular growths. *J Biol Chem* **283**, 20473-20483
95. Chiche, J., Brahimi-Horn, M. C., and Pouyssegur, J. (2010) Tumour hypoxia induces a metabolic shift causing acidosis: a common feature in cancer. *J Cell Mol Med* **14**, 771-794
96. Pinheiro, C., Longatto-Filho, A., Azevedo-Silva, J., Casal, M., Schmitt, F. C., and Baltazar, F. (2012) Role of monocarboxylate transporters in human cancers: state of the art. *J Bioenerg Biomembr* **44**, 127-139
97. Kroeger, N., Klatte, T., Chamie, K., Rao, P. N., Birkhauser, F. D., Sonn, G. A., Riss, J., Kabbinavar, F. F., Belldegrun, A. S., and Pantuck, A. J. (2013) Deletions of chromosomes 3p and 14q molecularly subclassify clear cell renal cell carcinoma. *Cancer* **119**, 1547-1554

98. Shen, C., Beroukhim, R., Schumacher, S. E., Zhou, J., Chang, M., Signoretti, S., and Kaelin, W. G., Jr. (2011) Genetic and functional studies implicate HIF1alpha as a 14q kidney cancer suppressor gene. *Cancer Discov* **1**, 222-235
99. Imamura, T., Kikuchi, H., Herraiz, M. T., Park, D. Y., Mizukami, Y., Mino-Kenduson, M., Lynch, M. P., Rueda, B. R., Benita, Y., Xavier, R. J., and Chung, D. C. (2009) HIF-1alpha and HIF-2alpha have divergent roles in colon cancer. *Int J Cancer* **124**, 763-771
100. Nangaku, M., and Eckardt, K. U. (2006) Pathogenesis of renal anemia. *Semin Nephrol* **26**, 261-268
101. Coresh, J., Selvin, E., Stevens, L. A., Manzi, J., Kusek, J. W., Eggers, P., Van Lente, F., and Levey, A. S. (2007) Prevalence of chronic kidney disease in the United States. *JAMA* **298**, 2038-2047
102. Grabe, D. W. (2007) Update on clinical practice recommendations and new therapeutic modalities for treating anemia in patients with chronic kidney disease. *Am J Health Syst Pharm* **64**, S8-14; quiz S23-15
103. Kim, S. Y., and Yang, E. G. (2015) Recent Advances in Developing Inhibitors for Hypoxia-Inducible Factor Prolyl Hydroxylases and Their Therapeutic Implications. *Molecules* **20**, 20551-20568
104. Flamme, I., Oehme, F., Ellinghaus, P., Jeske, M., Keldenich, J., and Thuss, U. (2014) Mimicking hypoxia to treat anemia: HIF-stabilizer BAY 85-3934 (Molidustat) stimulates erythropoietin production without hypertensive effects. *PLoS One* **9**, e111838
105. Provenzano, R., Besarab, A., Sun, C. H., Diamond, S. A., Durham, J. H., Cangiano, J. L., Aiello, J. R., Novak, J. E., Lee, T., Leong, R., Roberts, B. K., Saikali, K. G., Hemmerich, S., Szczech, L. A., Yu, K. H., and Neff, T. B. (2016) Oral Hypoxia-Inducible Factor Prolyl Hydroxylase Inhibitor Roxadustat (FG-4592) for the Treatment of Anemia in Patients with CKD. *Clin J Am Soc Nephrol* **11**, 982-991
106. Eltzschig, H. K., Bratton, D. L., and Colgan, S. P. (2014) Targeting hypoxia signalling for the treatment of ischaemic and inflammatory diseases. *Nat Rev Drug Discov* **13**, 852-869
107. Eckle, T., Kohler, D., Lehmann, R., El Kasmi, K., and Eltzschig, H. K. (2008) Hypoxia-inducible factor-1 is central to cardioprotection: a new paradigm for ischemic preconditioning. *Circulation* **118**, 166-175
108. Eckle, T., Hartmann, K., Bonney, S., Reithel, S., Mittelbronn, M., Walker, L. A., Lowes, B. D., Han, J., Borchers, C. H., Buttrick, P. M., Kominsky, D. J., Colgan, S. P., and Eltzschig, H. K. (2012) Adora2b-elicited Per2 stabilization promotes a HIF-dependent metabolic switch crucial for myocardial adaptation to ischemia. *Nat Med* **18**, 774-782
109. Cummins, E. P., Doherty, G. A., and Taylor, C. T. (2013) Hydroxylases as therapeutic targets in inflammatory bowel disease. *Lab Invest* **93**, 378-383
110. Biddlestone, J., Bandarra, D., and Rocha, S. (2015) The role of hypoxia in inflammatory disease (review). *Int J Mol Med* **35**, 859-869
111. Rosenberger, P., Schwab, J. M., Mirakaj, V., Masekowsky, E., Mager, A., Morote-Garcia, J. C., Unertl, K., and Eltzschig, H. K. (2009) Hypoxia-inducible factor-dependent induction of netrin-1 dampens inflammation caused by hypoxia. *Nat Immunol* **10**, 195-202
112. Cummins, E. P., Seeballuck, F., Keely, S. J., Mangan, N. E., Callanan, J. J., Fallon, P. G., and Taylor, C. T. (2008) The hydroxylase inhibitor dimethyloxalylglycine is protective in a murine model of colitis. *Gastroenterology* **134**, 156-165

113. Robinson, A., Keely, S., Karhausen, J., Gerich, M. E., Furuta, G. T., and Colgan, S. P. (2008) Mucosal protection by hypoxia-inducible factor prolyl hydroxylase inhibition. *Gastroenterology* **134**, 145-155
114. Tambuwala, M. M., Manresa, M. C., Cummins, E. P., Aversa, V., Coulter, I. S., and Taylor, C. T. (2015) Targeted delivery of the hydroxylase inhibitor DMOG provides enhanced efficacy with reduced systemic exposure in a murine model of colitis. *J Control Release* **217**, 221-227
115. Marks, E., Goggins, B. J., Cardona, J., Cole, S., Minahan, K., Mateer, S., Walker, M. M., Shalwitz, R., and Keely, S. (2015) Oral delivery of prolyl hydroxylase inhibitor: AKB-4924 promotes localized mucosal healing in a mouse model of colitis. *Inflamm Bowel Dis* **21**, 267-275
116. Albina, J. E., Mastrofrancesco, B., Vessella, J. A., Louis, C. A., Henry, W. L., Jr., and Reichner, J. S. (2001) HIF-1 expression in healing wounds: HIF-1alpha induction in primary inflammatory cells by TNF-alpha. *Am J Physiol Cell Physiol* **281**, C1971-1977
117. Botusan, I. R., Sunkari, V. G., Savu, O., Catrina, A. I., Grunler, J., Lindberg, S., Pereira, T., Yla-Herttuala, S., Poellinger, L., Brismar, K., and Catrina, S. B. (2008) Stabilization of HIF-1alpha is critical to improve wound healing in diabetic mice. *Proc Natl Acad Sci U S A* **105**, 19426-19431
118. Kalucka, J., Ettinger, A., Franke, K., Mamlouk, S., Singh, R. P., Farhat, K., Muschter, A., Olbrich, S., Breier, G., Katschinski, D. M., Huttner, W., Weidemann, A., and Wielockx, B. (2013) Loss of epithelial hypoxia-inducible factor prolyl hydroxylase 2 accelerates skin wound healing in mice. *Mol Cell Biol* **33**, 3426-3438
119. Zhang, X., Yan, X., Cheng, L., Dai, J., Wang, C., Han, P., and Chai, Y. (2013) Wound healing improvement with PHD-2 silenced fibroblasts in diabetic mice. *PLoS One* **8**, e84548
120. Thangarajah, H., Yao, D., Chang, E. I., Shi, Y., Jazayeri, L., Vial, I. N., Galiano, R. D., Du, X. L., Grogan, R., Galvez, M. G., Januszyk, M., Brownlee, M., and Gurtner, G. C. (2009) The molecular basis for impaired hypoxia-induced VEGF expression in diabetic tissues. *Proc Natl Acad Sci U S A* **106**, 13505-13510
121. Pirenne, J., Gunson, B., Khaleef, H., Hubscher, S., Afford, S., McMaster, P., and Adams, D. (1997) Influence of ischemia-reperfusion injury on rejection after liver transplantation. *Transplant Proc* **29**, 366-367
122. Watt, K. D., Lyden, E. R., Gulizia, J. M., and McCashland, T. M. (2006) Recurrent hepatitis C posttransplant: early preservation injury may predict poor outcome. *Liver Transpl* **12**, 134-139
123. Cheng, K., Ho, K., Stokes, R., Scott, C., Lau, S. M., Hawthorne, W. J., O'Connell, P. J., Loudovaris, T., Kay, T. W., Kulkarni, R. N., Okada, T., Wang, X. L., Yim, S. H., Shah, Y., Grey, S. T., Biankin, A. V., Kench, J. G., Laybutt, D. R., Gonzalez, F. J., Kahn, C. R., and Gunton, J. E. (2010) Hypoxia-inducible factor-1alpha regulates beta cell function in mouse and human islets. *J Clin Invest* **120**, 2171-2183
124. Amm, I., Sommer, T., and Wolf, D. H. (2014) Protein quality control and elimination of protein waste: the role of the ubiquitin-proteasome system. *Biochim Biophys Acta* **1843**, 182-196
125. Lilienbaum, A. (2013) Relationship between the proteasomal system and autophagy. *Int J Biochem Mol Biol* **4**, 1-26
126. Hershko, A., and Ciechanover, A. (1998) The ubiquitin system. *Annual review of biochemistry* **67**, 425-479

127. Lecker, S. H., Goldberg, A. L., and Mitch, W. E. (2006) Protein degradation by the ubiquitin-proteasome pathway in normal and disease states. *J Am Soc Nephrol* **17**, 1807-1819
128. Skaar, J. R., Pagan, J. K., and Pagano, M. (2014) SCF ubiquitin ligase-targeted therapies. *Nat Rev Drug Discov* **13**, 889-903
129. Metzger, M. B., Pruneda, J. N., Klevit, R. E., and Weissman, A. M. (2014) RING-type E3 ligases: master manipulators of E2 ubiquitin-conjugating enzymes and ubiquitination. *Biochim Biophys Acta* **1843**, 47-60
130. Dove, K. K., Stieglitz, B., Duncan, E. D., Rittinger, K., and Klevit, R. E. (2016) Molecular insights into RBR E3 ligase ubiquitin transfer mechanisms. *EMBO Rep* **17**, 1221-1235
131. Komander, D., and Rape, M. (2012) The ubiquitin code. *Annu Rev Biochem* **81**, 203-229
132. Yau, R., and Rape, M. (2016) The increasing complexity of the ubiquitin code. *Nat Cell Biol* **18**, 579-586
133. Bosu, D. R., and Kipreos, E. T. (2008) Cullin-RING ubiquitin ligases: global regulation and activation cycles. *Cell Div* **3**, 7
134. Bulatov, E., and Ciulli, A. (2015) Targeting Cullin-RING E3 ubiquitin ligases for drug discovery: structure, assembly and small-molecule modulation. *Biochem J* **467**, 365-386
135. Hua, Z., and Vierstra, R. D. (2011) The cullin-RING ubiquitin-protein ligases. *Annu Rev Plant Biol* **62**, 299-334
136. Duda, D. M., Borg, L. A., Scott, D. C., Hunt, H. W., Hammel, M., and Schulman, B. A. (2008) Structural insights into NEDD8 activation of cullin-RING ligases: conformational control of conjugation. *Cell* **134**, 995-1006
137. Zheng, J., Yang, X., Harrell, J. M., Ryzhikov, S., Shim, E. H., Lykke-Andersen, K., Wei, N., Sun, H., Kobayashi, R., and Zhang, H. (2002) CAND1 binds to unneddylated CUL1 and regulates the formation of SCF ubiquitin E3 ligase complex. *Mol Cell* **10**, 1519-1526
138. Latif, F., Tory, K., Gnarra, J., Yao, M., Duh, F. M., Orcutt, M. L., Stackhouse, T., Kuzmin, I., Modi, W., Geil, L., and et al. (1993) Identification of the von Hippel-Lindau disease tumor suppressor gene. *Science* **260**, 1317-1320
139. Kaelin, W. G. (2007) Von Hippel-Lindau disease. *Annu Rev Pathol* **2**, 145-173
140. Gossage, L., Eisen, T., and Maher, E. R. (2015) VHL, the story of a tumour suppressor gene. *Nat Rev Cancer* **15**, 55-64
141. Maher, E. R., Neumann, H. P., and Richard, S. (2011) von Hippel-Lindau disease: a clinical and scientific review. *Eur J Hum Genet* **19**, 617-623
142. Chen, F., Kishida, T., Yao, M., Hustad, T., Glavac, D., Dean, M., Gnarra, J. R., Orcutt, M. L., Duh, F. M., Glenn, G., and et al. (1995) Germline mutations in the von Hippel-Lindau disease tumor suppressor gene: correlations with phenotype. *Hum Mutat* **5**, 66-75
143. Hoffman, M. A., Ohh, M., Yang, H., Klco, J. M., Ivan, M., and Kaelin, W. G., Jr. (2001) von Hippel-Lindau protein mutants linked to type 2C VHL disease preserve the ability to downregulate HIF. *Hum Mol Genet* **10**, 1019-1027
144. Richards, F. M., Payne, S. J., Zbar, B., Affara, N. A., Ferguson-Smith, M. A., and Maher, E. R. (1995) Molecular analysis of de novo germline mutations in the von Hippel-Lindau disease gene. *Hum Mol Genet* **4**, 2139-2143
145. Iliopoulos, O., Ohh, M., and Kaelin, W. G., Jr. (1998) pVHL19 is a biologically active product of the von Hippel-Lindau gene arising from internal translation initiation. *Proc Natl Acad Sci U S A* **95**, 11661-11666
146. Schoenfeld, A., Davidowitz, E. J., and Burk, R. D. (1998) A second major native von Hippel-Lindau gene product, initiated from an internal translation

start site, functions as a tumor suppressor. *Proc Natl Acad Sci U S A* **95**, 8817-8822

147. Blankenship, C., Naglich, J. G., Whaley, J. M., Seizinger, B., and Kley, N. (1999) Alternate choice of initiation codon produces a biologically active product of the von Hippel Lindau gene with tumor suppressor activity. *Oncogene* **18**, 1529-1535
148. Iliopoulos, O., Kibel, A., Gray, S., and Kaelin, W. G., Jr. (1995) Tumour suppression by the human von Hippel-Lindau gene product. *Nat Med* **1**, 822-826
149. Gnarra, J. R., Tory, K., Weng, Y., Schmidt, L., Wei, M. H., Li, H., Latif, F., Liu, S., Chen, F., Duh, F. M., and et al. (1994) Mutations of the VHL tumour suppressor gene in renal carcinoma. *Nat Genet* **7**, 85-90
150. Richards, F. M., Schofield, P. N., Fleming, S., and Maher, E. R. (1996) Expression of the von Hippel-Lindau disease tumour suppressor gene during human embryogenesis. *Hum Mol Genet* **5**, 639-644
151. Kessler, P. M., Vasavada, S. P., Rackley, R. R., Stackhouse, T., Duh, F. M., Latif, F., Lerman, M. I., Zbar, B., and Williams, B. R. (1995) Expression of the Von Hippel-Lindau tumor suppressor gene, VHL, in human fetal kidney and during mouse embryogenesis. *Mol Med* **1**, 457-466
152. Gnarra, J. R., Ward, J. M., Porter, F. D., Wagner, J. R., Devor, D. E., Grinberg, A., Emmert-Buck, M. R., Westphal, H., Klausner, R. D., and Linehan, W. M. (1997) Defective placental vasculogenesis causes embryonic lethality in VHL-deficient mice. *Proc Natl Acad Sci U S A* **94**, 9102-9107
153. Haase, V. H., Glickman, J. N., Socolovsky, M., and Jaenisch, R. (2001) Vascular tumors in livers with targeted inactivation of the von Hippel-Lindau tumor suppressor. *Proc Natl Acad Sci U S A* **98**, 1583-1588
154. Ohh, M., Yauch, R. L., Lonergan, K. M., Whaley, J. M., Stemmer-Rachamimov, A. O., Louis, D. N., Gavin, B. J., Kley, N., Kaelin, W. G., Jr., and Iliopoulos, O. (1998) The von Hippel-Lindau tumor suppressor protein is required for proper assembly of an extracellular fibronectin matrix. *Mol Cell* **1**, 959-968
155. Esteban-Barragan, M. A., Avila, P., Alvarez-Tejado, M., Gutierrez, M. D., Garcia-Pardo, A., Sanchez-Madrid, F., and Landazuri, M. O. (2002) Role of the von Hippel-Lindau tumor suppressor gene in the formation of beta1-integrin fibrillar adhesions. *Cancer Res* **62**, 2929-2936
156. Pause, A., Lee, S., Worrell, R. A., Chen, D. Y., Burgess, W. H., Linehan, W. M., and Klausner, R. D. (1997) The von Hippel-Lindau tumor-suppressor gene product forms a stable complex with human CUL-2, a member of the Cdc53 family of proteins. *Proc Natl Acad Sci U S A* **94**, 2156-2161
157. Kibel, A., Iliopoulos, O., DeCaprio, J. A., and Kaelin, W. G., Jr. (1995) Binding of the von Hippel-Lindau tumor suppressor protein to Elongin B and C. *Science* **269**, 1444-1446
158. Cardote, T. A. F., Gadd, M. S., and Ciulli, A. (2017) Crystal Structure of the Cul2-Rbx1-EloBC-VHL Ubiquitin Ligase Complex. *Structure* **25**, 901-911 e903
159. Mahrour, N., Redwine, W. B., Florens, L., Swanson, S. K., Martin-Brown, S., Bradford, W. D., Staehling-Hampton, K., Washburn, M. P., Conaway, R. C., and Conaway, J. W. (2008) Characterization of Cullin-box sequences that direct recruitment of Cul2-Rbx1 and Cul5-Rbx2 modules to Elongin BC-based ubiquitin ligases. *J Biol Chem* **283**, 8005-8013
160. Stebbins, C. E., Kaelin, W. G., Jr., and Pavletich, N. P. (1999) Structure of the VHL-ElonginC-ElonginB complex: implications for VHL tumor suppressor function. *Science* **284**, 455-461
161. Anderson, K., Nordquist, K. A., Gao, X., Hicks, K. C., Zhai, B., Gygi, S. P., and Patel, T. B. (2011) Regulation of cellular levels of Sprouty2 protein by prolyl

hydroxylase domain and von Hippel-Lindau proteins. *J Biol Chem* **286**, 42027-42036

162. Okuda, H., Saitoh, K., Hirai, S., Iwai, K., Takaki, Y., Baba, M., Minato, N., Ohno, S., and Shuin, T. (2001) The von Hippel-Lindau tumor suppressor protein mediates ubiquitination of activated atypical protein kinase C. *J Biol Chem* **276**, 43611-43617
163. Zhou, L., and Yang, H. (2011) The von Hippel-Lindau tumor suppressor protein promotes c-Cbl-independent poly-ubiquitylation and degradation of the activated EGFR. *PLoS One* **6**, e23936
164. Maynard, M. A., and Ohh, M. (2004) Von Hippel-Lindau tumor suppressor protein and hypoxia-inducible factor in kidney cancer. *Am J Nephrol* **24**, 1-13
165. Feldman, D. E., Thulasiraman, V., Ferreyra, R. G., and Frydman, J. (1999) Formation of the VHL-elongin BC tumor suppressor complex is mediated by the chaperonin TRiC. *Mol Cell* **4**, 1051-1061
166. Hansen, W. J., Ohh, M., Moslehi, J., Kondo, K., Kaelin, W. G., and Welch, W. J. (2002) Diverse effects of mutations in exon II of the von Hippel-Lindau (VHL) tumor suppressor gene on the interaction of pVHL with the cytosolic chaperonin and pVHL-dependent ubiquitin ligase activity. *Mol Cell Biol* **22**, 1947-1960
167. McClellan, A. J., Scott, M. D., and Frydman, J. (2005) Folding and quality control of the VHL tumor suppressor proceed through distinct chaperone pathways. *Cell* **121**, 739-748
168. Martinez-Saez, O., Gajate Borau, P., Alonso-Gordoa, T., Molina-Cerrillo, J., and Grande, E. (2017) Targeting HIF-2 alpha in clear cell renal cell carcinoma: A promising therapeutic strategy. *Crit Rev Oncol Hematol* **111**, 117-123
169. Zhang, H., Qian, D. Z., Tan, Y. S., Lee, K., Gao, P., Ren, Y. R., Rey, S., Hammers, H., Chang, D., Pili, R., Dang, C. V., Liu, J. O., and Semenza, G. L. (2008) Digoxin and other cardiac glycosides inhibit HIF-1alpha synthesis and block tumor growth. *Proc Natl Acad Sci U S A* **105**, 19579-19586
170. Wong, C. C., Zhang, H., Gilkes, D. M., Chen, J., Wei, H., Chaturvedi, P., Hubbi, M. E., and Semenza, G. L. (2012) Inhibitors of hypoxia-inducible factor 1 block breast cancer metastatic niche formation and lung metastasis. *J Mol Med (Berl)* **90**, 803-815
171. Lee, K., Zhang, H., Qian, D. Z., Rey, S., Liu, J. O., and Semenza, G. L. (2009) Acriflavine inhibits HIF-1 dimerization, tumor growth, and vascularization. *Proc Natl Acad Sci U S A* **106**, 17910-17915
172. Yin, T., He, S., Shen, G., and Wang, Y. (2014) HIF-1 Dimerization Inhibitor Acriflavine Enhances Antitumor Activity of Sunitinib in Breast Cancer Model. *Oncol Res* **22**, 139-145
173. Weijer, R., Broekgaarden, M., Krekorian, M., Alles, L. K., van Wijk, A. C., Mackaaij, C., Verheij, J., van der Wal, A. C., van Gulik, T. M., Storm, G., and Heger, M. (2016) Inhibition of hypoxia inducible factor 1 and topoisomerase with acriflavine sensitizes perihilar cholangiocarcinomas to photodynamic therapy. *Oncotarget* **7**, 3341-3356
174. Cheloni, G., Tanturli, M., Tusa, I., Ho DeSouza, N., Shan, Y., Gozzini, A., Mazurier, F., Rovida, E., Li, S., and Dello Sbarba, P. (2017) Targeting chronic myeloid leukemia stem cells with the hypoxia-inducible factor inhibitor acriflavine. *Blood* **130**, 655-665
175. Richardson, P. G., Hideshima, T., and Anderson, K. C. (2003) Bortezomib (PS-341): a novel, first-in-class proteasome inhibitor for the treatment of multiple myeloma and other cancers. *Cancer Control* **10**, 361-369

176. Shin, D. H., Chun, Y. S., Lee, D. S., Huang, L. E., and Park, J. W. (2008) Bortezomib inhibits tumor adaptation to hypoxia by stimulating the FIH-mediated repression of hypoxia-inducible factor-1. *Blood* **111**, 3131-3136
177. Kaluz, S., Kaluzova, M., and Stanbridge, E. J. (2006) Proteasomal inhibition attenuates transcriptional activity of hypoxia-inducible factor 1 (HIF-1) via specific effect on the HIF-1alpha C-terminal activation domain. *Mol Cell Biol* **26**, 5895-5907
178. Kortuem, K. M., and Stewart, A. K. (2013) Carfilzomib. *Blood* **121**, 893-897
179. Huang, X., and Dixit, V. M. (2016) Drugging the undruggables: exploring the ubiquitin system for drug development. *Cell Res* **26**, 484-498
180. Scheuermann, T. H., Tomchick, D. R., Machius, M., Guo, Y., Bruick, R. K., and Gardner, K. H. (2009) Artificial ligand binding within the HIF2alpha PAS-B domain of the HIF2 transcription factor. *Proc Natl Acad Sci U S A* **106**, 450-455
181. Scheuermann, T. H., Li, Q., Ma, H. W., Key, J., Zhang, L., Chen, R., Garcia, J. A., Naidoo, J., Longgood, J., Frantz, D. E., Tambar, U. K., Gardner, K. H., and Bruick, R. K. (2013) Allosteric inhibition of hypoxia inducible factor-2 with small molecules. *Nat Chem Biol* **9**, 271-276
182. Chen, W., Hill, H., Christie, A., Kim, M. S., Holloman, E., Pavia-Jimenez, A., Homayoun, F., Ma, Y., Patel, N., Yell, P., Hao, G., Yousuf, Q., Joyce, A., Pedrosa, I., Geiger, H., Zhang, H., Chang, J., Gardner, K. H., Bruick, R. K., Reeves, C., Hwang, T. H., Courtney, K., Frenkel, E., Sun, X., Zojwalla, N., Wong, T., Rizzi, J. P., Wallace, E. M., Josey, J. A., Xie, Y., Xie, X. J., Kapur, P., McKay, R. M., and Brugarolas, J. (2016) Targeting renal cell carcinoma with a HIF-2 antagonist. *Nature* **539**, 112-117
183. Cho, H., Du, X., Rizzi, J. P., Liberzon, E., Chakraborty, A. A., Gao, W., Carvo, I., Signoretti, S., Bruick, R. K., Josey, J. A., Wallace, E. M., and Kaelin, W. G. (2016) On-target efficacy of a HIF-2alpha antagonist in preclinical kidney cancer models. *Nature* **539**, 107-111
184. Wallace, E. M., Rizzi, J. P., Han, G., Wehn, P. M., Cao, Z., Du, X., Cheng, T., Czerwinski, R. M., Dixon, D. D., Goggin, B. S., Grina, J. A., Halfmann, M. M., Maddie, M. A., Olive, S. R., Schlachter, S. T., Tan, H., Wang, B., Wang, K., Xie, S., Xu, R., Yang, H., and Josey, J. A. (2016) A Small-Molecule Antagonist of HIF2alpha Is Efficacious in Preclinical Models of Renal Cell Carcinoma. *Cancer Res* **76**, 5491-5500
185. Tian, Y. M., Yeoh, K. K., Lee, M. K., Eriksson, T., Kessler, B. M., Kramer, H. B., Edelmann, M. J., Willam, C., Pugh, C. W., Schofield, C. J., and Ratcliffe, P. J. (2011) Differential sensitivity of hypoxia inducible factor hydroxylation sites to hypoxia and hydroxylase inhibitors. *J Biol Chem* **286**, 13041-13051
186. McDonough, M. A., McNeill, L. A., Tilliet, M., Papamicael, C. A., Chen, Q. Y., Banerji, B., Hewitson, K. S., and Schofield, C. J. (2005) Selective inhibition of factor inhibiting hypoxia-inducible factor. *J Am Chem Soc* **127**, 7680-7681
187. Chan, M. C., Ilott, N. E., Schodel, J., Sims, D., Tumber, A., Lippl, K., Mole, D. R., Pugh, C. W., Ratcliffe, P. J., Ponting, C. P., and Schofield, C. J. (2016) Tuning the Transcriptional Response to Hypoxia by Inhibiting Hypoxia-inducible Factor (HIF) Prolyl and Asparaginyl Hydroxylases. *J Biol Chem* **291**, 20661-20673
188. Hill, P., Shukla, D., Tran, M. G., Aragones, J., Cook, H. T., Carmeliet, P., and Maxwell, P. H. (2008) Inhibition of hypoxia inducible factor hydroxylases protects against renal ischemia-reperfusion injury. *J Am Soc Nephrol* **19**, 39-46
189. Xi, L., Taher, M., Yin, C., Salloum, F., and Kukreja, R. C. (2004) Cobalt chloride induces delayed cardiac preconditioning in mice through selective

activation of HIF-1alpha and AP-1 and iNOS signaling. *Am J Physiol Heart Circ Physiol* **287**, H2369-2375

190. Wang, G. L., and Semenza, G. L. (1993) Desferrioxamine induces erythropoietin gene expression and hypoxia-inducible factor 1 DNA-binding activity: implications for models of hypoxia signal transduction. *Blood* **82**, 3610-3615
191. Mobarra, N., Shanaki, M., Ehteram, H., Nasiri, H., Sahmani, M., Saeidi, M., Goudarzi, M., Pourkarim, H., and Azad, M. (2016) A Review on Iron Chelators in Treatment of Iron Overload Syndromes. *Int J Hematol Oncol Stem Cell Res* **10**, 239-247
192. Guo, C., Zhang, Y. X., Wang, T., Zhong, M. L., Yang, Z. H., Hao, L. J., Chai, R., and Zhang, S. (2015) Intranasal deferoxamine attenuates synapse loss via up-regulating the P38/HIF-1alpha pathway on the brain of APP/PS1 transgenic mice. *Front Aging Neurosci* **7**, 104
193. Wu, Y., Li, X., Xie, W., Jankovic, J., Le, W., and Pan, T. (2010) Neuroprotection of deferoxamine on rotenone-induced injury via accumulation of HIF-1 alpha and induction of autophagy in SH-SY5Y cells. *Neurochem Int* **57**, 198-205
194. Okumura, C. Y., Hollands, A., Tran, D. N., Olson, J., Dahesh, S., von Kockritz-Blickwede, M., Thienphrapa, W., Corle, C., Jeung, S. N., Kotsakis, A., Shalwitz, R. A., Johnson, R. S., and Nizet, V. (2012) A new pharmacological agent (AKB-4924) stabilizes hypoxia inducible factor-1 (HIF-1) and increases skin innate defenses against bacterial infection. *J Mol Med (Berl)* **90**, 1079-1089
195. Keely, S., Campbell, E. L., Baird, A. W., Hansbro, P. M., Shalwitz, R. A., Kotsakis, A., McNamee, E. N., Eltzschig, H. K., Kominsky, D. J., and Colgan, S. P. (2014) Contribution of epithelial innate immunity to systemic protection afforded by prolyl hydroxylase inhibition in murine colitis. *Mucosal Immunol* **7**, 114-123
196. Soucy, T. A., Smith, P. G., Milhollen, M. A., Berger, A. J., Gavin, J. M., Adhikari, S., Brownell, J. E., Burke, K. E., Cardin, D. P., Critchley, S., Cullis, C. A., Doucette, A., Garnsey, J. J., Gaulin, J. L., Gershman, R. E., Lublinsky, A. R., McDonald, A., Mizutani, H., Narayanan, U., Olhava, E. J., Peluso, S., Rezaei, M., Sintchak, M. D., Talreja, T., Thomas, M. P., Traore, T., Vyskocil, S., Weatherhead, G. S., Yu, J., Zhang, J., Dick, L. R., Claiborne, C. F., Rolfe, M., Bolen, J. B., and Langston, S. P. (2009) An inhibitor of NEDD8-activating enzyme as a new approach to treat cancer. *Nature* **458**, 732-736
197. Brownell, J. E., Sintchak, M. D., Gavin, J. M., Liao, H., Bruzzese, F. J., Bump, N. J., Soucy, T. A., Milhollen, M. A., Yang, X., Burkhardt, A. L., Ma, J., Loke, H. K., Lingaraj, T., Wu, D., Hamman, K. B., Spelman, J. J., Cullis, C. A., Langston, S. P., Vyskocil, S., Sells, T. B., Mallender, W. D., Visiers, I., Li, P., Claiborne, C. F., Rolfe, M., Bolen, J. B., and Dick, L. R. (2010) Substrate-assisted inhibition of ubiquitin-like protein-activating enzymes: the NEDD8 E1 inhibitor MLN4924 forms a NEDD8-AMP mimetic in situ. *Mol Cell* **37**, 102-111
198. Curtis, V. F., Ehrentraut, S. F., Campbell, E. L., Glover, L. E., Bayless, A., Kelly, C. J., Kominsky, D. J., and Colgan, S. P. (2015) Stabilization of HIF through inhibition of Cullin-2 neddylation is protective in mucosal inflammatory responses. *FASEB J* **29**, 208-215
199. Lan, H., Tang, Z., Jin, H., and Sun, Y. (2016) Neddylation inhibitor MLN4924 suppresses growth and migration of human gastric cancer cells. *Sci Rep* **6**, 24218
200. Swords, R. T., Erba, H. P., DeAngelo, D. J., Bixby, D. L., Altman, J. K., Maris, M., Hua, Z., Blakemore, S. J., Faessel, H., Sedarati, F., Dezube, B. J., Giles, F.

J., and Medeiros, B. C. (2015) Pevonedistat (MLN4924), a First-in-Class NEDD8-activating enzyme inhibitor, in patients with acute myeloid leukaemia and myelodysplastic syndromes: a phase 1 study. *Br J Haematol* **169**, 534-543

201. Locatelli, F., Fishbane, S., Block, G. A., and Macdougall, I. C. (2017) Targeting Hypoxia-Inducible Factors for the Treatment of Anemia in Chronic Kidney Disease Patients. *Am J Nephrol* **45**, 187-199
202. Flight, M. H. (2013) Deal watch: AstraZeneca bets on FibroGen's anaemia drug. *Nat Rev Drug Discov* **12**, 730
203. Chowdhury, R., Candela-Lena, J. I., Chan, M. C., Greenald, D. J., Yeoh, K. K., Tian, Y. M., McDonough, M. A., Tumber, A., Rose, N. R., Conejo-Garcia, A., Demetriades, M., Mathavan, S., Kawamura, A., Lee, M. K., van Eeden, F., Pugh, C. W., Ratcliffe, P. J., and Schofield, C. J. (2013) Selective small molecule probes for the hypoxia inducible factor (HIF) prolyl hydroxylases. *ACS Chem Biol* **8**, 1488-1496
204. Chan, M. C., Atasoylu, O., Hodson, E., Tumber, A., Leung, I. K., Chowdhury, R., Gomez-Perez, V., Demetriades, M., Rydzik, A. M., Holt-Martyn, J., Tian, Y. M., Bishop, T., Claridge, T. D., Kawamura, A., Pugh, C. W., Ratcliffe, P. J., and Schofield, C. J. (2015) Potent and Selective Triazole-Based Inhibitors of the Hypoxia-Inducible Factor Prolyl-Hydroxylases with Activity in the Murine Brain. *PLoS One* **10**, e0132004
205. Cohen, P., and Tcherpakov, M. (2010) Will the ubiquitin system furnish as many drug targets as protein kinases? *Cell* **143**, 686-693
206. Arkin, M. R., Tang, Y., and Wells, J. A. (2014) Small-molecule inhibitors of protein-protein interactions: progressing toward the reality. *Chem Biol* **21**, 1102-1114
207. Scott, D. E., Bayly, A. R., Abell, C., and Skidmore, J. (2016) Small molecules, big targets: drug discovery faces the protein-protein interaction challenge. *Nat Rev Drug Discov* **15**, 533-550
208. Arrowsmith, C. H., Audia, J. E., Austin, C., Baell, J., Bennett, J., Blagg, J., Bountra, C., Brennan, P. E., Brown, P. J., Bunnage, M. E., Buser-Doepner, C., Campbell, R. M., Carter, A. J., Cohen, P., Copeland, R. A., Cravatt, B., Dahlin, J. L., Dhanak, D., Edwards, A. M., Frederiksen, M., Frye, S. V., Gray, N., Grimshaw, C. E., Hepworth, D., Howe, T., Huber, K. V., Jin, J., Knapp, S., Kotz, J. D., Kruger, R. G., Lowe, D., Mader, M. M., Marsden, B., Mueller-Fahrnow, A., Muller, S., O'Hagan, R. C., Overington, J. P., Owen, D. R., Rosenberg, S. H., Roth, B., Ross, R., Schapira, M., Schreiber, S. L., Shoichet, B., Sundstrom, M., Superti-Furga, G., Taunton, J., Toledo-Sherman, L., Walpole, C., Walters, M. A., Willson, T. M., Workman, P., Young, R. N., and Zuercher, W. J. (2015) The promise and peril of chemical probes. *Nat Chem Biol* **11**, 536-541
209. Bunnage, M. E., Chekler, E. L., and Jones, L. H. (2013) Target validation using chemical probes. *Nat Chem Biol* **9**, 195-199
210. Workman, P., and Collins, I. (2010) Probing the probes: fitness factors for small molecule tools. *Chem Biol* **17**, 561-577
211. Buckley, D. L., Van Molle, I., Gareiss, P. C., Tae, H. S., Michel, J., Noblin, D. J., Jorgensen, W. L., Ciulli, A., and Crews, C. M. (2012) Targeting the von Hippel-Lindau E3 ubiquitin ligase using small molecules to disrupt the VHL/HIF-1alpha interaction. *J Am Chem Soc* **134**, 4465-4468
212. Van Molle, I., Thomann, A., Buckley, D. L., So, E. C., Lang, S., Crews, C. M., and Ciulli, A. (2012) Dissecting fragment-based lead discovery at the von Hippel-Lindau protein:hypoxia inducible factor 1alpha protein-protein interface. *Chem Biol* **19**, 1300-1312

213. Buckley, D. L., Gustafson, J. L., Van Molle, I., Roth, A. G., Tae, H. S., Gareiss, P. C., Jorgensen, W. L., Ciulli, A., and Crews, C. M. (2012) Small-molecule inhibitors of the interaction between the E3 ligase VHL and HIF1alpha. *Angew Chem Int Ed Engl* **51**, 11463-11467
214. Galdeano, C., Gadd, M. S., Soares, P., Scaffidi, S., Van Molle, I., Birced, I., Hewitt, S., Dias, D. M., and Ciulli, A. (2014) Structure-guided design and optimization of small molecules targeting the protein-protein interaction between the von Hippel-Lindau (VHL) E3 ubiquitin ligase and the hypoxia inducible factor (HIF) alpha subunit with in vitro nanomolar affinities. *J Med Chem* **57**, 8657-8663
215. Frost, J., Galdeano, C., Soares, P., Gadd, M. S., Grzes, K. M., Ellis, L., Epemolu, O., Shimamura, S., Bantscheff, M., Grandi, P., Read, K. D., Cantrell, D. A., Rocha, S., and Ciulli, A. (2016) Potent and selective chemical probe of hypoxic signalling downstream of HIF-alpha hydroxylation via VHL inhibition. *Nat Commun* **7**, 13312
216. Sakamoto, K. M., Kim, K. B., Kumagai, A., Mercurio, F., Crews, C. M., and Deshaies, R. J. (2001) Protacs: chimeric molecules that target proteins to the Skp1-Cullin-F box complex for ubiquitination and degradation. *Proc Natl Acad Sci U S A* **98**, 8554-8559
217. Zengerle, M., Chan, K. H., and Ciulli, A. (2015) Selective Small Molecule Induced Degradation of the BET Bromodomain Protein BRD4. *ACS Chem Biol* **10**, 1770-1777
218. Chan, K. H., Zengerle, M., Testa, A., and Ciulli, A. (2017) Impact of Target Warhead and Linkage Vector on Inducing Protein Degradation: Comparison of Bromodomain and Extra-Terminal (BET) Degraders Derived from Triazolodiazepine (JQ1) and Tetrahydroquinoline (I-BET726) BET Inhibitor Scaffolds. *J Med Chem*
219. Bondeson, D. P., Mares, A., Smith, I. E., Ko, E., Campos, S., Miah, A. H., Mulholland, K. E., Routly, N., Buckley, D. L., Gustafson, J. L., Zinn, N., Grandi, P., Shimamura, S., Bergamini, G., Faelth-Savitski, M., Bantscheff, M., Cox, C., Gordon, D. A., Willard, R. R., Flanagan, J. J., Casillas, L. N., Votta, B. J., den Besten, W., Famm, K., Kruidenier, L., Carter, P. S., Harling, J. D., Churcher, I., and Crews, C. M. (2015) Catalytic in vivo protein knockdown by small-molecule PROTACs. *Nat Chem Biol* **11**, 611-617
220. Buckley, D. L., Raina, K., Darricarrere, N., Hines, J., Gustafson, J. L., Smith, I. E., Miah, A. H., Harling, J. D., and Crews, C. M. (2015) HaloPROTACS: Use of Small Molecule PROTACs to Induce Degradation of HaloTag Fusion Proteins. *ACS Chem Biol* **10**, 1831-1837
221. Fischer, E. S., Bohm, K., Lydeard, J. R., Yang, H., Stadler, M. B., Cavadini, S., Nagel, J., Serluca, F., Acker, V., Lingaraju, G. M., Tichkule, R. B., Schebesta, M., Forrester, W. C., Schirle, M., Hassiepen, U., Ottl, J., Hild, M., Beckwith, R. E., Harper, J. W., Jenkins, J. L., and Thoma, N. H. (2014) Structure of the DDB1-CRBN E3 ubiquitin ligase in complex with thalidomide. *Nature* **512**, 49-53
222. Melvin, A., Mudie, S., and Rocha, S. (2011) The chromatin remodeler ISWI regulates the cellular response to hypoxia: role of FIH. *Mol Biol Cell* **22**, 4171-4181
223. Martinez Molina, D., Jafari, R., Ignatushchenko, M., Seki, T., Larsson, E. A., Dan, C., Sreekumar, L., Cao, Y., and Nordlund, P. (2013) Monitoring drug target engagement in cells and tissues using the cellular thermal shift assay. *Science* **341**, 84-87

224. Liao, Y., Smyth, G. K., and Shi, W. (2014) featureCounts: an efficient general purpose program for assigning sequence reads to genomic features. *Bioinformatics* **30**, 923-930
225. Robinson, M. D., McCarthy, D. J., and Smyth, G. K. (2010) edgeR: a Bioconductor package for differential expression analysis of digital gene expression data. *Bioinformatics* **26**, 139-140
226. van Uden, P., Kenneth, N. S., Webster, R., Muller, H. A., Mudie, S., and Rocha, S. (2011) Evolutionary conserved regulation of HIF-1beta by NF-kappaB. *PLoS Genet* **7**, e1001285
227. Loenarz, C., Mecinovic, J., Chowdhury, R., McNeill, L. A., Flashman, E., and Schofield, C. J. (2009) Evidence for a stereoelectronic effect in human oxygen sensing. *Angew Chem Int Ed Engl* **48**, 1784-1787
228. Hergovich, A., Lisztwan, J., Barry, R., Ballschmieter, P., and Krek, W. (2003) Regulation of microtubule stability by the von Hippel-Lindau tumour suppressor protein pVHL. *Nat Cell Biol* **5**, 64-70
229. Thoma, C. R., Toso, A., Gutbrodt, K. L., Reggi, S. P., Frew, I. J., Schraml, P., Hergovich, A., Moch, H., Meraldi, P., and Krek, W. (2009) VHL loss causes spindle misorientation and chromosome instability. *Nat Cell Biol* **11**, 994-1001
230. Hell, M. P., Duda, M., Weber, T. C., Moch, H., and Krek, W. (2014) Tumor suppressor VHL functions in the control of mitotic fidelity. *Cancer Res* **74**, 2422-2431
231. Goda, N., Ryan, H. E., Khadivi, B., McNulty, W., Rickert, R. C., and Johnson, R. S. (2003) Hypoxia-inducible factor 1alpha is essential for cell cycle arrest during hypoxia. *Mol Cell Biol* **23**, 359-369
232. Chan, M. C., Holt-Martyn, J. P., Schofield, C. J., and Ratcliffe, P. J. (2016) Pharmacological targeting of the HIF hydroxylases--A new field in medicine development. *Mol Aspects Med* **47-48**, 54-75
233. Forsythe, J. A., Jiang, B. H., Iyer, N. V., Agani, F., Leung, S. W., Koos, R. D., and Semenza, G. L. (1996) Activation of vascular endothelial growth factor gene transcription by hypoxia-inducible factor 1. *Mol Cell Biol* **16**, 4604-4613
234. Wang, Z., Gerstein, M., and Snyder, M. (2009) RNA-Seq: a revolutionary tool for transcriptomics. *Nat Rev Genet* **10**, 57-63
235. McAlister, G. C., Huttlin, E. L., Haas, W., Ting, L., Jedrychowski, M. P., Rogers, J. C., Kuhn, K., Pike, I., Grothe, R. A., Blethrow, J. D., and Gygi, S. P. (2012) Increasing the multiplexing capacity of TMTs using reporter ion isotopologues with isobaric masses. *Anal Chem* **84**, 7469-7478
236. Rauniyar, N., and Yates, J. R., 3rd. (2014) Isobaric labeling-based relative quantification in shotgun proteomics. *J Proteome Res* **13**, 5293-5309
237. Schurch, N. J., Schofield, P., Gierlinski, M., Cole, C., Sherstnev, A., Singh, V., Wrobel, N., Gharbi, K., Simpson, G. G., Owen-Hughes, T., Blaxter, M., and Barton, G. J. (2016) How many biological replicates are needed in an RNA-seq experiment and which differential expression tool should you use? *RNA* **22**, 839-851
238. Mense, S. M., Sengupta, A., Zhou, M., Lan, C., Bentsman, G., Volsky, D. J., and Zhang, L. (2006) Gene expression profiling reveals the profound upregulation of hypoxia-responsive genes in primary human astrocytes. *Physiol Genomics* **25**, 435-449
239. Elvidge, G. P., Glenny, L., Appelhoff, R. J., Ratcliffe, P. J., Ragoussis, J., and Gleadle, J. M. (2006) Concordant regulation of gene expression by hypoxia and 2-oxoglutarate-dependent dioxygenase inhibition: the role of HIF-1alpha, HIF-2alpha, and other pathways. *J Biol Chem* **281**, 15215-15226

240. Schodel, J., Oikonomopoulos, S., Ragoussis, J., Pugh, C. W., Ratcliffe, P. J., and Mole, D. R. (2011) High-resolution genome-wide mapping of HIF-binding sites by ChIP-seq. *Blood* **117**, e207-217
241. Hu, C. J., Iyer, S., Sataur, A., Covello, K. L., Chodosh, L. A., and Simon, M. C. (2006) Differential regulation of the transcriptional activities of hypoxia-inducible factor 1 alpha (HIF-1alpha) and HIF-2alpha in stem cells. *Mol Cell Biol* **26**, 3514-3526
242. Knowles, H. J., Cleton-Jansen, A. M., Korsching, E., and Athanasou, N. A. (2010) Hypoxia-inducible factor regulates osteoclast-mediated bone resorption: role of angiopoietin-like 4. *FASEB J* **24**, 4648-4659
243. An, X., Jin, Y., Guo, H., Foo, S. Y., Cully, B. L., Wu, J., Zeng, H., Rosenzweig, A., and Li, J. (2009) Response gene to complement 32, a novel hypoxia-regulated angiogenic inhibitor. *Circulation* **120**, 617-627
244. Ai, H., Yang, B., Li, J., Xie, X., Chen, H., and Ren, J. (2014) Population history and genomic signatures for high-altitude adaptation in Tibetan pigs. *BMC Genomics* **15**, 834
245. Le Jan, S., Le Meur, N., Cazes, A., Philippe, J., Le Cunff, M., Leger, J., Corvol, P., and Germain, S. (2006) Characterization of the expression of the hypoxia-induced genes neuritin, TXNIP and IGFBP3 in cancer. *FEBS Lett* **580**, 3395-3400
246. Chai, T. F., Leck, Y. C., He, H., Yu, F. X., Luo, Y., and Hagen, T. (2011) Hypoxia-inducible factor independent down-regulation of thioredoxin-interacting protein in hypoxia. *FEBS Lett* **585**, 492-498
247. Shin, D., Jeon, J. H., Jeong, M., Suh, H. W., Kim, S., Kim, H. C., Moon, O. S., Kim, Y. S., Chung, J. W., Yoon, S. R., Kim, W. H., and Choi, I. (2008) VDUP1 mediates nuclear export of HIF1alpha via CRM1-dependent pathway. *Biochim Biophys Acta* **1783**, 838-848
248. D'Ignazio, L., Bandarra, D., and Rocha, S. (2016) NF-kappaB and HIF crosstalk in immune responses. *FEBS J* **283**, 413-424
249. Murdoch, C., Muthana, M., and Lewis, C. E. (2005) Hypoxia regulates macrophage functions in inflammation. *J Immunol* **175**, 6257-6263
250. Arany, Z., Foo, S. Y., Ma, Y., Ruas, J. L., Bommi-Reddy, A., Girnun, G., Cooper, M., Laznik, D., Chinsomboon, J., Rangwala, S. M., Baek, K. H., Rosenzweig, A., and Spiegelman, B. M. (2008) HIF-independent regulation of VEGF and angiogenesis by the transcriptional coactivator PGC-1alpha. *Nature* **451**, 1008-1012
251. Li, Y., Padmanabha, D., Gentile, L. B., Dumur, C. I., Beckstead, R. B., and Baker, K. D. (2013) HIF- and non-HIF-regulated hypoxic responses require the estrogen-related receptor in Drosophila melanogaster. *PLoS Genet* **9**, e1003230
252. Padmanabha, D., Padilla, P. A., You, Y. J., and Baker, K. D. (2015) A HIF-independent mediator of transcriptional responses to oxygen deprivation in Caenorhabditis elegans. *Genetics* **199**, 739-748
253. Duran, R. V., MacKenzie, E. D., Boulahbel, H., Frezza, C., Heiserich, L., Tardito, S., Bussolati, O., Rocha, S., Hall, M. N., and Gottlieb, E. (2013) HIF-independent role of prolyl hydroxylases in the cellular response to amino acids. *Oncogene* **32**, 4549-4556
254. Ginouves, A., Ilc, K., Macias, N., Pouyssegur, J., and Berra, E. (2008) PHDs overactivation during chronic hypoxia "desensitizes" HIFalpha and protects cells from necrosis. *Proc Natl Acad Sci U S A* **105**, 4745-4750
255. Tanimoto, K., Makino, Y., Pereira, T., and Poellinger, L. (2000) Mechanism of regulation of the hypoxia-inducible factor-1 alpha by the von Hippel-Lindau tumor suppressor protein. *EMBO J* **19**, 4298-4309

256. Hubbi, M. E., Hu, H., Kshitiz, Ahmed, I., Levchenko, A., and Semenza, G. L. (2013) Chaperone-mediated autophagy targets hypoxia-inducible factor-1alpha (HIF-1alpha) for lysosomal degradation. *J Biol Chem* **288**, 10703-10714
257. Mellacheruvu, D., Wright, Z., Couzens, A. L., Lambert, J. P., St-Denis, N. A., Li, T., Miteva, Y. V., Hauri, S., Sardiu, M. E., Low, T. Y., Halim, V. A., Bagshaw, R. D., Hubner, N. C., Al-Hakim, A., Bouchard, A., Faubert, D., Fermin, D., Dunham, W. H., Goudreault, M., Lin, Z. Y., Badillo, B. G., Pawson, T., Durocher, D., Coulombe, B., Aebersold, R., Superti-Furga, G., Colinge, J., Heck, A. J., Choi, H., Gstaiger, M., Mohammed, S., Cristea, I. M., Bennett, K. L., Washburn, M. P., Raught, B., Ewing, R. M., Gingras, A. C., and Nesvizhskii, A. I. (2013) The CRAPome: a contaminant repository for affinity purification-mass spectrometry data. *Nat Methods* **10**, 730-736
258. Hochrainer, K., Mayer, H., Baranyi, U., Binder, B., Lipp, J., and Kroismayr, R. (2005) The human HERC family of ubiquitin ligases: novel members, genomic organization, expression profiling, and evolutionary aspects. *Genomics* **85**, 153-164
259. Tan, X., Calderon-Villalobos, L. I., Sharon, M., Zheng, C., Robinson, C. V., Estelle, M., and Zheng, N. (2007) Mechanism of auxin perception by the TIR1 ubiquitin ligase. *Nature* **446**, 640-645
260. Gandhi, A. K., Kang, J., Havens, C. G., Conklin, T., Ning, Y., Wu, L., Ito, T., Ando, H., Waldman, M. F., Thakurta, A., Klippel, A., Handa, H., Daniel, T. O., Schafer, P. H., and Chopra, R. (2014) Immunomodulatory agents lenalidomide and pomalidomide co-stimulate T cells by inducing degradation of T cell repressors Ikaros and Aiolos via modulation of the E3 ubiquitin ligase complex CRL4(CRBN.). *Br J Haematol* **164**, 811-821
261. Bilbao, A., Varesio, E., Luban, J., Strambio-De-Castillia, C., Hopfgartner, G., Muller, M., and Lisacek, F. (2015) Processing strategies and software solutions for data-independent acquisition in mass spectrometry. *Proteomics* **15**, 964-980
262. Kapitsinou, P. P., and Haase, V. H. (2008) The VHL tumor suppressor and HIF: insights from genetic studies in mice. *Cell Death Differ* **15**, 650-659
263. To, K. K., and Huang, L. E. (2005) Suppression of hypoxia-inducible factor 1alpha (HIF-1alpha) transcriptional activity by the HIF prolyl hydroxylase EGLN1. *J Biol Chem* **280**, 38102-38107
264. Lu, J., Qian, Y., Altieri, M., Dong, H., Wang, J., Raina, K., Hines, J., Winkler, J. D., Crew, A. P., Coleman, K., and Crews, C. M. (2015) Hijacking the E3 Ubiquitin Ligase Cereblon to Efficiently Target BRD4. *Chem Biol* **22**, 755-763
265. Jain, I. H., Zazzeron, L., Goli, R., Alexa, K., Schatzman-Bone, S., Dhillon, H., Goldberger, O., Peng, J., Shalem, O., Sanjana, N. E., Zhang, F., Goessling, W., Zapol, W. M., and Mootha, V. K. (2016) Hypoxia as a therapy for mitochondrial disease. *Science* **352**, 54-61
266. Varela, I., Tarpey, P., Raine, K., Huang, D., Ong, C. K., Stephens, P., Davies, H., Jones, D., Lin, M. L., Teague, J., Bignell, G., Butler, A., Cho, J., Dalgliesh, G. L., Galappaththige, D., Greenman, C., Hardy, C., Jia, M., Latimer, C., Lau, K. W., Marshall, J., McLaren, S., Menzies, A., Mudie, L., Stebbings, L., Largaespada, D. A., Wessels, L. F., Richard, S., Kahnoski, R. J., Anema, J., Tuveson, D. A., Perez-Mancera, P. A., Mustonen, V., Fischer, A., Adams, D. J., Rust, A., Chan-on, W., Subimerb, C., Dykema, K., Furge, K., Campbell, P. J., Teh, B. T., Stratton, M. R., and Futreal, P. A. (2011) Exome sequencing identifies frequent mutation of the SWI/SNF complex gene PBRM1 in renal carcinoma. *Nature* **469**, 539-542
267. Hakimi, A. A., Pham, C. G., and Hsieh, J. J. (2013) A clear picture of renal cell carcinoma. *Nat Genet* **45**, 849-850

9. Appendix

Table 9.1 – Chemical structures, and dissociation constants measured by FP and ITC of a new series of VHL inhibitors by Pedro Soares. Figures of chemical structures were made by Pedro Soares.

Inhibitor	Chemical Structure	Kd FP (nM)	Kd ITC (nM)
VH058	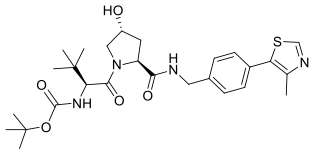	6500 ± 300	-
VH070	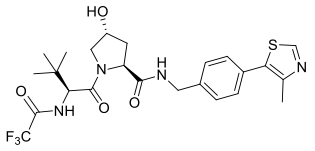	270 ± 50	-
VH071	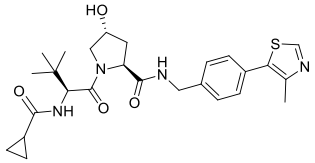	170 ± 30	130 ± 10
VH079	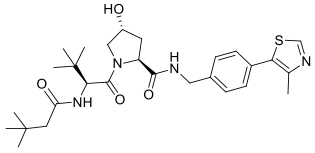	450 ± 90	-
VH080	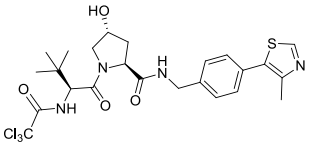	200 ± 30	-
VH089	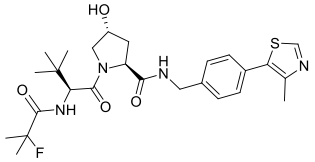	770 ± 30	-
VH100	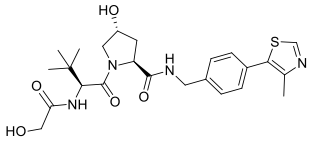	195 ± 30	105 ± 11
VH110	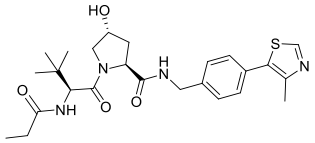	345 ± 90	-
VH185	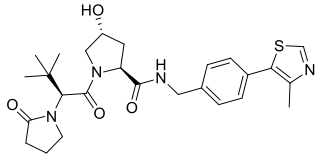	1400 ± 100	-

VH456	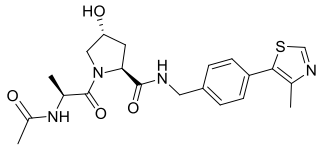	760 ± 20	-
VH235	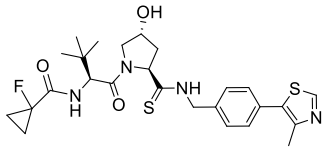	1670 ± 90	-
VH271	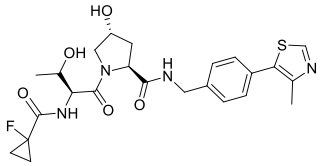	365 ± 40	-
VH285	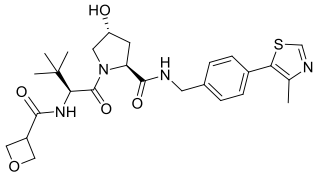	320 ± 20	232 ± 20
VH286	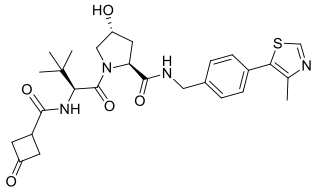	500 ± 30	-
VH302	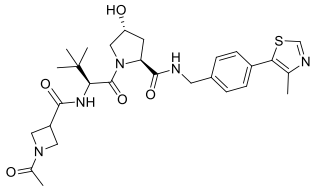	4895 ± 200	232 ± 20
VH311	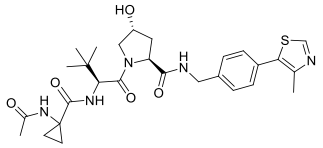	300 ± 40	140 ± 20
VH365	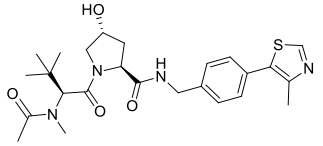	5510 ± 300	-

Table 9.2 – List of 4 genes downregulated in hypoxia, IOX2 and VH032 treatments compared to DMSO control. Genes were selected at FDR < 0.05 and logFC < –1. In red: selected for validation by qRT-PCR.

Ensembl gene ID	Gene name
ENSG00000133710	SPINK5
ENSG00000158050	DUSP2
ENSG00000187325	TAF9B
ENSG00000272711	RP11-259N19.1

Table 9.3 – List of 232 genes upregulated in hypoxia, IOX2 and VH032 treatments compared to DMSO control. Genes were selected at FDR < 0.05 and logFC > 1. Under 'Comparison' column, genes were reported in publicly available datasets. 1: list of 100 HIF targets. 2: list of 259 genes upregulated in several cell lines. 3: list of 1141 genes upregulated in hypoxia in HeLa cells. 4: list of 356 genes identified by ChIP-sequencing for HIF-1. 5: list of 301 genes identified by ChIP-sequencing for HIF-2. 6: list of 246 genes upregulated in hypoxia in MCF7 cells. In red: selected for validation by qRT-PCR.

Ensembl gene ID	Gene name	Comparison
ENSG00000007516	BAIAP3	
ENSG00000018280	SLC11A1	
ENSG00000025039	RRAGD	2, 6
ENSG00000044524	EPHA3	3
ENSG00000047457	CP	1, 3
ENSG00000048740	CELF2	
ENSG00000054356	PTPRN	4
ENSG00000059804	SLC2A3	2, 3, 4, 5
ENSG00000061656	SPAG4	4, 6
ENSG00000064225	ST3GAL6	
ENSG00000067057	PFKP	2, 4, 6
ENSG00000067992	PDK3	2, 3
ENSG00000068971	PPP2R5B	3
ENSG00000069667	RORA	2
ENSG00000072682	P4HA2	2, 3, 4, 6
ENSG00000079739	PGM1	6
ENSG00000087266	SH3BP2	
ENSG00000088340	FER1L4	
ENSG00000092421	SEMA6A	
ENSG00000095303	PTGS1	2, 3
ENSG00000099840	IZUMO4	
ENSG00000100290	BIK	
ENSG00000100593	ISM2	
ENSG00000102144	PGK1	1, 2, 3, 6
ENSG00000103184	SEC14L5	
ENSG00000104419	NDRG1	2, 3, 4, 5, 6
ENSG00000104765	BNIP3L	1, 2, 6
ENSG00000104812	GYS1	1, 2, 6
ENSG00000105220	GPI	1, 4, 5
ENSG00000105650	PDE4C	
ENSG00000105877	DNAH11	
ENSG00000107159	CA9	1, 4, 6

ENSG00000109107	ALDOC	3, 4, 6
ENSG00000111669	TPI1	1
ENSG00000111674	ENO2	2, 3, 6
ENSG00000112379	KIAA1244	
ENSG00000112715	VEGFA	1, 2
ENSG00000113083	LOX	1, 2, 3, 6
ENSG00000113739	STC2	2, 3, 4, 5, 6
ENSG00000114023	FAM162A	
ENSG00000114268	PFKFB4	2, 3, 4, 5
ENSG00000114480	GBE1	2, 3, 4, 5, 6
ENSG00000114646	CSPG5	
ENSG00000115548	KDM3A	1
ENSG00000116883	RP11-268J15.5	
ENSG00000116977	LGALS8	2
ENSG00000117266	CDK18	
ENSG00000117394	SLC2A1	1, 2, 3, 4, 6
ENSG00000119630	PGF	
ENSG00000119950	MXI1	
ENSG00000122884	P4HA1	2, 4, 5, 6
ENSG00000123095	BHLHE41	
ENSG00000124116	WFDC3	
ENSG00000125629	INSIG2	2, 4, 6
ENSG00000125895	TMEM74B	
ENSG00000127329	PTPRB	4
ENSG00000127578	WFIKKN1	3
ENSG00000127663	KDM4B	1
ENSG00000129521	EGLN3	1, 2, 4, 5
ENSG00000130821	SLC6A8	2
ENSG00000131094	C1QL1	
ENSG00000131668	BARX1	
ENSG00000132139	GAS2L2	
ENSG00000133138	TBC1D8B	3
ENSG00000133488	SEC14L4	
ENSG00000133874	RNF122	
ENSG00000134013	LOXL2	3, 4, 5, 6
ENSG00000134107	BHLHE40	3
ENSG00000134333	LDHA	1, 2, 4, 5
ENSG00000135245	HILPDA	
ENSG00000135766	EGLN1	1, 2
ENSG00000136352	NKX2-1	
ENSG00000137285	TUBB2B	
ENSG00000139832	RAB20	2
ENSG00000141526	SLC16A3	
ENSG00000141959	PFKL	1, 2, 4
ENSG00000143590	EFNA3	6
ENSG00000143847	PPFIA4	6
ENSG00000144063	MALL	
ENSG00000144320	KIAA1715	2
ENSG00000145491	ROPN1L	
ENSG00000145901	TNIP1	2
ENSG00000146094	DOK3	
ENSG00000146205	ANO7	
ENSG00000146674	IGFBP3	1, 4, 5, 6
ENSG00000147036	LANCL3	
ENSG00000147852	VLDLR	6
ENSG00000148926	ADM	1, 2, 3, 4, 6
ENSG00000149925	ALDOA	1, 4, 5

ENSG00000151882	CCL28	
ENSG00000152256	PDK1	1, 2, 4, 5, 6
ENSG00000152952	PLOD2	2, 3, 4, 5
ENSG00000153233	PTPRR	2
ENSG00000154493	C10orf90	
ENSG00000159167	STC1	2, 3, 6
ENSG00000159208	C1orf51	4
ENSG00000159399	HK2	1, 3, 4, 6
ENSG00000160999	SH2B2	
ENSG00000161544	CYGB	
ENSG00000161638	ITGA5	3, 4, 5
ENSG00000161921	CXCL16	
ENSG00000161958	FGF11	
ENSG00000162433	AK4	
ENSG00000163516	ANKZF1	4
ENSG00000163689	C3orf67	
ENSG00000164056	SPRY1	4
ENSG00000164078	MST1R	
ENSG00000164096	C4orf3	
ENSG00000164638	SLC29A4	
ENSG00000164849	GPR146	
ENSG00000166046	TCP11L2	3
ENSG00000167619	TMEM145	
ENSG00000167695	FAM57A	
ENSG00000167771	RCOR2	1
ENSG00000167772	ANGPTL4	4, 6
ENSG00000167971	CASKIN1	
ENSG00000168333	C8orf22	
ENSG00000168350	DEGS2	
ENSG00000170075	GPR37L1	4, 5
ENSG00000170379	FAM115C	
ENSG00000170525	PFKFB3	1, 2, 3, 4, 5, 6
ENSG00000171314	PGAM1	4
ENSG00000171388	APLN	
ENSG00000172081	MOB3A	
ENSG00000173281	PPP1R3B	3
ENSG00000173376	NDNF	
ENSG00000173566	NUDT18	
ENSG00000173727	AP000769.1	
ENSG00000173890	GPR160	
ENSG00000175414	ARL10	
ENSG00000175874	CREG2	
ENSG00000175938	ORAI3	
ENSG00000176171	BNIP3	1, 2, 3, 6
ENSG00000176383	B3GNT4	6
ENSG00000176428	VPS37D	
ENSG00000177181	RIMKLA	
ENSG00000177453	NIM1K	
ENSG00000177606	JUN	2, 3, 6
ENSG00000178802	MPI	2, 4
ENSG00000179148	ALOXE3	4
ENSG00000179344	HLA-DQB1	
ENSG00000179403	VWA1	
ENSG00000180448	HMHA1	
ENSG00000180815	MAP3K15	
ENSG00000181350	FAM211A	
ENSG00000181458	TMEM45A	4

ENSG00000181577	C6orf223	
ENSG00000181652	ATG9B	
ENSG00000182580	EPHB3	
ENSG00000182896	TMEM95	
ENSG00000183111	ARHGEF37	
ENSG00000183775	KCTD16	
ENSG00000184441	AP001062.7	
ENSG00000184731	FAM110C	4
ENSG00000185022	MAFF	2, 3
ENSG00000185100	ADSSL1	
ENSG00000186314	PRELID2	
ENSG00000186352	ANKRD37	1, 4, 5
ENSG00000186765	FSCN2	
ENSG00000186918	ZNF395	2, 4, 5
ENSG00000187479	C11orf96	
ENSG00000187642	C1orf170	
ENSG00000187667	WHAMMP3	
ENSG00000188820	FAM26F	
ENSG00000196968	FUT11	5, 6
ENSG00000197358	BNIP3P1	
ENSG00000197557	TTC30A	
ENSG00000197635	DPP4	
ENSG00000197930	ERO1L	2, 5, 6
ENSG00000199038	MIR210	
ENSG00000203780	FANK1	
ENSG00000204128	C2orf72	
ENSG00000205129	C4orf47	
ENSG00000212864	RNF208	
ENSG00000213290	PGK1P2	
ENSG00000213700	RPL17P50	
ENSG00000213859	KCTD11	5
ENSG00000214110	LDHAP4	
ENSG00000214193	SH3D21	
ENSG00000214274	ANG	3
ENSG00000216285	RP11-490H24.5	
ENSG00000219607	PPP1R3G	
ENSG00000223573	TINCR	
ENSG00000225205	AC093818.1	
ENSG00000226415	TPI1P1	
ENSG00000226510	UPK1A-AS1	
ENSG00000227036	LINC00511	
ENSG00000227533	SLC2A1-AS1	
ENSG00000228288	PCAT6	
ENSG00000228328	RP11-516A11.1	
ENSG00000228451	SDAD1P1	
ENSG00000230432	AC114803.3	
ENSG00000230479	AP000695.6	
ENSG00000230581	RP11-390F4.8	
ENSG00000231881	RP5-1120P11.3	
ENSG00000231890	AC093391.2	
ENSG00000232788	AC078883.3	
ENSG00000233818	AP000695.4	
ENSG00000235601	RP11-231K24.2	
ENSG00000235847	LDHAP7	
ENSG00000236064	RP6-191P20.4	
ENSG00000236090	LDHAP3	
ENSG00000237330	RNF223	

ENSG00000237686	RP5-1120P11.1
ENSG00000240032	RP11-274H2.3
ENSG00000241129	RPL22P19
ENSG00000242114	MTFP1
ENSG00000247095	MIR210HG
ENSG00000251259	AC004069.2
ENSG00000251359	WWC2-AS2
ENSG00000253882	RP11-61L23.2
ENSG00000254414	RP11-182J1.1
ENSG00000254554	RP11-351I24.1
ENSG00000255966	RP5-940J5.3
ENSG00000256006	AC084117.3
ENSG00000257913	RP11-386G11.5
ENSG00000260822	GS1-358P8.4
ENSG00000260919	CTD-3154N5.1
ENSG00000261051	RP11-274H2.5
ENSG00000263535	AK4P1
ENSG00000263893	CTD-3010D24.3
ENSG00000266677	RP11-258F1.1
ENSG00000267424	CTD-2265O21.3
ENSG00000267964	AC022400.2
ENSG00000267976	AP000695.1
ENSG00000268485	AC104841.2
ENSG00000268603	RP11-316O14.1
ENSG00000268852	AC132872.2
ENSG00000268856	AP001579.1
ENSG00000269968	RP5-940J5.9
ENSG00000272114	RP1-261G23.7
ENSG00000272870	RP11-798M19.6

Table 9.4 – List of 100 HIF targets. Data adapted from (84)

Ensembl gene ID	Gene name
ENSG00000074800	ENO1
ENSG00000130635	COL5A1
ENSG00000163235	TGFA
ENSG00000104812	GYS1
ENSG00000117984	CTSD
ENSG00000164442	CITED2
ENSG00000105976	MET
ENSG00000141682	PMAIP1
ENSG00000178467	P4HTM
ENSG00000149925	ALDOA
ENSG00000011422	PLAUR
ENSG00000102144	PGK1
ENSG00000140564	FURIN
ENSG00000146678	IGFBP1
ENSG00000197461	PDGFA
ENSG00000156515	HK1
ENSG00000173077	DEC1
ENSG00000211445	GPX3
ENSG00000121966	CXCR4
ENSG00000026025	VIM
ENSG00000104765	BNIP3L
ENSG00000115548	KDM3A
ENSG00000167600	CYP2S1
ENSG00000164867	NOS3
ENSG00000130427	EPO
ENSG00000002586	CD99
ENSG00000169764	UGP2
ENSG00000118523	CTGF
ENSG00000135318	NT5E
ENSG00000105220	GPI
ENSG00000047457	CP
ENSG00000107562	CXCL12
ENSG00000066926	FECH
ENSG00000146674	IGFBP3
ENSG00000119950	MXI1
ENSG00000186847	KRT14
ENSG00000198959	TGM2
ENSG00000078401	EDN1
ENSG00000007171	NOS2
ENSG00000143384	MCL1
ENSG00000085563	ABCB1
ENSG00000112715	VEGFA
ENSG00000111669	TPI1
ENSG00000118777	ABCG2
ENSG00000135766	EGLN1
ENSG00000087245	MMP2
ENSG00000170214	ADRA1B
ENSG00000134333	LDHA
ENSG00000124762	CDKN1A
ENSG00000117394	SLC2A1
ENSG00000141959	PFKL
ENSG00000115457	IGFBP2
ENSG00000100292	HMOX1

ENSG00000067225	PKM
ENSG00000159399	HK2
ENSG00000160255	ITGB2
ENSG00000115738	ID2
ENSG00000176171	BNIP3
ENSG00000106991	ENG
ENSG00000143125	PROK1
ENSG00000127663	KDM4B
ENSG00000113083	LOX
ENSG00000174697	LEP
ENSG00000138764	CCNG2
ENSG00000147853	AK3
ENSG00000181163	NPM1
ENSG00000148926	ADM
ENSG00000167771	RCOR2
ENSG00000123384	LRP1
ENSG00000157227	MMP14
ENSG00000091513	TF
ENSG00000129521	EGLN3
ENSG00000170525	PFKFB3
ENSG00000115414	FN1
ENSG00000114113	RBP2
ENSG00000160180	TFF3
ENSG00000111640	GAPDH
ENSG00000152256	PDK1
ENSG00000167244	IGF2
ENSG00000168209	DDIT4
ENSG00000111057	KRT18
ENSG00000107077	KDM4C
ENSG00000107159	CA9
ENSG00000011485	PPP5C
ENSG00000134954	ETS1
ENSG00000123358	NR4A1
ENSG00000164362	TERT
ENSG00000072274	TFRC
ENSG00000166598	HSP90B1
ENSG00000171345	KRT19
ENSG00000119699	TGFB3
ENSG00000106366	SERPINE1
ENSG00000186352	ANKRD37
LRG_343	TERT
LRG_365	HK1
LRG_399	TGFB3
LRG_458	NPM1
LRG_51	CXCR4
LRG_662	MET
LRG_76	ITGB2

Table 9.5 – List of 259 genes upregulated in hypoxia in 16 cell lines. Data was provided by Prof. Luis del Peso Ovalle, Madrid, Spain, after meta-analysis of hypoxia-treated gene profiling datasets across 19 experiments and 16 cell lines (85).

Ensembl gene ID	Gene name
ENSG00000115657	ABCB6
ENSG00000107897	ACBD5
ENSG00000075624	ACTB
ENSG00000148700	ADD3
ENSG00000148926	ADM
ENSG00000101745	ANKRD12
ENSG00000166825	ANPEP
ENSG00000177879	AP3S1
ENSG00000102606	ARHGEF7
ENSG00000163466	ARPC2
ENSG00000138303	ASCC1
ENSG00000115966	ATF2
ENSG00000162772	ATF3
ENSG00000128272	ATF4
ENSG00000145782	ATG12
ENSG00000088812	ATRN
ENSG00000119986	AVPI1
ENSG00000174483	BBS1
ENSG00000103507	BCKDK
ENSG00000183337	BCOR
ENSG00000176171	BNIP3
ENSG00000104765	BNIP3L
ENSG00000133639	BTG1
ENSG00000074410	CA12
ENSG00000167535	CACNB3
ENSG00000153048	CARHSP1
ENSG00000138764	CCNG2
ENSG00000118816	CCNI
ENSG00000163660	CCNL1
ENSG00000026508	CD44
ENSG00000117335	CD46
ENSG00000002586	CD99
ENSG00000111276	CDKN1B
ENSG00000135837	CEP350
ENSG00000166037	CEP57
ENSG00000173575	CHD2
ENSG00000131873	CHSY1
ENSG00000013441	CLK1
ENSG00000179335	CLK3
ENSG00000113240	CLK4
ENSG00000155508	CNOT8
ENSG00000113712	CSNK1A1
ENSG00000175183	CSRP2
ENSG00000137770	CTDSPL2
ENSG00000158290	CUL4B
ENSG00000121966	CXCR4
ENSG00000035664	DAPK2
ENSG00000115866	DARS
ENSG00000134574	DDB2
ENSG00000168209	DDIT4
ENSG00000204580	DDR1

ENSG00000128590	DNAJB9
ENSG00000136770	DNAJC1
ENSG00000101152	DNAJC5
ENSG00000120129	DUSP1
ENSG00000135766	EGLN1
ENSG00000129521	EGLN3
ENSG00000063046	EIF4B
ENSG00000074800	ENO1
ENSG00000111674	ENO2
ENSG00000197930	ERO1L
ENSG00000128923	FAM63B
ENSG00000037637	FBXO42
ENSG00000079459	FDFT1
ENSG00000145780	FEM1C
ENSG00000111790	FGFR1OP2
ENSG00000115414	FN1
ENSG00000187239	FNBP1
ENSG00000217128	FNIP1
ENSG00000118689	FOXO3
ENSG00000114416	FXR1
ENSG00000033327	GAB2
ENSG00000139112	GABARAPL1
ENSG00000099860	GADD45B
ENSG00000111640	GAPDH
ENSG00000114480	GBE1
ENSG00000090863	GLG1
ENSG00000066455	GOLGA5
ENSG00000175265	GOLGA8A
ENSG00000104812	GYS1
ENSG00000105856	HBP1
ENSG00000184678	HIST2H2BE
ENSG00000010818	HIVEP2
ENSG00000156515	HK1
ENSG00000206503	HLA-A
ENSG00000234745	HLA-B
ENSG00000204592	HLA-E
ENSG00000204632	HLA-G
ENSG00000112972	HMGCS1
ENSG00000153936	HS2ST1
ENSG00000166598	HSP90B1
ENSG00000182054	IDH2
ENSG00000010404	IDS
ENSG00000241489	IDS
ENSG00000137331	IER3
ENSG00000115461	IGFBP5
ENSG00000196083	IL1RAP
ENSG00000134460	IL2RA
ENSG00000153487	ING1
ENSG00000168556	ING2
ENSG00000186480	INSIG1
ENSG00000125629	INSIG2
ENSG00000140575	IQGAP1
ENSG00000185950	IRS2
ENSG00000172183	ISG20
ENSG00000150093	ITGB1
ENSG00000136156	ITM2B
ENSG00000177606	JUN

ENSG00000171223	JUNB
ENSG00000130522	JUND
ENSG00000144320	KIAA1715
ENSG00000116685	KIAA2013
ENSG00000155090	KLF10
ENSG00000067082	KLF6
ENSG00000118263	KLF7
ENSG00000114796	KLHL24
ENSG00000134333	LDHA
ENSG00000100097	LGALS1
ENSG00000116977	LGALS8
ENSG00000074695	LMAN1
ENSG00000168216	LMBRD1
ENSG00000113083	LOX
ENSG00000185022	MAFF
ENSG00000140941	MAP1LC3B
ENSG00000047849	MAP4
ENSG00000166987	MBD6
ENSG00000068305	MEF2A
ENSG00000198408	MGEA5
ENSG00000240972	MIF
ENSG00000133606	MKRN1
ENSG00000119684	MLH3
ENSG00000123562	MORF4L2
ENSG00000178802	MPI
ENSG00000100330	MTMR3
ENSG00000146085	MUT
ENSG00000119950	MXI1
ENSG00000104419	NDRG1
ENSG00000165030	NFIL3
ENSG00000151092	NGLY1
ENSG00000113580	NR3C1
ENSG00000119508	NR4A3
ENSG00000139496	NUPL1
ENSG00000046651	OFD1
ENSG00000135506	OS9
ENSG00000164830	OXR1
ENSG00000172939	OXSR1
ENSG00000122884	P4HA1
ENSG00000072682	P4HA2
ENSG00000145730	PAM
ENSG00000138617	PARP16
ENSG00000180628	PCGF5
ENSG00000163710	PCOLCE2
ENSG00000152256	PDK1
ENSG00000067992	PDK3
ENSG00000170525	PFKFB3
ENSG00000114268	PFKFB4
ENSG00000141959	PFKL
ENSG00000067057	PFKP
ENSG00000102144	PGK1
ENSG00000135365	PHF21A
ENSG00000118482	PHF3
ENSG00000165195	PIGA
ENSG00000102096	PIM2
ENSG00000107679	PLEKHA1
ENSG00000169499	PLEKHA2

ENSG00000083444	PLOD1
ENSG00000152952	PLOD2
ENSG00000146278	PNRC1
ENSG00000214517	PPME1
ENSG00000120910	PPP3CC
ENSG00000156011	PSD3
ENSG00000095303	PTGS1
ENSG00000142949	PTPRF
ENSG00000153233	PTPRR
ENSG00000183255	PTTG1IP
ENSG00000135631	RAB11FIP5
ENSG00000139832	RAB20
ENSG00000181467	RAP2B
ENSG00000158987	RAPGEF6
ENSG00000099849	RASSF7
ENSG00000089902	RCOR1
ENSG00000164327	RICTOR
ENSG00000101782	RIOK3
ENSG00000101654	RNMT
ENSG00000069667	RORA
ENSG00000116251	RPL22
ENSG00000162244	RPL29
ENSG00000089157	RPLP0
ENSG00000231500	RPS18
ENSG00000137154	RPS6
ENSG00000170889	RPS9
ENSG00000025039	RRAGD
ENSG00000081019	RSBN1
ENSG00000115310	RTN4
ENSG00000163602	RYBP
ENSG00000164105	SAP30
ENSG00000151748	SAV1
ENSG00000085365	SCAMP1
ENSG00000099194	SCD
ENSG00000137575	SDCBP
ENSG00000132432	SEC61G
ENSG00000111897	SERINC1
ENSG00000132824	SERINC3
ENSG00000106366	SERPINE1
ENSG00000179833	SERTAD2
ENSG00000115524	SF3B1
ENSG00000107819	SFXN3
ENSG00000097033	SH3GLB1
ENSG00000114120	SLC25A36
ENSG00000147454	SLC25A37
ENSG00000117394	SLC2A1
ENSG00000059804	SLC2A3
ENSG00000127526	SLC35E1
ENSG00000131389	SLC6A6
ENSG00000130821	SLC6A8
ENSG00000101665	SMAD7
ENSG00000102172	SMS
ENSG00000101972	STAG2
ENSG00000164211	STARD4
ENSG00000159167	STC1
ENSG00000113739	STC2
ENSG00000117614	SYF2

ENSG00000054611	TBC1D22A
ENSG00000163659	TIPARP
ENSG00000133872	TMEM66
ENSG00000116857	TMEM9
ENSG00000144747	TMF1
ENSG00000145901	TNIP1
ENSG00000105048	TNNT1
ENSG00000076554	TPD52
ENSG00000198467	TPM2
ENSG00000144935	TRPC1
ENSG00000157514	TSC22D3
ENSG00000182670	TTC3
ENSG00000143367	TUFT1
ENSG00000150991	UBC
ENSG00000148154	UGCG
ENSG00000169764	UGP2
ENSG00000213585	VDAC1
ENSG00000112715	VEGFA
ENSG00000026025	VIM
ENSG00000167397	VKORC1
ENSG00000132970	WASF3
ENSG00000163872	YEATS2
ENSG00000119801	YPEL5
ENSG00000170949	ZNF160
ENSG00000188994	ZNF292
ENSG00000186918	ZNF395
	AK3L1
	CCDC52
	CDC2L6
	FAM62B
	KIAA1128
	MTP18
	PKM2
	PLDN
	RP11-529I10.4
	SC4MOL

Table 9.6 – List of 1141 genes upregulated in hypoxia in HeLa cells. Data provided by Prof. Luis del Peso Ovalle, Madrid, Spain. Authors re-analysed microarray data taken from (238) and re-analysis was described in (85).

Ensembl gene ID	Gene name	Ensembl gene ID	Gene name
ENSG00000139193	CD27	ENSG00000176809	LRRC37A3
ENSG00000171060	C8orf74	ENSG00000165029	ABCA1
ENSG00000170262	MRAP	ENSG00000147613	PSKH2
ENSG00000159788	RGS12	ENSG00000068366	ACSL4
ENSG00000278468	MUC4	ENSG00000163636	PSMD6
ENSG00000133703	KRAS	ENSG00000158825	CDA
ENSG00000231479	SLC44A4	ENSG00000095303	PTGS1
ENSG00000141639	MAPK4	ENSG00000173612	GPRC6A
ENSG00000170264	FAM161A	ENSG00000243902	ELFN2
ENSG00000248874	C5orf17	ENSG00000166897	ELFN2
ENSG00000197776	KLHDC1	ENSG00000113070	HBEGF
ENSG00000100612	DHRS7	ENSG00000147655	RSPO2
ENSG00000118454	ANKRD13C	ENSG00000174944	P2RY14
ENSG00000177606	JUN	ENSG00000156976	EIF4A2
ENSG00000196839	ADA	ENSG00000242852	ZNF709
ENSG00000131791	PRKAB2	ENSG00000178573	MAF
ENSG00000273587	SNORA78	ENSG00000149948	HMGA2
ENSG00000227720	PPP1R11	ENSG00000182168	UNC5C
ENSG00000164266	SPINK1	ENSG00000242247	ARFGAP3
ENSG00000145012	LPP	ENSG00000070495	JMJD6
ENSG00000277209	RPPH1	ENSG00000234058	PPP1R11
ENSG00000234444	ZNF736	ENSG00000046889	PREX2
ENSG00000279386	GAFA3	ENSG00000115828	QPCT
ENSG00000145692	BHMT	ENSG00000134046	MBD2
ENSG00000117139	KDM5B	ENSG00000182752	PAPPA
ENSG00000273608	SRCIN1	ENSG00000173852	DPY19L1
ENSG00000225091	SNORA71A	ENSG00000182866	LCK
ENSG00000200959	SNORA74A	ENSG00000173480	ZNF417
ENSG00000109046	WSB1	ENSG00000197928	ZNF677
ENSG00000273562	NAP1L4	ENSG00000182827	ACBD3
ENSG00000145623	OSMR	ENSG00000188641	DPYD
ENSG00000110203	FOLR3	ENSG00000136603	SKIL
ENSG00000005381	MPO	ENSG00000166046	TCP11L2
ENSG00000167978	SRRM2	ENSG00000006607	FARP2
ENSG00000275099	GGNBP2	ENSG00000186818	LILRB4
ENSG00000075151	EIF4G3	ENSG00000181374	CCL13
ENSG00000213654	GPSM3	ENSG00000230128	IER3
ENSG00000117595	IRF6	ENSG00000150627	WDR17
ENSG00000170688	OR5E1P	ENSG00000159023	EPB41
ENSG00000215301	DDX3X	ENSG00000011600	TYROBP
ENSG00000154556	SORBS2	ENSG00000180219	FAM71C
ENSG00000205592	MUC19	ENSG00000136868	SLC31A1
ENSG00000162999	DUSP19	ENSG00000275498	PDXDC1
ENSG00000164418	GRIK2	ENSG00000196267	ZNF836
ENSG00000124508	BTN2A2	ENSG00000128739	SNRPN
ENSG00000196826	ZNF709	ENSG00000173482	PTPRM
ENSG00000112365	ZBTB24	ENSG00000147130	ZMYM3
ENSG00000276709	PDXDC1	ENSG00000169314	C22orf15
ENSG00000183303	OR5P2	ENSG00000117036	ETV3
ENSG00000151164	RAD9B	ENSG00000058335	RASGRF1

ENSG00000110841	PPFIBP1	ENSG00000149557	FEZ1
ENSG00000115970	THADA	ENSG00000198851	CD3E
ENSG00000149084	HSD17B12	ENSG00000273822	MUC4
ENSG00000259581	TYRO3P	ENSG00000138641	HERC3
ENSG00000172367	PDZD3	ENSG00000189376	C8orf76
ENSG00000166896	XRCC6BP1	ENSG00000163867	ZMYM6
ENSG00000155754	ALS2CR11	ENSG00000142515	KLK3
ENSG00000197261	C6orf141	ENSG00000183814	LIN9
ENSG00000179094	PER1	ENSG00000138767	CNOT6L
ENSG00000169442	CD52	ENSG00000128590	DNAJB9
ENSG00000179242	CDH4	ENSG00000077279	DCX
ENSG00000119138	KLF9	ENSG00000127074	RGS13
ENSG00000277956	MAPT	ENSG00000186529	CYP4F3
ENSG00000186231	KLHL32	ENSG00000105426	PTPRS
ENSG00000141543	EIF4A3	ENSG00000122644	ARL4A
ENSG00000164751	PEX2	ENSG00000227231	IER3
ENSG00000143768	LEFTY2	ENSG00000205358	MT1H
ENSG00000229972	IQCF3	ENSG00000144130	NT5DC4
ENSG00000260873	SNTB2	ENSG00000156273	BACH1
ENSG00000064989	CALCRL	ENSG00000160584	SIK3
ENSG00000115966	ATF2	ENSG00000080822	CLDND1
ENSG00000132703	APCS	ENSG00000070614	NDST1
ENSG00000138495	COX17	ENSG00000248098	BCKDHA
ENSG00000196569	LAMA2	ENSG00000145819	ARHGAP26
ENSG00000060237	WNK1	ENSG00000197548	ATG7
ENSG00000151746	BICD1	ENSG00000203879	GDI1
ENSG00000184619	KRBA2	ENSG00000162714	ZNF496
ENSG00000148795	CYP17A1	ENSG00000091656	ZFHX4
ENSG00000096088	PGC	ENSG00000081277	PKP1
ENSG00000136250	AOAH	ENSG00000014914	MTMR11
ENSG00000121741	ZMYM2	ENSG00000170122	FOXD4
ENSG00000116685	KIAA2013	ENSG00000150540	HNMT
ENSG00000136872	ALDOB	ENSG00000102144	PGK1
ENSG00000162735	PEX19	ENSG00000145191	EIF2B5
ENSG00000187210	GCNT1	ENSG00000137975	CLCA2
ENSG00000143839	REN	ENSG00000146809	ASB15
ENSG00000237155	IER3	ENSG00000206372	C2
ENSG00000166171	DPCD	ENSG00000196131	VN1R2
ENSG00000174177	CTU2	ENSG00000175582	RAB6A
ENSG00000113739	STC2	ENSG00000111728	ST8SIA1
ENSG00000215595	C20orf202	ENSG00000128881	TTBK2
ENSG00000165383	LRRC18	ENSG00000142512	SIGLEC10
ENSG00000179195	ZNF664	ENSG00000162571	TTLL10
ENSG00000179889	PDXDC1	ENSG00000186001	LRCH3
ENSG00000179869	ABCA13	ENSG00000179774	ATOH7
ENSG00000233490	GPSM3	ENSG00000235336	SLC44A4
ENSG00000233931	TRIM40	ENSG00000164142	FAM160A1
ENSG00000102172	SMS	ENSG00000277585	MUC4
ENSG00000141977	CIB3	ENSG00000169967	MAP3K2
ENSG00000090020	SLC9A1	ENSG00000156515	HK1
ENSG00000198844	ARHGEF15	ENSG00000163913	IFT122
ENSG00000170683	OR10A3	ENSG00000136235	GPNMB
ENSG00000144724	PTPRG	ENSG00000255794	RMST
ENSG00000149633	KIAA1755	ENSG00000178974	FBXO34
ENSG00000175262	C1orf127	ENSG00000065923	SLC9A7
ENSG00000140521	POLG	ENSG00000163660	CCNL1
ENSG00000169398	PTK2	ENSG00000128645	HOXD1

ENSG00000144824	PHLDB2	ENSG00000106089	STX1A
ENSG00000155816	FMN2	ENSG00000176731	C8orf59
ENSG00000278555	LILRB4	ENSG00000237621	OR9A1P
ENSG00000114316	USP4	ENSG00000163349	HIPK1
ENSG00000104419	NDRG1	ENSG00000013503	POLR3B
ENSG00000134668	SPOCD1	ENSG00000147894	C9orf72
ENSG00000011405	PIK3C2A	ENSG00000018625	ATP1A2
ENSG00000158427	TMSB15B	ENSG00000136750	GAD2
ENSG00000006530	AGK	ENSG00000231543	C2
ENSG00000198898	CAPZA2	ENSG00000111011	RSRC2
ENSG00000127603	MACF1	ENSG00000169764	UGP2
ENSG00000087074	PPP1R15A	ENSG00000116874	WARS2
ENSG00000186094	AGBL4	ENSG00000047315	POLR2B
ENSG00000160226	C21orf2	ENSG00000113532	ST8SIA4
ENSG00000206501	PPP1R11	ENSG00000143257	NR1I3
ENSG00000169495	HTRA4	ENSG00000215580	BCORP1
ENSG00000099942	CRKL	ENSG00000198839	ZNF277
ENSG00000081181	ARG2	ENSG00000171487	NLRP5
ENSG00000163749	CCDC158	ENSG00000092200	RPGRIP1
ENSG00000183696	UPP1	ENSG00000206314	GPSM3
ENSG00000128683	GAD1	ENSG00000142409	ZNF787
ENSG00000064012	CASP8	ENSG00000034239	EFCAB1
ENSG00000100084	HIRA	ENSG00000169035	KLK7
ENSG00000198650	TAT	ENSG00000137868	STRA6
ENSG00000185477	GPRIN3	ENSG00000162761	LMX1A
ENSG00000105737	GRIK5	ENSG00000235017	C2
ENSG00000126785	RHOJ	ENSG00000136160	EDNRB
ENSG00000112293	GPLD1	ENSG00000047457	CP
ENSG00000109061	MYH1	ENSG00000153774	CFDP1
ENSG00000168615	ADAM9	ENSG00000132530	XAF1
ENSG00000125144	MT1G	ENSG00000203668	CHML
ENSG00000184647	PRSS55	ENSG00000104953	TLE6
ENSG00000205856	C22orf42	ENSG00000157152	SYN2
ENSG00000129595	EPB41L4A	ENSG00000164123	C4orf45
ENSG00000142621	FHAD1	ENSG00000120029	C10orf76
ENSG00000110436	SLC1A2	ENSG00000229252	HLA-E
ENSG00000278828	HIST1H3H	ENSG00000196071	OR2L13
ENSG00000160588	MPZL3	ENSG00000224227	OR2L1P
ENSG00000119688	ABCD4	ENSG00000281530	DGCR12
ENSG00000139436	GIT2	ENSG00000136381	IREB2
ENSG00000280641	CDH4	ENSG00000171180	OR2M4
ENSG00000153094	BCL2L11	ENSG00000179059	ZFP42
ENSG00000224196	OR5AK4P	ENSG00000262327	AGK
ENSG00000196932	TMEM26	ENSG00000006128	TAC1
ENSG00000125414	MYH2	ENSG00000127578	WFIKKN1
ENSG00000159348	CYB5R1	ENSG00000152952	PLOD2
ENSG00000075239	ACAT1	ENSG00000154277	UCHL1
ENSG00000188559	RALGAPA2	ENSG00000186350	RXRA
ENSG00000079841	RIMS1	ENSG00000183023	SLC8A1
ENSG00000105649	RAB3A	ENSG00000168806	LCMT2
ENSG00000079263	SP140	ENSG00000273953	OR10A3
ENSG00000118263	KLF7	ENSG00000114127	XRN1
ENSG00000165704	HPRT1	ENSG00000184012	TMPRSS2
ENSG00000144668	ITGA9	ENSG00000103966	EHD4
ENSG00000137331	IER3	ENSG00000160401	C9orf117
ENSG00000154316	TDH	ENSG00000100433	KCNK10
ENSG00000026025	VIM	ENSG00000164291	ARSK

ENSG00000112941	PAPD7	ENSG00000228001	TRIM40
ENSG00000102796	DHRS12	ENSG00000259905	PWRN1
ENSG00000253313	C1orf210	ENSG00000225201	HLA-E
ENSG00000152760	TCTEX1D1	ENSG00000010404	IDS
ENSG00000100490	CDKL1	ENSG00000104343	UBE2W
ENSG00000184203	PPP1R2	ENSG00000180777	ANKRD30B
ENSG00000228567	VN1R4	ENSG00000072682	P4HA2
ENSG00000067992	PDK3	ENSG00000183255	PTTG1IP
ENSG00000130066	SAT1	ENSG00000114480	GBE1
ENSG00000213203	GIMAP1	ENSG00000237403	PPP1R11
ENSG00000280497	OR5E1P	ENSG00000185013	NT5C1B
ENSG00000278466	MUC2	ENSG00000276429	PLCH2
ENSG00000133138	TBC1D8B	ENSG00000131778	CHD1L
ENSG00000116748	AMPD1	ENSG00000269226	TMSB15B
ENSG00000156076	WIF1	ENSG00000165030	NFIL3
ENSG00000118689	FOXO3	ENSG00000174473	GALNTL6
ENSG00000078142	PIK3C3	ENSG00000152684	PELO
ENSG00000039068	CDH1	ENSG00000170310	STX8
ENSG00000239305	RNF103	ENSG00000130414	NDUFA10
ENSG00000106511	MEOX2	ENSG00000168421	RHOH
ENSG00000120693	SMAD9	ENSG00000116151	MORN1
ENSG00000118046	STK11	ENSG00000078043	PIAS2
ENSG00000136488	CSH1	ENSG00000159167	STC1
ENSG00000241697	TMEFF1	ENSG00000141279	NPEPPS
ENSG00000186868	MAPT	ENSG00000135253	KCP
ENSG00000161638	ITGA5	ENSG00000153707	PTPRD
ENSG00000078304	PPP2R5C	ENSG00000172890	NADSYN1
ENSG00000146143	PRIM2	ENSG00000186952	TMEM232
ENSG00000133835	HSD17B4	ENSG00000119950	MXI1
ENSG00000171044	XKR6	ENSG00000059804	SLC2A3
ENSG00000164761	TNFRSF11B	ENSG00000120738	EGR1
ENSG00000119771	KLHL29	ENSG00000130592	LSP1
ENSG00000166747	AP1G1	ENSG00000177842	ZNF620
ENSG00000144285	SCN1A	ENSG00000013588	GPRC5A
ENSG00000107518	ATRNL1	ENSG00000185070	FLRT2
ENSG00000103275	UBE2I	ENSG00000049167	ERCC8
ENSG00000213901	SLC23A3	ENSG00000112964	GHR
ENSG00000078114	NEBL	ENSG00000198908	BHLHB9
ENSG00000075539	FRYL	ENSG00000129226	CD68
ENSG00000232641	MOG	ENSG00000111674	ENO2
ENSG00000147753	TTTY7	ENSG00000243335	KCTD7
ENSG00000082126	MPP4	ENSG00000006740	ARHGAP44
ENSG00000164287	CDC20B	ENSG00000145794	MEGF10
ENSG00000166278	C2	ENSG00000116717	GADD45A
ENSG00000134757	DSG3	ENSG00000121064	SCPEP1
ENSG00000152348	ATG10	ENSG00000172243	CLEC7A
ENSG00000229077	SLC44A4	ENSG00000117394	SLC2A1
ENSG00000164161	HHIP	ENSG00000163602	RYBP
ENSG00000168386	FILIP1L	ENSG00000179335	CLK3
ENSG00000170788	DYDC1	ENSG00000172578	KLHL6
ENSG00000018408	WWTR1	ENSG00000115457	IGFBP2
ENSG00000145321	GC	ENSG00000214274	ANG
ENSG00000044524	EPHA3	ENSG00000100292	HMOX1
ENSG00000127831	VIL1	ENSG00000147571	CRH
ENSG00000143384	MCL1	ENSG00000108239	TBC1D12
ENSG00000153933	DGKE	ENSG00000060069	CTDP1
ENSG00000134452	FBXO18	ENSG00000258818	RNASE4

ENSG00000203837	PNLIPRP3	ENSG00000162105	SHANK2
ENSG00000169403	PTAFR	ENSG00000155093	PTPRN2
ENSG00000277363	SRCIN1	ENSG00000146926	ASB10
ENSG00000184678	HIST2H2BE	ENSG00000203463	SLC44A4
ENSG00000082153	BZW1	ENSG00000166183	ASPG
ENSG00000197343	ZNF655	ENSG00000276042	LILRB4
ENSG00000173575	CHD2	ENSG00000241489	IDS
ENSG00000188277	C15orf62	ENSG00000171759	PAH
ENSG00000124151	NCOA3	ENSG00000206478	IER3
ENSG00000175315	CST6	ENSG00000265241	RBM8A
ENSG00000186452	TMPRSS12	ENSG00000186866	POFUT2
ENSG00000137968	SLC44A5	ENSG00000187987	ZSCAN23
ENSG00000105855	ITGB8	ENSG00000278311	GGNBP2
ENSG00000173258	ZNF483	ENSG00000173848	NET1
ENSG00000262145	XRCC6BP1	ENSG00000101236	RNF24
ENSG00000138670	RASGEF1B	ENSG00000171223	JUNB
ENSG00000178538	CA8	ENSG00000151729	SLC25A4
ENSG00000163661	PTX3	ENSG00000156873	PHKG2
ENSG00000204592	HLA-E	ENSG00000140538	NTRK3
ENSG00000183643	C15orf32	ENSG00000138722	MMRN1
ENSG00000110315	RNF141	ENSG00000159399	HK2
ENSG00000148357	HMCN2	ENSG00000176177	ENTHD1
ENSG00000179387	ELMOD2	ENSG00000150961	SEC24D
ENSG00000111880	RNGTT	ENSG00000117519	CNN3
ENSG00000230254	HLA-E	ENSG00000237046	TRIM40
ENSG00000198408	MGEA5	ENSG00000186051	TAL2
ENSG00000187193	MT1X	ENSG00000187144	SPATA21
ENSG00000221818	EBF2	ENSG00000149573	MPZL2
ENSG00000186260	MKL2	ENSG00000139496	NUPL1
ENSG00000150593	PDCD4	ENSG00000152578	GRIA4
ENSG00000115310	RTN4	ENSG00000175602	CCDC85B
ENSG00000103227	LMF1	ENSG00000115461	IGFBP5
ENSG00000147647	DPYS	ENSG00000121691	CAT
ENSG00000168918	INPP5D	ENSG00000187608	ISG15
ENSG00000147488	ST18	ENSG00000118245	TNP1
ENSG00000112576	CCND3	ENSG00000155876	RRAGA
ENSG00000137672	TRPC6	ENSG00000204161	C10orf128
ENSG00000102218	RP2	ENSG00000065609	SNAP91
ENSG00000113971	NPHP3	ENSG00000175592	FOSL1
ENSG00000075292	ZNF638	ENSG00000213231	TCL1B
ENSG00000112077	RHAG	ENSG00000152104	PTPN14
ENSG00000204381	LAYN	ENSG00000100368	CSF2RB
ENSG00000150275	PCDH15	ENSG00000169026	MFSD7
ENSG00000145850	TIMD4	ENSG00000176171	BNIP3
ENSG00000277276	OTUB2	ENSG00000163995	ABLIM2
ENSG00000185022	MAFF	ENSG00000168297	PXK
ENSG00000120519	SLC10A7	ENSG00000189152	GRAPL
ENSG00000171617	ENC1	ENSG00000140945	CDH13
ENSG00000166592	RRAD	ENSG00000080371	RAB21
ENSG00000186575	NF2	ENSG00000236399	TRIM40
ENSG00000142627	EPHA2	ENSG00000163406	SLC15A2
ENSG00000185920	PTCH1	ENSG00000040341	STAU2
ENSG00000002016	RAD52	ENSG00000134013	LOXL2
ENSG00000126581	BECN1	ENSG00000251493	FOXD1
ENSG00000142867	BCL10	ENSG00000160321	ZNF208
ENSG00000089199	CHGB	ENSG00000236561	MOG
ENSG00000157168	NRG1	ENSG00000138439	FAM117B

ENSG00000275730	LILRB4	ENSG00000100842	EFS
ENSG00000198125	MB	ENSG00000010610	CD4
ENSG00000089723	OTUB2	ENSG00000236560	PPP1R11
ENSG00000172575	RASGRP1	ENSG00000175445	LPL
ENSG00000048540	LMO3	ENSG00000041982	TNC
ENSG00000139793	MBNL2	ENSG00000169242	EFNA1
ENSG00000112299	VNN1	ENSG00000175155	YPEL2
ENSG00000113734	BNIP1	ENSG00000137857	DUOX1
ENSG00000235696	C2	ENSG00000160013	PTGIR
ENSG00000177694	NAALADL2	ENSG00000107819	SFXN3
ENSG00000281486	SNTG2	ENSG00000120254	MTHFD1L
ENSG00000138735	PDE5A	ENSG00000177570	SAMD12
ENSG00000140332	TLE3	ENSG00000138792	ENPEP
ENSG00000091317	CMTM6	ENSG00000126091	ST3GAL3
ENSG00000136169	SETDB2	ENSG00000214456	PLIN5
ENSG00000159958	TNFRSF13C	ENSG00000185915	KLHL34
ENSG00000145687	SSBP2	ENSG00000113083	LOX
ENSG00000162882	HAAO	ENSG00000164684	ZNF704
ENSG00000074695	LMAN1	ENSG00000080224	EPHA6
ENSG00000129535	NRL	ENSG00000112096	SOD2
ENSG00000124762	CDKN1A	ENSG00000072364	AFF4
ENSG00000135929	CYP27A1	ENSG00000138083	SIX3
ENSG00000224496	TRIM40	ENSG00000088926	F11
ENSG00000104714	ERICH1	ENSG00000178694	NSUN3
ENSG00000164483	SAMD3	ENSG00000163646	CLRN1
ENSG00000161649	CD300LG	ENSG00000217128	FNIP1
ENSG00000172236	TPSAB1	ENSG00000075420	FNDC3B
ENSG00000170423	KRT78	ENSG00000132681	ATP1A4
ENSG00000198133	TMEM229B	ENSG00000178243	C9orf62
ENSG00000170579	DLGAP1	ENSG00000206378	SLC44A4
ENSG00000121361	KCNJ8	ENSG00000183114	FAM43B
ENSG00000125810	CD93	ENSG00000185742	C11orf87
ENSG00000142484	TM4SF5	ENSG00000118407	FILIP1
ENSG00000153071	DAB2	ENSG00000204385	SLC44A4
ENSG00000179420	OR6W1P	ENSG00000101782	RIOK3
ENSG00000184194	GPR173	ENSG00000164304	CAGE1
ENSG00000147570	DNAJC5B	ENSG00000104371	DKK4
ENSG00000113448	PDE4D	ENSG00000123384	LRP1
ENSG00000175229	GAL3ST3	ENSG00000116675	DNAJC6
ENSG00000117500	TMED5	ENSG00000130164	LDLR
ENSG00000033178	UBA6	ENSG00000196104	SPOCK3
ENSG00000233314	PPP1R11	ENSG00000050438	SLC4A8
ENSG00000259001	RPPH1	ENSG00000177879	AP3S1
ENSG00000102096	PIM2	ENSG00000168447	SCNN1B
ENSG00000168243	GNG4	ENSG00000227458	TRIM40
ENSG00000138738	PRDM5	ENSG00000163141	BNIPL
ENSG00000181982	CCDC149	ENSG00000183963	SMTN
ENSG00000189195	BTBD8	ENSG00000156218	ADAMTSL3
ENSG00000161944	ASGR2	ENSG00000204614	TRIM40
ENSG00000104549	SQLE	ENSG00000134107	BHLHE40
ENSG00000123610	TNFAIP6	ENSG00000145782	ATG12
ENSG00000204655	MOG	ENSG00000111700	SLCO1B3
ENSG00000138764	CCNG2	ENSG00000176566	DCAF4L2
ENSG00000198574	SH2D1B	ENSG00000138642	HERC6
ENSG00000196177	ACADSB	ENSG00000237834	MOG
ENSG00000012504	NR1H4	ENSG00000197465	GYPE
ENSG00000198682	PAPSS2	ENSG00000174957	OR5J2

ENSG00000182035	ADIG	ENSG00000149527	PLCH2
ENSG00000143727	ACP1	ENSG00000135423	GLS2
ENSG00000116260	QSOX1	ENSG00000114098	ARMC8
ENSG00000122420	PTGFR	ENSG00000115808	STRN
ENSG00000184650	ODF4	ENSG00000137766	UNC13C
ENSG00000127377	CRYGN	ENSG00000163424	C3orf30
ENSG00000151229	SLC2A13	ENSG00000155380	SLC16A1
ENSG00000127481	UBR4	ENSG00000100934	SEC23A
ENSG00000146282	RARS2	ENSG00000169032	MAP2K1
ENSG00000153046	CDYL	ENSG00000141194	OR4D1
ENSG00000135740	SLC9A5	ENSG00000078596	ITM2A
ENSG00000184786	TCTE3	ENSG00000164385	C6orf195
ENSG00000140416	TPM1	ENSG00000121904	CSMD2
ENSG00000206493	HLA-E	ENSG00000267206	LCN6
ENSG00000155508	CNOT8	ENSG00000109103	UNC119
ENSG00000120149	MSX2	ENSG00000198453	ZNF568
ENSG00000234508	GPSM3	ENSG00000168032	ENTPD3
ENSG00000186340	THBS2	ENSG00000171133	OR2K2
ENSG00000125398	SOX9	ENSG00000104722	NEFM
ENSG00000137770	CTDSPL2	ENSG00000122335	SERAC1
ENSG00000125675	GRIA3	ENSG00000255713	OR4D2
ENSG00000198467	TPM2	ENSG00000164879	CA3
ENSG00000100285	NEFH	ENSG00000226560	C2
ENSG00000148926	ADM	ENSG00000102032	RENBP
ENSG00000076944	STXBP2	ENSG00000110218	PANX1
ENSG00000141985	SH3GL1	ENSG00000276613	MUC4
ENSG00000206190	ATP10A	ENSG00000155313	USP25
ENSG00000101311	FERMT1	ENSG00000143774	GUK1
ENSG00000169469	SPRR1B	ENSG00000237829	PPP1R11
ENSG00000162645	GBP2	ENSG00000114388	NPRL2
ENSG00000168556	ING2	ENSG00000099783	HNRNPM
ENSG00000162391	FAM151A	ENSG00000140479	PCSK6
ENSG00000139990	DCAF5	ENSG00000161594	KLHL10
ENSG00000173281	PPP1R3B	ENSG00000198961	PJA2
ENSG00000163492	CCDC141	ENSG00000142599	RERE
ENSG00000183347	GBP6	ENSG00000221866	PLXNA4
ENSG00000067798	NAV3	ENSG00000141519	CCDC40
ENSG00000160305	DIP2A	ENSG00000138395	CDK15
ENSG00000162772	ATF3	ENSG00000111335	OAS2
ENSG00000168807	SNTB2	ENSG00000156500	FAM122C
ENSG00000113712	CSNK1A1	ENSG00000173421	CCDC36
ENSG00000234623	MOG	ENSG00000138435	CHRNA1
ENSG00000155545	MIER3	ENSG00000182230	FAM153B
ENSG00000141314	RHBDL3	ENSG00000067066	SP100
ENSG00000168658	VWA3B	ENSG00000069966	GNB5
ENSG00000141469	SLC14A1	ENSG00000139973	SYT16
ENSG00000213639	PPP1CB	ENSG00000130270	ATP8B3
ENSG00000162928	PEX13	ENSG00000135365	PHF21A
ENSG00000070756	PABPC1	ENSG00000137345	MOG
ENSG00000241484	ARHGAP8	ENSG00000164691	TAGAP
ENSG00000004846	ABCB5	ENSG00000123500	COL10A1
ENSG00000197779	ZNF81	ENSG00000259207	ITGB3
ENSG00000084112	SSH1	ENSG00000103507	BCKDK
ENSG00000171843	MLLT3	ENSG00000033122	LRRC7
ENSG00000276644	DACH1	ENSG00000135924	DNAJB2
ENSG00000276025	OR5P2	ENSG00000107447	DNTT
ENSG00000130254	SAFB2	ENSG00000185043	CIB1

ENSG00000120708	TGFBI	ENSG00000133742	CA1
ENSG00000063854	HAGH	ENSG00000057663	ATG5
ENSG00000151692	RNF144A	ENSG00000170525	PFKFB3
ENSG00000137809	ITGA11	ENSG00000161542	PRPSAP1
ENSG00000095370	SH2D3C	ENSG00000109107	ALDOC
ENSG00000280055	TMEM75	ENSG00000163803	PLB1
ENSG00000237052	GPSM3	ENSG00000002587	HS3ST1
ENSG00000198788	MUC2	ENSG00000180008	SOCS4
ENSG00000010327	STAB1	ENSG00000154485	MMP21
ENSG00000221995	TIAF1	ENSG00000163131	CTSS
ENSG00000015171	ZMYND11	ENSG00000006576	PHTF2
ENSG00000089847	ANKRD24	ENSG00000176293	ZNF135
ENSG00000142233	NTN5	ENSG00000002079	MYH16
ENSG00000172594	SMPDL3A	ENSG00000204619	PPP1R11
ENSG00000176659	C20orf197	ENSG00000137962	ARHGAP29
ENSG00000115414	FN1	ENSG00000104888	SLC17A7
ENSG00000085274	MYNN	ENSG00000148848	ADAM12
ENSG00000102678	FGF9	ENSG00000273984	MUC4
ENSG00000197976	AKAP17A	ENSG00000152049	KCNE4
ENSG00000164124	TMEM144	ENSG00000273579	C22orf15
ENSG00000173545	ZNF622	ENSG00000144426	NBEAL1
ENSG00000100116	GCAT	ENSG00000011347	SYT7
ENSG00000177947	ODF3	ENSG00000221914	PPP2R2A
ENSG00000126217	MCF2L	ENSG00000174953	DHX36
ENSG00000137802	MAPKBP1	ENSG00000233904	HLA-E
ENSG00000198743	SLC5A3	ENSG00000152056	AP1S3
ENSG00000167995	BEST1	ENSG00000275368	TCTE3
ENSG00000155066	PROM2	ENSG00000068971	PPP2R5B
ENSG00000183826	BTBD9	ENSG00000243064	ABCC13
ENSG00000164327	RICTOR	ENSG00000077157	PPP1R12B
ENSG00000204120	GIGYF2	ENSG00000074410	CA12
ENSG00000165338	HECTD2	ENSG00000236697	GPSM3
ENSG00000180532	ZSCAN4	ENSG00000167797	CDK2AP2
ENSG00000204403	CASP12	ENSG00000281020	SNTG2
ENSG00000234096	MOG	ENSG00000176597	B3GNT5
ENSG00000115956	PLEK	ENSG00000228263	SLC44A4
ENSG00000151014	CCRN4L	ENSG00000143632	ACTA1
ENSG00000232180	SLC44A4	ENSG00000114315	HES1
ENSG00000145113	MUC4	ENSG00000162992	NEUROD1
ENSG00000131389	SLC6A6	ENSG00000113645	WWC1
ENSG00000177324	BEND2	ENSG00000168542	COL3A1
ENSG00000179133	C10orf67	ENSG00000076067	RBMS2
ENSG00000180336	C17orf104	ENSG00000184863	RBM33
ENSG00000130021	HDHD1	ENSG00000163879	DNALI1
ENSG00000122121	XPNPEP2	ENSG00000122641	INHBA
ENSG00000172554	SNTG2	ENSG00000185087	FAM169B
ENSG00000205277	MUC12	ENSG00000115232	ITGA4
ENSG00000100504	PYGL	ENSG00000009790	TRAF3IP3
ENSG00000115020	PIKFYVE	ENSG00000162852	CNST
ENSG00000077585	GPR137B	ENSG00000184292	TACSTD2
ENSG00000196876	SCN8A	ENSG00000150907	FOXO1
ENSG00000144218	AFF3	ENSG00000111676	ATN1
ENSG00000236632	HLA-E	ENSG00000055483	USP36
ENSG00000114857	NKTR	ENSG00000216937	CCDC7
ENSG00000280278	FLJ30679	ENSG00000100784	RPS6KA5
ENSG00000166819	PLIN1	ENSG00000162692	VCAM1
ENSG00000155304	HSPA13	ENSG00000113889	KNG1

ENSG00000136110	LECT1	ENSG00000076554	TPD52
ENSG00000168268	NT5DC2	ENSG00000278303	MUC4
ENSG00000152910	CNTNAP4	ENSG00000158113	LRRC43
ENSG00000180061	TMEM150B	ENSG00000175077	RTP1
ENSG00000170180	GYPA	ENSG00000007933	FMO3
ENSG00000230885	MOG	ENSG00000065135	GNAI3
ENSG00000085265	FCN1	ENSG00000155890	TRIM42
ENSG00000103316	CRYM	ENSG00000146192	FGD2
ENSG00000145016	KIAA0226	ENSG00000146592	CREB5
ENSG00000058063	ATP11B	ENSG00000275052	SMEK2
ENSG00000048828	FAM120A	ENSG00000161040	FBXL13
ENSG00000183117	CSMD1	ENSG00000150076	CCDC7
ENSG00000170743	SYT9	ENSG00000170417	TMEM182
ENSG00000163975	MFI2	ENSG00000135679	MDM2
ENSG00000114841	DNAH1	ENSG00000129990	SYT5
ENSG00000137825	ITPKA	ENSG00000159527	PGLYRP3
ENSG00000205531	NAP1L4	ENSG00000135801	TAF5L
ENSG00000110852	CLEC2B	ENSG00000052749	RRP12
ENSG00000147316	MCPH1	ENSG00000222047	C10orf55
ENSG00000120645	IQSEC3	ENSG00000187783	TMEM72
ENSG00000126216	TUBGCP3	ENSG00000048052	HDAC9
ENSG00000172179	PRL	ENSG00000163814	CDCP1
ENSG00000160471	COX6B2	ENSG00000196123	KIAA0895L
ENSG00000180043	FAM71E2	ENSG00000111790	FGFR1OP2
ENSG00000163081	CCDC140	ENSG00000185112	FAM43A
ENSG00000272602	ZNF595	ENSG00000127249	ATP13A4
ENSG00000181355	OFCC1	ENSG00000001084	GCLC
ENSG00000112655	PTK7	ENSG00000043462	LCP2
ENSG00000170166	HOXD4	ENSG00000115657	ABCB6
ENSG00000185684	EP400NL	ENSG00000173273	TNKS
ENSG00000128652	HOXD3	ENSG00000138036	DYNC2LI1
ENSG00000102984	ZNF821	ENSG00000092295	TGM1
ENSG00000239827	SUGT1P3	ENSG00000128563	PRKRIP1
ENSG00000103642	LACTB	ENSG00000113361	CDH6
ENSG00000130182	ZSCAN10	ENSG00000143514	TP53BP2
ENSG00000116117	PARD3B	ENSG00000138640	FAM13A
ENSG00000198155	ZNF876P	ENSG00000121594	CD80
ENSG00000133858	ZFC3H1	ENSG00000172995	ARPP21
ENSG00000164588	HCN1	ENSG00000164494	PDSS2
ENSG00000281763	DHX36	ENSG00000204364	C2
ENSG00000013725	CD6	ENSG00000124249	KCNK15
ENSG00000062038	CDH3	ENSG00000160678	S100A1
ENSG00000155097	ATP6V1C1	ENSG00000064205	WISP2
ENSG00000077420	APBB1IP	ENSG00000180263	FGD6
ENSG00000156413	FUT6	ENSG00000083444	PLOD1
ENSG00000119979	FAM45A	ENSG00000158473	CD1D
ENSG00000126391	FRMD8	ENSG00000184635	ZNF93
ENSG00000234243	GPSM3	ENSG00000160683	CXCR5
ENSG00000128585	MKLN1	ENSG00000161640	SIGLEC11
ENSG00000189144	ZNF573	ENSG00000148136	OR13C4
ENSG00000070019	GUCY2C	ENSG00000131477	RAMP2
ENSG00000089472	HEPH	ENSG00000166342	NETO1
ENSG00000140749	IGSF6	ENSG00000176641	RNF152
ENSG00000173221	GLRX	ENSG00000101443	WFDC2
ENSG00000196361	ELAVL3	ENSG00000197471	SPN
ENSG00000048707	VPS13D	ENSG00000264943	SH3GL1P2
ENSG00000147183	CPXCR1	ENSG00000186081	KRT5

ENSG00000147459	DOCK5	ENSG00000138777	PPA2
ENSG00000185942	NKAIN3	ENSG00000172183	ISG20
ENSG00000109684	CLNK	ENSG00000164934	DCAF13
ENSG00000221869	CEBPD	ENSG00000126218	F10
ENSG00000163961	RNF168	ENSG00000242441	GTF2A1L
ENSG00000166598	HSP90B1	ENSG00000165527	ARF6
ENSG00000131969	ABHD12B	ENSG00000128016	ZFP36
ENSG00000163568	AIM2	ENSG00000106366	SERPINE1
ENSG00000143520	FLG2	ENSG00000148175	STOM
ENSG00000122545	SEPT7	ENSG00000164591	MYOZ3
ENSG00000072041	SLC6A15	ENSG00000166507	NDST2
ENSG00000172524	TRIM40	ENSG00000136827	TOR1A
ENSG00000104332	SFRP1	ENSG00000278279	LILRB4
ENSG00000143226	FCGR2A	ENSG00000125910	S1PR4
ENSG00000114120	SLC25A36	ENSG00000276155	MAPT
ENSG00000071991	CDH19	ENSG00000049246	PER3
ENSG00000262607	IQSEC3	ENSG00000235030	IER3
ENSG00000173404	INSM1	ENSG00000103723	AP3B2
ENSG00000126457	PRMT1	ENSG00000056050	C4orf27
ENSG00000107798	LIPA	ENSG00000095777	MYO3A
ENSG00000155052	CNTNAP5	ENSG00000128242	GAL3ST1
ENSG00000124145	SDC4	ENSG00000164543	STK17A
ENSG00000114268	PFKFB4	ENSG00000281614	INPP5D
ENSG00000186480	INSIG1	ENSG00000281434	NDUFA10
ENSG00000156966	B3GNT7	ENSG00000281917	SLC16A1
ENSG00000077522	ACTN2	ENSG00000280931	OR5P2
ENSG00000127241	MASP1	ENSG00000281056	OR5E1P
ENSG00000026297	RNASET2	ENSG00000281680	OR10A3
ENSG00000140285	FGF7	LRG_16	ADA
ENSG00000075340	ADD2	LRG_165	STXBP2
ENSG00000101928	MOSPD1	LRG_179	CLEC7A
ENSG00000113916	BCL6	LRG_184	TNFRSF13C
ENSG00000135749	PCNXL2	LRG_185	RNF168
ENSG00000204397	CARD16	LRG_236	CTDP1
ENSG00000174611	KY	LRG_258	NDRG1
ENSG00000164746	C7orf57	LRG_26	C2
ENSG00000185811	IKZF1	LRG_274	LDLR
ENSG00000100055	CYTH4	LRG_3	COL3A1
ENSG00000164616	FBXL21	LRG_301	CDH1
ENSG00000143842	SOX13	LRG_319	STK11
ENSG00000196381	ZNF781	LRG_326	ZBTB24
ENSG00000092871	RFFL	LRG_34	CASP8
ENSG00000105398	SULT2A1	LRG_341	UNC119
ENSG00000005156	LIG3	LRG_349	MASP1
ENSG00000087510	TFAP2C	LRG_357	CD27
ENSG00000105835	NAMPT	LRG_365	HK1
ENSG00000154478	GPR26	LRG_38	CD3E
ENSG00000185250	PPIL6	LRG_409	LAMA2
ENSG00000171345	KRT19	LRG_411	NEBL
ENSG00000143061	IGSF3	LRG_451	ACADSB
ENSG00000100519	PSMC6	LRG_452	FOXD4
ENSG00000115590	IL1R2	LRG_466	ERCC8
ENSG00000119938	PPP1R3C	LRG_511	NF2
ENSG00000056487	PHF21B	LRG_515	PTCH1
ENSG00000141527	CARD14	LRG_6	ATP1A2
ENSG00000118520	ARG1	LRG_607	TYROBP
ENSG00000170948	MBD3L1	LRG_620	BCL2L11

ENSG00000169905	TOR1AIP2	LRG_653	ANG
ENSG00000221937	TAS2R40	LRG_700	CLRN1
ENSG00000197753	LHFPL5	LRG_722	DPYD
ENSG00000120129	DUSP1	LRG_725	MAP2K1
ENSG00000248144	ADH1C	LRG_8	SCN1A
ENSG00000169057	MECP2	LRG_84	MPO
ENSG00000149021	SCGB1A1		

Table 9.7 – List of top ten conserved motifs in genes found overlapped between hypoxia and IOX2 only (not VH032) with potential transcription factor binding site.

#	Gene Set Name	# Genes in Gene Set (K)	Description	# Genes in Overlap (k)	k/K	p-value	FDR q-value
1	TTTNNANAGCYR_UNKNOWN	2274	Genes having at least one occurrence of the highly conserved motif M169 TTTNNANAGCYR in the region spanning up to 4 kb around their transcription start sites. The motif does not match any known transcription factor binding site.	26	0.0114	9.97E-09	6.13E-06
2	GGGAGGRR_MAZ_Q6	766	Genes having at least one occurrence of the highly conserved motif M24 GGGAGGRR in the region spanning up to 4 kb around their transcription start sites. The motif matches transcription factor binding site V$MAZ_Q6 in v7.4 TRANSFAC.	15	0.0196	2.18E-08	6.54E-06
3	YRTCANNRCGC_UNKNOWN	2940	Genes having at least one occurrence of the highly conserved motif M115 YRTCANNRCGC in the region spanning up to 4 kb around their transcription start sites. The motif does not match any known transcription factor binding site.	29	0.0099	3.19E-08	6.54E-06
4	TGANTCA_AP1_C	2485	Genes having at least one occurrence of the highly conserved motif M7 TGANTCA in the region spanning up to 4 kb around their transcription start sites. The motif matches transcription factor binding site V$AP1_C in v7.4 TRANSFAC.	24	0.0097	8.59E-07	1.32E-04
5	TGACAGNY_MEIS1_01	1524	Genes having at least one occurrence of the highly conserved motif M41 TGACAGNY in the region spanning up to 4 kb around their transcription start sites. The motif matches transcription factor binding site V$MEIS1_01 in v7.4 TRANSFAC.	17	0.0112	6.34E-06	7.80E-04
6	YTCCC	1296	Genes having at least one	15	0.0116	1.50E-	1.54E-

	RNNAGGY_UNKNOWN		occurrence of the highly conserved motif M114 YTCCCRNNAGGY in the region spanning up to 4 kb around their transcription start sites. The motif does not match any known transcription factor binding site.			05	03
7	GATA6_01	265	Genes having at least one occurrence of the transcription factor binding site V$GATA6_01 (v7.4 TRANSFAC) in the regions spanning up to 4 kb around their transcription starting sites.	7	0.0264	2.20E-05	1.93E-03
8	TGGAAA_NFAT_Q4_01	2061	Genes having at least one occurrence of the highly conserved motif M55 TGGAAA in the region spanning up to 4 kb around their transcription start sites. The motif matches transcription factor binding site V$NFAT_Q4_01 in v7.4 TRANSFAC.	19	0.0092	2.55E-05	1.96E-03
9	HIF1_Q3	230	Genes having at least one occurrence of the transcription factor binding site V$HIF1_Q3 (v7.4 TRANSFAC) in the regions spanning up to 4 kb around their transcription starting sites.	6	0.0261	9.23E-05	6.31E-03
10	TTCYRGAA_UNKNOWN	1232	Genes having at least one occurrence of the highly conserved motif M72 TTCYRGAA in the region spanning up to 4 kb around their transcription start sites. The motif does not match any known transcription factor binding site.	13	0.0106	1.43E-04	8.68E-03

Table 9.8 – List of genes found overlapped between hypoxia and IOX2 (not VH032) containing at least one conserved motifs stated in Appendix Table 9.7. Entrez gene ID for each gene is listed. Number 1-10 correspond to # in **Appendix Table 9.7**, which contains details of conserved motifs. X indicates that the gene contains the conserved motif.

Entrez Gene Id	Gene Symbol	1	2	3	4	5	6	7	8	9	10
2597	GAPDH	X	X	X	X		X				X
4035	LRP1	X	X	X		X					
30008	EFEMP2	X	X	X							
9066	SYT7	X	X		X		X	X			
222171	PRR15	X	X		X						
3861	KRT14	X	X				X		X		
8541	PPFIA3	X	X								X
9770	RASSF2	X		X	X	X	X		X		
6261	RYR1	X		X	X	X					
28951	TRIB2	X		X	X						
3201	HOXA4	X		X				X	X		X
901	CCNG2	X		X					X		
205428	C3orf58	X		X					X		
5460	POU5F1	X		X							X
1026	CDKN1A	X		X							
6920	TCEA3	X		X							
84929	FIBCD1	X		X							
4607	MYBPC3	X			X			X			
9744	ACAP1	X			X						
139728	PNCK	X			X						
1852	DUSP9	X			X						
154743	C7orf60	X				X			X	X	
9094	UNC119	X				X					X
8642	DCHS1	X									X
54890	ALKBH5	X									
242	ALOX12B	X									
8572	PDLIM4		X	X		X			X		
139596	UPRT		X	X							
4582	MUC1		X	X							
7511	XPNPEP1		X			X				X	
1755	DMBT1		X				X				
5493	PPL		X								
963	CD53		X								
1132	CHRM4		X								
84251	SGIP1			X	X	X		X	X		X
92359	CRB3			X	X						
50619	DEF6			X	X						
64866	CDCP1			X	X						
7138	TNNT1			X		X	X				
56901	NDUFA4L2			X		X					
8325	FZD8			X			X				
151556	GPR155			X				X			
5794	PTPRH			X							
3300	DNAJB2			X							
91373	UAP1L1			X							
9022	CLIC3			X							
23480	SEC61G			X							
11156	PTP4A3				X	X					

113791	PIK3IP1	X			X	X	
10865	ARID5A	X			X		X
10529	NEBL	X					
79152	FA2H	X					
5604	MAP2K1	X					
2706	GJB2	X					
54852	PAQR5	X					
113828	FAM83F	X					
5737	PTGFR	X					
5054	SERPINE1		X	X			
54541	DDIT4		X		X	X	
5066	PAM		X		X		X
51760	SYT17		X				
5365	PLXNB3		X				
2825	GPR1		X				
9241	NOG			X	X		X
55279	ZNF654			X	X		
4783	NFIL3			X		X	X
4093	SMAD9			X			
3237	HOXD11			X			
3868	KRT16			X			
50506	DUOX2			X			
7036	TFR2				X	X	
164633	CABP7					X	X
3484	IGFBP1					X	
79858	NEK11					X	
8780	RIOK3					X	
55760	DHX32					X	
5507	PPP1R3C						X
771	CA12						X